DOKUZ EYLÜL UNIVERSITY
GRADUATE SCHOOL OF NATURAL AND APPLIED SCIENCES

GEOLOGIC EVOLUTION OF İZMİR-BALIKESİR TRANSFER ZONE: A CRUSTAL-SCALE STRUCTURE REORGANIZING EXTENSIONAL TECTONICS IN WESTERN ANATOLIA

by
Bora UZEL

April, 2013
İZMİR

GEOLOGIC EVOLUTION OF İZMİR-BALIKESİR TRANSFER ZONE: A CRUSTAL-SCALE STRUCTURE REORGANIZING EXTENSIONAL TECTONICS IN WESTERN ANATOLIA

A Thesis Submitted to the
Graduate School of Natural and Applied Sciences of Dokuz Eylül University
In Partial Fulfillment of the Requirements for the Degree of Doctor of Philosophy in Geological Engineering, Applied Geology Program

by
Bora UZEL

April, 2013
İZMİR

Ph.D. THESIS EXAMINATION RESULT FORM

We have read the thesis entitled **"GEOLOGIC EVOLUTION OF İZMİR-BALIKESİR TRANSFER ZONE: A CRUSTAL-SCALE STRUCTURE REORGANIZING EXTENSIONAL TECTONICS IN WESTERN ANATOLIA"** completed by **BORA UZEL** under supervision of **PROF.DR. HASAN SÖZBİLİR** and we certify that in our opinion it is fully adequate, in scope and in quality, as a thesis for the degree of Doctor of Philosophy.

Prof.Dr. Hasan SÖZBİLİR

Supervisor

Prof.Dr. Uğur İNCİ

Thesis Committee Member

Prof.Dr. Rahmi PINAR

Thesis Committee Member

Examining Committee Member

Examining Committee Member

Prof.Dr. Ayşe OKUR

Director

Graduate School of Natural and Applied Sciences

ACKNOWLEDGEMENTS

The success and outcome of this study required a lot of guidance and assistance from many important people. Of course, everything is started with my supervisor. I respect and thank to him, to Hasan Sözbilir for giving me an opportunity to do this study and providing me all support and guidance, which made me complete this doctorate project on time. Çağlar Özkaymak, my teammate, deserves here a big appreciation in this acknowledge. He was with me in the field every time. We share everything; knowledge, energy, food (he eats always more than me, of course), and support each other in all situations. I would like to thank everyone who has contributed to my thesis, but there are some people need to be particularly remarked here.

Actually, this all started in 2006 at an icebreaker dinner of 58th Geological Congress of Turkey, when Nuretdin Kaymakci sit just next to Hasan Sözbilir & me. After reading his PhD and papers (especially Denizli paper), I was willing to work with him, and there was no way to escape from me in that situation. So, we talked about a new brand project on western Anatolia and my future plan, and then my PhD came true. He is also the person who gave me the opportunity to meet and work together with the marvelous people from "The Fort".

I want to start with Cor Langereis for his never-ending support throughout more than 5 years. Cor, *dankjewel* for your everlasting patience and knowledge to explain the various Pmag techniques, and for sharing his priceless experiences at the field. It is not possible to forget those times spending at his place: tasting marvelous wines, cooking/eating delicious foods (special asparagus is still my favorite), listening great songs, watching great movies with the heat of open fire, working and talking over the midnights, and of course kindly company of his family (Nora, Shelly, and Vince). I am such a lucky guy that I met & work with Cor & Nuri.

All my Holland time would not have been instructive and joyful without the people of Fort. They were always positive and cheerful to me, so it makes everything

easier, especially to adapt the laboratory and to understand the paleomagnetism, indeed. Pınar (I had the best integration into my new atmosphere of Fort and Holland by sharing with her, and by learning every single step of paleomagnetism from her), Ahmet (aka. Peynircizade, was one of my mentors reminding me how to stand up after hard times), Tom (not only a technician, he is a magician and brilliant person), Mark (thanks for theoretical advices on Curie), Murat (has also been a part of the dating and paleomagnetic stories), Maud & Come (it was always good to communicate with you, half Turkish friends), Arjan (thank you for sincerely talks, and to giving me a hand on interpretation of my first year geochronology samples), Maxim (thanks for the bike trips all around the Utrecht), Iuliana (and her sweet family), Douwe van Hinsbergen (who inspiring me with his productivity and the way of his papers), Silja, Wout, Lenaard, Roderic, Nathan, Karin, and all other members. Thank you for your support, and great Friday-presentation-borrels during the last couple years.

From Vrije Universiteit (Free University) Amsterdam, Klaudia Kuiper (marvelous Ar/Ar dater) put a lot of effort on my geochronology chapter and answered my all questions (even nonsense ones) patient and directly. She processed and cared about my Ar/Ar samples. I also would like to express my best to Roel van Elsas for his endless and attentive assistance during the mineral separation processes, to Jan Wijbrans for his collaborate.

Thank you Ökmen, who guided to me during the Söke basin. I'll never forget his support on my mood, unique constructive critics on the geological (plus un-geological) things. Here, I particularly would like to thank my (ex-) colleagues and friends of the Karaburun project: Cahit Helvacı, Yalçın Ersoy, and Fuat Erkül. Thanks for the discussions and contributions all along the project. I also need to send my best wishes to inspiring Erdin Bozkurt & Ali Koçyiğit for always encouraging me. Special thanks must go to Burak (my Awesome! brother), Ertepınar Family (Maskot & Goldie, indeed), Mustafa & Zeynep (my roommates), and Yasin for their technical and emotional support. Without forgetting the company of Esad, Deniz, Mert, and Aykut; it was so enjoyable playing basketball, and hanging at Alsancak

with you. If you are in such a kind of study, you barely have time, but madly need relaxation. That means you need good friends around.

Thank you all for making this study possible!

This study was accomplished with financial support from the Scientific and Technical Research Council of Turkey (TÜBİTAK) research grant (ÇAYDAĞ Project No: 109Y044), and partly from the Dokuz Eylül University Scientific Research Project (BAP Project No: 2007.KB.FEN.039). The thesis (& examining) committee thanked for their guidance, support and giving their feedback.

This PhD thesis is dedicated to the memory of Orhan Kaya & Tom Mullender...

Bora UZEL

GEOLOGIC EVOLUTION OF İZMİR-BALIKESİR TRANSFER ZONE: A CRUSTAL-SCALE STRUCTURE REORGANIZING EXTENSIONAL TECTONICS IN WESTERN ANATOLIA

ABSTRACT

This thesis attempts to expose the structural implication of a crustal scale zone of weakness, the İzmir–Balıkesir transfer zone (İBTZ) which is a recently recognized as strike-slip dominated shear zone that accommodates the differential deformation between the Cycladic and Menderes core complexes within the Aegean Extensional System. Here, I present new stratigraphic, structural, paleomagnetic, geochronologic and kinematic data and 1/25,000 scale mapping of Miocene to Recent rock units within the İBTZ. The results point out that the İBTZ is a transtensional brittle shear zone that deforms the pre-Neogene basement rock units, the early-middle Miocene volcano-sedimentary units and the Plio–Quaternary continental units.

The analysis of large-scale structures and fault kinematic data indicate that three different deformation phases prevailed in the İBTZ during the late Cenozoic. The first phase (Phase 1) is characterized by N–S directed extension and E–W contraction that gave way to the development of strike-slip faults with normal components and likely took place during the early (?) to late Miocene. This transtensional phase, forming the volcano-sedimentary basin was overprinted by the second phase (Phase 2) which is characterized by variable extension and contraction directions indicating wrench-to extension-dominated transtension. The structures related to Phase 2 are observed all around the İzmir Bay and indicate a distributed nature of the deformation that probably took place during the early Pliocene, coeval with the end of the activity of the mid-Cycladic lineament and the last exhumation of the central Menderes core complex. The latest deformation phase (Phase 3) is characterized by an association of NW–SE trending left-lateral and NE–SW trending right-lateral strike-slip faults and E–W trending normal faults forming extensional deformation.

During Phase 3, the İBTZ evolved from a wider shear zone into a relatively narrow discrete fault zone by the late Pliocene, during which the strike-slip and extensional deformation were completely decoupled from each other.

With respect to new paleomagnetic data, İBTZ is a clockwise rotated structural shear zone that separated two counterclockwise rotated rigid blocks; the Menderes and Cycladic complexes, and can be interpreted as the surface reflection of the teared part of the subduction beneath the Anatolian plate.

Keywords: paleomagnetism, block rotation, geochronology, kinematic analysis, İzmir-Balıkesir Transfer Zone, western Anatolia.

İZMİR-BALIKESİR TRANSFER ZONU'NUN JEOLOJİK EVRİMİ: BATI ANADOLU'DAKİ GENİŞLEME TEKTONİĞİNİ YENİDEN ORGANİZE EDEN KITASAL ÖLÇEKTE BİR YAPI

ÖZ

Bu tez, Ege Genişleme Sistemindeki Menderes Çekirdek Kompleksi ile Kikladlar arasındaki farklı deformasyonu karşılayan ve kabuksal ölçekli bir makaslama zonu olarak tanımlanan İzmir-Balıkesir Transfer Zonu'nun yapısal önemini tanımlamayı amaçlar. Bu çalışmada, İBTZ içindeki Miyosen-Kuvaterner birimleri 1/25.000 ölçeğinde haritalanmış ve birimlerden stratigrafik, yapısal, jeomorfolojik, paleomanyetik ve jeokronolojik veriler elde edilmiştir. Veriler İBTZ'nin transtansiyonal bir makaslama zonu olduğunu ve Neojen öncesi temel kayaları, Neojen volkanosedimanter istifleri ve Pliyo-Kuvaterner birimlerini deforme ettiğini göstermiştir.

Yapısal ve kinematik verilere göre, İBTZ'de Geç Senozoyik'te üç deformasyon evresi tanımlanmıştır. Miyosen dönemine karşılık gelen ilk evrede K-G genişleme ve D-B sıkışma sonucunda gelişen doğrultu atımlı faylarca baskındır. Bu evrede KD-GB uzanımlı Miyosen volkanosedimanter havzaların oluşumu gerçekleşmiştir. İkinci evre doğrultu atım-baskın transtansiyondan genişleme-baskın transtansiyona dönüşen tektonizmayla ilişkilidir. Bu evre olasılıkla Erken Pliyosen'deki orta Kiklad çizgiselliğinin aktivitesini yitirmesi ve Menderes çekirdek kompleksinin orta bölümünün en son yüzeylemesiyle eşyaşlıdır. Son evre KB-GD sol yönlü doğrultu atımlı fay, KD-GB sağ yönlü doğrultu atımlı fay ve D-B doğrultulu normal fayların birlikte çalışmasıyla karakteristiktir. Son evrede İBTZ parçalanarak daha dar bir makaslama zonuna dönüşmüştür.

Yeni paleomagnetik veriler İBTZ'nin saat ibresinin tersi yönünde rijit bloklar şeklinde rotasyona uğrayan Menderes Çekirdek Kompleksi ve Kikladları ayıran ve

zon içinde saatibresi yönünde rotasyonların geliştiği bir makaslama zonu olduğunu göstermektedir. Tüm verilere göre, İBTZ Anadolu levhası altındaki yitim zonundaki bir yırtığın yüzeye yansımış şekli olarak yorumlanabilir.

Anahtar Sözcükler: paleomanyetizma, blok rotasyonu, jeokronoloji, kinematic analiz, İzmir-Balıkesir Transfer Zonu, Batı Anadolu.

CONTENTS

Page

PH.D. THESIS EXAMINATION RESULT FORM ii
ACKNOWLEDGEMENTS iii
ABSTRACT vi
ÖZ viii
FIGURE LIST xiv
TABLE LIST xix

CHAPTER ONE – INTRODUCTION 1

1.1 Prologue and Synopsis 1
1.2 Organization of the Thesis 3

CHAPTER TWO – STRATIGRAPHY AND TYPES OF CENOZOIC BASINS WITHIN AND ADJACENT TO THE İZMİR-BALIKESİR TRANSFER ZONE 7

2.1 Introduction 7
2.1.1 Molasse Basins 9
2.1.2 Supra-detachment Basins 10
2.1.3 Strike-slip Basins 10
2.2 Pre-Cenozoic Stratigraphy: Basement Units 13
2.3 Cenozoic Stratigraphy 18
2.3.1 Çandarlı-Dikili Area 19
2.3.2 Cumaovası Basin 22
2.3.3 Didim Area 27
2.3.4 Foça Area 28
2.3.5 Gördes Basin 32
2.3.6 E–W Grabens 36
2.3.6.1. Salihli Area 37
2.3.6.2. Tire Area 41

2.3.6.3 Syn-extensional Granitoids 44
2.3.7 Karaburun Area 44
2.3.8 Kocaçay Basin 51
2.3.9 Söke Basin 55
2.3.10 Spildağı-Yamanlar Area 59
2.3.11 Urla Basin 66
2.3.12 Yuntdağ Area 68
2.4 Plio-Quaternary Stratigraphy 71

CHAPTER THREE – GEOCHRONOLOGY OF LATE CENOZOIC MAGMATISM WITHIN THE İZMİR-BALIKESIR TRANSFER ZONE 74

3.1 Introduction 74
3.2 Geological Setting of the Cenozoic Magmatism 76
3.3 $^{40}Ar/^{39}Ar$ Dating 80
3.3.1 Methodology 80
3.3.2 Sample Preparation Procedure 81
3.3.3 Results of $^{40}Ar/^{39}Ar$ Dating 84

CHAPTER FOUR – STRUCTURAL FEATURES AND TECTONICS OF THE İZMİR–BALIKESİR TRANSFER ZONE 90

4.1 Introduction 90
4.2 Tectonic Framework of the Region 92
4.3 Late Cenozoic Structures 95
4.3.1 Karaburun Area 95
4.3.1.1 Karaburun Fault Zone (KbFZ) 95
4.3.1.2 Karareis Fault Zone (KrFZ) 98
4.3.1.3 NNE-striking Faults 100
4.3.1.4 Folds 101
4.3.2 Menemen Area 101
4.3.2.1 Harmandalı Fault Zone (HFZ) 101

4.3.2.2 E–W-trending Faults 103
4.3.2.3 NW-trending Faults 105
4.3.2.4 Folds 105
4.3.3 Yaka Area 106
4.3.3.1 Karaçay Fault Zone (KçFZ) 106
4.3.3.2 Kemalpaşa (KFZ) & Spildağı Fault Zones (SdFZ) 109
4.3.3.3 Cross-faults 110
4.3.3.4 Folds 110
4.3.4 Inner Bay Area 112
4.3.4.1 Seferihisar Fault Zone (SFZ)) 112
4.3.4.2 İzmir Fault Zone (İFZ) 113
4.3.4.3 Karşıyaka Fault Zone (KyFZ) 116
4.3.4.4 Orhanlı Fault Zone (OFZ) 119
4.3.4.5 N–S-trending Faults 119
4.3.4.6 Folds 120
4.4 Paleostress Analysis of Fault-slip Data 121
4.4.1 Methodology 121
4.4.2 Palaeostress Configurations 122
4.4.2.1 Phase 1 124
4.4.2.2 Phase 2 127
4.4.2.3 Phase 3 128

CHAPTER FIVE – PALEOMAGNETIC STUDIES 130

5.1 Introduction 130
5.2 Paleomagnetic Measurements and Analysis 134
5.3 Sampling Procedure 136
5.3.1 Paleomagnetic Studies within the İBTZ 138
5.3.1.1 Yuntdağ Area 138
5.3.1.2 Spildağı-Yamanlar Area 145
5.3.1.3 Urla Basin 147
5.3.1.4 Cumaovası Basin 148

5.3.1.5 Kocaçay Basin 151
5.4.2 Paleomagnetic Studies outside the İBTZ 153
5.4.2.1 Dikili-Çandarlı Area 153
5.4.2.2 Foça Area 155
5.4.2.3 Karaburun Area 155
5.4.2.4 Gördes Basin 157
5.4.2.5 Gediz, Küçük Menderes, and Büyük Menderes Grabens 159
5.4.2.6 Söke Basin & Didim Area 161
5.5 Paleomagnetic Results 165
5.5.1 Paleomagnetic Results within the İBTZ 165
5.5.2 Paleomagnetic Results outside the İBTZ 172

CHAPTER SIX – DISCUSSION AND CONCLUSION 177

6.1 Spatio-Temporal Characteristics of Volcanism and Sedimentation 177
6.2 Deformation Phases 182
6.3 Paleomagnetism 185
6.3.1 Previous Paleomagnetic Studies in the Region 185
6.3.2 Discussion on the Paleomagnetic Results of This Study 191
6.3.2.1 Early-Middle Miocene Rotations 192
6.3.2.2 Implications Early Miocene Rotations 194
6.3.2.3 Middle-Late Miocene Rotations 195
6.3.2.4 Implications Early Miocene Rotations 195
6.4 Regional Implications 196

REFERENCES 202

FIGURE LIST

Page

Figure 1.1 Simplified tectonic and geologic maps of the Aegean region 4
Figure 2.1 Simplified tectonic map of the western Anatolia showing tectonic units and the distribution of Cenozoic successions 8
Figure 2.2 Geological map of the pre-Miocene basement rocks 14
Figure 2.3 Simplified geological map of western Anatolia 18
Figure 2.4 Geological map of Çandarlı-Dikili area 19
Figure 2.5 Generalized stratigraphic columnar section of Çandarlı-Dikili area 21
Figure 2.6 Field photos of Miocene stratigraphic units exposed in the Çandarlı-Dikili area..... 22
Figure 2.7 Detailed geological map of the Cumaovası basin..... 24
Figure 2.8 Generalized stratigraphic columnar section of the Cumaovası basin 25
Figure 2.9 Field photos of stratigraphic units exposed in the Cumaovası basin 26
Figure 2.10 Field photos of stratigraphic units exposed in the Didim area 28
Figure 2.11 Geological maps of the Foça area 29
Figure 2.12 Generalized stratigraphic columnar section of Foça area..... 31
Figure 2.13 Field photos of volcano-sedimentary units exposed in the Foça area 32
Figure 2.14 Geological map of the Gördes basin..... 33
Figure 2.15 Generalized stratigraphic columnar section of the Gördes basin 34
Figure 2.16 Field photos of volcano-sedimentary units exposed in the Gördes basin..... 35
Figure 2.17 Simplified geological map showing the Neogene–Quaternary basins ... 38
Figure 2.18 Generalized stratigraphic columnar section of Gediz Graben around Salihli area 39
Figure 2.19 Field photos of Gediz detachment fault and sedimentary units on top of it..... 40
Figure 2.20 Generalized stratigraphic columnar section of the Küçük Menderes Graben around Tire area..... 41
Figure 2.21 Field photos of stratigraphic units exposed in the Tire area 43
Figure 2.22 Geological map of the Karaburun area and Urla basin..... 45
Figure 2.23 Detailed geological map of the Karaburun area 47

Figure 2.24 Generalized stratigraphic columnar section of northern Karaburun..... 48
Figure 2.25 Detailed geological map of the Karaburun area around Çeşme 49
Figure 2.26 Field photos of stratigraphic units exposed in the Karaburun area 50
Figure 2.27 Detailed geological map of the Kocaçay basin 52
Figure 2.28 Generalized stratigraphic columnar section of Kocaçay basin 53
Figure 2.29 Field photos of stratigraphic units exposed in Kocaçay basin 54
Figure 2.30 Generalized geological map of the western margin of the Büyük Menderes and Küçük Menderes grabens and the detailed geological map of the Söke basin 56
Figure 2.31 Generalized stratigraphic columnar section of Söke basin 57
Figure 2.32 Field photos of stratigraphic units exposed in the Söke basin 58
Figure 2.33 Detailed geological map of western hillside of the Yamanlar high around Menemen village 60
Figure 2.34 Detailed geological map of southern hillside of the Spil-Yamanlar area around Bornova village 61
Figure 2.35 Detailed geological map of the central part of Spil-Yamanlar area 62
Figure 2.36 Generalized stratigraphic columnar section of Spil-Yamanlar area 63
Figure 2.37 Field photos of the Miocene units exposed around Spil-Yamanlar area 65
Figure 2.38 Detailed geological map of the Urla basin around İskele village 66
Figure 2.39 Generalized stratigraphic columnar section of the Urla basin 67
Figure 2.40 Field photos from the upper sequence of the Miocene units exposed in the Urla basin 68
Figure 2.41 Detailed geological map of the Yuntdağ area around Manisa basin 69
Figure 2.42 Field photos of Miocene units exposed around Yuntdağ area 70
Figure 3.1 Simplified tectonic map showing major neotectonic elements and Cenozoic volcanic rocks in Anatolian Plate 75
Figure 3.2 Simplified geological maps showing main distribution of the Eocene to Quaternary magmatic rocks in the western Anatolia 77
Figure 3.3 Simplified geological map of volcanic areas and sample locations for $^{40}Ar/^{39}Ar$ geochronology study 82
Figure 3.4 Figure showing the incremental heating $^{40}Ar/^{39}Ar$ spectra of samples ... 86

Figure 3.5 Figure showing the chronologic positions of $^{40}Ar/^{39}Ar$ results of this study and spatio-temporal relationship between volcanism and studied areas ... 88
Figure 4.1 Simplified tectonic maps showing the major (plate) tectonic elements and configuration of the Aegean region ... 91
Figure 4.2 Simplified geological map of the İzmir Bay area draped on topographic data ... 93
Figure 4.3 Detailed geological map of Karaburun area ... 96
Figure 4.4 Field photos of post-Miocene structures from the Yaka area ... 98
Figure 4.5 Lower-hemisphere equal-area projection of fault planes, slickenlines, and constructed palaeostress configurations for the Karaburun area ... 99
Figure 4.6 Detailed geological map of the Menemen area ... 102
Figure 4.7 Field photos of post-Miocene structures from Menemen area ... 104
Figure 4.8 Lower-hemisphere equal-area projections of fault planes, slickenlines and constructed palaeostress configurations for the Menemen area ... 105
Figure 4.9 Detailed geological map of the Yaka area ... 107
Figure 4.10 Field photos of post-Miocene structures from the Yaka area ... 108
Figure 4.11 Lower-hemisphere equal-area projection of fault planes, slickenlines, and constructed palaeostress configurations for the Yaka area ... 109
Figure 4.12 Interpretation of fault interactions in the Yaka area ... 111
Figure 4.13 Detailed geological map of Güzelbahçe area and geological cross-section ... 114
Figure 4.14 Field photos of the Seferihisar and İzmir fault zones ... 115
Figure 4.15 Lower-hemisphere equal-area projection of fault planes, slickenlines and constructed palaeostress configurations for the Inner Bay area ... 116
Figure 4.16 Detailed geological map of the southern margin of the Inner Bay area around Altındağ ... 117
Figure 4.17 Field photographs of the E–W-trending İzmir fault zone ... 118
Figure 4.18 Orientation and temporal variation of horizontal components of principal paleostrain axes ... 123
Figure 5.1 Published paleomagnetic results from the eastern Mediterranean region ... 131

Figure 5.2 Simplified geological map of western Anatolia draped onto a Digital Elevation Model image showing distribution of Neogene sediments, granitoids and volcanic suits 132
Figure 5.3 Simplified geological map showing the distribution of sampling locations and codes of ninety-six paleomagnetic sampling localities 137
Figure 5.4 Sketch cross-sections and a field picture of the sample sites within the Yuntdağ area 139
Figure 5.5 Sketch cross-sections and field pictures of the sample sites within the Yuntdağ area 141
Figure 5.6 Sketch cross-sections and field pictures of the sample sites within the Yuntdağ area 143
Figure 5.7 Sketch cross-sections and field pictures of the sample sites within the Spil-Yamanlar area 144
Figure 5.8 Sketch cross-sections and field pictures of the sample sites within the Spil-Yamanlar area 146
Figure 5.9 Sketch cross-sections and a field photo of the sample sites within the Urla basin 148
Figure 5.10 Sketch cross-sections and field pictures of the sampling sites illustrating positions of the samples within each section in the Cumaovası basin 150
Figure 5.11 Sketch cross-sections and a field photo, indicating stratigraphic positions of the paleomagnetic samples within the Kocaçay basin 152
Figure 5.12 Sketch cross-sections and field photos showing stratigraphic positions of the paleomagnetic samples within the Çandarlı-Dikili and Foça areas 154
Figure 5.13 Sketch cross-sections and a field photo showing stratigraphic positions of the paleomagnetic samples within the Karaburun area 156
Figure 5.14 Sketch cross-sections and filed photos showing stratigraphic positions of the paleomagnetic samples within the Gördes basin 158
Figure 5.15 Sketch cross-sections and filed photos indicating positions of the paleomagnetic samples within the E–W-trending grabens 160
Figure 5.16 Sketch cross-sections and field photos showing stratigraphic positions of the paleomagnetic samples within the Söke basin 162

Figure 5.17 Equal area projections of the ChRM directions and orthogonal vector diagrams 166
Figure 5.18 Calculated mean directions for each area 168
Figure 5.19 Equal area projections of the ChRM directions and orthogonal vector diagram 173
Figure 6.1 Figure showing temporal relationship between the different volcanic edifices in İBTZ 178
Figure 6.2 Iso-age contour map of the Miocene volcanics and age versus altitude diagram..... 180
Figure 6.3 Stratigraphical correlation of the Cenozoic basins in the İBTZ 181
Figure 6.4 Miocene and post-Miocene kinematic data from the İBTZ, the Aegean and West Anatolian Extensional Systems 184
Figure 6.5 Paleomagnetic data from this study and previous paleomagnetic studies..... 190
Figure 6.6 Paleomagnetic results from this study 193
Figure 6.7 Rigid body rotation model for the study area 195
Figure 6.7 Present dynamics in western Anatolian and Aegean region drapped on the surface/subsurface topography 199

TABLE LIST

Page

Table 3.1 Summary of available age data from the areas or basins that studied in this thesis 79
Table 3.2 Summary of $^{40}Ar/^{39}Ar$ results 83
Table 4.1 Characteristics of stress states used to reconstruct the stress regimes 125
Table 4.2 Published palaeostress tensors used for the reconstruction of the deformational history of the area 126
Table 5.1 Table showing all paleomagnetic data from this study 169
Table 6.1 Published paleomagnetic results in western Anatolia..... 186

CHAPTER ONE
INTRODUCTION

1.1 Prologue and Synopsis

For over 30 years, earth scientists have conducted field-oriented studies in western Anatolia and they attributed the deformation in the brittle upper crust to the activities of accompanied normal faults since the early Miocene (e.g. Seyitoğlu & Scott, 1994). Most of these studies revealed that Neogene evolution of Aegean and Western Anatolia region is dominated by extensional deformation that gave way to the exhumation of Menderes core complex (MCC) which was associated with well-defined NE-SW trending and E-W trending horst-graben complexes (Dewey & Şengör, 1987; Pichon & Angelier, 1980; Şengör et al., 1985; Şengör, 1987; Bozkurt, 1994, 2001, 2003, and references therein). Although, the extensional tectonics in the region is relatively well studied, the strike-slip tectonics and related structures in the region is generally received less attention or omitted. On the other hand, Kaya (1981) was one of the pioneers that realized the importance of strike-slip faults in western Anatolia. Then, Ring et al. (1999) gave another perspective to these structures in terms of crustal scale deformation. Recently, Uzel & Sözbilir (2008), Sözbilir et al. (2011), Uzel et al. (2012, 2013) and Özkaymak et al. (2013) provided a plausible explanation for the tectonic significance of these structures. They argued that differential stretching of MCC (MCC) and Cycladic core complex (CCC) is accommodated by the İzmir-Balıkesir Transfer Zone (İBTZ), a strike-slip fault zone experienced multi-phase deformation history. Recent earthquakes (Doğanbey Mw= 6.0 in 1992; Urla Mw= 5.7 in 2003; Sığacık Bay Mw= 5.4–5.8 in 2005) also indicate that strike-slip deformation in the region is as important as the normal faulting both in terms of tectonics and their seismic hazard potential (e.g. Benetatos et al., 2006; Tan, 2012).

In fact, Kaya (1981) studied the sedimentary basins lying within the zone and archived using Miocene stratigraphic record that these NE-trending structures inherited from late Cretaceous reactivated. After that, the İBTZ was first identified by Okay and Siyako (1991) as a NE-trending transform zone of weakness, and was interpreted as the depositional loci of the Bornova Flysch Zone during the late Cretaceous. Then, Ring et al. (1999) discussed that this feature was a sinistral wrench corridor and propose that the zone has offset the Vardar-İzmir-Ankara Suture Zone left laterally and resulted in about ~150 km bent of the belt southwards. Finally, Kaya et al. (2007) associate these NE-trending structures with convergence along the Hellenic Trench and the mechanism of retreatment of slab. After all, the most recent paper about this subject is the study of Gessner et al. (2013), which argues the remarkable differences between the Aegean and western Anatolian parts of the convergent plate using with the gravity, earthquake locations, seismic velocity anomalies, and the surface geological data. They suggest that the differences between these two micro plates accommodate with a lithospheric-scale shear zone (West Anatolian Shear Zone). According to researchers this zone reflect to the surface as the NE-trending İBTZ.

However, the tectonic significance, deformation mechanism, kinematics and timing of strike-slip tectonics and its association with the normal faulting in the region are not well-known yet. This is mainly due to lack of structural, kinematic, paleontological and radiometric data. In order to shed light on some of these problems the main purpose of this study is to understand timing and kinematics of İBTZ in the context of western Anatolian–Aegean extension. In other words, using geochronology, structural geology and paleomagnetism as a tool, the present study seeks answers for the following questions:

- What is the role of strike-slip faulting (particularly İBTZ) on Aegean–West Anatolian extensional system?
- What is the mechanism of stress partitioning between normal and strike-slip faulting in the region?
- What is the timing of these events and how they evolve in time?

In order to reach the above-mentioned goals, the problem is tackled with multi-disciplinary approach. These include conventional 1/25.000-scale field mapping, structural mapping and analysis, fault kinematics using fault slip-data, radiometric dating techniques for constraining the timing of the events precisely, and paleomagnetic techniques to determine the amount and sense of vertical axis rotations. The study area covers mainly the extent of the İBTZ from its northern end around Balikesir to onshore southern end around western margin of the Büyük Menderes Graben near Söke to Didim (Fig. 1.1). The study is concentrated mostly on the volcanic rocks and associated sedimentary infill of the Miocene basins in the İBTZ.

1.2 Organization of the Thesis

This multi-disciplinary study comprises six chapters. First and the last chapters give introducing the study and final implications of gathered data in a regional aspect, respectively. Others were designed as each of chapters includes one different tool; stratigraphy, geochronology, structural geology and paleomagnetism. The brief information of the chapters are following:

Chapter 1 contains preliminary information about the purpose and aim of this study and it's extended. Additionally, some previous works have been mentioned, and their determinations about the region have been given in this chapter.

Second chapter (*Chapter 2*) is about the stratigraphy of the İBTZ and neighbor areas. Here stratigraphical information related to Neogene volcano-sedimentary basins in the region are presented. The main purposes are: (i) to present each stratigraphic unit basin by basin, (ii) to construct a well-defined stratigraphic correlation scheme to explore the effect of the İBTZ on depositional process (if there), (iv) using the lacks of the deposition to simplify whole stratigraphy in terms of different names of the same unit in the literature, (iii) to understand the spatio-temporal relationships of the geochronologic, kinematic, and paleomagnetic

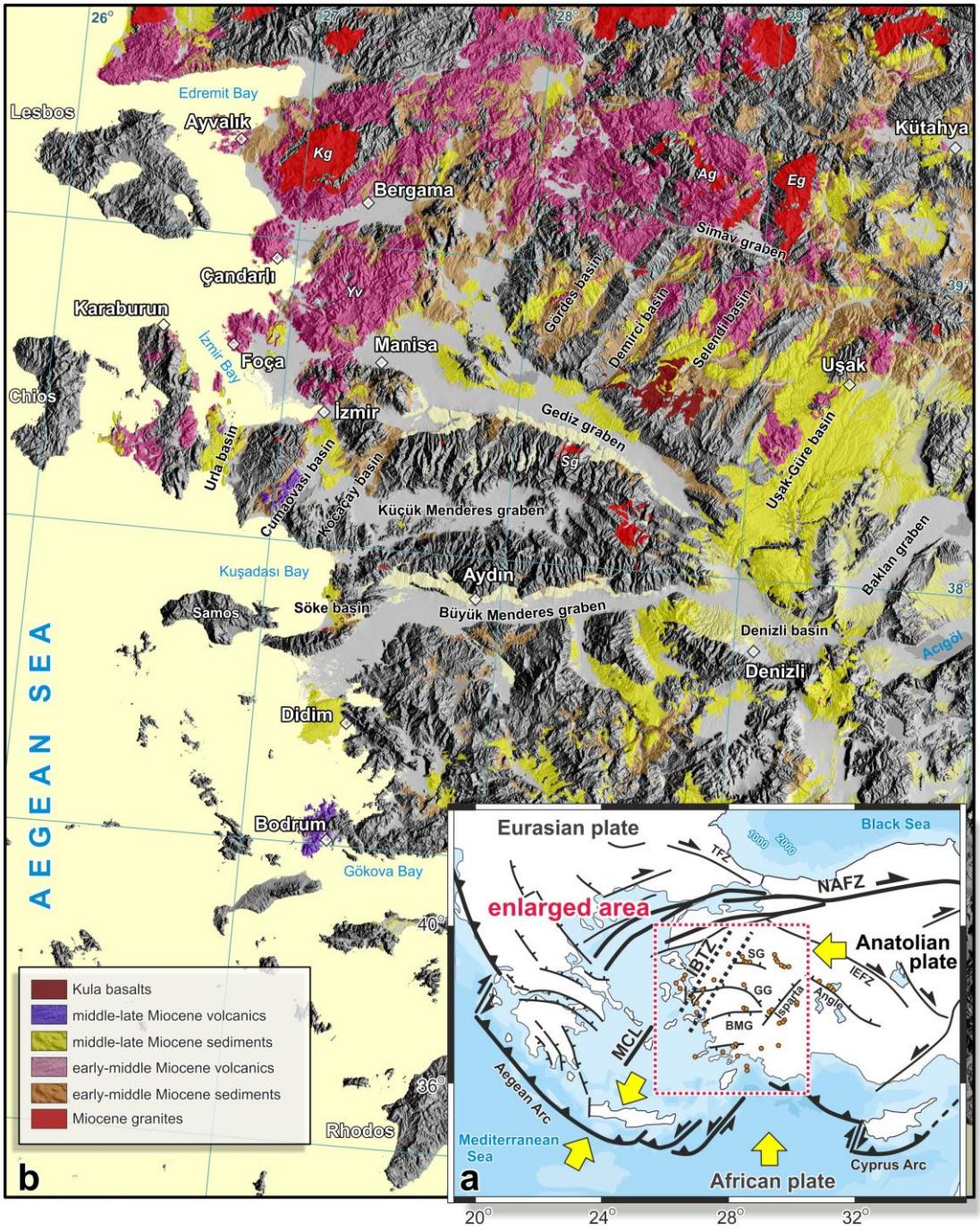


Figure 1.1 a) Simplified map showing the major (plate) tectonic elements and configuration of the Aegean region. NAFZ, North Anatolian Fault Zone; CAFZ, Central Anatolian Fault Zone; TGF, Tuz Gölü Fault; IEFZ, İnönü-Eskişehir Fault Zone; AFZ, Akşehir Fault Zone; G, Gökova Bay; BMG, Büyük Menderes Graben; GG, Gediz Graben; SG, Simav Graben; TFZ, Thrace Fault Zone (complied from Şengör et al., 1985; Barka, 1992; Bozkurt, 2001; Koçyiğit & Özaçar, 2003; Uzel & Sözbilir, 2008; Tan et al., 2008; Biryol et al., 2011). b) Simplified geological map of western Anatolia (MTA, 2002) draped onto a Digital Elevation Model image. Kg, Kozak granite; Eg, Eğrigöz granite; Ag, Alaçamdağ granite; Sg, Salihli granite.

sampling sites with each other. Data from this chapter has been published as "*Neotectonic evolution of an actively growing superimposed basin in western Anatolia: The Inner Bay of İzmir, Turkey*" in *Turkish Journal of Earth Sciences*.

Dating of the events means to compare different geological events and to understand how these are building up in time. In this context, *Chapter 3* uses $^{40}Ar/^{39}Ar$ geochronology technique and provides a new geochronological data set from Miocene volcanic rocks exposed along the İBTZ (37 new ages from 34 different lava levels), mostly in Çandarlı, Foça, Yuntdağ, Yamanlar, Karaburun, Urla, and Cumaovası magmatic suits. Due to the fact that the internal structures of the volcanic areas are very complex (particularly within the İBTZ) and presence of a number of cross-cutting relationships encountered during field studies implies multiple phases of volcanism. The idea is dating the samples from each volcanic site that paleomagnetically drilled. But here, it should be also noted that these volcanic rocks are locally intercalated with the Neogene sediments; so they are also used to date the Neogene deposits precisely. Data from this chapter is in preparation as "*$^{40}Ar/^{39}Ar$ geochronology and integrated tectonostratigraphy of the Miocene volcano-sedimentary successions within the İzmir–Balıkesir transfer zone"*.

The *Chapter 4* gives field-based data on main structures they can possibly defined boundaries of rotating tectonic blocks. It also points out the main structures that responsible for deformation (and/or sedimentation) of the stratigraphical units, and rotation of the tectonic blocks. After: (i) geological mapping of structural elements at a scale of 1/25000, (ii) identifying stratigraphic units for relative dating of the deformation phases, (iii) collection of kinematic data from the mesoscopic structures to construct palaeostress configurations; different deformation phases have been described. To understand the nature of each phase a computer-based inversion technique of Angelier (1979, 1984) is performed by integrating with field observations. The available palaeostress data sets in the literature are also merged. Data from this chapter has been published as "*Structural evidence for strike-slip deformation in the İzmir–Balıkesir transfer zone and consequences for late Cenozoic evolution of western Anatolia (Turkey)*" in *Journal of Geodynamics*.

Chapter 5 presents paleomagnetic data from the Miocene basins within and adjacent to İBTZ. In total, 1398 cores were sampled at 96 localities disturbed within the İBTZ and adjacent areas; the data set is to be used as reference to the fault block rotations within the İBTZ. The drilling locations are concentrated on Miocene volcano-stratigraphic units exposed along the İBTZ, E-W trending graben basins, and NE-trending basins. In addition to these syn-extensional granites intruded into the Menderes Core Complex during its exhumation are also sampled. For each area, in addition to site based result a common paleomagnetic vector is calculated. Then, tectonically induced rotations are determined for each tectonic block. Data from this chapter is in preparation as "*Paleomagnetic results from Miocene sediments and lavas of the west Anatolian extensional basins*".

The main conclusions and results of the present study are discussed in the final as *Chapter 6*. A tectonic scenario is constructed to explain the geological events, and to document the role of İBTZ. Previous scenarios are also discussed and the whole story building step by step is hammered out. Data from this chapter is in preparation as "*Geological evolution of İzmir-Balikesir transfer zone: A crustal structure reorganizing extensional deformation in western Anatolia*".

CHAPTER TWO
STRATIGRAPHY AND TYPES OF CENOZOIC BASINS WITHIN AND ADJACENT TO THE İZMİR-BALIKESİR TRANSFER ZONE

2.1 Introduction

In this chapter, first I will give short information about the late Cenozoic basin types in western Anatolia, in chronological order; molasse basin, supradetachment basin, and strike-slip basin. Then I present the spatial stratigraphy of these basins which is also the loci of or adjacent to a NE-trending intermittently active zone of weakness, the İzmir-Balıkesir Transfer Zone (İBTZ).

Field-oriented studies in western Anatolia revealed that the E–W trending late Cenozoic basins are bounded by approximately E–W-oriented detachments and high-angle normal faults (e.g. Koçyiğit et al., 1999; Bozkurt, 2000, 2001; Sözbilir, 2001, 2002; Bozkurt & Sözbilir, 2004, 2006; Emre & Sözbilir, 2007; Çiftçi & Bozkurt, 2007, 2008, 2009). The detachment faults that are kinematically linked with a crustal-scale metamorphic core complex, the Menderes core complex (MCC), and approximately E–W and NE–SW dissecting basins form the most prominent features of western Anatolia (Fig. 2.1; e.g. Hetzel et al., 1995; Yılmaz et al., 2000; Bozkurt & Oberhänsli, 2001; Gessner et al., 2001; Işık & Tekeli, 2001; Ring et al., 2003; Purvis & Robertson, 2004; Bozkurt & Sözbilir, 2004). Detachment fault systems in this province are associated with domal uplift of the Menderes core complex of the lower plate and the formation of asymmetric supradetachment basins in the upper plate. In addition, there are also some studies revealing the presence of a number of NE–SW trending strike-slip faults controlling the NE-trending Miocene deposition on the western Anatolian crust onshore (e.g. Kaya, 1981; Genç et al., 2001; Kaya et al., 2004; Kaya et al., 2007; Uzel & Sözbilir, 2008; Sözbilir et al., 2011) and offshore (Ocakoğlu et al., 2004, 2005). This transversely orientated strike-slip- dominated zone that accommodated the lateral termination of E–W-trending graben bounding

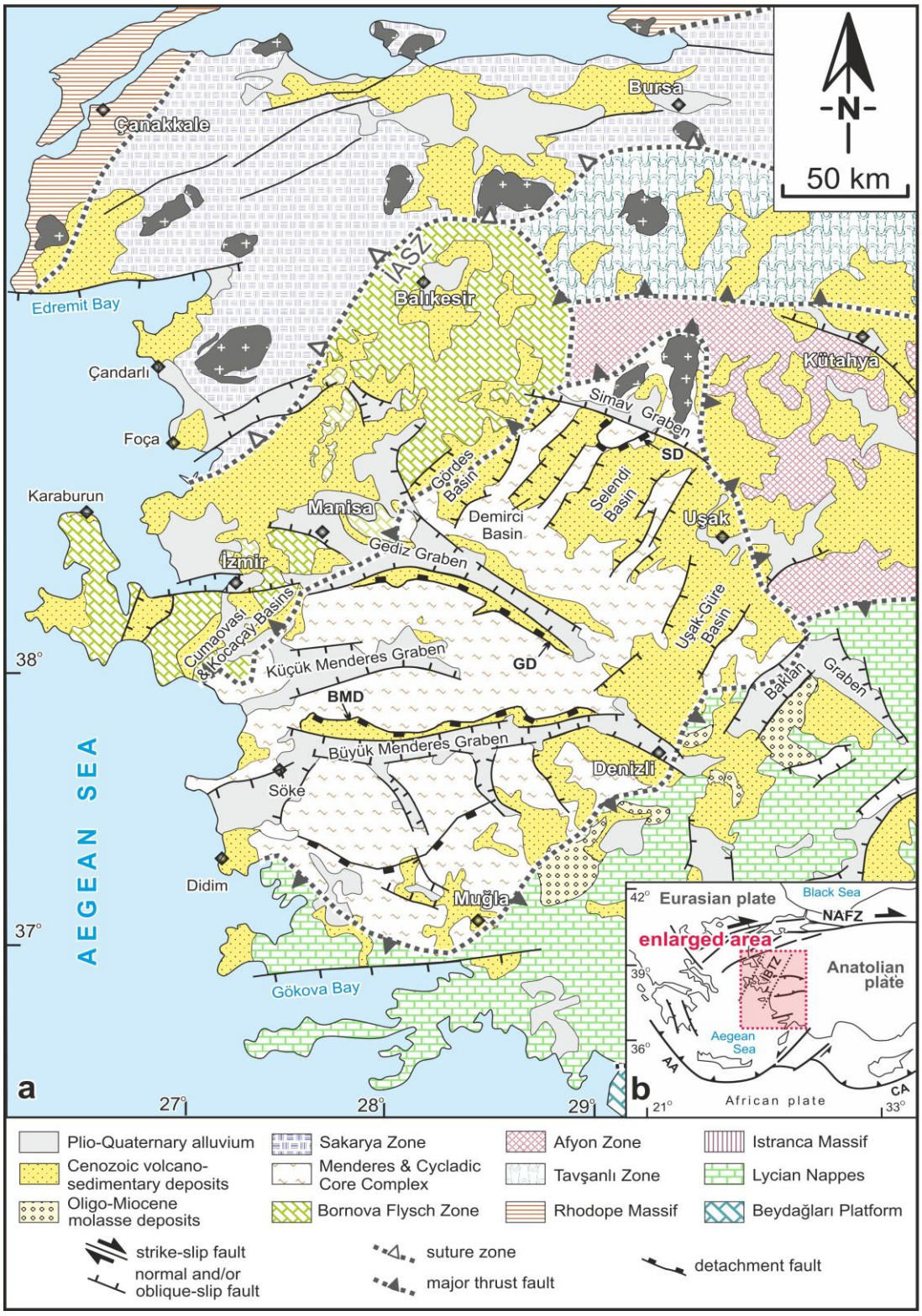


Figure 2.1 a) Simplified tectonic map of the western Anatolia showing the main tectonic units and the distribution of Cenozoic successions (Okay & Siyako, 1993; Bozkurt & Park, 1994; Bozkurt, 2001, 2004; Bozkurt & Sözbilir, 2004; Sözbilir, 2001, 2002b; Işık et al., 2003, 2004; Collins & Robertson, 2003; Özer & Sözbilir, 2003; Sözbilir, 2005).

faults, linking spatially discrete loci of extension, includes the İBTZ. Along the zone, the main structural contacts between the tectonostratigraphic units were reactivated as transtensional shear zones and resulted in NE–SW trending elongated strike-slip basins of Miocene age.

The models for the tectonic evolution of these basins include (summarized in Bozkurt 2003): tectonic escape (Dewey and Şengör, 1979; Şengör, 1979, 1980, 1982, 1987; Şengör et al., 1985; Görür et al., 1995), back arc spreading (McKenzie, 1978; Le Pichon and Angelier, 1979; Jackson & McKenzie, 1988; Meulenkamp et al., 1994; Okay and Satır, 2000), orogenic collapse (Seyitoğlu & Scott, 1992; Seyitoğlu et al., 1992), episodic two-stage extension model (Sözbilir & Emre, 1996; Koçyiğit et al. 1999; Bozkurt, 2000, 2001a, 2003; Işık & Tekeli, 2001; Lips et al., 2001; Sözbilir, 2001, 2002; Bozkurt & Sözbilir 2004; Koçyiğit 2005), and the velocity differences between the overriding plates (Aegean and Anatolian plates) on the African plate (Doglioni et al., 2002; Tokçaer et al., 2005).

2.1.1 Molasse Basins

The Oligo-Miocene molasse basin of western Anatolia named as the Lycian molasse basin by Sözbilir (2005) is composed of a sequence of late to early-post orogenic deposits including both continental and shallow-marine sediments (Sözbilir, 2005). These sediments lie on the Mesozoic Lycian Nappes with ophiolites, and Paleocene-Eocene supra-allochthonous sediments (Fig. 2.1). Molasse deposits have long been recognized as an important tool in the analysis of late orogenic histories (c.f. Allen et al., 1986). The term of ‘molasse’ was originally applied to the molasse of the Alps by Swiss geologists as a distinctive sedimentary facies, consisting of alluvial and shallow-marine deposits that formed within or adjacent to fold belts in foreland or intermontane basins (Miall, 1978). The characteristic features of molasses are: (i) they are usually lying within or adjacent to emergent fold belts during and following orogenic activity; (ii) there is an obvious relationship between sedimentation and tectonism; (iii) because of the discrete uplift events occurring the source area and subsidence in the basin, the intrabasinal unconformities are common;

(iv) metamorphic core complexes, exhumed simultaneously with deposition of the molasse units (Miall, 1978).

2.1.2 Supra-detachment Basins

In western Anatolia, a series of supra-detachment basins are postulated. They are: NE-trending Kocaçay (Sözbilir et al., 2011), Gördes, Selendi and Uşak-Güre basins (Şengör, 1987; Ersoy et al., 2008; 2012); and E-W-trending Gediz and Büyük Menderes grabens (Emre, 1996; Sözbilir, 2001; Çiftçi & Bozkurt, 2010). Supradetachment basins, which form in the hanging walls of low-angle normal faults, are a special class of basins; their formation and stratigraphic development are closely related to tectonic processes. They form in areas of extensional tectonics where extension rates and finite strains are high, such as in the Basin and Range province, the North American Cordillera, and the Aegean region (e.g. Emre, 1996; Sözbilir, 2001; van Hinsbergen & Meulenkamp, 2006; Jolivet, 2010). According to Fillmore et al. (1994), basically, there are three detachment related basin types: footwall basin behind the breakaway fault, classical breakaway basins, and basins formed within the hanging wall due to upper-plate faulting.

2.1.3 Strike-slip Basins

Many sedimentary basins of variable sizes are formed under the control of both strike-slip and normal fault systems. These are defined as transtensional basins that have various geometries and complex tectonic and depositional histories. Transtensional basins are most likely to form along oblique-divergent plate boundaries or in transfer and accommodation zones in major rifts and extensional provinces (Christie-Blick & Bilddle, 1985; Fauld & Varga, 1998). Ingersoll & Busby (1995) defined transtensional basins as those basins formed by extension along strike-slip fault systems. The classic examples of the transtensional basin are the pull-apart basins that are elongated depressions where one strike-slip fault steps over to another strike-slip fault (Aydın & Nur, 1982; Christie-Blick & Bilddle, 1985). These basins are commonly bounded by large strike-slip fault zones, adjacent to

which sediments are strongly deformed. The pull-apart origin of these basins is clearly demonstrated by the character of the basin. Proximal provenance of high-energy mass-flow deposits indicates areas of local basement uplift and erosion adjacent to areas with rapid subsidence and deposition features characteristic of a pull-apart origin (Sylvester, 1988). However, basins that form where normal or oblique-slip faults splay from large strike-slip faults without a step to another strike-slip fault are best defined as transtensional fault-termination basins (Miall, 2000). Fault-termination basins have characteristics of both classic rift and pull-apart (strike-slip) basins (Umhoefer et al., 2007). Examples are present in the northern Aegean Sea (Mann, 1997; Koukouvelas & Aydın, 2002), along ancient strike-slip faults (Olsen & Schlische, 1990), and in the southern Gulf of California − an oblique-divergent plate boundary (Dorsey & Umhoefer, 2000; Dorsey et al., 2001; Umhoefer et al., 2007).

A few studies have documented some characteristic structures of strike-slip basins, based on solid structural and sedimentological data (e.g., Crowel, 1982; Aydın and Nur, 1985; Christie-Blick and Biddle, 1985; Nilsen and McLaughlin, 1985; Ingersoll, 1988; Sylvester 1988; May et al., 1993; Campagna and Aydın, 1994; Ingersoll and Busby, 1995; Nilsen and Sylvester 1995; Dooley and McClay, 1997; Rahe et al., 1998; Lee and Chough, 1999; Ryang and Chough, 1999; Barka et al., 2000; Miall 2000; Wysocka and Swierczewska, 2003). For example, the Ridge basin in southern California is one of the best studied strike-slip basins in the world (Crowel, 1982; Nilsen and McLaughlin, 1985). It was developed during the late Miocene-Pliocene time under the control of the dextral San Gabriel Fault, which bounds it to the southwest, while the San Andreas Fault forms its northwest boundary. The Ridge basin is a syncline-like asymmetrical basin filled with up to 14-km-thick sedimentary sequence. Across the southwestern margin of the basin, there is a thick alluvial fan to deltaic clastics shed from the San Gabriel Fault into the lacustrine sediments (May et al. 1993). Another well-defined pull-apart basin is the rhomb-shaped Eumsung basin in Korea (Ryang and Chough, 1999). It is approximately 40-km long and 5-km wide. It was formed in a stepover along the sinistral Kongju fault system. The southwestern part of the Eumsung basin, three

alluvial-to-lacustrine systems are recognized: (1) a volcaniclastics-dominated alluvial fan, (2) an alluvial plain dominated by channel shifting within floodplain, and (3) a floodplain and lake. The Lo River basin, which is located in Vietnam also demonstrates many of the characteristic structures of a pull-apart basin (Wysocka and Swierczewska, 2003). The basin was formed in relation to sinistral transtensional regime through the Red River and Lo River fault zones. It has an alluvial sedimentary fill (6000 m thick) consisting of three main packages: (1) alluvial fan deposits, (2) gravel- and/or sand-dominated fluvial channel deposits, and (3) alluvial plain deposits. The basin fill was accompanied by syn-depositional tectonism responsible for the development of intra-formational folds and local unconformities. These unconformities were attributed to transition from transtension to transpression in the basin (Wysocka and Swierczewska, 2003).

Most of the strike-slip basins that have been described in Turkey occur along North Anatolian and East Anatolian fault zones (e.g., Koçyiğit, 1988, 1989, 1990; Westaway & Arger, 1996; Barka et al., 2000; Koçyiğit & Erol, 2001; Şengör et al., 2004). The Taşova-Erbaa basin, as an example, developed along the North Anatolian Fault Zone (Barka et al., 2000). It is approximately 65-km long and 15−18-km wide. Barka et al. (2000) have mapped numerous extensional and compressional faults, which deformed the basin fill. The compressional structures are isolated and associated with master faults, whereas the pervasive extensional faults trend perpendicular to the principal displacement zone of master faults that accommodates secondary pull-apart stretching within the basin.

An example of the strike-slip basin evolved in western Anatolia is recently documented in İBTZ by Uzel and Sözbilir (2008), Cumaovası basin. The basin is located at the western end of Gediz and Küçük Menderes grabens in the west Anatolian extensional province. It is 5–17 km wide and 35-km-long, NNE–SSW-trending, asymmetric basin that was formed under the control of strike-slip and oblique-slip normal faults. The basin contains three different Cenozoic infills that are separated by angular unconformities: controlled/deformed by synchronous NE–SW-trending strike-slip faulting; and E–W-trending normal faulting. Basin tectonics is

characterized by episodic activity, where superposed transpressional and transtensional deformation occurred.

The rock units exposed in the west Anatolian basins ranges from Silurian to Recent in age. For the sake of simplicity and tectonic history of the region, the pre-Cenozoic metamorphosed or strongly deformed units (considered here as basement), the Eocene-Oligocene sedimentary units are only briefly described. However, the Miocene to Recent rock units are described in detail since they are deposited under the influence of tectonic events related to the current tectonic scheme of the region.

2.2 Pre-Cenozoic Stratigraphy: Basement Units

The basement consists mainly of six tectonic units comprising, from NW to SE, the Rhodope-Vardar-Sakarya Zone, the Bornova Flysch Zone (including the Karaburun Belt), the Tavşanlı Zone, the Menderes Core Complex, the Cycladic Core Complex and the Lycian Nappes (Fig. 2.2).

The Rhodope-Vardar-Sakarya Zone is a mountain range, which is located to the north- northwest of the Aegean Sea, northern Greece and southern Bulgaria (Fig 2.1). It is mainly composed of high- to low-grade metamorphic rocks (Rhodope and Vardar massifs), limestones and highly deformed sedimentary rocks (Sakarya Zone). The unit is regarded as a complex of Mesozoic syn-metamorphic stacked in an Alpine active margin that later underwent extension and related exhumation of high-grade rocks (Ring et al., 1999; Jolivet et al., 2004; Okay et al., 2012). According to internal structures and exhumation history of Rhodope-Vardar-Sakarya Zone has several core complexes which are tectonically lying within Aegean subduction zone caused convergence between the Eurasian and African plates (Fig 2.1). The closest core complex formation to the study area is cropped out in Biga Peninsula, its Kazdağ Core Complex. The main rock units of the complex are gneiss (and associated migmatites), amphibolite, marble, and meta-serpentines (Cavazza et al., 2008). The exhumation of Kazdağ Core Complex encompasses two stages. The first stage took place between late Oligocene and early Miocene along in the footwalls of

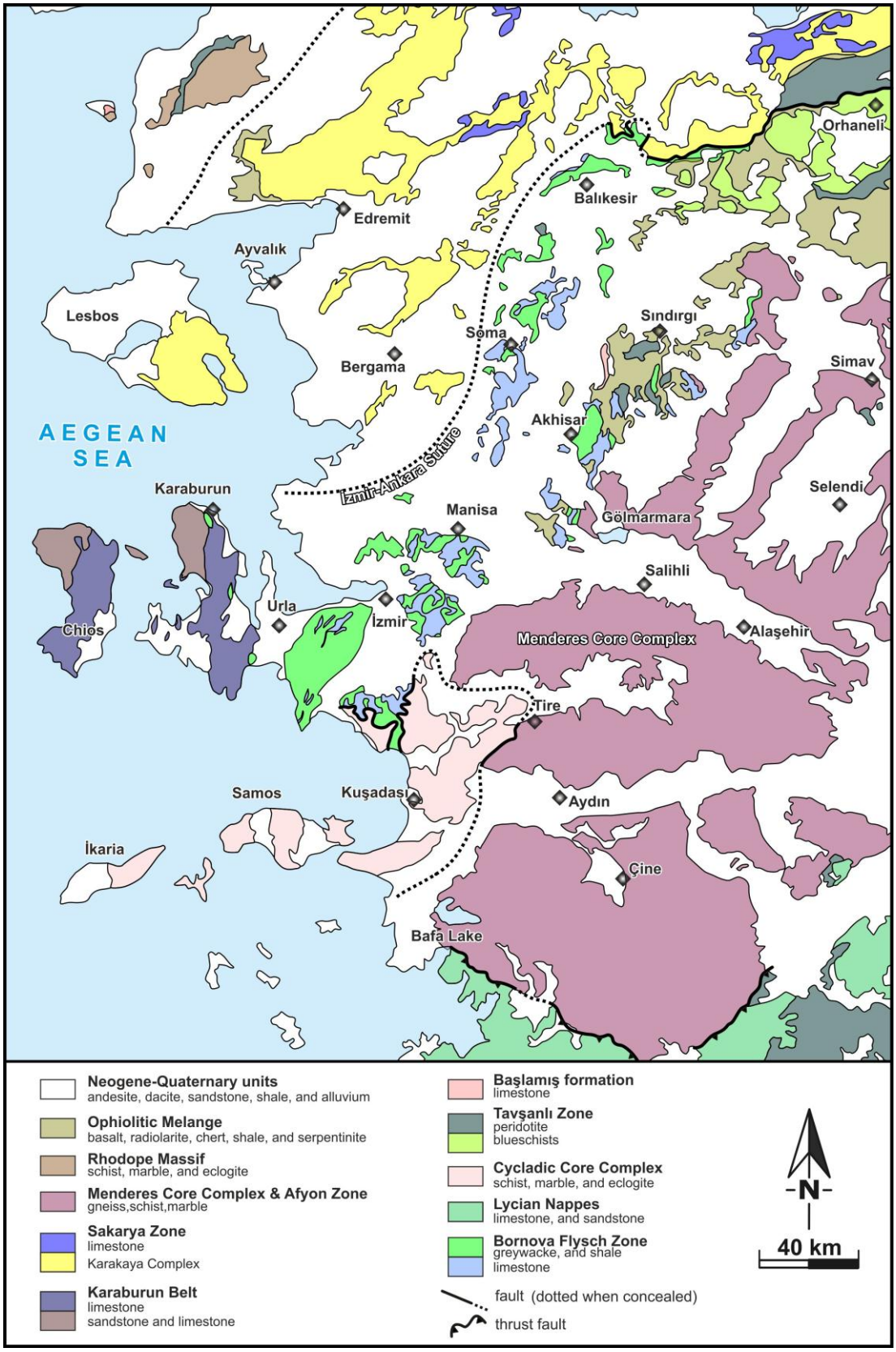


Figure 2.2 Geological map of the pre-Miocene basement rocks (modified from Okay et al., 2012).

opposing (Alakeçi and Şelale) detachment faults. The second stage is dominated by strike-slip faulting along the southern branches of North Anatolian Fault Zone during the Plio-Quaternary.

The Bornova Flysch Zone, also known as Bornova Mélange (Erdoğan, 1990), is defined as a tectonic belt on the northern margin of the Anatolide-Tauride Block (Okay and Altıner, 2007; Okay et al, 2011). It is a 60–90 km wide and approximately 230 km long, NE-trending tectonic zone lying between the Menderes Massif and the Karaburun Belt. It is well exposed in the Seferihisar high along the southern margin of the İzmir Bay (Fig. 2.2). The Bornova Flysch Zone is composed of an extremely deformed (locally metamorphosed) flysch-like sedimentary matrix of Maastrichtian–Paleocene age with blocks of Mesozoic limestones, serpentinites and submarine mafic volcanic rocks (Erdoğan, 1990; Sarı, 2012).

The Karaburun Belt comprises rock units extending from Paleozoic to late Cretaceous and records opening and closure of the Tethyan Ocean (Erdoğan, 1990; Kozur, 1997; Robertson and Pickett, 2000). It has a wide range of rock types including granites, turbiditic sequences with olistholits (i.e. wild flysch), having ages extending from Paleozoic to Cretaceous and belonging to different tectonic settings and depositional environments (see Erdoğan, 1990; Kozur, 1997, Çakmakoğlu and Bilgin, 2006 for detail).

A 50-km-wide coherent blueschist belt pointing out the northward-subducted margin of the Anatolide-Tauride Platform is called as the Tavşanlı Zone (Okay, 1984; Okay et al, 1998). It is a high pressure/low temperature zone (Okay, 1984). The unit mainly consists of two packages: (1) The metamorphic rocks of the Tavşanlı Zone are made up of schist, phyllite and massive platform metacarbonates intercalating with meta-basite, shale and cherts (Okay, 1986; Candan et al., 2005). (2) Unmetamorphic part of the unit is characterized by imbricated and highly deformed volcano-sedimentary rocks intercalated with spilites, agglomerates, cherts, shales, limestones and greywackes (Kaya, 1972; Okay, 1986; Bozkurt and Oberhänsli, 2001).

The Cycladic (Metamorphic) Core Complex (CCC) is an Eocene high-pressure metamorphic belt exposed mainly at the southern margin of Kocaçay Basin in western Turkey. It extends westwards and is also exposed in some Greek Islands within a crescent shape belt extending from Turkey to the southernmost part of mainland Greece (Figs. 2.1 and 2.2). It consists primarily of large marble bodies embedded in schists. In the Kocadağ High, it comprises mica- and calc-schists, marbles, meta-cherts, serpentines and meta-volcanic rocks (Fig. 2.1; Okay, 2001; Sözbilir et al., 2011).

The Menderes Metamorphic Core Complex (MCC), also known as Menderes Massif, is one of the largest metamorphic series in the Alpine-Himalayan chain and has suffered from metamorphic events related to late Proterozoic to early Paleozoic Pan-African events as well as to Mesozoic to Cenozoic Alpine orogenic events (e.g. Bozkurt and Park, 1997; Okay, 2001; Candan et al., 2001; Lips et al., 2001). It is delimited in the west by the İBTZ, which is the main topic of this paper (Figs. 2.1 and 2.2) and is exhumed along low-angle normal faults, which uplifted and exposed medium to high-grade metamorphic rocks and separated the metamorphic core from the un-metamorphosed to lower grade metamorphic cover series in its footwall. These low angle detachment faults are dissected by high angle normal faults (e.g. Koçyiğit et al., 1999; Sözbilir, 2001; Bozkurt and Sözbilir, 2004) that control mainly the northern and southern margins of major E–W trending basins in western Anatolia, such as the Gediz and Büyük Menderes grabens (Emre and sözbilir, 1997, Çiftçi and Bozkurt, 2010 and references therein).

At the south of the MCC and CCC, the Lycian Nappes tectonically overlies the metamorphic rocks (Fig. 2.2; Okay, 1989, 2001; Rimmelé et al., 2004; Bozkurt, 2007). The Lycian Nappes represents an allochthonous rift to passive margin succession translated towards the SE during late Cretaceous–late Miocene time interval. It includes blocks of recrystallized limestones, cherty limestones, bauxite-bearing limestones, dolomites, gabbros, submarine volcanics and radiolarites mixed in a matrix of turbiditic sandstone-shale alternations and sheared serpentinites (Sözbilir, 2002). The contact between the MCC and the Lycian Nappes is

characterized by a detachment fault, where red-green phyllite slices acted as a décollement zone (Bozkurt & Oberhänsli; 2001).

2.3 Cenozoic Stratigraphy

The Eocene Başlamış Formation described in Akhisar basin is the oldest non-metamorphic rock unit of the Cenozoic stratigraphic record in the region. It is exposed in a very small area (a couple of ten km^2) around the vicinity of Başlamış village (Fig. 2.2). The unit lies on the ophiolitic basement rocks with an angular unconformity and includes mainly of conglomerates dominated by ophiolitic clasts at the base (Akdeniz, 1980). This level is followed gradationally by sandstones marls and limestones to the top. Several fossiliferous levels have been described in the unit, particularly through the sandstone and limestone levels; nummulitic limestones are remarkable. The Başlamış Formation is unconformably overlain by conglomerates and volcanic rocks of the Miocene units (Akdeniz, 1980).

The Oligo-Miocene Lycian molasse basin is a NE-SW-oriented basin that developed along the contact between the MCC and the Lycian nappes on an imbricated basement (Fig. 2.1), comprising the allochthonous Mesozoic rocks of the Lycian nappes and Paleocene-Eocene supra-allochthonous sediments (Sözbilir, 2002). The Lycian Oligo-Miocene molasse basin units mainly consist of a sequence of late to early-post orogenic deposits that contain both continental and shallow-marine sediments (Sözbilir, 2002, 2005). The units are characterized by fining- and coarsening-upward sedimentary cycles with syn-depositional intrabasinal unconformities. Those units generally indicate shallow marine environments and consist of thick, coarse-grained alluvial fans and fan-delta deposits with some patch reefs (Sözbilir, 2005).

The Miocene stratigraphic record of the İBTZ and adjacent region (it's the main objective of this thesis; Fig. 2.3) has several units with different names in the literature. Generally, it is characterized by two main volcano-sedimentary packages

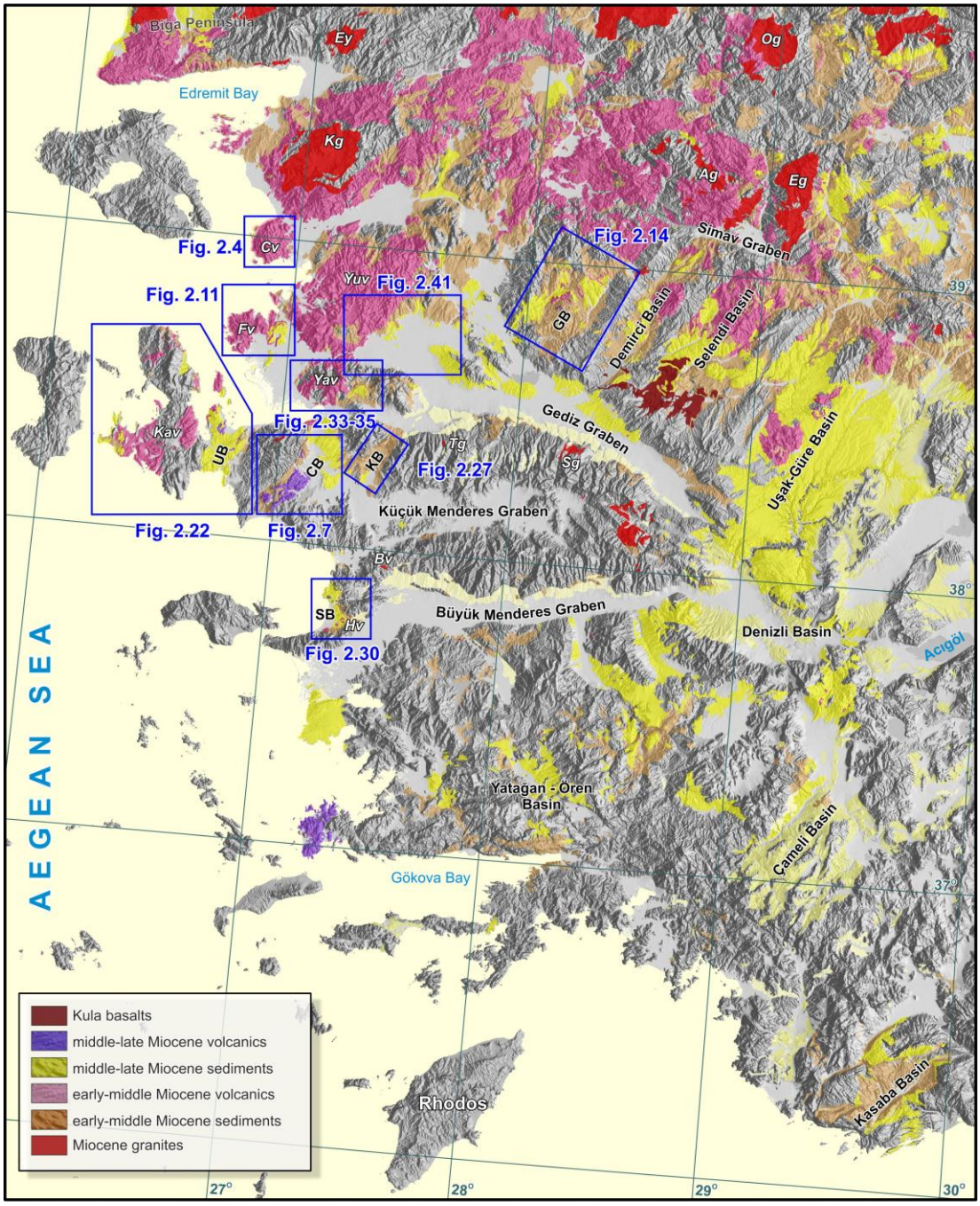


Figure 2.3 Simplified geological map of western Anatolia (MTA, 2002) draped onto a Digital Elevation Model image. It shows distribution of the Neogene basins. inset map locations will be mentioned below. Kg, Kozak granite; GB, Gördes basin; UB, Urla basin; CB, Cumaovası basin; KB, Kocaçay basin; SB, Söke basin; Ey, Eybek granite; Og, Orhaneli granite; Eg, Eğrigöz granite; Ag, Alaçamdağ granite; Sg, Salihli granite; Tg, Turgutlu granite; Kav, Karaburun volcanic suite, Yuv, Yuntdağ volcanic suite; Yav, Yamanlar volcanic suite; Fv, Foça volcanic suite; Cv, Çandarlı volcanic suite; Hv, Hisartepe volcanics; Bv, Balatçık volcanics; Kv, Kula volcanics.

separated by an angular unconformity and to simplify main story they will be termed as: (i) *lower sequence*, and (ii) *upper sequence*. Here, I focus on the main geometry and characteristics of these successions within following basins/areas, in alphabetic order: Çandarlı-Dikili area, Cumaovası basin, Didim area, Foça area, Gördes basin, E-W Graben basins, Karaburun area, Kocaçay basin, Söke basin, Spil-Yamanlar area, Urla basin, and Yuntdağ area (Fig. 2.3).

2.3.1 Çandarlı-Dikili Area

The area located in the northwestern part of the İBTZ contains several products of the western Anatolian Miocene volcanism (Figs. 2.3 & 2.4). The Miocene stratigraphy can be divided into two main groups (Kaya, 1981; Karacık and Yılmaz, 2000; Karacık et al., 2007): (i) the early–middle Miocene Dikili group, comprising of mainly pyroclastic rocks, andesitic-dacitic lavas, lava breccias, lahars and associated sedimentary rocks; and (ii) the middle(?)–late Miocene (Pliocene?) Çandarlı group, made up of lava and intercalated sedimentary rocks.

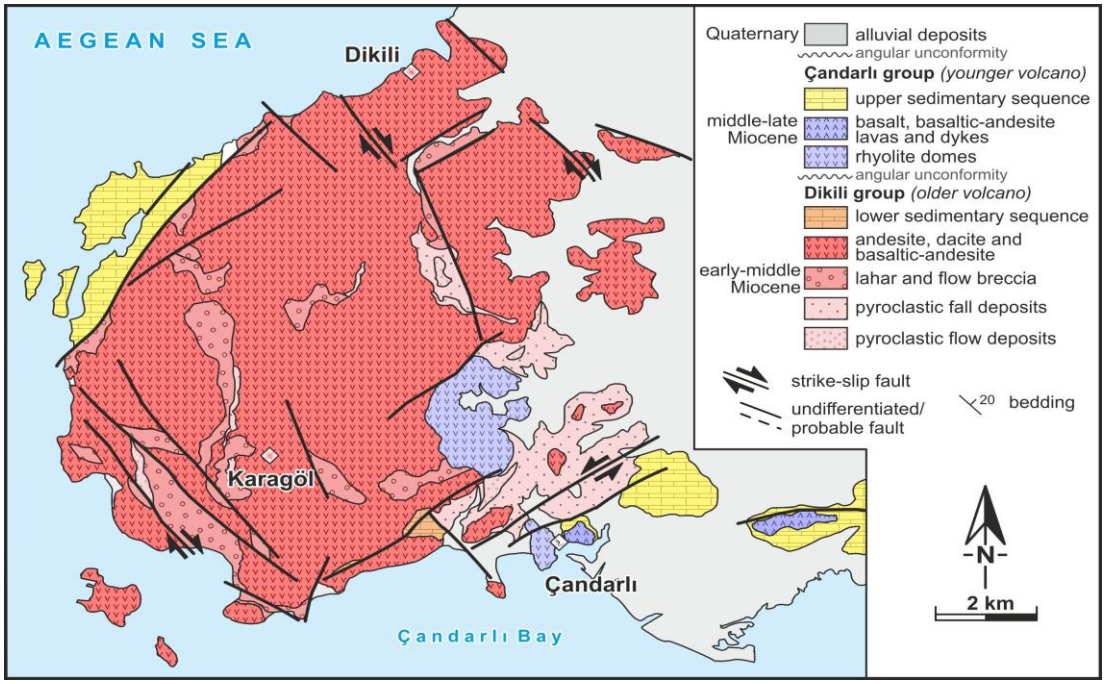


Figure 2.4 Geological map of Çandarlı-Dikili area (modified from Karacık et al., 2007). See Fig. 2.3 for location.

At the base of the Miocene sequence, *lower sequence* starts with grayish colored epiclastic conglomerates (Yeniköy conglomerate of Kaya, 1981). It is generally massive to thick-bedded and intercalated with pebbly sandstones and mudstones. From base to top, sedimentary rocks are composed mainly of volcanogenic mudstone, sandstone, reworked tuff, limestone lenses and rarely conglomerates. This sedimentary level can laterally be correlated with Aliağa limestone exposed in Yamanlar, Yuntdağ, Foça and Karaburun areas and with Çatalca Formation of Cumaovası basin. Dikili group, which is the first product of the Miocene volcanism in the area, is composed mainly of pyroclastic fall and flow deposits and passes laterally and vertically into lava flows. The other common lithology of the Dikili group is andesitic and dacitic lava flows and stocks (Fig. 2.6). Borsi et al. (1972) dated volcanism at 16.7 Ma (K–Ar whole rock age).

The *upper sequence* lies unconformably on the volcanic successions of Dikili Group (Fig. 2.5). It begins with grey-green shales, and followed by sandstone, mudstone and marl alternation. Upward, the sequence then passes into whitish lacustrine limestones. This level is possibly lateral equivalent of Urla limestone in Karaburun area and Urla basin (Kaya, 1981). The late Miocene volcanics in Çandarlı-Dikili area commences with mafic and felsic lava flows and associated with with sedimentary sequence (Karacık et al., 2007). The extrusion of the second stage lavas is controlled mainly by margin-boundary faults of the Çandarlı-Dikili topographic high (Fig. 2.4).

The whole explosive volcanism of the Çandarlı-Dikili area is represented mainly by rhyolitic domes and basaltic andesite to trachyandesite lavas; they are closely associated with the NW–SE- and NE–SW-trending fault systems that controlled the initiation of the Çandarlı depression (Fig. 2.5; Karacık et al., 2007).

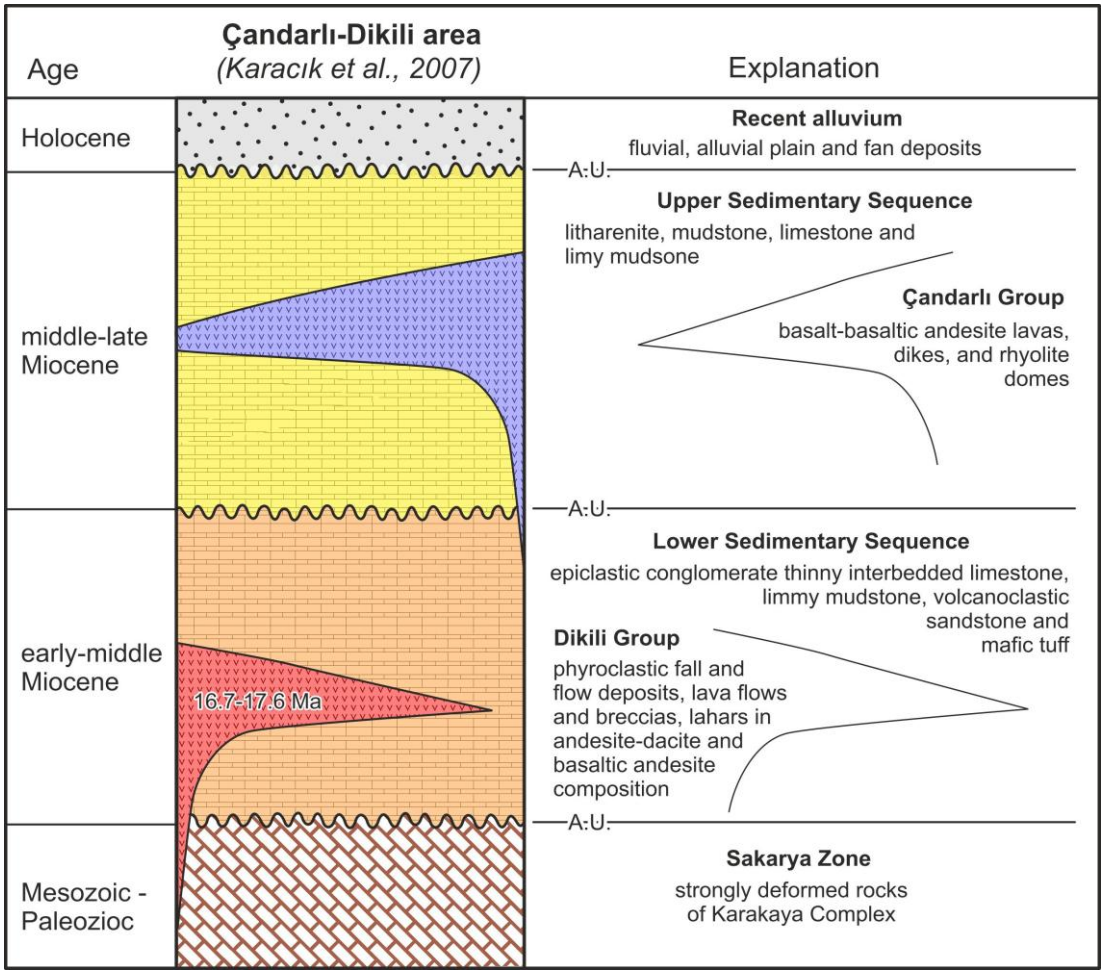


Figure 2.5 Generalized stratigraphic columnar section of Çandarlı-Dikili area (modified from Kaya, 1981; Karacık et al., 2007). AU, Angular unconformity.



Figure 2.6 Field photos of Miocene stratigraphic units exposed in Çandarlı-Dikili area.

2.3.2 Cumaovası Basin

The Cumaovası basin is located across a topographic depression between the Seferihisar and Nifdağı highs (Fig. 2.7) and comprises five major lithostratigraphic units, from base to top they comprise: Çatalca Formation and Yamanlar volcanics as the *lower sequence*; Ürkmez Formation, Yeniköy Formation and Cumaovası volcanics as the *upper sequence* (Fig. 2.8; Genç et al., 2001; Uzel and Sözbilir, 2008).

The *lower sequence* starts with the Çatalca Formation which is composed of thin-to-thick bedded conglomerates, sandstones, siltstones and shale alternations, including lignite lenses (Fig. 2.9b). Formation is interpreted as a lacustrine-fan delta facies and dated, based on the paleontological and palynological studies, at early–

middle Miocene (Akartuna, 1962; Kaya, 1979, 1981; Genç et al., 2001; Sözbilir et al., 2004). Early–middle Miocene lacustrine deposits outcrop at various localities in the western Anatolian basins; e.g., Dereköy Formation in the Kocaçay basin (Sözbilir et al., 2011), Soma Formation in the Soma basin (İnci 1991, 1998, 2002), Demirci Formation in the Demirci basin (İnci, 1998; Yılmaz et al., 2000), Hacıbekir group in the Selendi basin (Seyitoğlu, 1997; Ersoy & Helvacı, 2007), Hasköy and Başçayır Formations in the Büyük Menderes graben (Sözbilir & Emre 1990; Emre & Sözbilir, 1995; Çemen et al. 2006), and Alaşehir Formation in the Gediz Graben (Koçyiğit et al., 1999; Yılmaz et al., 2000; Sözbilir, 2001, 2002; Seyitoğlu et al., 2002; Bozkurt & Sözbilir, 2004) can be correlated with the Çatalca Formation. In the north of the study area, the fine-grained clastics of the Çatalca Formation are intercalated with the lavas and tuffs of the Karaburun volcanics. It is dated as 19.2 Ma (K-Ar age) by Borsi et al. (1972).

The *upper sequence* of the Cumaovası basin starts with the Ürkmez Formation (Fig. 2.8; Eşder and Şimşek, 1975; Genç et al., 2001), which is dominated by reddish-brown conglomerate and sandstone containing with brownish-gray lacustrine limestone lenses (Fig. 2.9a). Upward in the sequence, lithology displays a fining-upward profile where the conglomerates are grades into fine- grained conglomerates, sandstones and mudstones. According to Genç et al. (2001), the Ürkmez Formation is of latest middle (?)–late Miocene in age and is interpreted as alluvial fan and lateral fan deposits interfingering with low energy lacustrine facies. These clastic rocks are interbedded with lacustrine limestones of the Yeniköy Formation in the upper parts of the unit (Eşder & Şimşek, 1975; Genç et al., 2001). The Yeniköy Formation also contains sandstone, mudstone and claystone alternations with thin lignite seams (Fig. 2.9d).

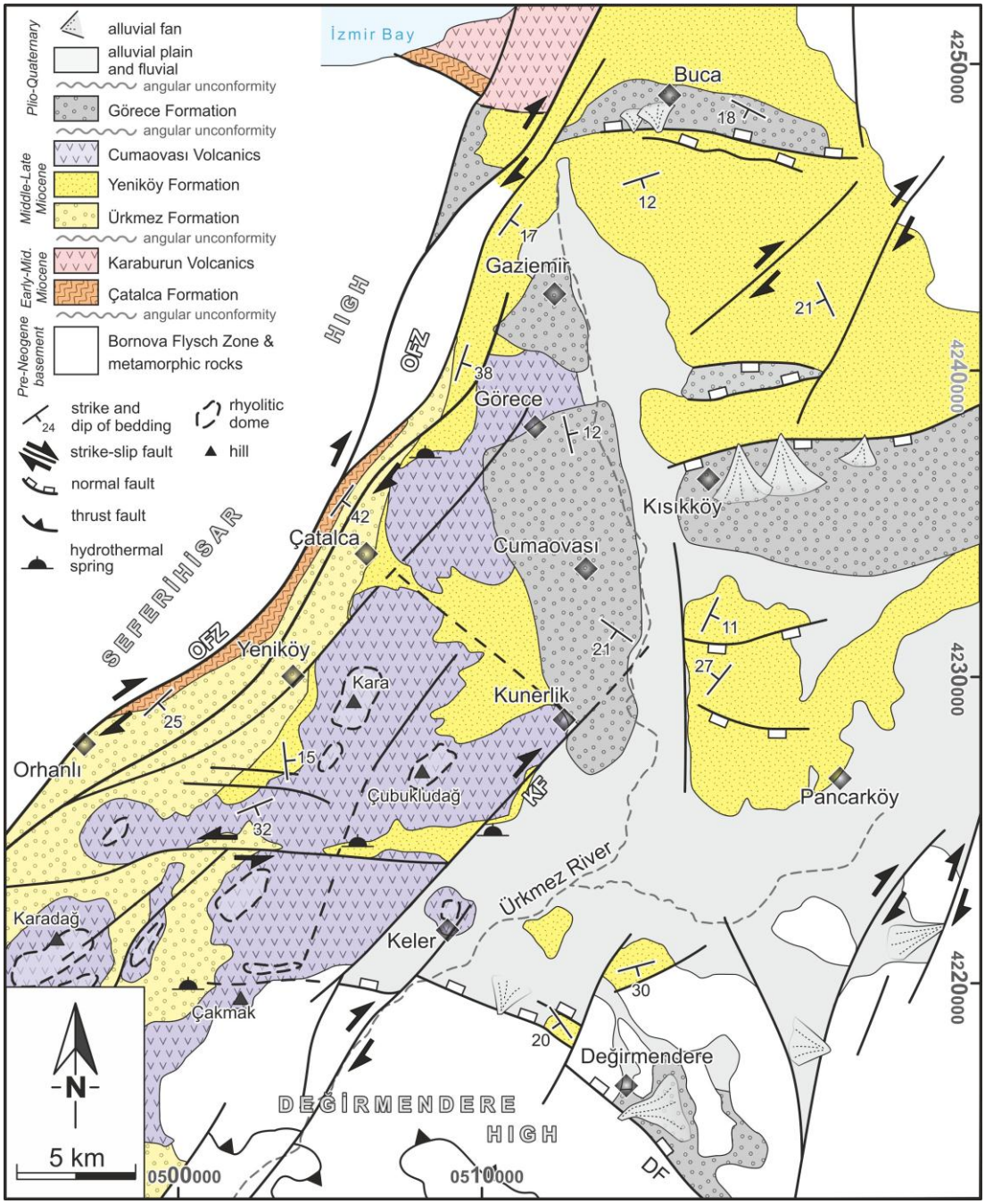


Figure 2.7 Detailed geological map of the Cumaovası basin. OFZ, Orhanlı fault zone; KF, Kunerlik fault. See Fig. 2.3 for location.

Upward, the sequence is dominated by thin- to medium-bedded lacustrine limestones and green laminated claystone alternations. These are interbedded with pyroclastic rocks of the Cumaovası volcanics (Eşder & Şimşek, 1975; Özgenç, 1978; Genç et al., 2001). The outcrops of the Cumaovası volcanics are aligned in the NNE–SSW direction and forms ‘central volcanics’ in the basin. They are exposed around

the Karadağ, Dededağ, Karakaya, Kızılcaağaç, Çakmaktepe, Dikmendağı and Çubukludağ hills (Fig 2.9c). The rhyolitic volcanic rocks of the Cumaovası volcanics yielded 11.5–9 Ma K/Ar whole rock and biotite ages (Borsi et al., 1972; Özgenç, 1978; Genç et al., 2001). They are mostly rhyolitic pyroclastic rocks and lava flows with local domes. Genç et al. (2001) suggested that the Cumaovası volcanics begin with air fall tuffs of about 15 m thick; they form early products of the volcanic activity. They are overlain by pyroclastic flow deposits composed of angular fragments of lavas within a pumiceous matrix. These are intercalated with rhyolitic lavas, locally included obsidian flows and perlites.

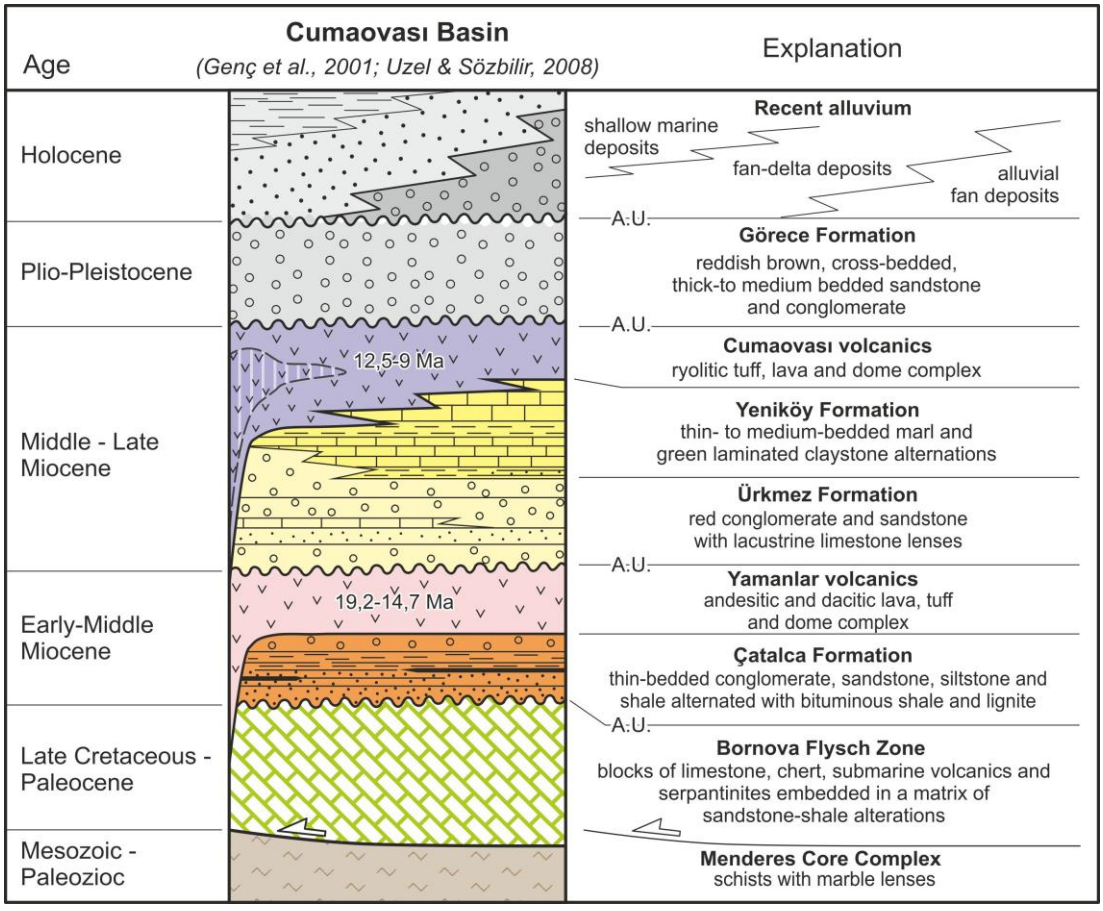


Figure 2.8 Generalized stratigraphic columnar section of Cumaovası basin (Uzel and Sözbilir, 2008). AU, Angular unconformity.

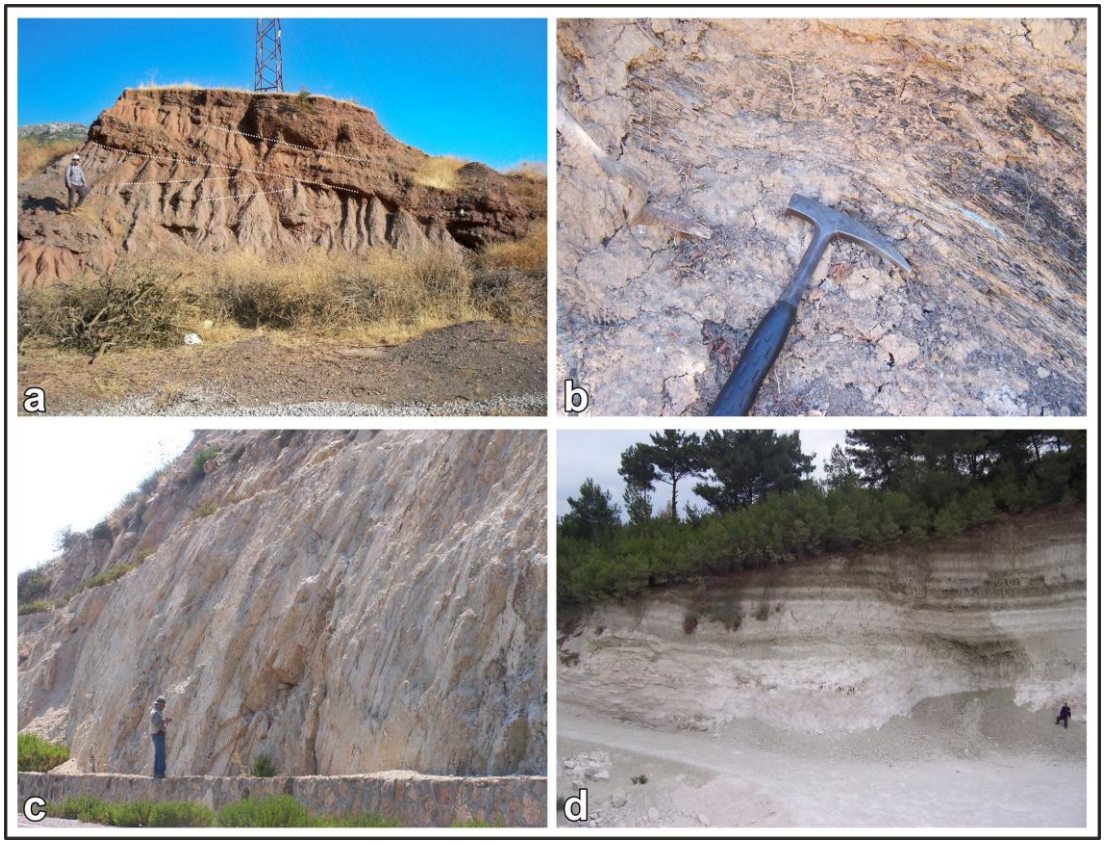


Figure 2.9 Field photos of stratigraphic units exposed in Cumaovası basin. a) Large-scale cross-bedding in reddish conglomerate and sandstone alternation of the Ürkmez Formation, b) close up view of coal-bearing Çatalca Formation, c) rhyolitic lavas of Cumaovası volcanics, d) whitish lacustrine limestone and greenish mudstone alternation of Yeniköy Formation.

The rhyolitic domes are aligned in NE–SW direction giving rise to NE−SW-directed hills in map view. The lava domes are located between Orhanlı fault zone and Kunerlik fault; these faults are interpreted to control transtensional opening (Uzel & Sözbilir, 2008). This structural origin of the domes is similar to that for the central volcanics as previously documented in the NE−SW-trending basins located north of the Gediz Graben (e.g., the Gördes, Demirci, Selendi and Uşak-Güre basins; see Bozkurt 2003 for detail). An ideal pull-apart basin model shows the presence of volcanic products within the centre of the basin (c.f. Crowell, 1974). There transtensional forces caused rupture in the centre of the basin and then localized the emplacement of volcanic rocks and shallow intrusions. Thus the strata would pass into volcanoclastics and lava flows, below which diapiric masses of hypabyssal rocks

occur. The readers are referred to Genç et al. (2001) for more detailed description of the Cumaovası basin fill units.

2.3.3 Didim Area

According to geological map of MTA (2002), only the late Miocene lacustrine limestones (*upper sequence*) are exposed in Didim area. Also in the literature there are not many recent studies about those sedimentary rocks. The limestones are termed as Milet Formation by Becker-Platen (1970) and Hakyemez and Örçen (1982). Atalay (1980) also proposed "Bozarmut member" name to the same unit. Metamorphic rocks of the MCC are unconformably overlain by the Milet Formation. Dominant lithology of the sedimentary succession is whitish, micritic, and thick-bedded limestone with clayey limestone intercalations. Gastropoda fossils are common in the sections of the unit (Fig. 2.10). This stratigraphic level is laterally equivalent to Kuşadası Formation exposed in Söke basin. Detailed discussion about this area will be given in the "Söke basin".



Figure 2.10 Field photos of stratigraphic units exposed in Didim area. a) Gently dipping thick bedded lacustrine limestones of the Milet Formation, b) a crystallized gastropoda fossil in the Formation, c) a close up view of whitish, thick and micritic limestone beds of the Milet Formation.

2.3.4 Foça Area

A thick volcanic succession made up of andesitic to rhyolitic lavas and sedimentary rocks in the *lower sequence* of Miocene strata crops out in Foça area, northwestern side of the İBTZ (Foça volcanic complex of Akay & Erdoğan, 2004; Figs. 2.11a, and 2.12). There, the Yuntdağ volcanics are composed mainly of andesitic and trachy-andesitic lava flows, domes and dykes, with coarse-grained to blocky pyroclastic flow deposits. Reddish-black-coloured porphyritic andesites, black aphanitic andesites, flow breccias and perlites are also common in this unit (Fig. 2.13d). The age of the Yuntdağ volcanics is of 16.8–21.0 Ma (whole rock and Rb–Sr ages of Borsi et al., 1972; Ercan et al., 1985). The unit grades laterally into, and is overlain by, the Foça volcanics (Akay and Erdoğan, 2004); they comprise rhyolitic pyroclastic rocks and small rhyolitic domes, dykes and lava flows. The

upper part of the unit includes mafic alkaline lavas and distinctively NE–SW-oriented dykes, called Foça alkaline volcanics (Fig. 2.13a-d). The overlying Aliağa limestone is composed primarily of yellowish-white-colored, medium- to thick-bedded, gastropod-rich lacustrine limestones with brownish-yellow clayey limestone and greenish-brown mudstone interbeds (Fig. 2.13f). The Aliağa limestone conformably and gradationally overlies both the Yuntdağ volcanics and the Foça volcanics (Kaya, 1981; Akay and Erdoğan, 2004) as in Karaburun area.

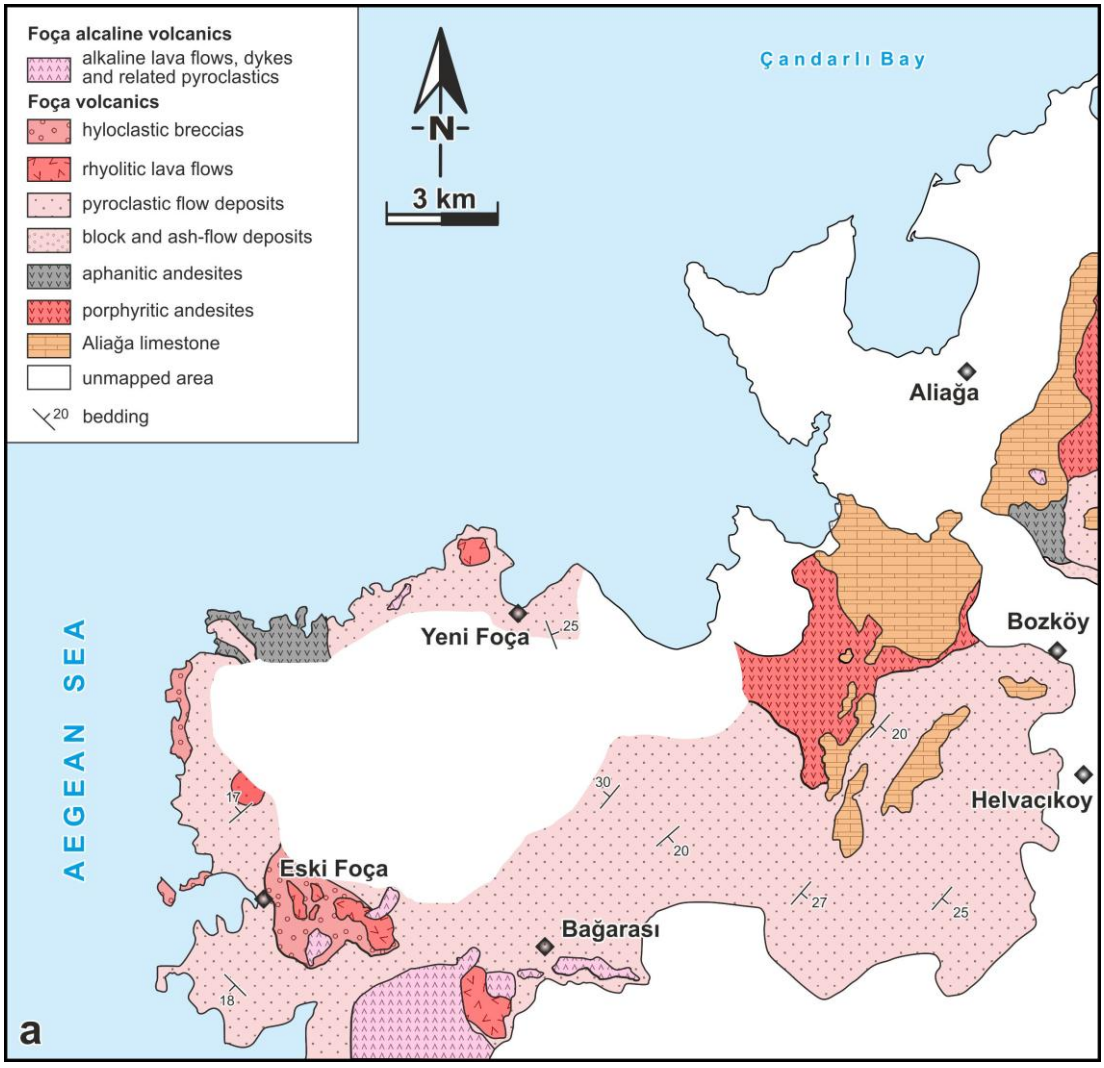


Figure 2.11 Geological maps of the Foça area showing distribution of the Miocene successions: a) modified from Akay and Erdoğan (2004). See Fig. 2.3 for location.

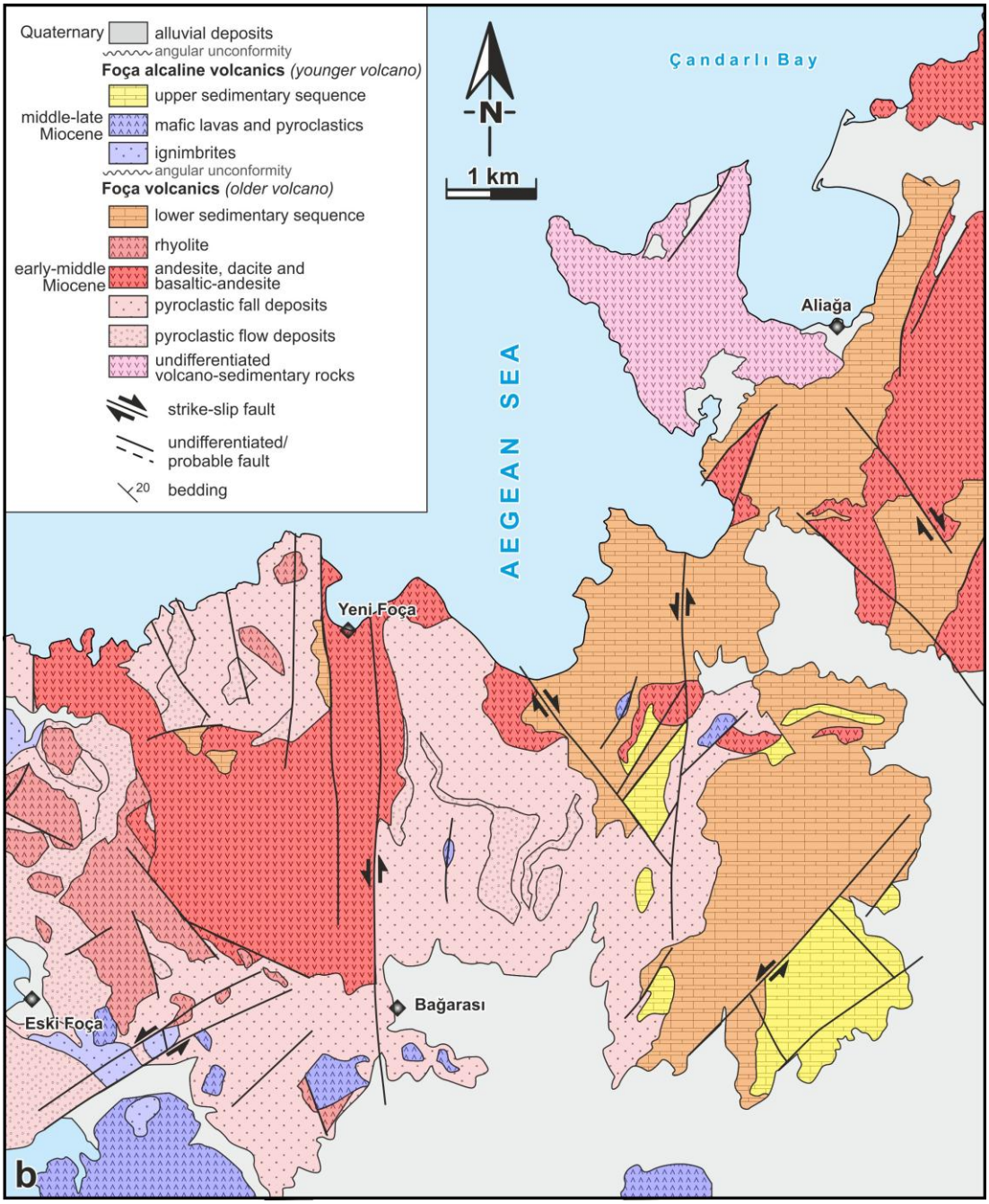


Figure 2.11 continued. b) modified and simplified from Altunkaynak & Yılmaz (2000) and Altunkaynak et al., 2010). See Fig. 2.3 for location.

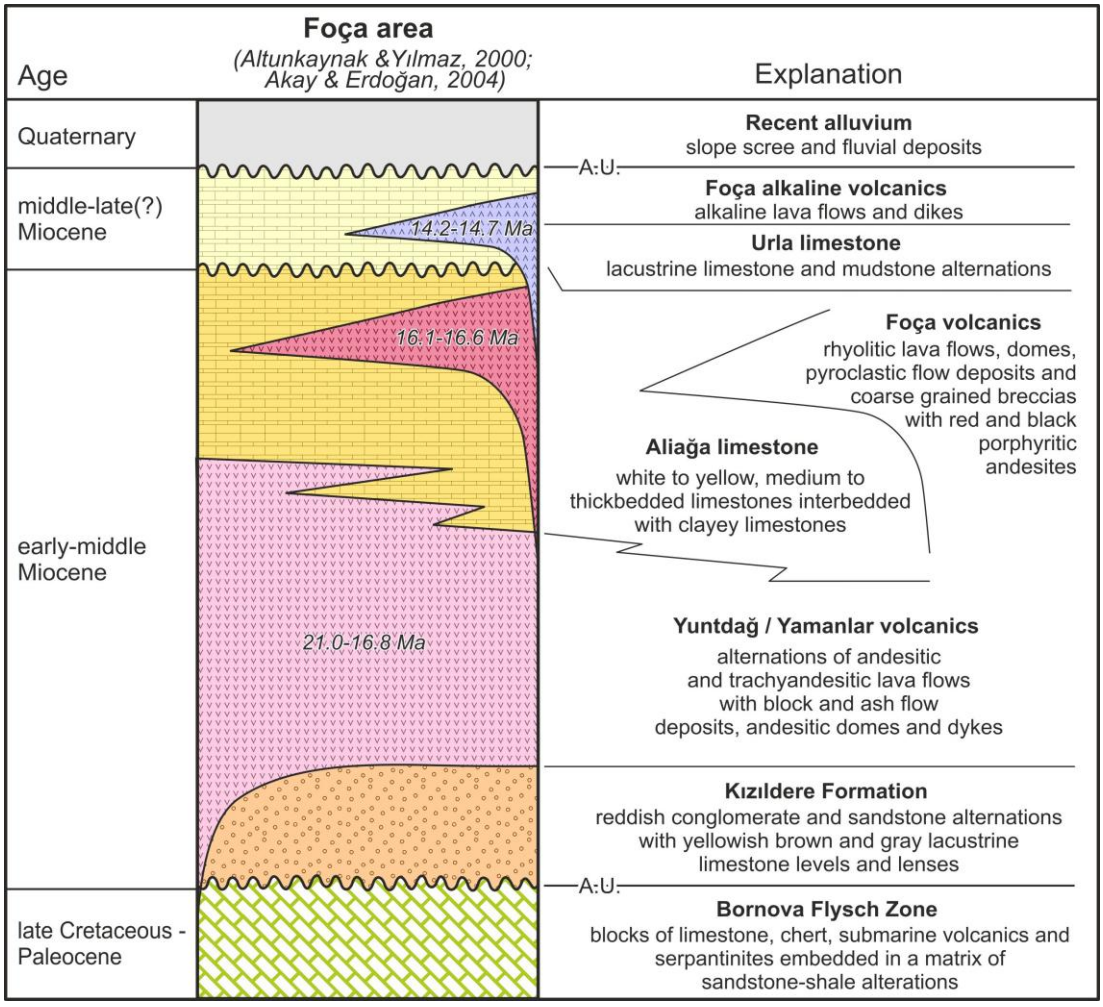


Figure 2.12 Generalized stratigraphic columnar section of Foça area (compiled from Altunkaynak and Yılmaz (2000), Akay and Erdoğan (2004), and field observations of this study). AU, Angular unconformity.

Although Akay and Erdoğan (2004) merge the whole volcanism in Foça area, Altunkaynak and Yılmaz (2000) separate the volcanic successions into two episodes; older volcano it's the Foça volcanics, and younger volcano it's the Foça alkaline volcanics (Figs. 2.11b, and Fig. 2.12). Age of the Foça volcanics ranges between 16.2–16.7 Ma, while the Foça alkaline volcanics have radiometrically dated at 14.2–14.7 Ma (biotite and plagioclase Ar–Ar ages of Altunkaynak et al., 2010).



Figure 2.13 Field photos of volcano-sedimentary units exposed in Foça area. a-d) from distance and close up views of intrusion of Foça alkaline volcanics (dark basaltic andesite dyke) into the Foça volcanics (whitish pyroclastics), e) a close up view of black and massive aphanitic andesites of Foça volcanics, f) a field photo showing the alternation of the Foça volcanics and Aliağa limestones.

2.3.5 Gördes Basin

The stratigraphy of the Gördes basin is characterized by the early Miocene volcanic and sedimentary units of *lower sequence* (Fig 2.14; Seyitoğlu and Scott, 1994; Purvis and Robertson, 2004; Ersoy et al., 2011). The basin fill lies upon the metamorphics of the MCC and Mesozoic sedimentary and ophiolitic rocks of the BFZ, and has been the subjected of many studies (Yağmurlu, 1984; Akgün & Akyol,

1987; Seyitoğlu and Scott, 1994; Purvis and Robertson, 2004; Ersoy et al., 2011). In this study we sampled *lower sequence* units and used previously established stratigraphy (Seyitoğlu & Scott, 1994; Ersoy et al., 2011).

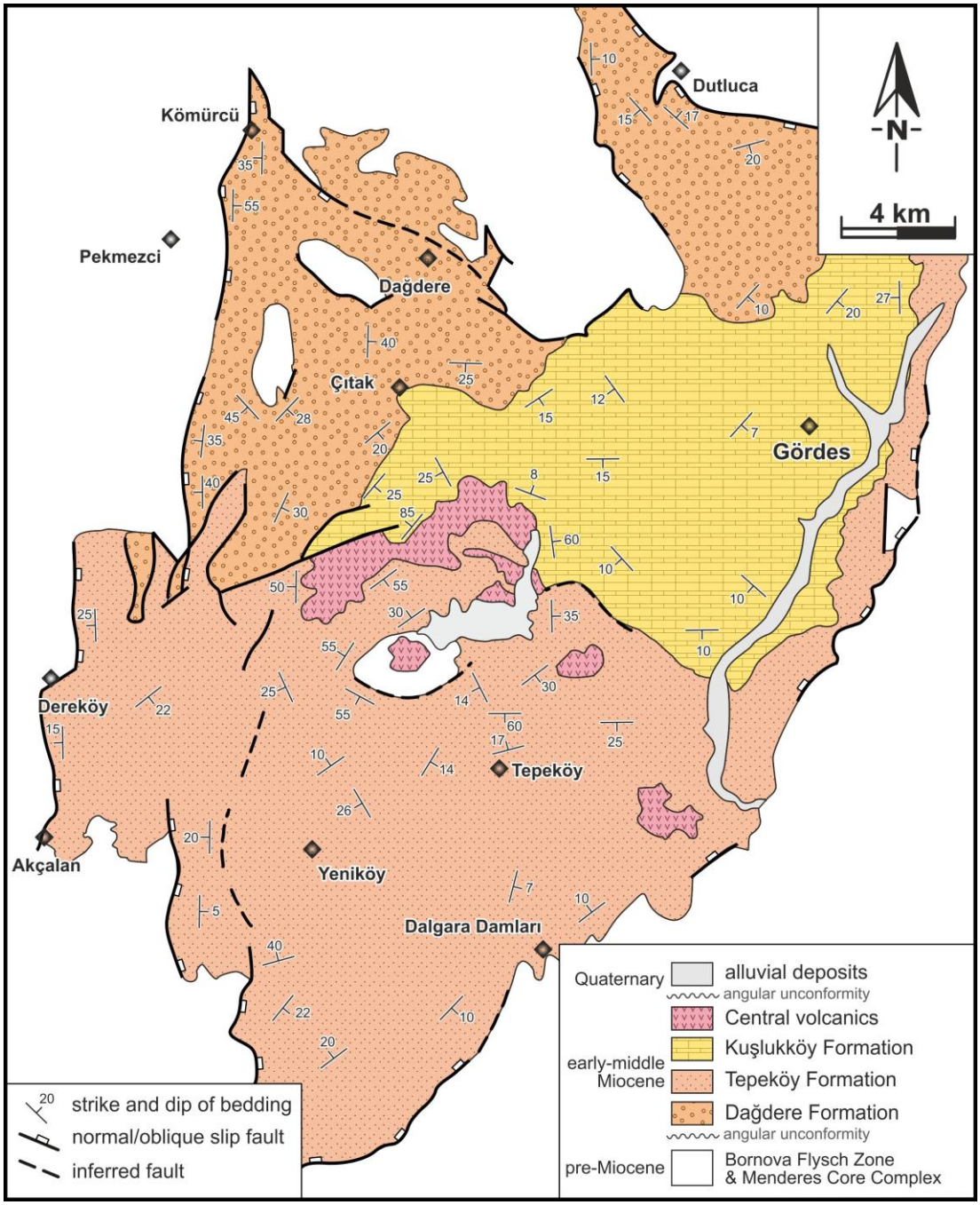


Figure 2.14 Geological map of the Gördes basin (Seyitoğlu & Scott, 1994). See Fig. 2.3 for location.

The sedimentary part of the early Miocene *lower sequence* is represented by the conglomerates and sandstones of the Dağdere, Kuşlukköy and Tepeköy Formations in the basin (Figs. 2.15 & 2.16). The Dağdere Formation is represented by a fining upward sequence, composed of cobble-pebble conglomerates, sandstones and mudstones with fossil (mainly gastropod) rich marls and lignite layers (Yağmurlu, 1984; Seyitoğlu and Scott, 1994). The clastic levels contain pebbles of tourmaline leucogranites, dated at 24.0-21.1 Ma (Seyitoğlu and Scott, 1992).

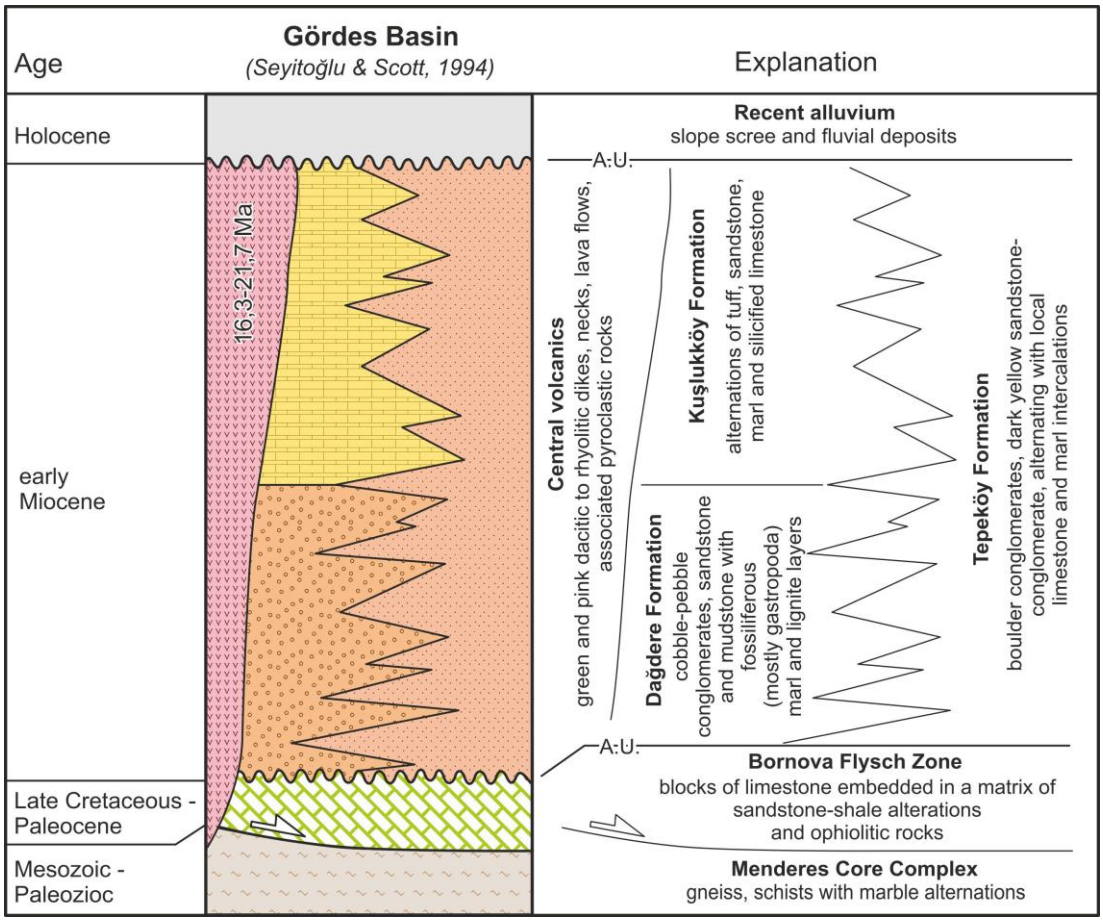


Figure 2.15 Generalized stratigraphic columnar section of Gördes basin (Seyitoğlu and Scott, 1994). AU, Angular unconformity.

The alternations of sandstone, marl, silicified limestone and acidic tuffs of the Kuşlukköy Formation comfortably overlie the Dağdere Formation. The Tepeköy Formation consists mainly of boulder conglomerates with sandstone layers at the base. And this level laterally and vertically grades into fine-grained sandstone and

dark yellow sandstone-conglomerate alternating with local limestone and marl intercalations. This unit shows lateral gradation relationship with the Dağdere and Kuşlukköy Formations (Seyitoğlu and Scott, 1994; Ersoy et al., 2011).



Figure 2.16 Field photos of volcano-sedimentary units exposed in Gördes basin. a-c) Close up view of sandstone, mudstone and limestone alternations of Kuşlukköy Formation, d) field relationship between central volcanics and sedimentary units, e) a close up view of volcanic dyke near Kayacık village.

The sedimentary basin fill of Gördes basin is cut by volcanic rocks (Fig. 2.15; Seyitoğlu and Scott, 1994; Purvis and Robertson, 2004; Ersoy et al., 2011). Seyitoğlu and Scott (1994) define this volcanism as "central volcanics", while Ersoy et al. (2011) considered them as two separate volcanic units, namely Güneşli and Kayacık volcanics. In the northern part of the basin, the volcanics included pinkish-whitish rhyolitic dykes and lava flows, associated pyroclastics interfingering with the sedimentary rocks (Kuşlukköy Formation).

In the center of the basin, the volcanics are characterized mainly by greenish dacitic-rhyolitic volcanic dykes and necks (cutting and deforming the sandstones) with lava flows and associated pyroclastic rocks interfingering with the fine-grained sediments of the Kuşlukköy Formation. According to previous studies the volcanic products of the Gördes basin yielded 21.7–16.3 Ma K–Ar and Ar–Ar mica ages (Seyitoğlu and Scott, 1994; Purvis et al., 2005).

2.3.6 E–W Grabens

Field studies in western Anatolia revealed that the E–W-trending Miocene basins are bounded by approximately E–W-oriented low- and high-angle normal faults (e.g. Koçyiğit et al., 1999; Bozkurt, 2000, 2001; Sözbilir, 2001, 2002; Bozkurt & Sözbilir, 2004, 2006; Emre & Sözbilir ,2007; Çiftçi & Bozkurt, 2007, 2008, 2009), and defined as graben basins. Low-angle normal faults (detachment faults) are kinematically linked with a crustal-scale metamorphic core complex, the MCC, and approximately E–W- and NE–SW-dissected basins and they form the most prominent features of western Anatolia (Fig. 17; e.g. Hetzel et al., 1995; Bozkurt & Oberhänsli, 2001; Gessner et al., 2001; Işık & Tekeli, 2001; Ring et al. 2003 and references therein). These basins are referred as E–W grabens and NE–SW cross-grabens, respectively (Şengör, 1987). From north to south, the most prominent E–W-oriented graben basins are Gediz, Küçük Menderes and Büyük Menderes grabens, respectively. According stratigraphic records of the graben basin fill, Miocene deposition is uninterrupted (Koçyiğit et al., 1999; Bozkurt, 2001; Sözbilir, 2002; Çiftçi & Bozkurt, 2009; Gürer et al., 2009), unlikely the basins at the westerns side

of the graben system (along the İBTZ) have *lower* and *upper sequences* separated with an unconformity.

In the context of thesis, brief stratigraphical information from the Salihli area of the Gediz graben, Tire area of the Küçük Menderes graben and syn-extensional granitic intrusions in the MCC will be given below (Fig. 17).

2.3.6.1 Salihli Area

The Gediz graben (also known as Alaşehir graben) forms a convex structural pattern with a length of 140 km and a width of 10–15 km (Fig. 2.17). The major syn-depositional normal faults in the hanging-wall of the Gediz detachment fault eventually controlled sedimentation during the Miocene (e.g. Emre, 1996; Koçyiğit et al., 1999; Seyitoğlu et al., 2000, 2002; Yılmaz et al., 2000; Sözbilir, 2001, 2002; Çiftçi and Bozkurt, 2007, 2009, 2010). The Gediz graben is filled with Miocene to Recent sediments with minor volcanics (only along the northern margin. The Miocene infill is described with a stratigraphic package, the Salihli group (Koçyiğit et al., 1999). The group is subdivided into many formations, namely Sağlıkdere, Kartaluçan, Acıdere, Göbekli and Kaletepe Formations, exposed along the southern margin of the graben, in the area between the Salihli and Turgutlu. The deposition of these Miocene units, the Salihli group, occurred in the hangingwall of the low-angle normal fault, the Gediz detachment fault (Figs. 2.18 and 2.19; Emre, 1996; Koçyiğit et al., 1999; Seyitoğlu et al., 2000, 2002; Yılmaz et al., 2000; Sözbilir, 2001, 2002; Çiftçi & Bozkurt, 2007, 2009, 2010).

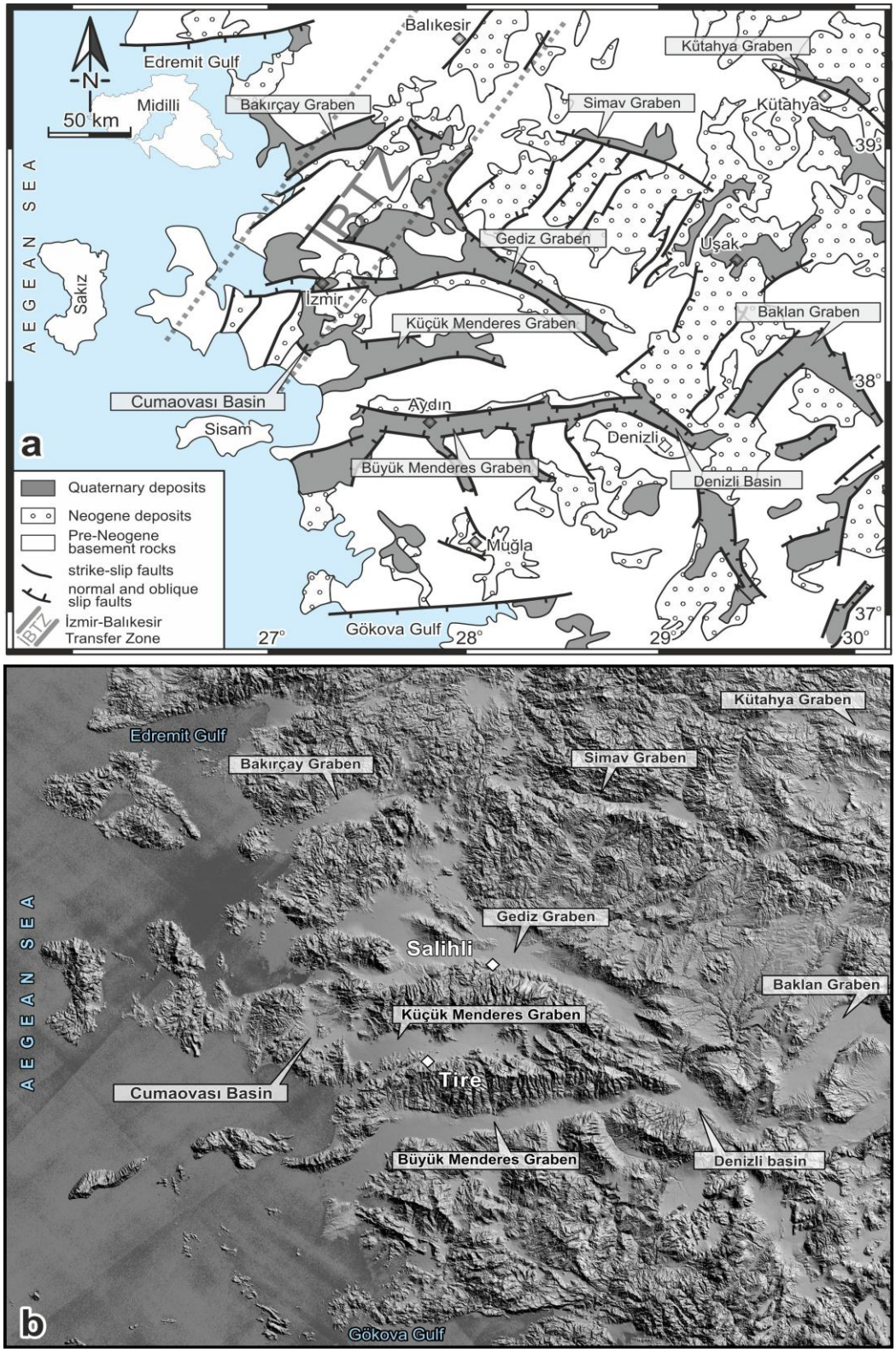


Figure 2.17 a) Simplified geological map showing the Neogene–Quaternary basins in western Anatolia with main tectonic lines (modified from MTA 2002, Geological Map of Turkey, Scale 1:500.000; Bozkurt 2000, 2001). b) Topographic map of western Anatolia. Topographic data were obtained by a Digital Elevation Model (DEM) image adapting from Global Mapper Program.

The Salihli group commences with gray conglomerate, sandstone and mudstone alternations (lacustrine-fan delta setting) and continues mostly with red conglomerate, sandstone and mudstones and limestone lenses (Sözbilir, 2002). Seyitoğlu & Scott (1996) name these sediments as Kurşunlu Formation; an age of early-middle Miocene is assigned to this unit. According to Sözbilir (2002), the age of unit may extent up to early Pliocene (Figs. 2.18, 2.19c-e).

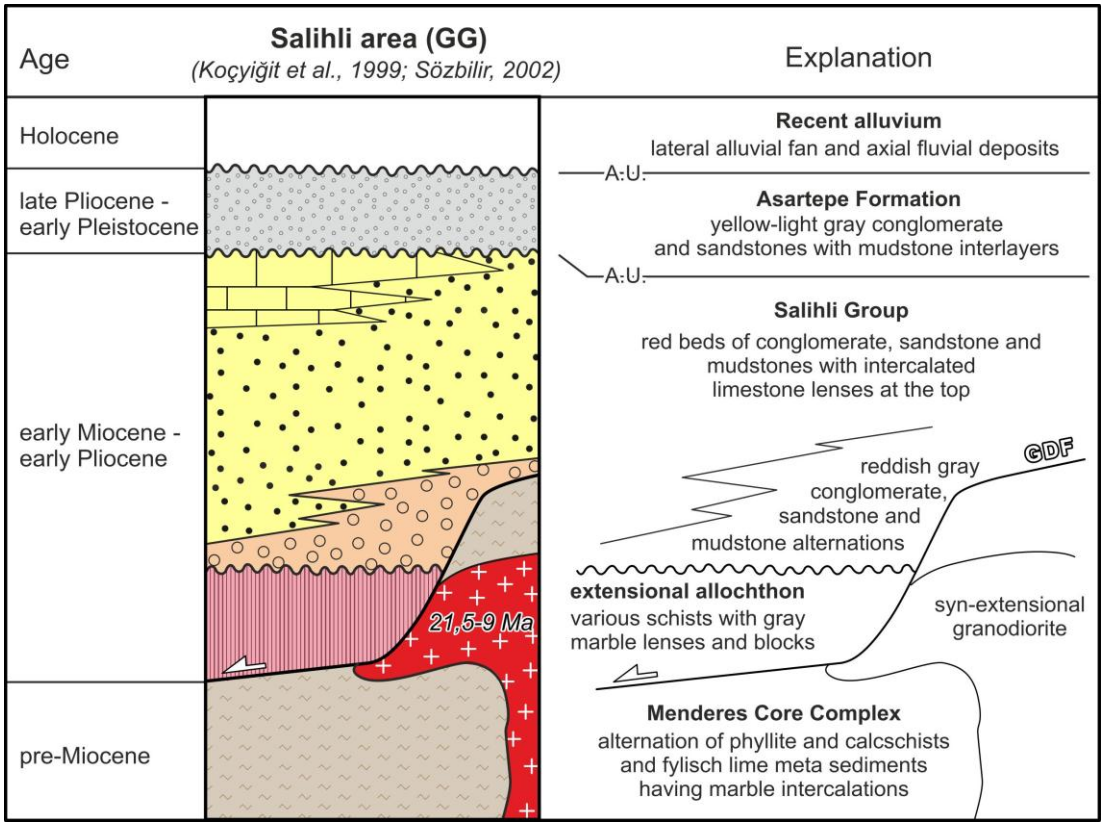


Figure 2.18 Generalized stratigraphic columnar section of Gediz Graben around Salihli area (compiled from Koçyiğit et al., 1999; Sözbilir, 2002). GDF, Gediz detachment fault; GG, Gediz graben; AU, Angular unconformity.



Figure 2.19 Field photos of Gediz detachment fault; from distance (a), and close-up view (b). c) Field relationship between the detachment fault and sedimentary units on top of it. d-e) Field photos of the Miocene basin fill of the Gediz Graben around Salihli area.

2.3.6.2 Tire Area

There are several studies concerning the stratigraphy and evolution of the Küçük Menderes Graben (Ercan et al., 1996; Emre et al., 2003; Rojay et al., 2005; Bozkurt & Rojay, 2005; Emre et al., 2005, 2006b; Emre & Sözbilir, 2005; 2007; Rojay et al., 2001, 2005; Seyitoğlu & Işık, 2009; Emre et al., 2012). The rock units around the Tire area is divided into three sedimentary packages separated by angular unconformities: the (latest early to earliest late) Miocene Ayaklıkırı Formation, the Plio−Pleistocene Aydoğdu Formation, and Recent alluvium (Fig. 2.20; Emre et al., 2012).

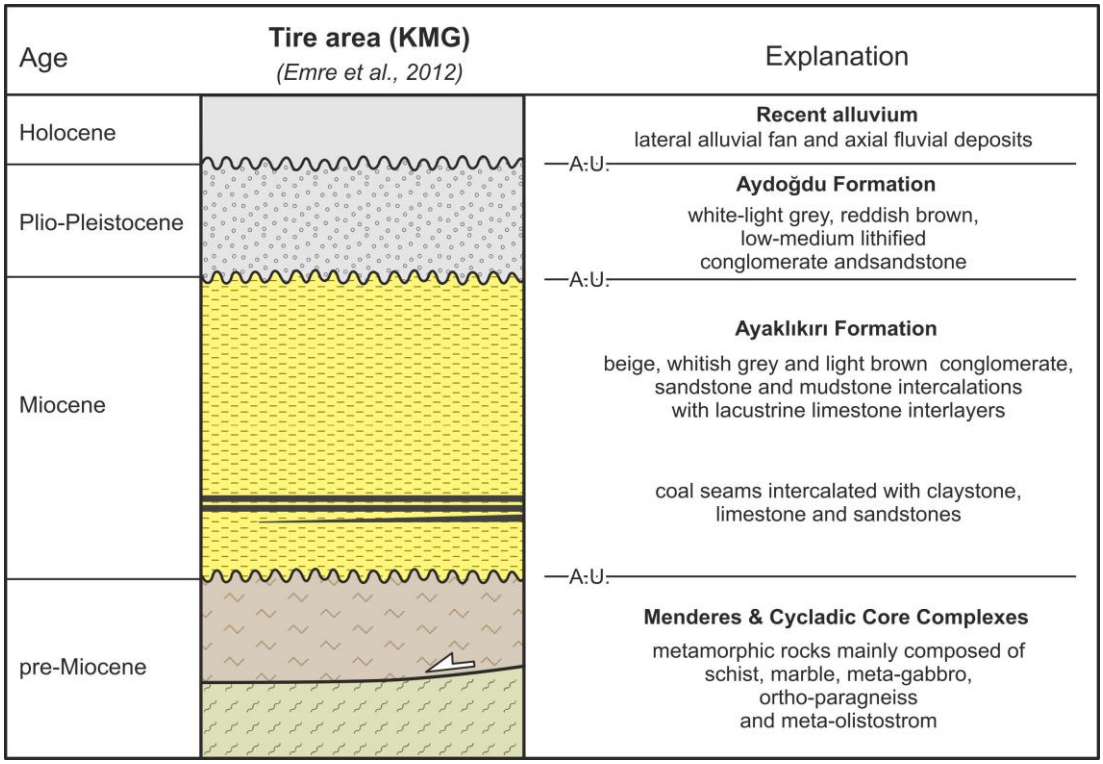


Figure 2.20 Generalized stratigraphic columnar section of the Küçük Menderes Graben around Tire area (compiled from Emre et al., 2012). KMG, Küçük Menderes Graben; AU, Angular unconformity.

The Miocene Ayaklıkırı Formation lying unconformably above the metamorphic rocks of the MCC and CCC is composed mainly of white-grey and reddish brown conglomerate, sandstone, mudstone and limestones with some coal levels forming in a lacustrine to fluvial setting (Emre et al., 2012). According to field observations of Rojay et al. (2005) and Emre et al. (2012), the conglomerates are generally beige,

grey and reddish brown colored, thick bedded and semi to well lithified, and sedimentologically moderately matured in the field. In the unit fining-upward conglomerate-sandstone sequences with marl and clayey limestones are common. Sandstones are mainly beige, grey, greenish grey and yellowish brown colored, medium bedded and well lithified, and rarely display cross-stratification along the sections. Limestones are described as brownish and white to cream colored, thin to medium bedded, mostly algal and well lithified and generally intercalated with silty-sandy-clayey limestones or mudstones (Fig. 2.21). Coal levels are generally intercalated with mudstones, limestones and sandstones in the succession. Palynological data of Emre et al. (2012) from the coal beds in the Ayaklıkırı Formation indicate that the deposition of this level was between the latest early Miocene–earliest late Miocene.

Basically, the sedimentary infill of the graben has two different sequences around Salihli area; (i) Miocene units controlled by the detachment fault (Salihli Group) and (ii) Plio-Quaternary units formed in front of the high-angle normal faults (Asartepe Formation and recent alluvium; Fig. 2.18, 2.19). The Karataş group is characterized by Plio-Quaternary faulted and terraced alluvial fan deposits (Asartepe Formation), the alkaline volcanic rocks (the Kula basalt), and undeformed continental clastics (Recent alluvium).

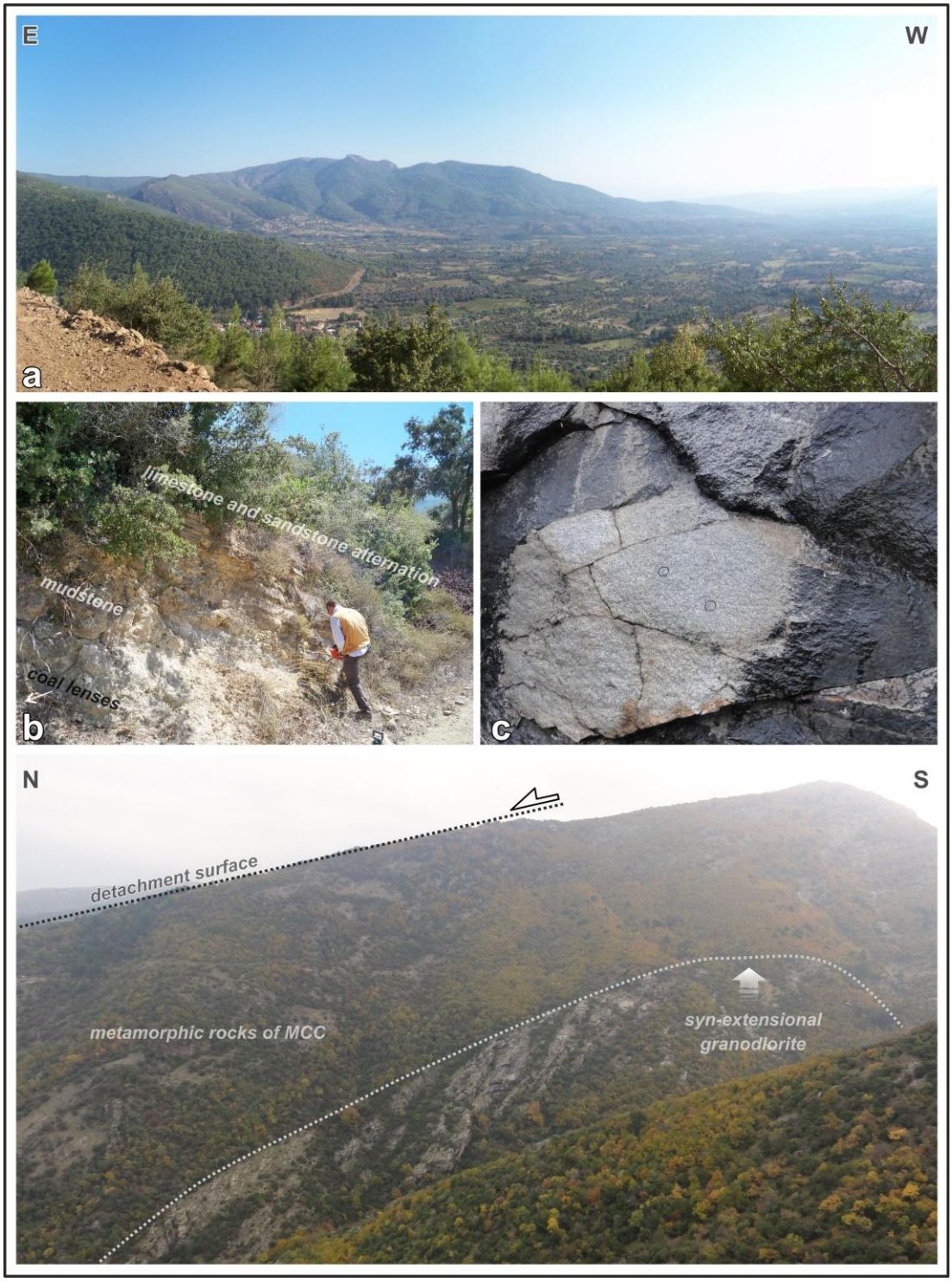


Figure 2.21 a) From distance view of the Küçük Menderes Graben near Tire area. b) A field photo of mudstone, sandstone and limestone alternation from the Ayaklıkırı Formation just top of the coal seam. c) Close up view of syn-extensional granitoids in Salihli area. d) Field relationship between the metamorphics rocks and granitic intrusion along the footwall of the Gediz Detachment Fault.

2.3.6.3 Syn-extensional Granitoids

As is known from the literature, major movement along the Gediz and Büyük Menderes detachment faults occurred during the Miocene, and it has resulted in the denudation of metamorphic core complexes (e.g. Hetzel et al., 1995; Emre and Sözbilir, 1997; Koçyiğit et al., 1999; Lips et al., 2001; Sözbilir, 2001, 2002; Seyitoğlu et al., 2002; Işık et al., 2003, 2004; Bozkurt and Sözbilir, 2004). The footwall metamorphic rocks were progressively mylonitised, exhumed, and simultaneously intruded by syn-extensional (or deformational) granitoids, the Turgutlu and Salihli granodiorites (Figs. 2.18, 2.21c-d). Here, the stratigraphic position and the timing of their emplacement have critical importance in the understanding of the core complex development.

The Salihli granodiorite yielded a wide range of ages, all obtained from the same granitoids: $^{39}Ar/^{40}Ar$ amphibole isochron and biotite plateau cooling ages of 19.5±1.4 and 12.2±0.4 Ma (Hetzel et al., 1995), U-Pb allanite ages of 15.0 ± 0.3 Ma (Glodny & Hetzel, 2007), and Th–Pb ion microprobe monazite ages ranging from 21.7±4.5 Ma to 9.6±1.6 Ma (Catlos et al., 2010). The timing of the syn-extensional magmatism in the footwall of the Gediz detachment fault coincides with a period of widespread volcanism (21.5 to 9 Ma) in the NE-trending transtensional basins located within the İBTZ.

2.3.7 Karaburun Area

The Miocene stratigraphic record cropped out in Karaburun area is characterized by two main volcano-sedimentary successions separated by an angular unconformity: (i) lo*wer sequence*, and (ii) *upper sequence*. Lower sequence includes widespread volcanic rocks composed by Karaburun, Kocadağ, Armağandağ, Yaylaköy volcanics and Uzunkuyu intrusion, and associated sedimentary succession (Bozköy Formation and Aliağa limestone). The upper sequence is a younger volcano-sedimentary succession and comprises Karaburun Formation, Urla limestone, İskele trachyte and Ovacık basalt (Figs. 2.3, and 2.22).

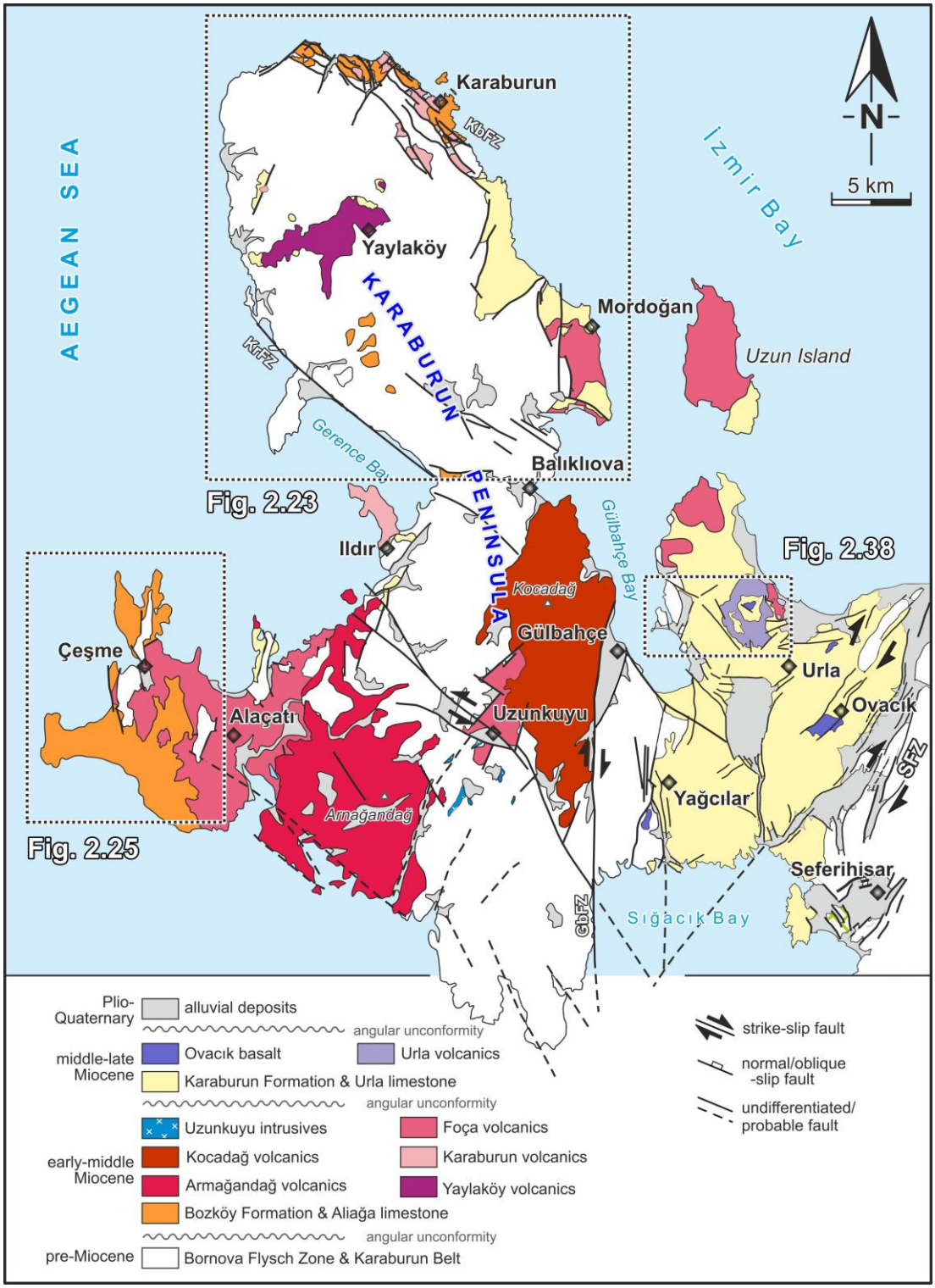


Figure 2.22 Geological map of the Karaburun area and Urla basin (compiled from Tatar-Erkül et al., 2008; Helvacı et al., 2009; Sözbilir et al., 2009; and this study). KbFZ, Karaburun fault zone; KrFZ, Karareis fault zone; GbFZ, Güzelbahçe fault zone; SFZ, Seferihisar fault zone.

The Miocene volcano-sedimentary deposit of the Karaburun area commences with *lower sequence*, the Bozköy Formation (Figs. 2.22, 2.23 and 2.24; Helvacı et al., 2009). It crops out mainly in the northwestern part of the area in the vicinity of Salman village, where the formation consists of reddish- to grayish-brown conglomerate, gray sandstone and greenish-gray mudstone alternations; it rests with an erosional surface on the rocks of the Karaburun Belt. Around the north of Sarpıncık village, the Bozköy Formation laterally and vertically passes into an alternation of white to brown lacustrine limestone and claystone (Aliağa limestone of Kaya, 1981).

During the deposition of the *lower sequence* sedimentation during the early Miocene, several volcanic units are emplaced (Figs. 2.22–25). The first products of volcanic activity in the Karaburun area, known as Yaylaköy volcanics, are composed by lava flows and associated pyroclastic rocks with a basaltic–andesite composition; they are dated as 21.3–17.0 Ma (whole rock ages of Borsi et al., 1972; Helvacı et al., 2009). Higher in the section, Karaburun volcanics of (18.5–16.0 Ma, whole rock K–Ar and Ar–Ar ages) and Foça volcanics (16.7–12.7 Ma, biotite and plagioclase Ar–Ar ages) are emplaced during the deposition of the Aliağa limestone (Kaya, 1981; Helvacı et al., 2009). The main lithologies of the Karaburun volcanics are reddish brown altered pyroclastic rocks and lava flows. The lavas interfinger with sediments of the Aliağa limestone.

The Armağandağ volcanics are composed mainly of pyroclastic rocks and massive lava flows with related dykes and domes. The pyroclastic rocks are characterized by white pumice, ash-fall deposits with regular bedding planes, lithic-rich ignimbrites with reverse/normal grading of lithic clasts and block and ash-flow-deposits. The lavas are usually composed of pinkish grey andesitic lava flows with a glassy matrix. These pyroclastic rocks and lavas interfinger with the limestones and mudstones of the Aliağa limestone; they have local peperitic contacts (Helvacı et al., 2009). The unit dated 18.2, 17.3 Ma (groundmass and biotite K–Ar ages) by Borsi et al. (1972), and 17.0 Ma (groundmass Ar–Ar age) by Helvacı et al. (2009).

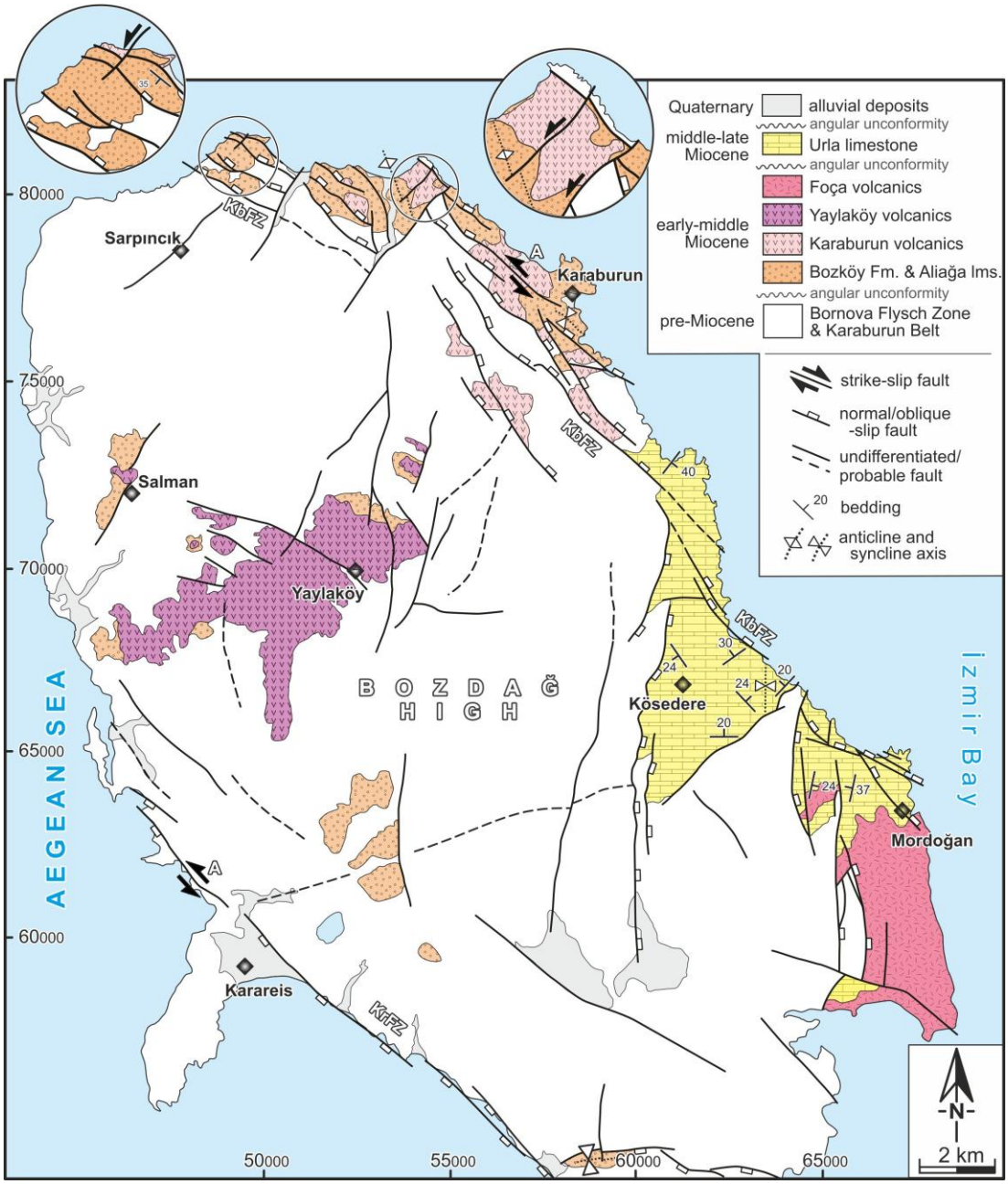


Figure 2.23 Detailed geological map of the Karaburun area (compiled from Tatar-Erkül et al., 2008; Helvacı et al., 2009, and this study). "A" refers to pre-Miocene strike-slip faulting along the Karaburun fault zone (KbFZ) and Karareis fault zone (KrFZ). See Fig. 2.22 for location.

The Kocadağ volcanics crop out in the southern part of the Karaburun area. It has almost similar lithologic description and stratigraphic position to the Armağandağ volcanics, but geochemically and petrographically has distinct features (Helvacı et al., 2009). Additionally, the pyroclastic products are dominated generally by block and ash flow deposits. The Kocadağ volcanics dated 16.6 Ma (whole rock K–Ar age)

by Borsi et al. (1972) and 17.5 Ma (whole rock Ar–Ar age) by Helvacı et al. (2009). The volcano-sedimentary units of the lower sequence are cut by mafic dykes of the Uzunkuyu intrusive in the central part of the Karaburun area. It is dated 15.4 (whole rock K–Ar age) by Türkecan et al. (1998) and 16.7 Ma (whole rock Ar–Ar age) by Helvacı et al. (2009).

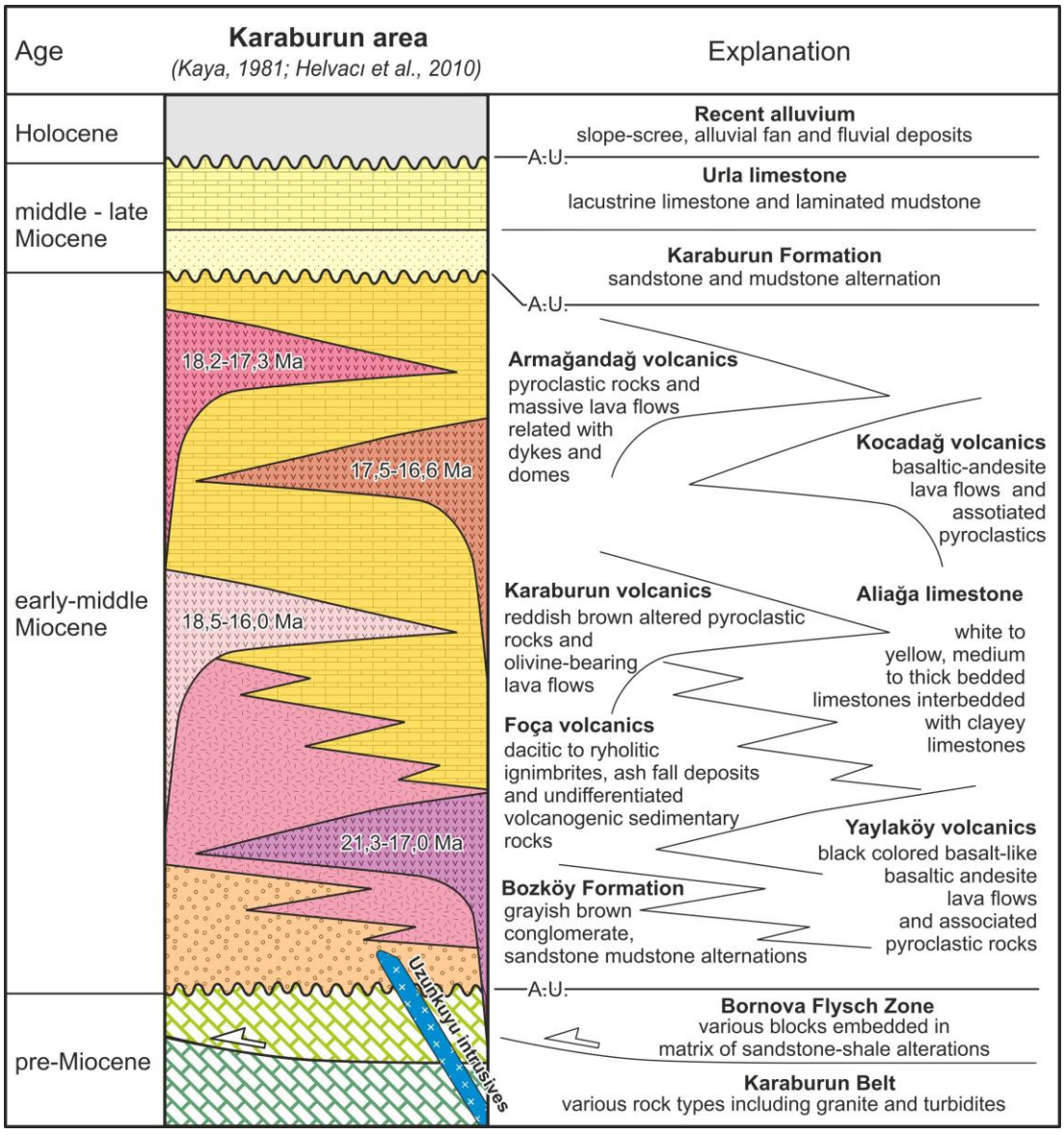


Figure 2.24 Generalized stratigraphic columnar section of northern Karaburun area (compiled from Kaya, 1981; Helvacı et al., 2009; and this study). AU, Angular unconformity.

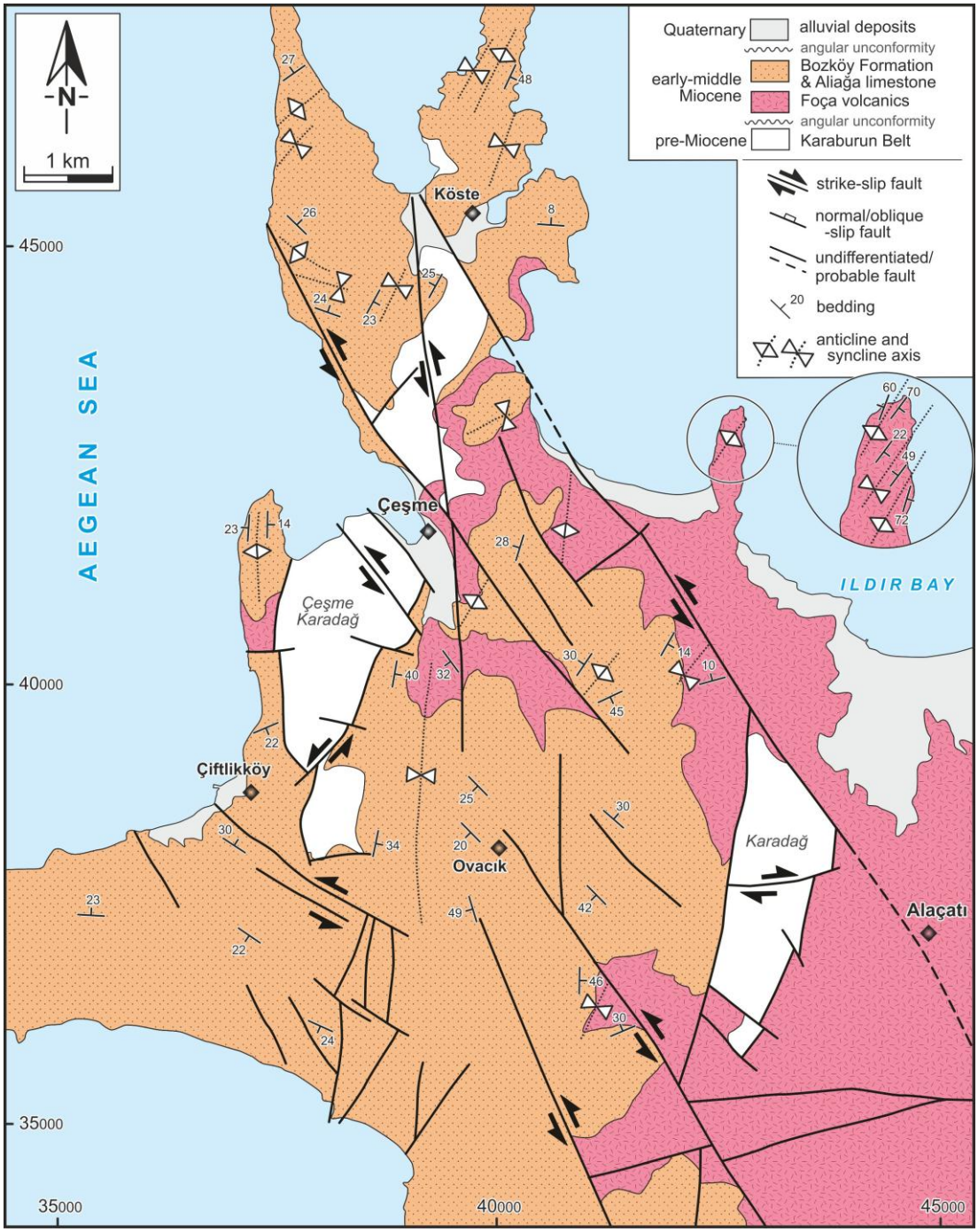


Figure 2.25 Detailed geological map of Karaburun area around Çeşme village (compiled from Helvacı et al., 2009, and this study). See Fig. 2.22 for location.

The *upper sequence* of the Miocene stratigraphic record starts with the Karaburun Formation and crops out at the northern part of the Karaburun area (Figs. 2.23 and 2.24). The unit consists mainly of brownish gray sandstone and grayish green

massive mudstone alternation with oolitic limestone interlayers and volcanogenic conglomerates. In some localities shale sublevels are also observed. The Urla limestone in the Karaburun area characterizes the youngest level of the upper sequence sedimentary unit. It consists mainly of yellowish white, thick-bedded limestone and brownish-gray to white mudstone, greenish-gray claystone alternations and gray sandstone interlayers. Fresh water algae and gastropoda fossils are common.



Figure 2.26 a) Field relationship between the platform carbonates of the Karaburun Belt (KB) and the Miocene sediments of the Urla limestone. b) Field view of the Bozköy Formation, composed of reddish brown sandstone, conglomerate and greenish gray mudstone alternations. c) A field photo from the dark gray lavas of the Yaylaköy volcanics. d) Intrusive relationship between the platform carbonates of the Karaburun Belt (KB) and a mafic dyke of the Uzunkuyu intrusion.

2.3.8 Kocaçay Basin

This NE-trending asymmetric basin is located between Nifdağı high in the west and Mahmutdağı high in the east and is more than 20 km in length (Fig. 2.3 and 2.27). The Miocene stratigraphic record is represented by two unconformity-bounded sequences: the Kemalpaşa group (the *lower sequence*) and the Kızılca Formation (the *upper sequence*). The Kemalpaşa group comprises two formations, namely Dereköy and Vişneli (Fig. 2.28; Sözbilir et al., 2011).

The Dereköy Formation is a more than 1300-m-thick coarsening upward and fining upward clastic sequence intercalated with lenses of limestone and minable coal beds. The unit at lower parts also includes blocks of recrystallized limestone-dolomite in various sizes. This blocky unit is named as 'Kesmedağı member' by Sözbilir et al. (2011). The sedimentary facies of the unit is made up of a sequence of alluvial and fluvial clastics that grade into lacustrine sediments; the latter thickens toward the eastern margin of the basin. The unit consists mainly of coarse-grained clastic facies near the Mahmutdağ and adjacent to the Mahmutdağı fault zone (Fig. 2.27). Clasts are mostly derived from the marbles and schists of the Menderes Core Complex; the limestones, sandstones and ophiolitic rocks of the Bornova Flysch Zone. Fining-upward conglomerates include erosive bases and co-occur with cross-bedded sandstones. Some erosive bed surfaces are observed within the underlying dark-brown to red sandstones (Fig. 2.29). Conglomerates at these levels also include clasts derived from the algal limestone lenses. Lacustrine micritic, algal limestone interlayers and organic-rich limestone lenses are observed in the Dereköy Formation. There are also syn-sedimentary unconformities within the sequence. In general, grain size decreases westwards from these localities. This indicates westwards transport of sediment from a topographic high (Mahmutdağ) east of the Mahmutdağı fault zone, and suggest that this fault zone forms the eastern margin of the basin where Dereköy Formation was deposited (Fig. 2.27; Sözbilir et al., 2011).

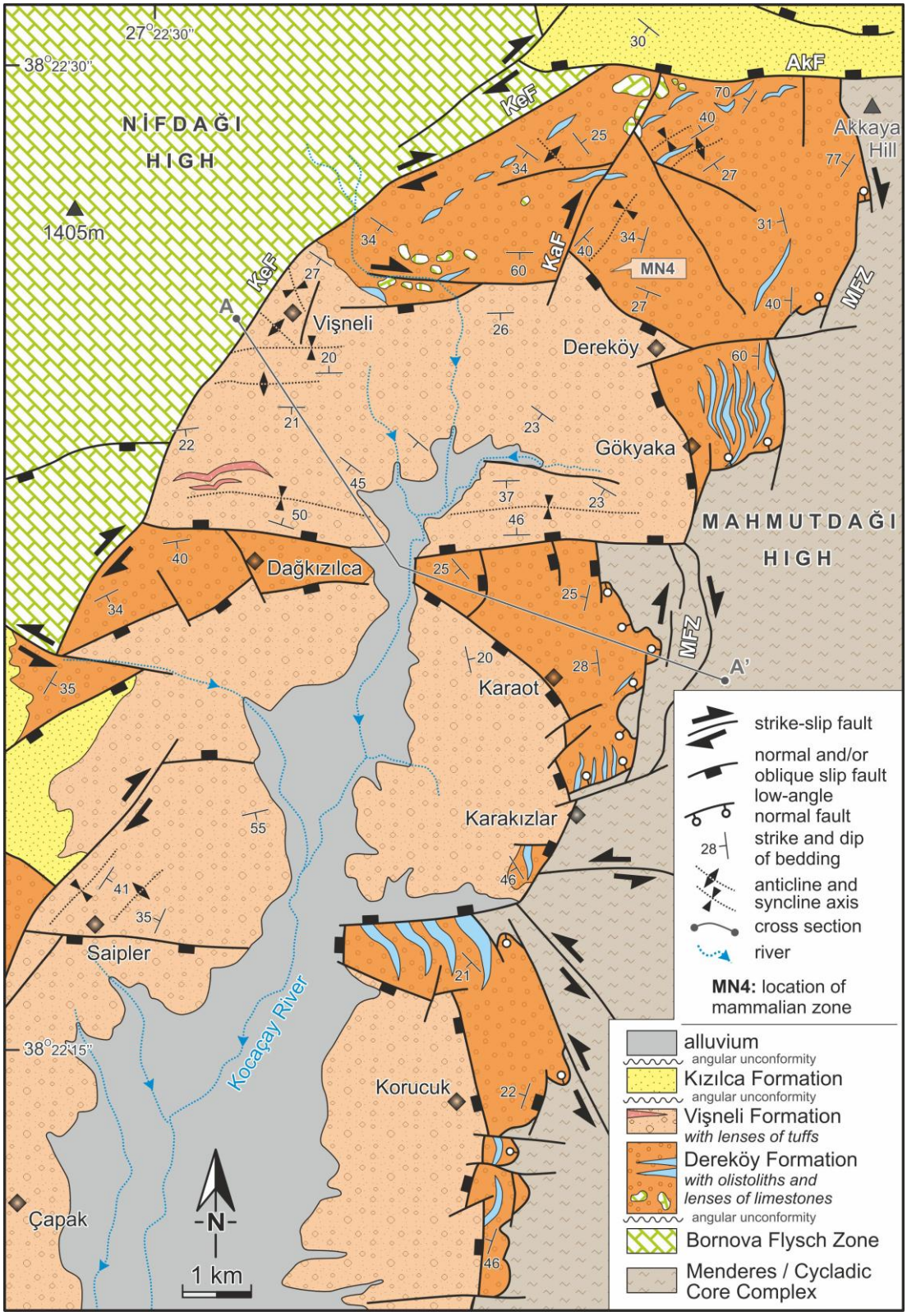


Figure 2.27 Detailed geological map of the Kocaçay basin (modified from Sözbilir et al., 2011). See Fig. 2.3 for location. MFZ, Mahmutdağı fault zone; KeF, Kesmadağı fault; KaF, Karabeldere fault. See Fig. 2.29e for cross section A-A'.

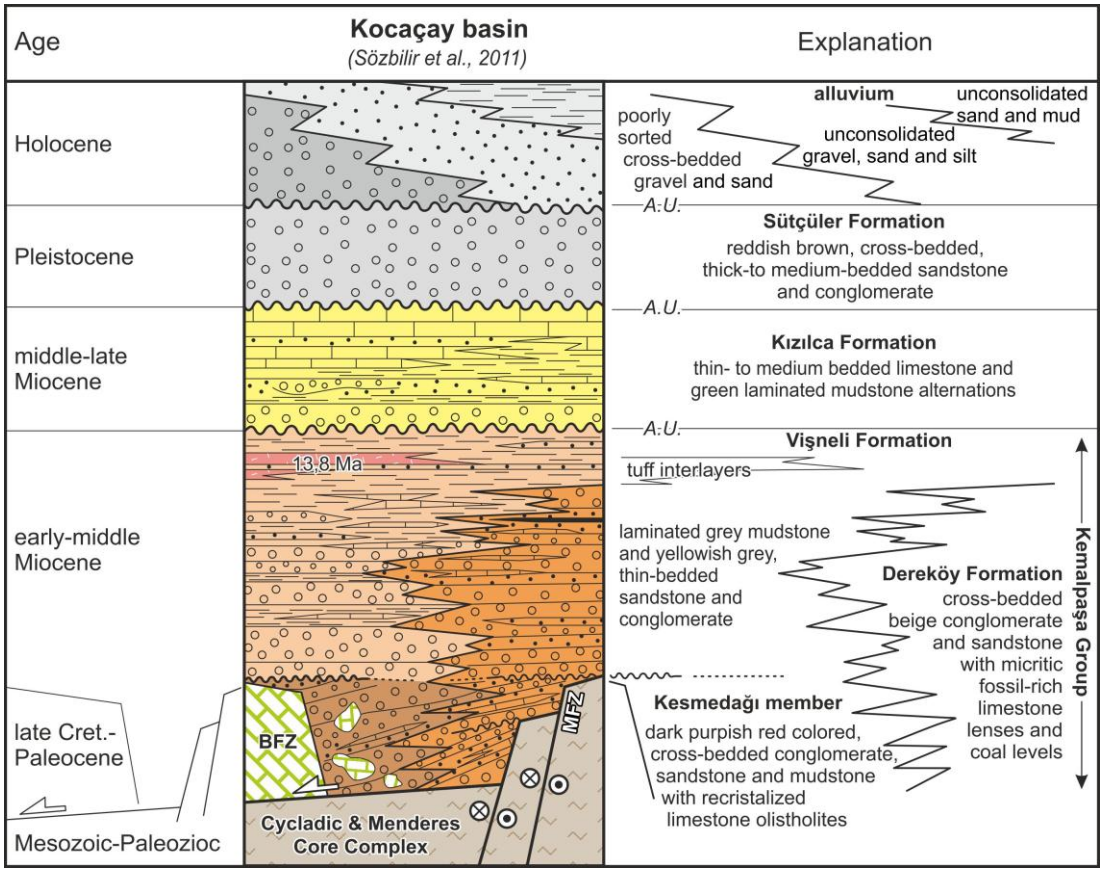


Figure 2.28 Generalized stratigraphic columnar section of Kocaçay basin (modified from Sözbilir et al., 2011). BFZ, Bornova Flysch Zone; MFZ, Mahmutdağı fault zone; AU, Angular unconformity.

The Vişneli Formation is described by Sözbilir et al. (2011) as a fining-upward succession of alluvial fan sediments and sheetflood to lacustrine deposits; these are also tuff interbeds suggesting a volcanically active setting. The formation starts with reddish-grey and light-green-grey conglomerate, laminated sandstone and mudstone alternations at the base. These deposits grades upwards into paper shales that contain sporadic thin sandstone and felsic tuff intercalations, and alternates upwards with volcaniclastic sandstone, lithic conglomerate and thicker felsic tuff layers (Fig. 2.28 and 2.29). At the top, the formation is characterized by laminated mudstones and volcanic interlayers that dated as 13.8 Ma by Sözbilir et al (2011). The early-middle Miocene Çatalca Formation is also observed in the Cumaovası basin (SW side of the Kocaçay basin) and is interpreted by Sözbilir et al. (2011) as the lateral equivalent of the Kemalpaşa group.

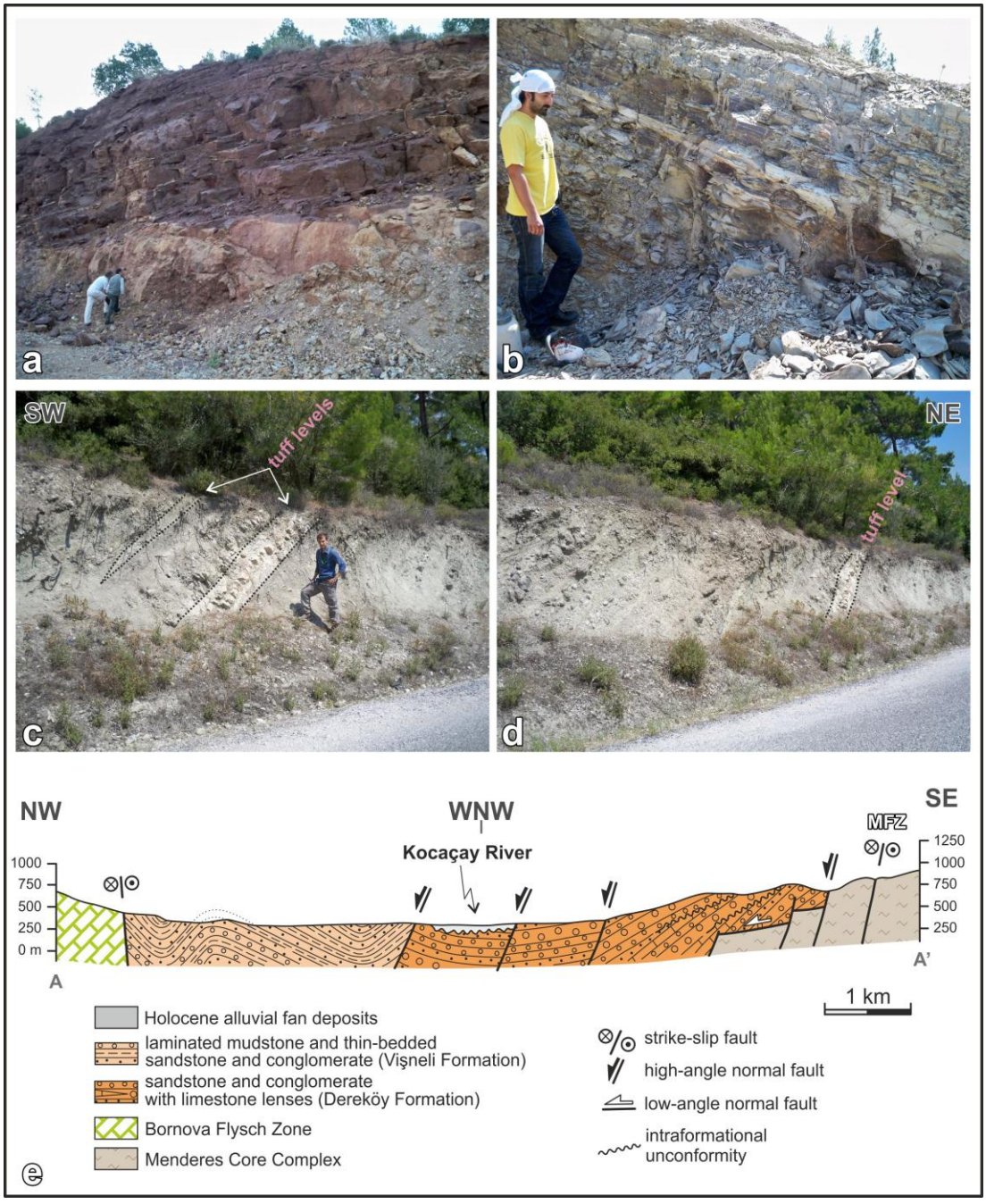


Figure 2.29 a) A field photo showing red beds of the Dereköy Formation. b) A close-up view of the Vişneli Formation showing the mudstone dominated part of the unit having leaf fossils and sandstone intercalations. c-d) Along the Vişneli-Dağkızılca road, the Vişneli Formation includes conglomerate and sandstone alternations with tuff interlayers and lenses. e) Geological cross-section illustrating stratigraphical relationships of the basin fill. See Fig. 2.27 for location of the section. MFZ, Mahmutdağı fault zone.

The *upper sequence* is characterized by the Kızılca Formation (Fig. 2.28). The unit is exposed in the northern side of it, and unconformably overlies the rocks of the Kemalpaşa group. It is represented by terrestrial clastic to lacustrine carbonate deposited in the southwestern tip of the Gediz graben. At the base, it is mainly composed of brown and poorly sorted alluvial conglomerates are passes upwards into grayish-brown sandstones and grayish-green mudstones. The succession ends with a light-grey and yellowish-white clayey limestone intercalation. According to the stratigraphic correlation with similar units in the neighboring basins successions, the age of the formation may be middle–late Miocene (Sözbilir, et al., 2011).

2.3.9 Söke Basin

The Söke basin is located at the western rim of the Büyük Menderes graben and extends from the Dilek Peninsula to the south and Kuşadası to the north (Figs. 2.3 and 2.30). It develops on the pre-Miocene rock units if the; (i) by metamorphic rocks of the Menderes and Cycladic Core Complexes, and (ii) sedimentary and ophiolitic rocks of the Lycian Nappes (Fig. 2.31; Candan et al., 1997; Okay, 2001; Gessner et al., 2001; Çetinkaplan, 2002; Jolivet et al., 2004; Rimmelé et al., 2006; Ring et al., 2007; Çakmakoğlu, 2007; Sümer et al., 2012). The unconformably overlying late Cenozoic basin fill units will be summarized from Sümer et al. (2013).

The Miocene stratigraphy of the Söke basin includes two main rock groups; (i) the early–middle Miocene (*lower sequence*) and (ii) middle–late Miocene (*upper sequence*), separated by an unconformity. From base to top, the *lower sequence* is characterized by the Söke Formation and consists of Kemalpaşa conglomerate, Şeytan member and Maden limestone, while the upper sequence comprises Davutlar member, Kuşadası Formation, Hisartepe and Balatçık volcanics (Figs. 2.31, and 2.32).

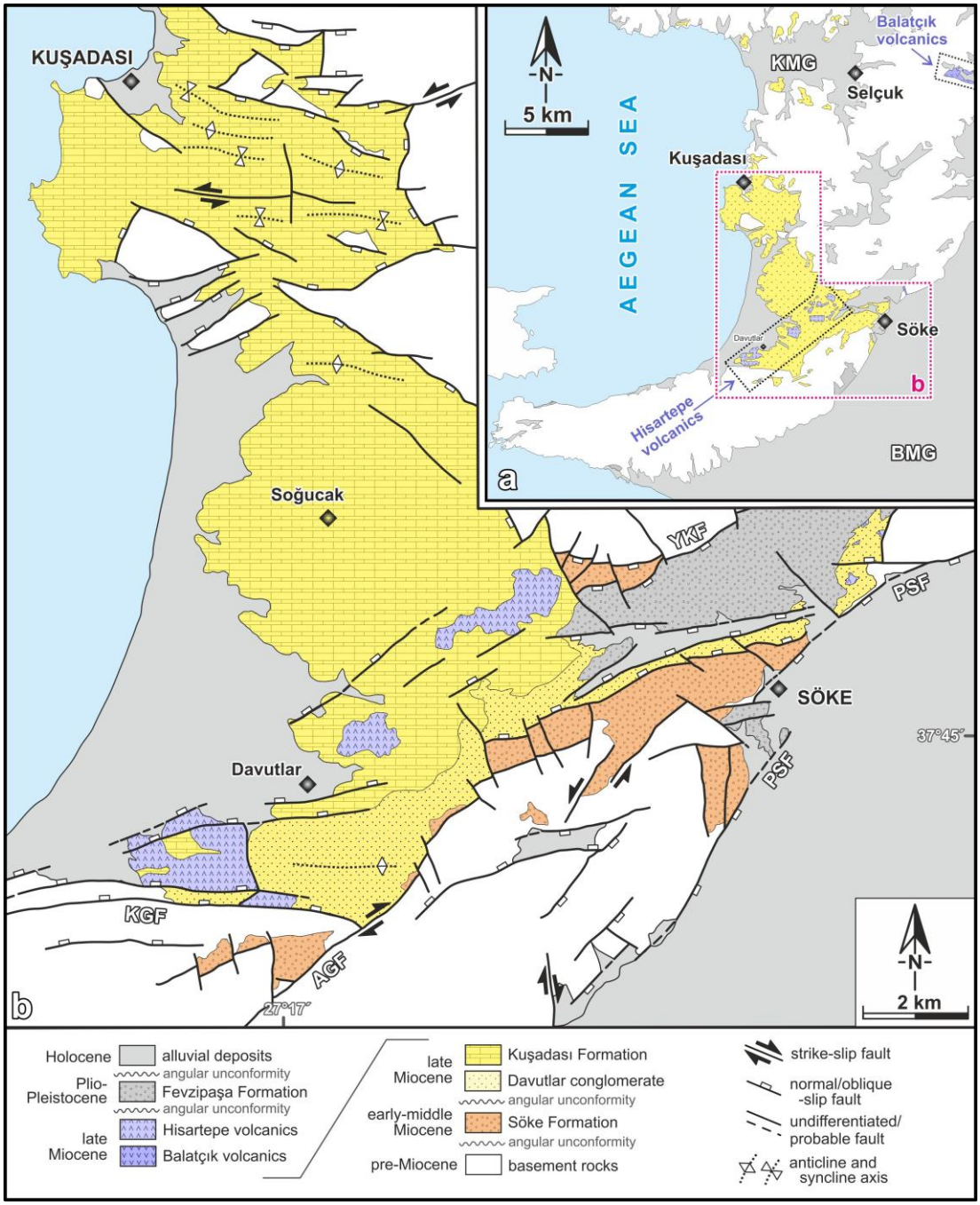


Figure 2.30 a) Generalized geological map of the western margin of the Büyük Menderes (BMG) and Küçük Menderes grabens (KMG) showing distribution of the Miocene sedimentary (yellow) and volcanic rocks (purple) in the region (modified from Çakmakoğlu, 2007). b) The detailed geological map of the Söke basin (simplified from Sümer et al., 2013). KGF, Karagedik fault; AGF, Ağaçlı fault; YKF, Yamaçköy fault; PSF, Priene-Sazlı fault. See Fig. 2.3 for location.

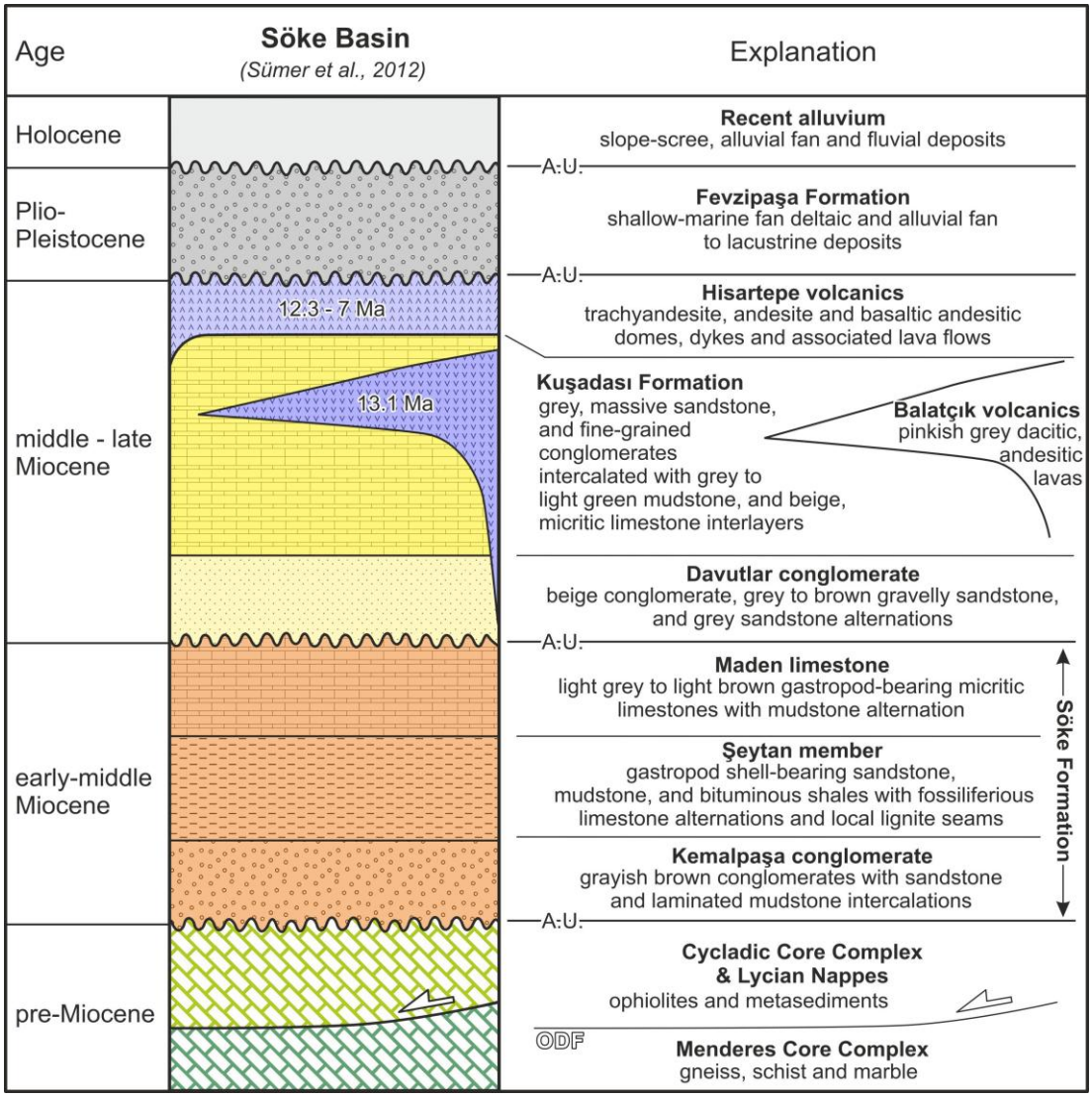


Figure 2.31 Generalized stratigraphic columnar section of Söke basin (simplified from Sümer et al., 2013). ODF, Oyukdağ detachment fault; AU, Angular unconformity.

The *lower sequence* of the basin (Söke Formation) is composed mainly of coarse-grained conglomerates, coarse- to fine-grained clastics, and carbonates, which show both lateral and vertical interfingering relationships throughout the basin (Fig. 2.31). It starts with grayish brown, massive and poorly sorted conglomerates with sandstone and parallel laminated mudstone intercalation (Kemalpaşa conglomerate). Upward, the clast size becomes finer, where the main lithology includes generally massive and gastropod shell-bearing sandstones, light grey to green and thin-bedded mudstones, and dark grey to brownish black and finely-laminated bituminous shales with light grey, thin- to medium-bedded, fossiliferious limestone alternations and

local lignite seams (Şeytan member). The sequence ends with light grey to light brown colored, medium- to thick-bedded and gastropod-bearing micritic limestones alternating with mudstone laminates and some lignite beds (Maden limestone). Becker-Platen (1970), Ünay and Göktaş (1999), Akgün and Akyol (1999) reported the presence of freshwater ostracods, micromammals and sporomorf assemblages, indicating early-middle Miocene age for the Söke Formation.



Figure 2.32 a-b) Field photos showing sandstone, mudstone and bituminous shale alternations (a) and gastropod shells-bearing sandstones of the Söke Formation (b). c) A road section across the Dededağ Formation showing cycles with conglomerate, sandstone and mudstone alternation; each cycle display erosional base levels. d) A close up view of a pinkish grey dacitic lava flow of the Balatçık volcanics. e) From distance field photo of dark grey and columnar jointed basaltic andesite lavas of the Hisartepe volcanics.

The *upper sequence* of Söke basin is dominated by beige, cross-bedded and fining-upward conglomerate, gravelly sandstone, and massive- to thick-bedded gray sandstone alternations at the base (Davutlar conglomerate). Conglomerates generally have erosional bottom contacts and are usually interbedded with gravelly sandstones. The sandstones display abrupt transitional contacts with the conglomerate levels. The sequence continues with massive grey sandstone, and fine-grained conglomerates intercalated with grey to light green laminated mudstone, and beige micritic limestones (Kuşadası Formation). According to several mammal, ostracod and gastropod determinations in the area, the age of the *upper sequence* is middle–late Miocene (Becker-Platen, 1970; Ünay et al., 1995; Ünay and Göktaş, 1999; Gürer et al., 2009).

During the deposition of the *upper sequence* sediments, Balatçık and Hisartepe volcanics were emplaced (Figs. 2.30 and 2.31). Balatçık volcanics named by Ercan et al. (1986) are exposed in a small area at the northeast of the Söke basin, east of Selçuk village (Fig. 2.30). The unit is dated 13.1 Ma by Ercan et al. (1986) is compose mainly of grey to pinkish grey dacitic, rhyodacitic and andesitic lavas. The Hisartepe volcanics are exposed at several hills trending in NE-direction through the Söke basin (Fig. 2.30). The unit is composed mainly of domes, dykes and associated lava flows with trachyandesite, andesite, and basaltic andesite composition. Along the contact between the carbonates of the Kuşadası Formation and lavas of the Hisartepe volcanics, a baked zone including peperitic texture is reported (Sümer et al., 2013). These lavas are dated as 12.3–7.0 Ma (K–Ar ages) by Ercan et al. (1986) and (Ar–Ar ages) by Sümer et al. (2013).

2.3.10 Spildağı-Yamanlar Area

The Miocene stratigraphy of the area can be divided into the *lower* and the *upper* (volcano-sedimentary) *sequences*, separated by an angular unconformity (Figs. 2.33–36). The *lower sequence* is well exposed within and beyond the western hillside of the Yamanlar high, and between the Yamanlar and Spildağı highs, it's located along the Karaçay fault zone (Figs. 2.33, and 2.34). The *lower sequence* is slightly folded

and crosscut by normal and strike-slip faults. The sequence consists primarily of conglomerates at the base, and grades into limestones, mudstones, and sandstone-

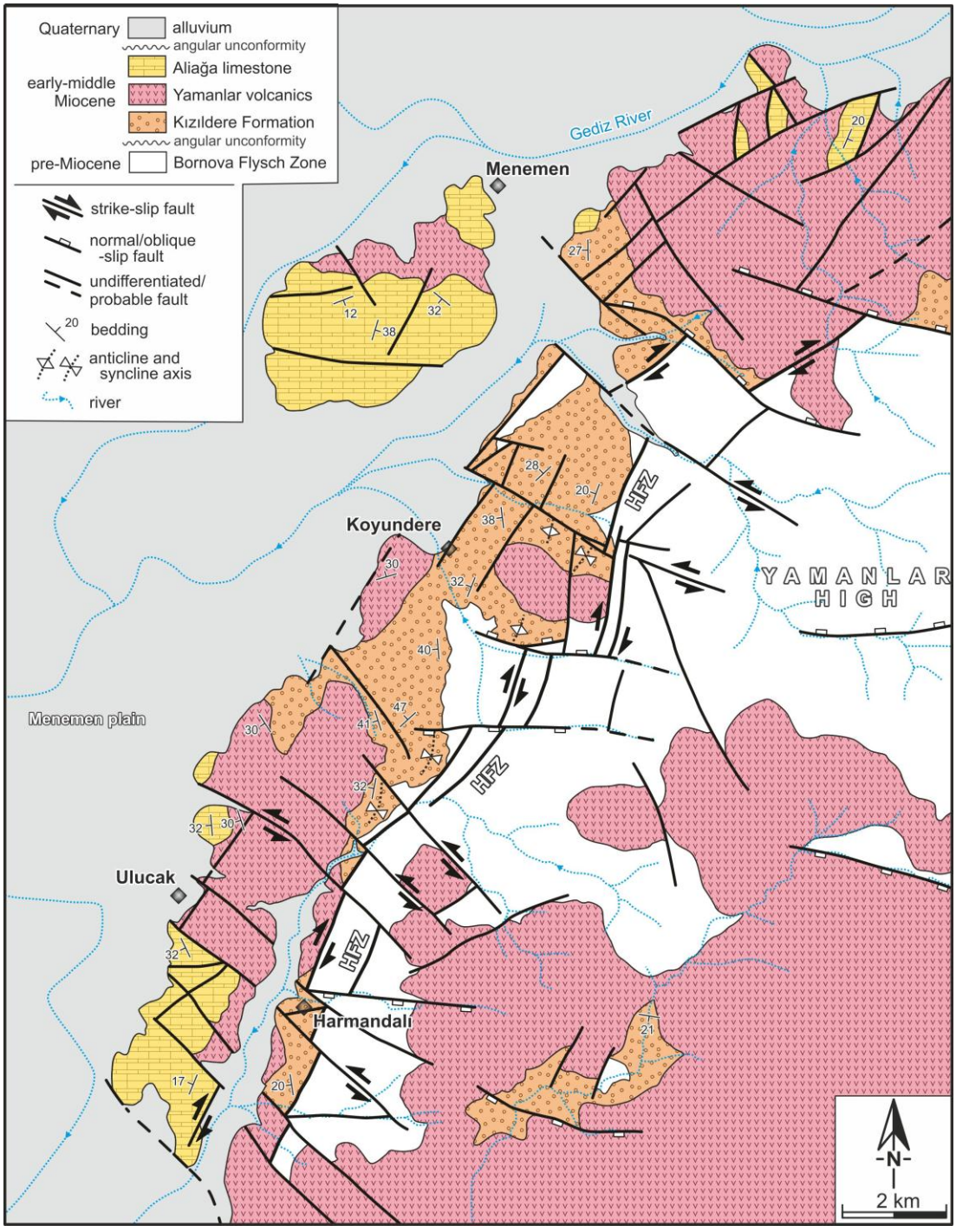


Figure 2.33 Detailed geological map of western hillside of the Yamanlar high around Menemen village. See Fig. 2.3 for location. HFZ, Harmandalı fault zone.

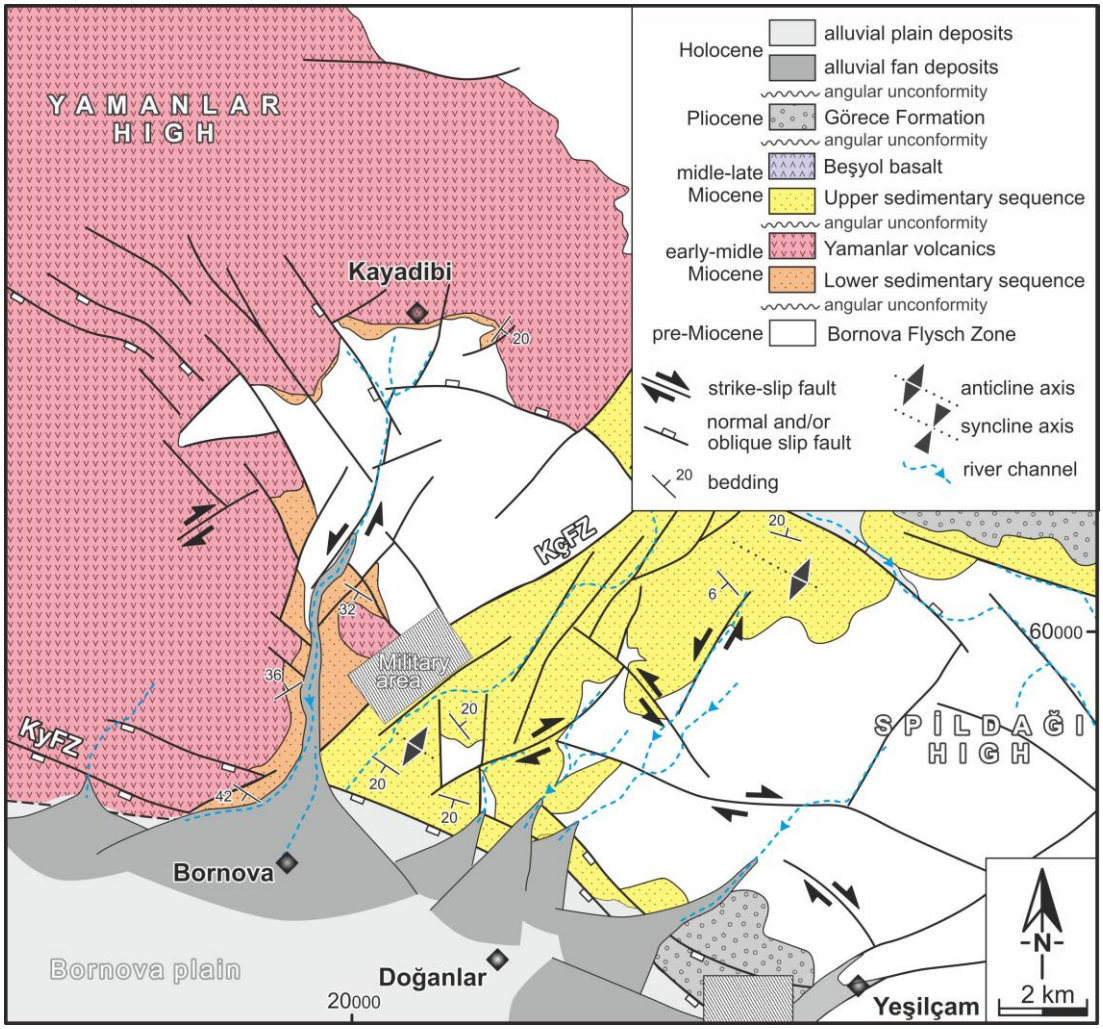


Figure 2.34 Detailed geological map of southern hillside of the Spil-Yamanlar area around Bornova village. See Fig. 2.3 for location. KyFZ, Karşıyaka fault zone; KçFZ, Karaçay fault zone.

shale alternations at the top. It unconformably overlies the basement rocks. The *lower sequence* consists of three formations and is overlain by the Yamanlar volcanics. The basal lithologies are named here as the Kızıldere Formation. Around the Menemen, a basal conglomerate overlies sandstone-shale alternation of the BFZ with an erosional surface (Fig. 2.33). The dominant lithology is brownish-red, thick-bedded to massive, poorly to moderately sorted polymictic conglomerates (Fig. 2.37a). Clasts are in range of pebble and are mainly derived from the rocks of Bornova Flysch Zone. The conglomerates alternate with gray-reddish-brown colored sandstone, siltstone and shale. Upward in the sequence, formation continues with a yellowish brown lacustrine limestone level (Figs. 2.36, and 4.37b).

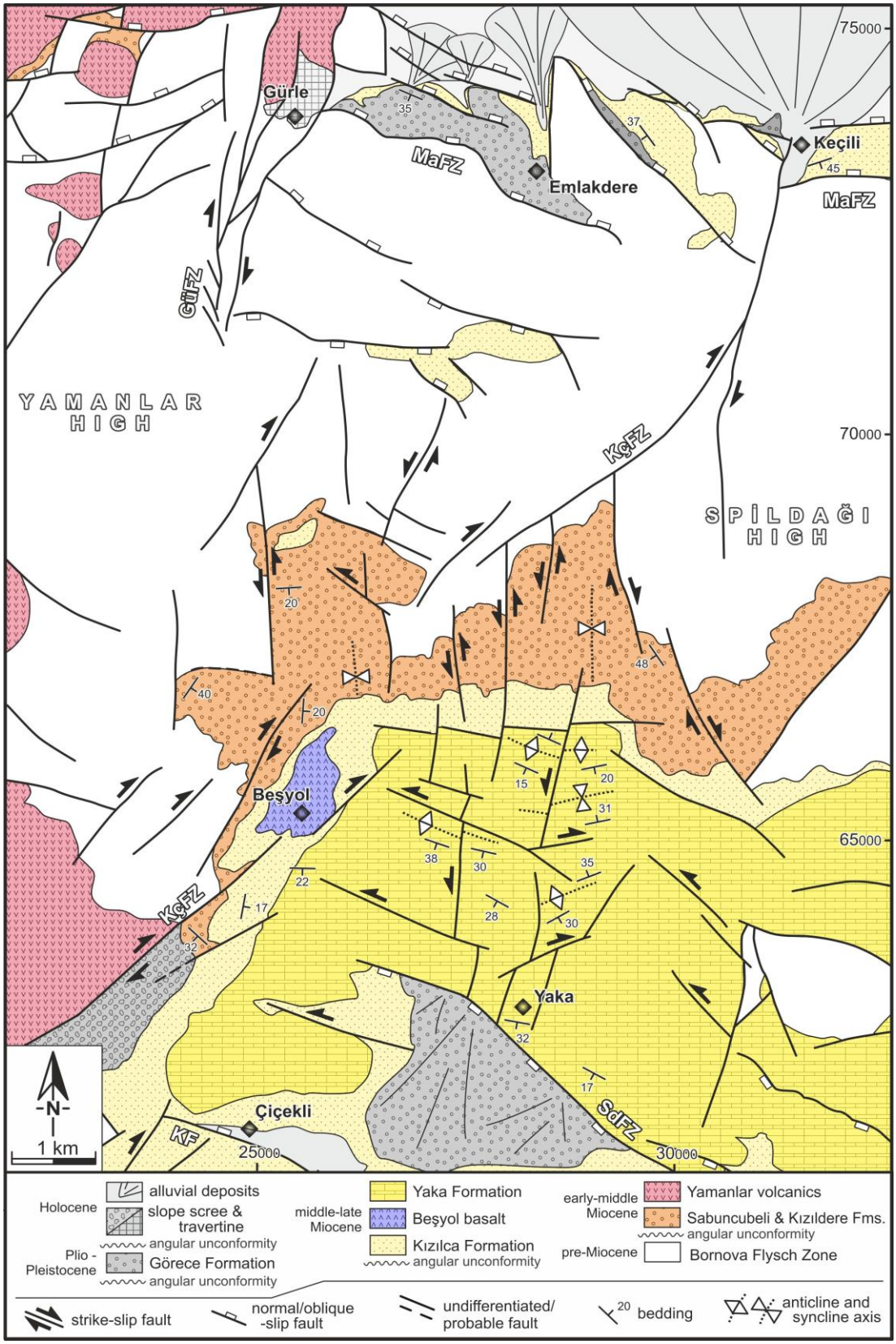


Figure 2.35 Detailed geological map of the central part of Spil-Yamanlar area. See Fig. 2.3 for location. GüFZ, Gürle fault zone; KçFZ, Karaçay fault zone; SdFZ, Spildağı fault zone; KF, Kemalpaşa fault.

The Kızıldere Formation may be interpreted as an alluvial to fluvial sequence; it is overlain by lacustrine carbonates of the Sabuncubeli Formation. The unit crops out between the Bornova and Kayadibi villages and north of Beşyol village. It is composed of thick-bedded conglomerate, sandstone and mudstone alternations with limestone lenses toward the top (Fig. 2.34). The overlying unit is calc-alkaline Yamanlar volcanics, which conformably rest on the sedimentary rocks of the *lower sequence* (Fig. 2.37c). In the area, the Yamanlar volcanics are composed of several lavas, pyroclastic rocks, dykes and domes of dacitic, andesitic, rhyolitic and basaltic compositions. K/Ar whole rock ages of 21.0–16.8 Ma have been reported for the Yamanlar volcanics (Borsi et al. 1972; Ercan et al. 1996), indicating an early to middle Miocene age.

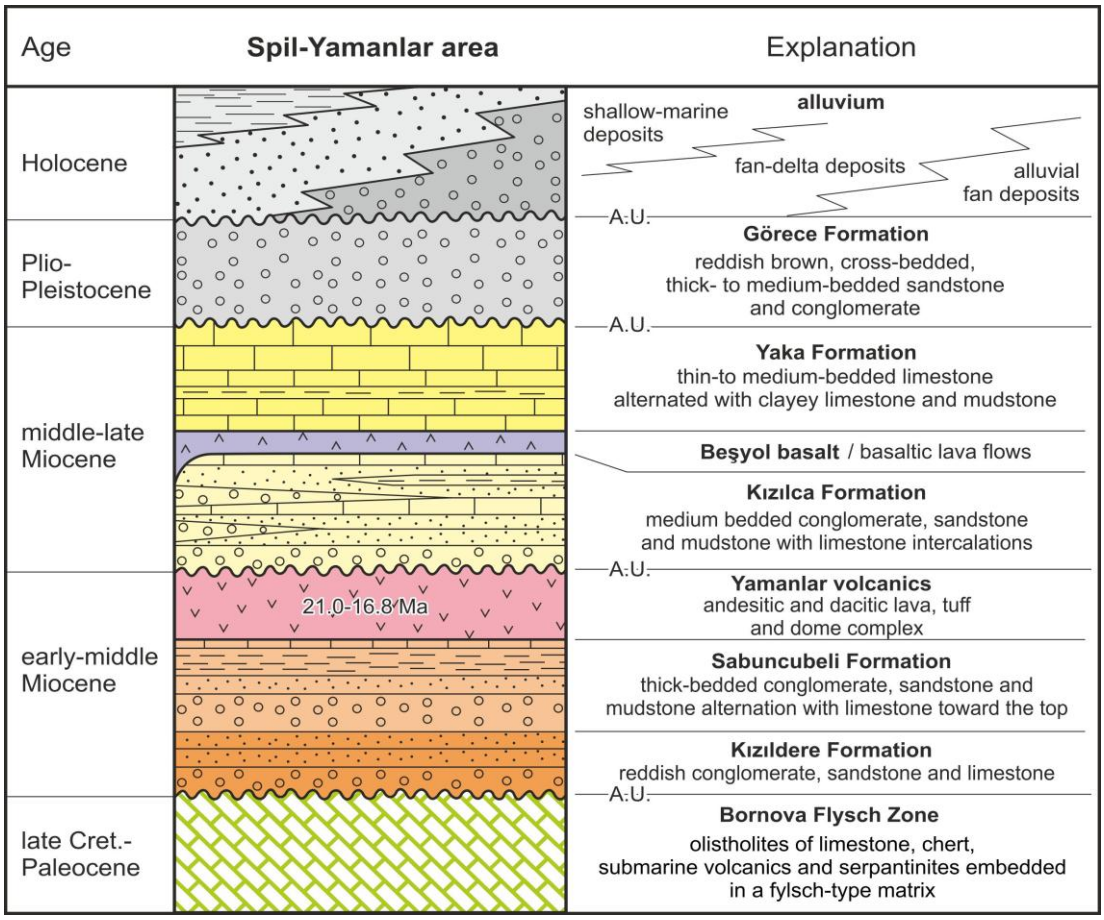


Figure 2.36 Generalized stratigraphic columnar section of Spil-Yamanlar area. AU, Angular unconformity.

Field observations and geological mapping show that the *upper sequence* is gently deformed, folded and faulted in the Spildağı-Yamanlar area. The sequence begins with the Kızılca Formation resting unconformably on the sedimentary and volcanic rocks of the lower sequence (Fig. 2.36). The Kızılca Formation is a packages of terrestrial clastic rocks, intercalated with lacustrine carbonate levels (Fig. 2.37d). The formation is made up of brown, poorly sorted alluvial conglomerates at the base, and passes upwards into grayish-brown sandstones and mudstones. The alluvial conglomerates contain clasts derived from the Yamanlar volcanics, lacustrine carbonates of the lower volcano-sedimentary sequence and the rocks of BFZ. The succession ends with a light-grey and yellowish-white clayey limestone intercalation at the top and is gradationally overlain by a carbonate-dominated sequence of the Yaka Formation (Fig. 2.37f-g).

At the transitional contact between these two units is marked by the Beşyol basalt (Fig. 2.36). It is characterized by dark brown to black olivine basalt lavas, showing peperitic texture at the contact with the lacustrine carbonates of the Yaka Formation (Fig. 2.37e). There is no accurate age data in the literature from these basalts. The age of this formation is suggested as late Miocene according to the stratigraphic correlation of the successions in the neighboring basins (see Dikili area and Cumaovası basin).

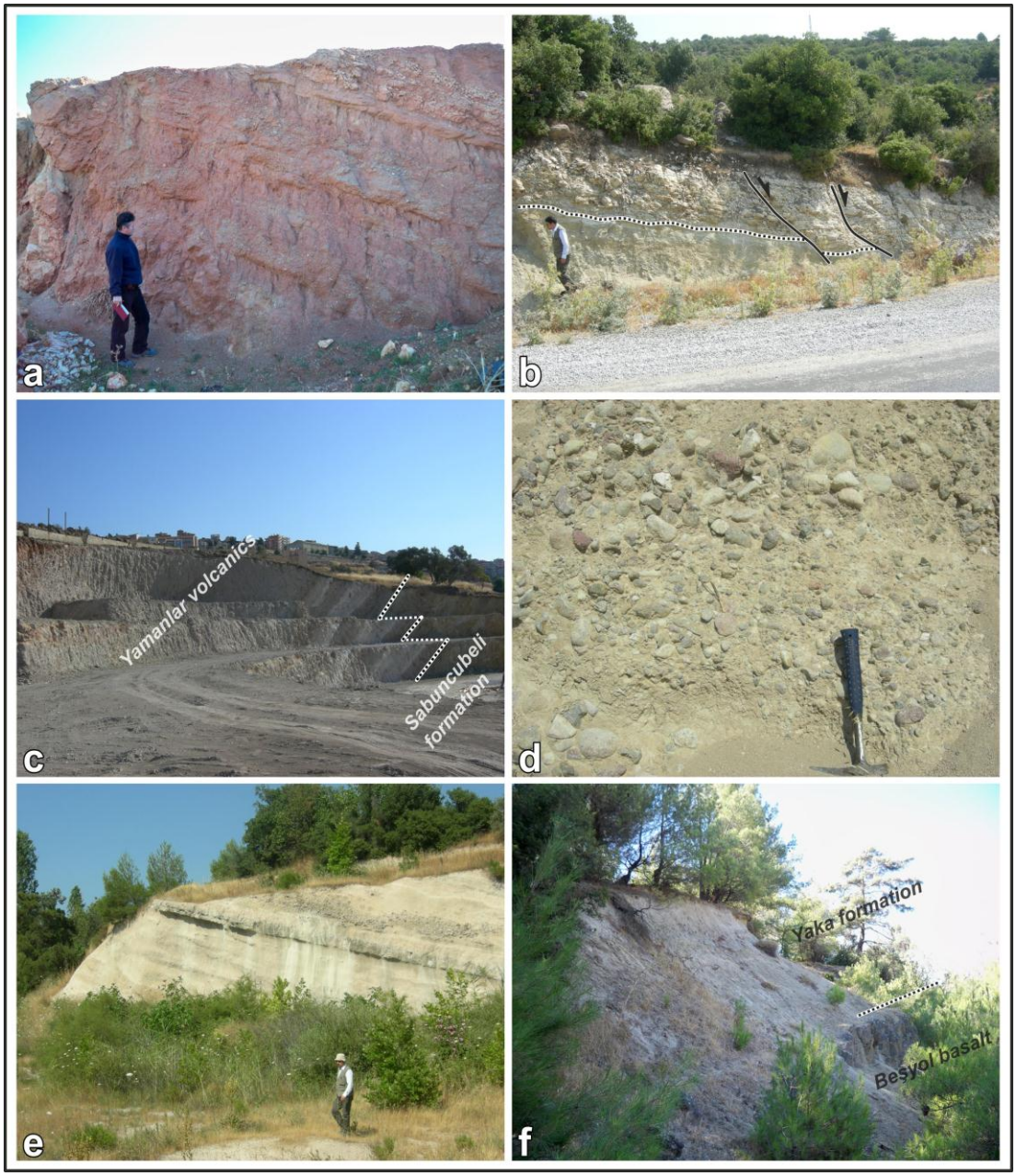


Figure 2.37 Field photos of the Miocene units exposed around Spil-Yamanlar area. a) The reddish sandstone and conglomerate alternation of the Kızıldere Formation. b) Field photograph of the main unconformity between flysch-type highly deformed rocks of the Bornova Flysch Zone and the overlying Miocene lacustrine sediments of the Sabuncubeli Formation. Note the NW–SE-trending faults cut and displace this boundary. c) Conformable contact between the Sabuncubeli Formation and Yamanlar volcanics. d) The base level of the Kızılca Formation. Note that the clasts are mostly derived from volcanic rocks of the Yamanlar volcanics. e) The top sections of the Kızılca Formation includes light-grey and yellowish-white clayey limestone and sandstone alternation. f) Field photo showing the conformable contact between the Beşyol basalt and overlying Yaka Formation.

2.3.11 Urla Basin

It is a NNE-trending basin located between the Karaburun Peninsula in the west and Seferihisar high in the east (Fig. 2.22). The basin fill is characterized by the middle to late Miocene strata (Figs. 2.38 and 2.39; Savaşçın, 1978; Kaya, 1981; Sümer, 2007). The base of the Urla basin is represented by Çamlı Formation, which comprises reddish- to brownish-gray, semi-consolidated conglomerates, alternations of sandstone and mudstone, with limestone interlayers.

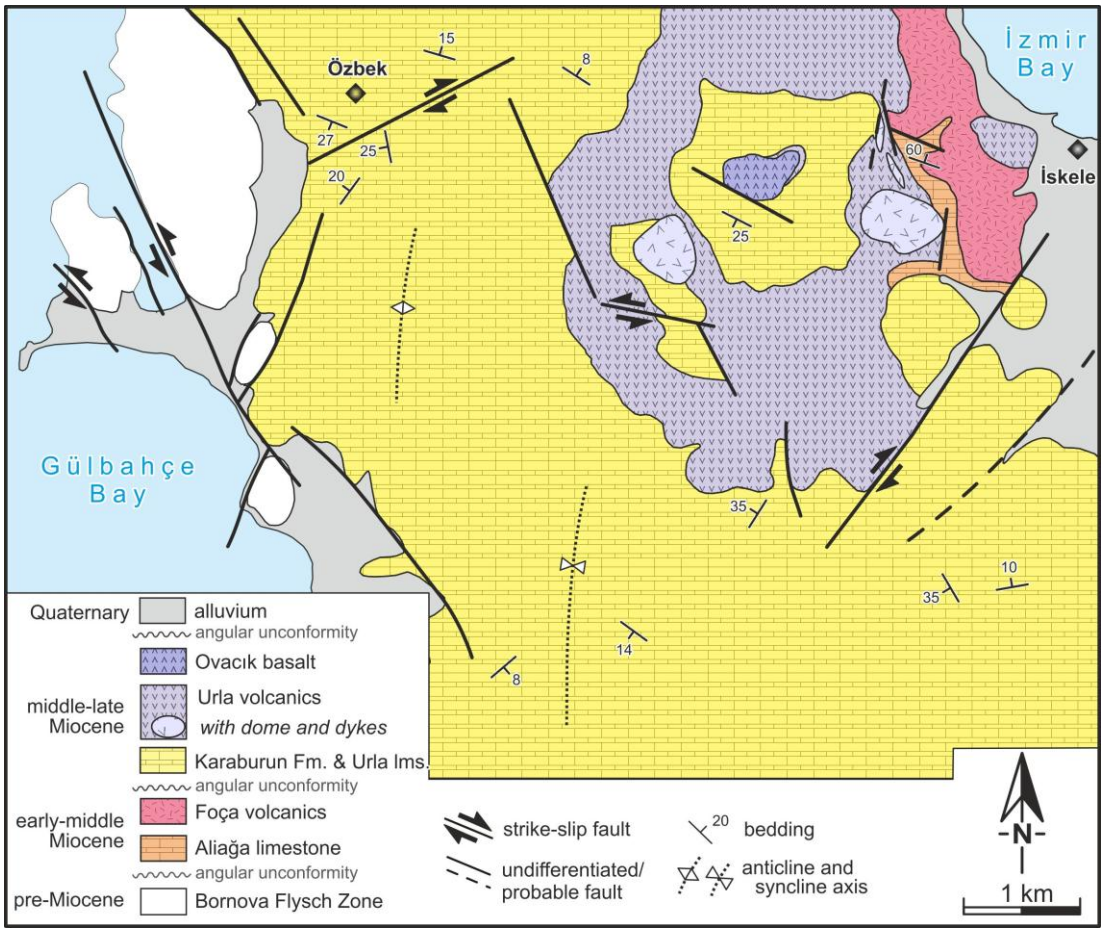


Figure 2.38 Detailed geological map of the Urla basin around İskele village (simplified from Sümer, 2007; and Helvacı et al., 2009). See Fig. 2.22 for location.

The conglomerates are poorly sorted and are composed of the fragments in variable sizes derived mainly from the rocks of the Bornova Flysch Zone, with minor clasts from the metamorphic rocks of the Menderes Core Complex and from volcanic rocks of the lower sequence of the Miocene units. It includes mudstone intercalations

and displayswell-developed sedimentary structures, such as cross beds, channel fills and graded bedding. The Urla limestone conformably overlies the other clastic units of the basin, and represents the upper part of the upper sequence.

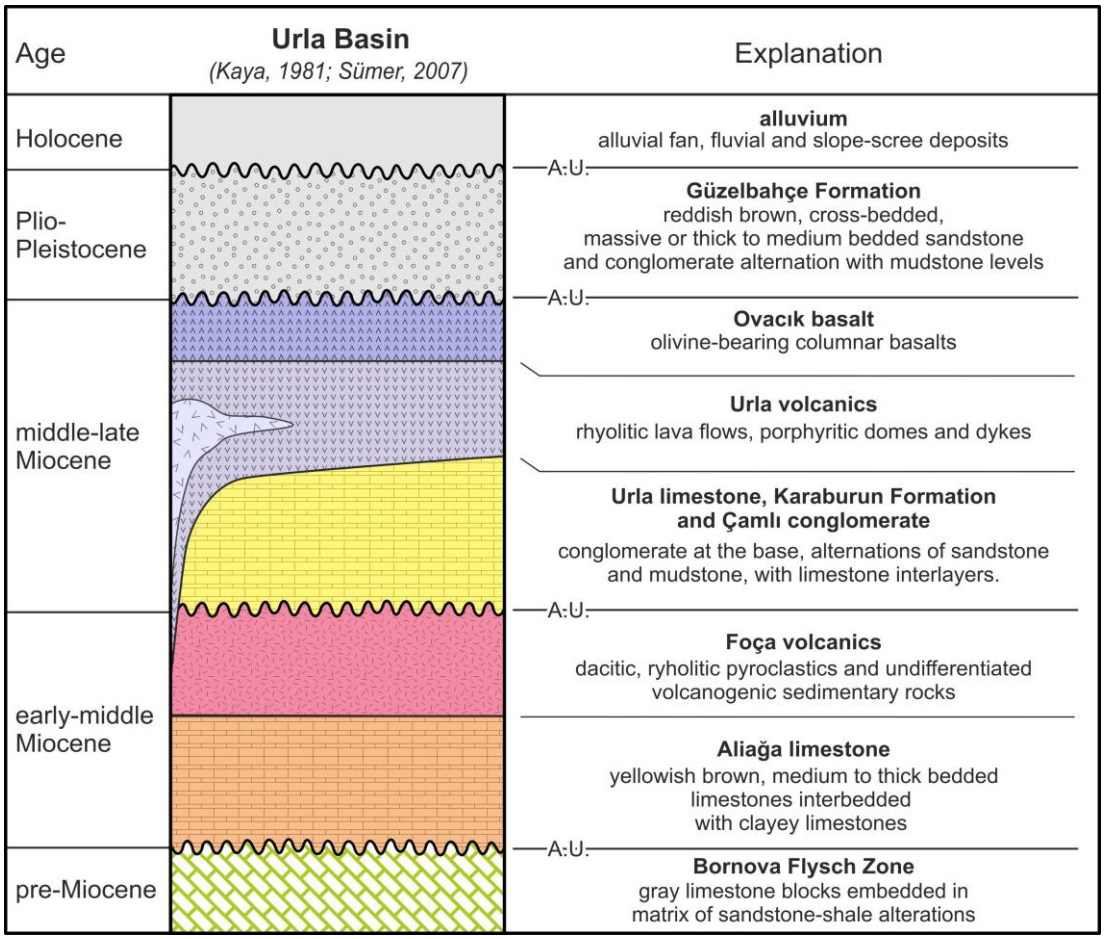


Figure 2.39 Generalized stratigraphic columnar section of the Urla basin (Kaya, 1981; Sümer, 2007). AU, Angular unconformity.

In the central part of the basin, the Urla volcanics and the Ovacık basalt are exposed (Kaya, 1981; Helvacı et al., 2009). The Urla volcanics are composed mainly of rhyolitic lava flows, domes and dykes. These lava flows yield (K–Ar biotite) age as 11.9 Ma (Borsi et al., 1972). The overlying Ovacık basalt is dated at 11.3 Ma (K–Ar whole rock age; Borsi et al., 1972). It is composed mainly of olivine-bearing columnar basalts (Fig. 2.40c).



Figure 2.40 Field photos from the upper sequence of the Miocene units exposed in the Urla basin. a) The top levels of the Karaburun Formation including yellowish sandstone, light-grey to whitish green mudstone and yellowish-white clayey limestone alternation. Note the NE-trending strike-slip faults with minor normal component cut and displace the unit. b) A typical field view of the Urla limestone with gently bedded yellowish-white lacustrine limestone and light-grey mudstone interlayers. c) A field photo from southwest of Yağcılar village (see Fig. 2.22), showing dark grey to black columnar lava flows of the Ovacık basalt.

2.3.12 Yuntdağ Area

The Neogene units consist of early–middle Miocene Kızıldere group (Sabuncubeli and Kızıldere Formations), early–middle Miocene Yuntdağı volcanics, and late Miocene Karadağ Formation (Figs. 2.41 and 2.42). The sequence of the Kızıldere group commences with reddish and grayish conglomerate alternation with a sandy matrix, which overlies above the Bornova Flysch Zone with an angular unconformity. The clasts are subrounded/rounded, poorly to moderately-sorted and are mostly derived from the Bornova Flysch Zone. The sequence grades upward into sandstone and mudstone with dark-gray coal interlayers and limestone alternation. They are strongly folded and deformed by NE- and NW-trending strike-slip fault (Fig. 2.41). Furthermore, the large-scale soft sediment deformation is characteristic

around the middle and upper part of the group. Upward in the sequence, thick-bedded yellowish-brown lacustrine limestones dominate the Kızıldere group may be interpreted as an alluvial to fluvial sequence overlain by lacustrine carbonates.

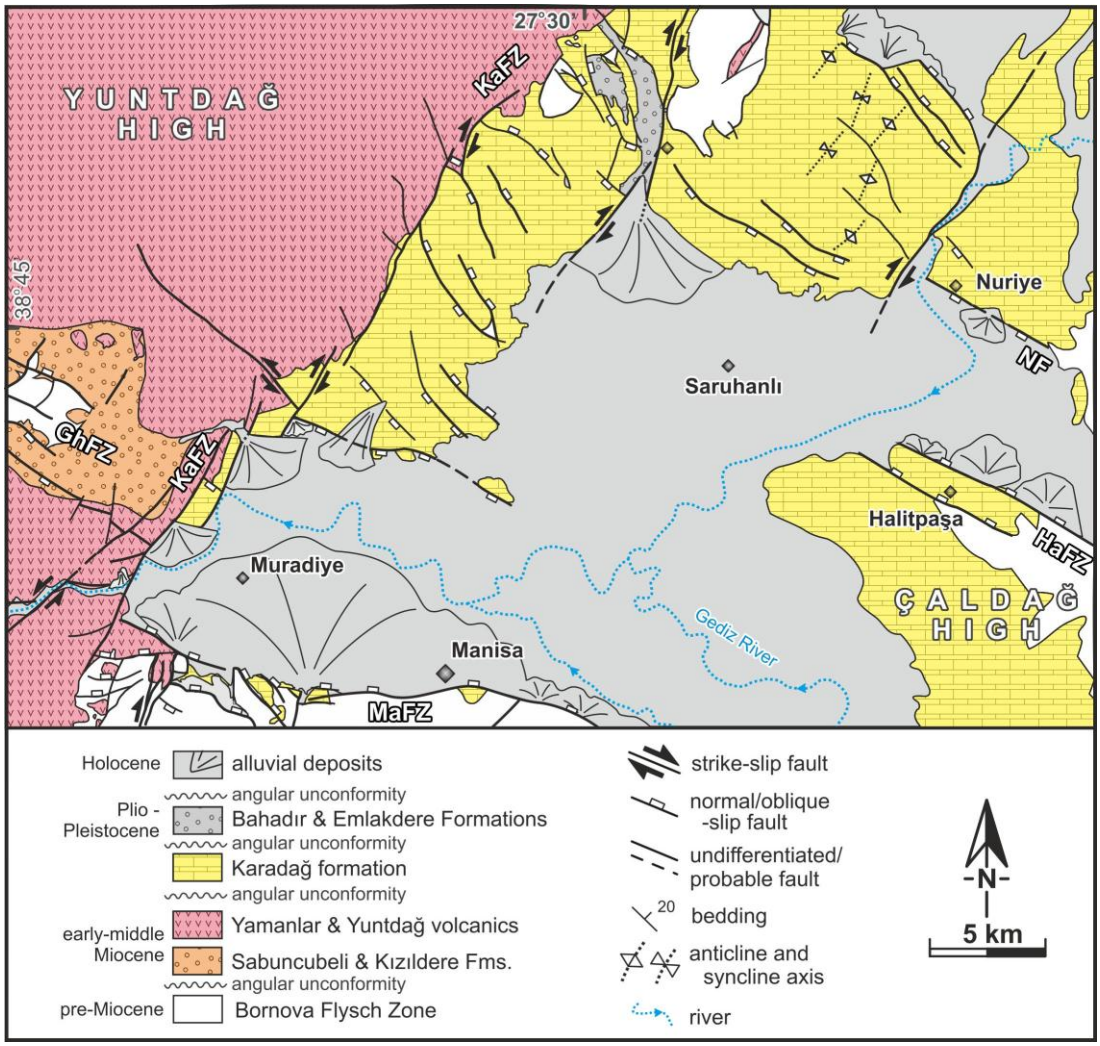


Figure 2.41 Detailed geological map of the Yuntdağ area around Manisa basin (simplified from Özkaymak et al., 2012). See Fig. 2.3 for location. MaFZ, Manisa fault zone; KaFZ, Kaleköy fault zone; GhFZ, Güzelhisar fault zone; HaFZ, Halitpaşa fault zone; NF, Nuriye fault.



Figure 2.42 Field photos of Miocene units exposed around Yuntdağ area. Field photos showing; a) The reddish conglomerates of the Kızıldere Formation; b) whitish pink pyroclastics and breccias, and c) dark gray lava flows of the Yamanlar volcanic; d–e) structural boundary between the Yuntdağ volcanics and Karadağ Formation; f) typical field views of Karadağ Formation; light brown lacustrine limestones; and g) greenish gray mudstones.

The conformably overlying Yuntdağı volcanics consists of pyroclastic rocks and lava flows. Lower part of the unit is represented by light-colored tuffs. In this part, thin-bedded lacustrine limestone interlayers of the Kızıldere group are the most prominent evidence of a conformably relationship between the lower Kızıldere group and the volcano-sedimentary sequence. Towards upper parts, coarse andesitic breccias overlie the tuff unit. At the top of the succession is represented by lava flows comprising the plateau-like topographic domains. Age of the unit is assigned as early–middle Miocene (Borsi et al., 1972; Savaşçın, 1978; Ercan et al., 1985, 1996).

The Yuntdağı volcanic unit is unconformably overlain by fluvial and lacustrine alternation of the Karadağ group that covers large areas in the Manisa basin (Fig. 2.41). The dominant lithology of the lower part of the group is made up of gray-colored, thick bedded, poorly to moderately sorted conglomerates with a sandy matrix. Clasts are in pebble sizes and are derived mainly from the Yuntdağı volcanics and the Bornova Flysch Zone. The conglomerates alternate with greenish grey sandstone and claystone. The unit grades upward into thin-bedded limestone and cross-bedded sandstone alternation. In the middle parts, cross-bedded grey sandstones are dominant. Upward in the sequence, the group ends with a yellowish-brown lacustrine limestone level. The upper part of the Miocene units, exposed throughout Manisa fault zone (Fig. 2.41) was mapped and documented by Bozkurt and Sözbilir (2006) and Özkaymak and Sözbilir (2008). According to Bozkurt and Sözbilir (2006), the unit is correlated with the late
Miocene lacustrine sediments exposed throughout western Anatolia (e.g., Hetzel et al., 1995; Yusufoğlu, 1996; Yılmaz et al., 2000).

2.4 Plio-Quaternary Stratigraphy

The post-Miocene continental and shallow-marine deposits unconformably overlie the Miocene volcano-sedimentary sequences. These are Plio–Pleistocene and Holocene alluvial and shallow-marine deposits. These Plio–Pleistocene successions are given different names in different basin; such as Görece Formation in Cumaovası

basin and Spil-Yamanlar area, Asartepe Formation in the Gediz graben, Aydoğdu Formation in the Küçük Menderes graben, Sütçüler Formation in the Kocaçay basin, Fevzipaşa Formation in the Söke basin, and Güzelbahçe Formation in the Urla basin. They rest on an erosional surface above the Miocene sequence or older rock units with a basal conglomerate. According to recent studies (Koçyiğit et al., 1999; Sümer, 2007; Uzel and Sözbilir, 2008; Emre, et al., 2012; Sümer et al., 2013) these units are deposited in an alluvial fan environment and they can well be correlated with each other.

In Salihli area (the Gediz graben), the Asartepe Formation deposited in the hangingwall block of of the margin-bounding high-angle normal faults that delineate the present day graben floor (Emre, 1996; Koçyiğit et al., 1999). The unit overlies the Salihli group with an angular unconformity and consists mainly of yellow–light gray conglomerate and sandstones with some mudstone levels (Emre, 1996; Koçyiğit et al., 1999; Sözbilir, 2002; Çiftçi and Bozkurt, 2009). The age of the Asartepe Formation is assigned as late Pliocene-early Pleistocene according to correlative units in other graben basins (Ünay et al., 1995; 1998, Sarıca et al., 2000). The youngest sedimentary unit, the recent alluvial deposits are occur in the present-day graben floor and are composed mainly of undeformed lateral alluvial fan and axial fluvial facies sediments. The Aydoğdu Formation as described by Emre et al. (2012) in Tire area (Küçük Menderes graben) is generally composed of white-light grey and reddish brown, poorly- to moderately-lithified thick-bedded conglomerate and sandstones. The unit displays a coarsening upward sequence, and includes sandstone lenses commonly. Sandstones are usually light brown colored, medium to thick bedded and coarse grained. According to Emre et al. (2006; 2012), the Aydoğdu Formation developed in an alluvial fan setting controlled by high-angle normal faults concurrent to the high-energy stream during the Plio−Pleistocene time interval. The Fevzipaşa Formation of the Söke basin studied by Ünay and Göktaş (1999), Gürer et al. (2001), and recently by Sümer et al. (2013) in detail. According to Sümer et al. (2013) the unit is described as alternation of conglomerates, gravelly sandstones, sandstones, and mudstones with lacustrine limestones and tuff levels towards the top. The conglomerates are generally grey, massive to horizontal bedded with erosional

basal contacts, poorly sorted and medium consolidated. The sandstones are grayish-beige to brown, very fine- to coarse-grained, well-sorted, and poorly consolidated. The cross bedding is common. The mudstones, which are laterally interfinger with sandstones, are mainly green to light grey colored, thick-bedded, and poorly consolidated. They also contain ostracod shells, planktonic diatoms, and plant detritus (Sümer et al,. 2012), and dated as Plio–Pleistocene. According to Uzel and Sözbilir (2008) the Görece Formation is exposed along marginal strike-slip and normal faults of the Cumaovası basin and in the Spil-Yamanlar area. The unit is characterized by red semi-consolidated continental clastics consisting of reddish-brown sandstone and conglomerate alterations. It begins with a basal conglomerate above an erosional surface of the volcano-sedimentary sequence. The unit is made up of alternations of poorly bedded, poorly- to moderately-sorted reddish-brown conglomerates and poorly bedded, moderately sorted yellowish-brown sandstone. Based on its sedimentary and geometric characters, the Görece Formation is interpreted as an alluvial fan deposit including the proximal, middle-distal and alluvial plain parts of the fan system (Uzel & Sözbilir 2008).

Holocene alluvial deposits of the western Anatolia are characterized by alluvial fan deposits that show interfingering relationships with alluvial plain deposits along the streams, and with fan-delta to shallow marine deposits along the shoreline of Aegean Sea (Hakyemez, et al., 1999). They are characterized by grey-beige sediments that occur in the present-day graben floor; they are composed mainly of undeformed lateral alluvial fan and axial fluvial facies gravel and sands with clay, silt and sand matrix (Koçyiğit et al., 1999; Sözbilir, 2001, 2002; Rojay et al., 2005; Emre & Sözbilir, 2007; Uzel & Sözbilir, 2008; Gürer et al., 2009; Uzel et al., 2012; Emre et al., 2012).

CHAPTER THREE
GEOCHRONOLOGY OF LATE CENOZOIC MAGMATISM WITHIN THE İZMİR-BALIKESIR TRANSFER ZONE

3.1 Introduction

Dating of the events is one of the fundamental tools in geology in order to understand sequence of events and their relative and absolute timing. This provides means to compare different geological events and to understand how the events are build up and evolved in time. Several geochronological techniques allow dating of the geological events. Widely used and relatively precise techniques include mostly the $^{40}K/^{40}Ar$, $^{40}Ar/^{39}Ar$, Rb–Sr, Sm–Nd, Lu–Hf, and U–Th–Pb radiogenic isotopes and their variations. These methods utilizes the dating of: (i) metamorphic fabric forming minerals to determine the timing of deformation along a fault zone or exhumation of footwall block below it, (ii) volcanic minerals or determine the age a magmatic event. The western Anatolia has a complex geodynamic evolution related to oceanic subduction, continental collision, crustal thickening, multi-stage metamorphism an extensional tectonics (e.g. Şengör & Yılmaz, 1981; Şengör 1987; Okay & Tüysüz, 1999; Ring et al., 1999; Bozkurt & Oberhänsli, 2001; Candan et al., 2001; Sözbilir 2001, 2002, 2005; van Hinsbergen et al., 2010). It is an actively deforming area essentially associated with the slab-edge processes related to the convergence of African and Eurasian plates since the Mesozoic (Fig. 3.1).

Present day tectonic configuration of the Aegean region (Fig. 3.1) has been controlled mainly by two large-scale plate tectonic processes operated simultaneously. These are; (i) subduction of African plate below the Eurasian plate and roll-back of the subducted slab below the Aegean region with respect to Eurasia (Le Pichon and Angelier, 1979; Meulenkamp et al., 1988, Van Hinsbergen et al. 2005, 2010, Biryol et al. 2011), and (ii) westwards escape of the Anatolian Block along North and East Anatolian fault zones. The first processes gave way to the development of Cycladic core complex (CCC) and the Menderes core complex (MCC) on top which a number of Late Cenozoic basins are developed during their

exhumation along detachment faults. It's very important to note here that the differential deformation between the CCC and MCC has been accommodated by the İzmir–Balıkesir Transfer Zone (İBTZ) and Mid-Cycladic Lineament (MCL) (Ring et al., 1999; Uzel and Sözbilir, 2008; Sözbilir et al., 2011, Uzel et al., 2013).

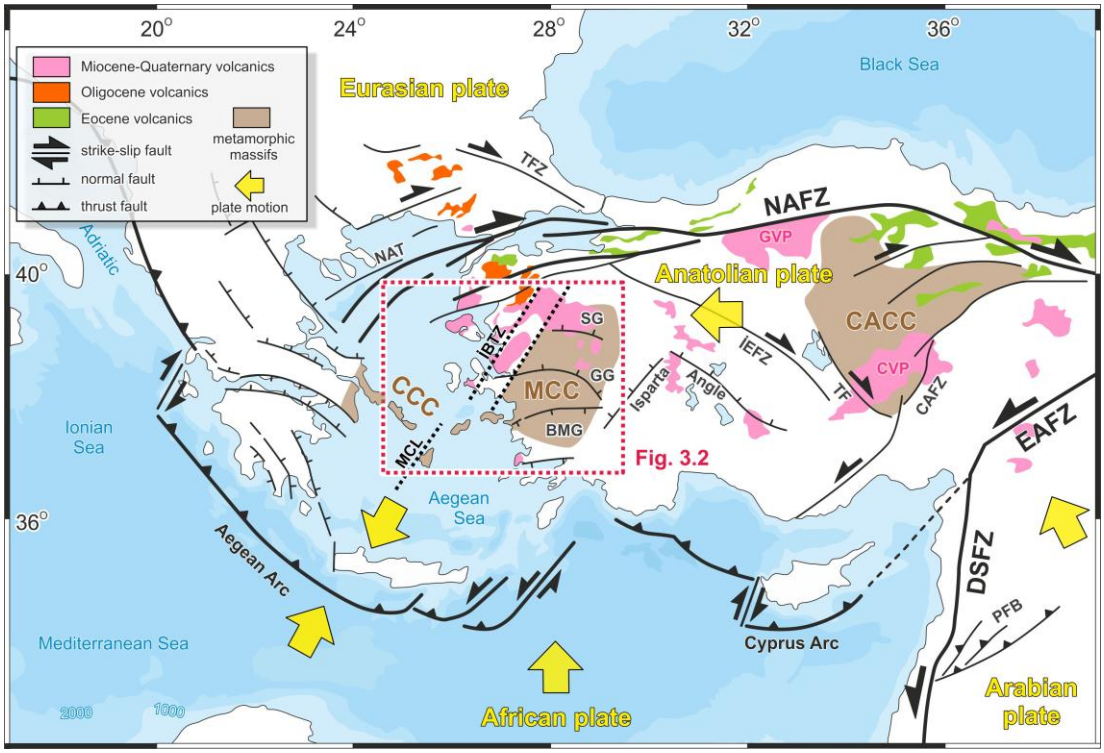


Figure 3.1 Simplified tectonic map showing distribution, plate tectonic configuration, and temporal relationships of the major neotectonic elements and Cenozoic volcanic rocks in Anatolian Plate. DFZ, Dead Sea Fault Zone; EAFZ, East Anatolian Fault Zone; NAFZ, North Anatolian Fault Zone; CAFZ, Central Anatolian Fault Zone; TF, Tuzgölü Fault; İEFZ, İnönü-Eskişehir Fault Zone; BMG, Büyük Menderes Graben; GG, Gediz Graben; SG, Simav Graben; NAT, North Anatolian Through; TFZ, Thrace Fault Zone; İBTZ, İzmir-Balıkesir Transfer Zone; MCL, Mid Cycladic Lineament (simplified from Şengör et al. 1985; Barka 1992; Bozkurt 2001; Koçyiğit and Özaçar, 2003, Biryol et al., 2011). Large yellow arrows indicate relative plate motion directions with respect to Eurasia. Locations of the main metamorphic core complexes, Cycladic Core Complex (CCC), Menderes Core Complex (MCC), and Central Anatolian Crystalline Core Complex (CACC) are also shown (Ring et al., 2001; Lefebvre et al., 2012).

The deformation styles, governing processes and exact timing of the events related to İBTZ, which form the main research questions of this study, are still under

debate. In order to shed light on the timing of events in the region, geochronology of the late Cenozoic volcanic rocks will be provided in this chapter. In this context, a new geochronological data set ($^{40}Ar/^{39}Ar$) from Miocene volcanic rocks along the İBTZ is presented. Results are compared with age data from the literature and paleontological records from the Miocene basin in-fills. In order to do this, brief information about Cenozoic volcanism in western Anatolia will be given first, then, the sampling and analytical procedure of the $^{40}Ar/^{39}Ar$ technique will be summarized from Kuiper et al. (2006) and Renne et al. (2009).

3.2 Geological Setting of the Cenozoic Magmatism

Main magmatic events in the western Anatolian can be classified, based on the processes and temporal relationships, basically into five distinct categories: (i) the Oligocene magmatism, (ii) early–middle Miocene volcanism, (iii) middle–late Miocene volcanism, (iv) Oligocene–late Miocene magmatism, and (v) Quaternary volcanism.

(i) The *Oligocene* volcanic rocks in western Anatolia are mainly cropped out at northeastern part of the Edremit Bay in Biga Peninsula (Fig. 3.2). It is represented geochemically by the calc-alkaline and high potassic basalt/trachybasalt to dacite, trachyandesite, and andesites (Altunkaynak and Genç, 2008). There is no reported evidence for the existence of Oligocene volcanic rocks within the Neogene grabens throughout the western Anatolia.

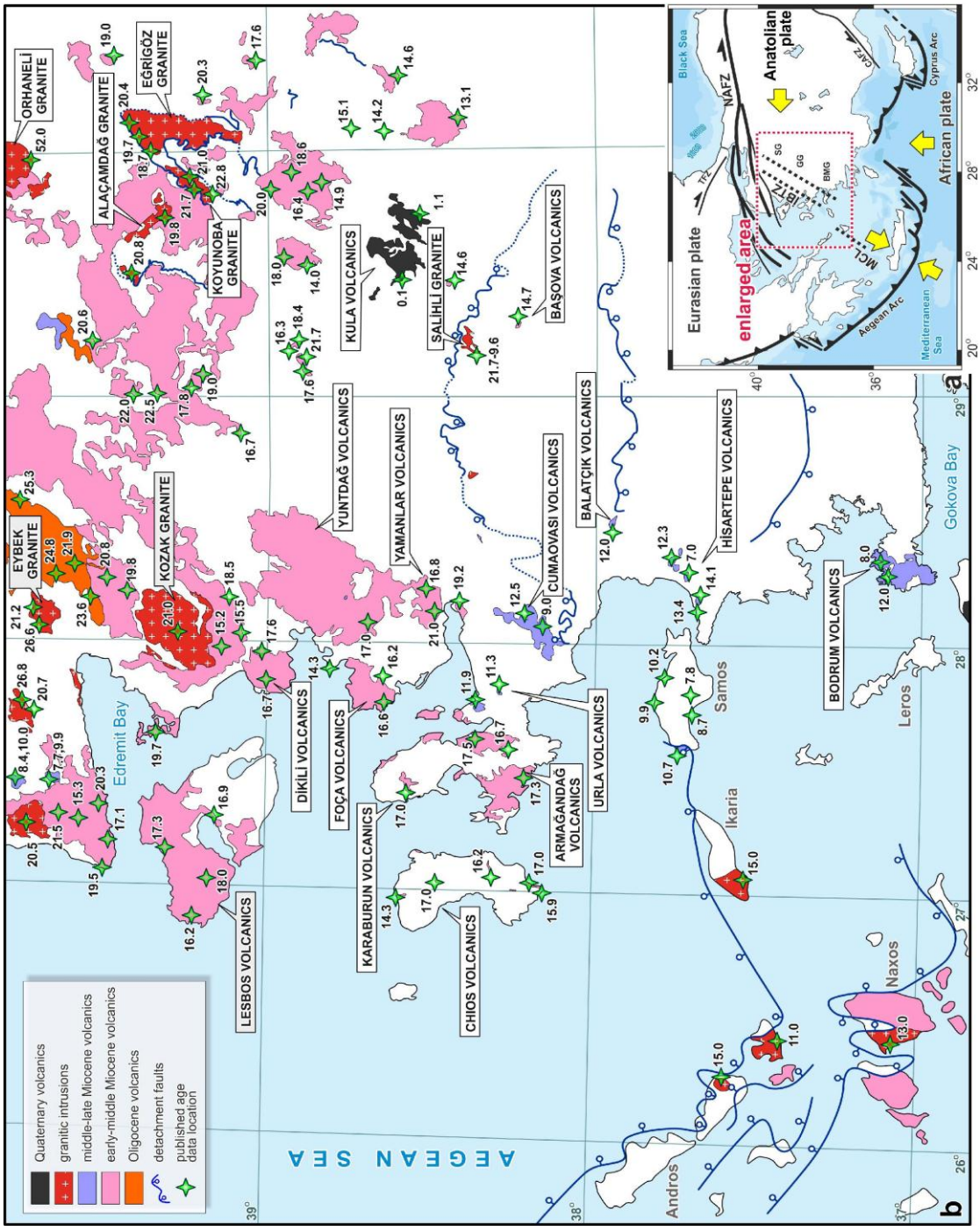


Figure 3.2 Simplified geological maps showing; a) geodynamic position of the area, and b) main distribution of the Eocene to Quaternary magmatic rocks in the western Anatolia with their available radiometric age data from literature (Krushensky, 1976; Borsi et al., 1972; Ercan et al., 1985; 1996; Seyitoğlu et al., 1992; Türkecan et al., 1998; Aldanmaz et al., 2000; Işık et al., 2004; Purvis et al., 2005; Kaymakçı et al., 2007; Helvacı et al, 2009; Erkül, 2010; Altunkaynak et al., 2010; Catlos et al., 2010; Hasözbek et al., 2010; 2011). NAFZ, North Anatolian Fault Zone; CAFZ, Central Anatolian Fault Zone; İBZT, İzmir–Balıkesir Transfer Zone; MCL, Mid-Cycladic Lineament; SG, Simav Graben; GG, Gediz Graben; BMG, Büyük Menderes Graben.

(ii) The following magmatic episode, the *early–middle Miocene* volcanism, is widespread in the area of northern Menderes core complex to the north of Gediz graben, along the İBTZ, and to the west of the İBTZ (Fig. 3.2). It consists mainly of andesitic, dacitic, trachytic, rhyolitic and basaltic lava flows and their pyroclastic deposits. Along the İBTZ, the volcanic rocks are predominated by coeval calc-alkaline and alkaline volcanic rocks with minor ultrapotassic and shoshonitic volcanic rocks (Akay and Erdoğan 2004; Erkül et al., 2005).

(iii) The *middle–late Miocene* volcanic rocks are observed in relatively small areas in the southwestern part of the Biga Peninsula, Soma, Urla, and Cumaovası basins (Fig. 3.2). It is represented by silica-rich rhyolite to andesites. Particularly, along the İBTZ, the volcanic centers lie mostly parallel to the major NE–SW trending faults. For example, in Cumaovası basin the volcanic centers and outcrops of the volcanic rocks are aligned in the NNE–SSW direction and they form the 'central volcanics'. The volcanic centers include Karadağ, Dededağ, Karakaya, Kızılcaağaç, Çakmaktepe, Dikmendağı and Çubukludağ hills (Fig. 2.7). Olivine-bearing high potassic basalts and potassic trachybasalts were also produced during this period. These basalts are chemically quite different with their strongly alkaline compositions (Helvacı et al., 2009; Altunkaynak et al., 2010), and mostly characterized by dark gray colored and relatively unaltered, columnar basalt lava flows and dykes.

(iv) The Oligo–Miocene magmatism produced very widespread *granitic plutons* such as Kozak, Evciler, Eybek, Orhaneli, Alaçamdağ, Eğrigöz, Koyunoba, Salihli, and Cycladic granites in the region (Fig. 3.2). The plutonic activity (9.6 Ma from Salihli granite by Catlos et al., 2010) and volcanic activity in the region lasted till the late Miocene (9.0 Ma from Cumaovası volcanics by Genç et al., 2009). These intrusions are described mainly as granodiorite, quartz diorite and monazite (Yılmaz, 1989; Hetzel et al., 1995b; Genç, 1998; Karacık & Yılmaz, 1998; Altunkaynak & Yılmaz, 1998, 1999; Pe-Piper et al., 2002; Glodny & Hetzel, 2007; Altunkaynak & Genç, 2008; Erkül et al., 2010; Jolivet et al., 2010; Hasözbek et al., 2011). Granitic pluton emplacements are attributed to core complex evolution/exhumation of the

metamorphic massifs along the detachment faults (e.g., Emre, 1996; Seyitoğlu, 1997a; Işık & Tekeli, 2001; Lips et al., 2001; Ring et al., 2003; Işık et al., 2003, 2004; Bozkurt & Sözbilir, 2004; Bozkurt & Mittwede, 2005; Catlos & Çemen, 2005; Ring & Collins, 2005; Thomson & Ring, 2006; Brichau et al., 2007; Catlos et al., 2010).

Table 3.1 Summary of available age data from the areas or basins that studied in this thesis. pla, plateau age; iso, isochron age; tgas, total gas age.

Area/basin	Unit	Study	Methods			
			Material used	Rb-Sr (Ma)	K-Ar (Ma)	Ar-Ar (Ma)
Çandarlı-Dikili	Dikili group	Borsi et al., 1972	biotite		16.7, 17.3, 17.6	
		Aldanmaz et al., 2000			15.2, 15.5	
Cumaovası	Cumaovası volcanics	Borsi et al., 1972	whole rock	12,5		
		Genç et al., 2001			9,0	
	Yamanlar volcanics	Borsi et al., 1972	mafic fraction		19,2	
Foça	Foça volcanics	Altunkaynak et al., 2010	biotite, plagioclase			16.6, 16.5, 16.1, 16.2 (pl
	Foça alcaline volcanics	Altunkaynak et al., 2010	biotite, plagioclase			14.2, 14.6, 14.7 (pla)
Karaburun	Yaylaköy volcanics	Helvacı et al., 2009	whole rock			17 (iso)
		Borsi et al., 1972	whole rock		21.3, 19.2	
	Karaburun basalt	Türkecan et al., 1998	ground mass		16.0, 18.5	
	Kocadağ volcanics	Helvacı et al., 2009	whole rock			17.5 (iso)
		Borsi et al., 1972	whole rock		16,6	
		Türkecan et al., 1998	whole rock		17,3	
	Armağandağ volcanics	Borsi et al., 1972	ground mass, biotite		18.2, 17.0	
		Helvacı et al., 2009	ground mass			17.3 (tgas)
	Uzunkuyu intrusives	Türkecan et al., 1998	whole rock		15,4	
		Helvacı et al., 2009	whole rock			16.7 (iso)
Urla	Urla volcanics	Borsi et al., 1972	biotite		11,9	
	Ovacık basalt	Borsi et al., 1972	whole rock		11,3	
Yamanlar	Yamanlar volcanics	Ercan et al., 1996			21.0, 16.8	
Yuntdağ	Yuntdağ volcanics	Ercan et al., 1996	whole rock	17,0		

(v) The *Quaternary* volcanism represents the latest volcanic products of the western Anatolia and is represented by the Kula volcanics (Fig. 3.2). The Kula volcanics are dominantly sodic in nature while the older volcanic rocks of western Anatolia are dominantly potassic in nature (e.g., Ercan, 1993; Richardson-Bunbury, 1996; Savaşçın et al., 1999; Tokçaer et al., 2005). The Kula volcanics are composed mainly of flood basalts, tuff and tephras produced from more than 80 small cinder cones within a couple of extrusion stages. It's interesting to note that, on the tuff layers belonging to Kula Volcanics human footprints are reported (Ercan, 1993; and references therein). According to Ercan (1993), Savaşçın et al. (1999), Tokçaer et al.

(2005) the Kula volcanics are located at the northern rim of the Gediz graben and are formed under the control of WNW–ESE-trending graben-bounding faults.

3.3 $^{40}Ar/^{39}Ar$ Dating

3.3.1 Methodology

The $^{40}Ar/^{39}Ar$ technique uses the decay of ^{40}K to ^{40}Ar to determine the age of a mineral and in this sense the method is similar to the more conventional K-Ar method (see MacDougall and Harrison, 1999 for detailed comparison). In the $^{40}Ar/^{39}Ar$ technique samples are irradiated in a nuclear reactor to convert a portion of the non-radiogenic ^{39}K to ^{39}Ar (produced from irradiation of ^{39}K). The produced ^{39}Ar acts as a proxy parent isotope with the ratio of ^{40}Ar and produced ^{39}Ar used to calculate an age. One advantage of the $^{40}Ar/^{39}Ar$ technique is that the daughter and 'parent' products can be measured simultaneously on the same aliquot of sample. In a $^{40}Ar/^{39}Ar$ stepwise heating experiment samples are progressively heated *in vacuum* by either a laser or vacuum furnace until fusion. The gas released from each step is purified and 5 isotopes of argon are measured using a static mass spectrometer. $^{40}Ar/^{39}Ar$ ages are calculated after correcting the data for system backgrounds, radioactive decay of ^{37}Ar and produced ^{39}Ar, mass discrimination, isotopic interferences, fluency gradients and atmospheric contamination (see MacDougall and Harrison, 1999 for a detailed discussion). $^{40}Ar/^{39}Ar$ age spectra are obtained by combining results from a step-heating experiment in order of increasing temperature or cumulative release of produced ^{39}Ar.

A plateau age represents a flat portion of the age spectrum and is normally defined as comprising at least three consecutive steps that are within 2σ of the plateau age and contain more than 50% of the gas released. The term "mean age" is commonly used to define the mean of age steps that do not fit the criterion for a plateau.

3.3.2 Sample Preparation Procedure

The thirty-seven freshest samples within the İBTZ (Çandarlı, Cumaovası, Karaburun, Urla, Yamanlar and Yuntdağ) were selected for $^{40}Ar/^{39}Ar$ dating (Fig. 3.3, Table 3.2). The specimens were taken from dykes, lava flows (some of them columnar jointed), and associated pyroclastic rocks. The field identifications of the samples were noted as andesite, dacite, rhyolite, basaltic andesite and basalt. They are processed in Vrije Universitate (Free University) of Amsterdam (the Netherlands) for mineral separation and isotopic calculations.

First, all the samples were crushed, washed and sieved separately. From each crushed bulk fractions of 250–500 μm were extracted. Depend on the lithology one or two (if possible) of main mineral fractions for each rock sample; such as sanidine, biotite, plagioclase and groundmass were separated using standard heavy liquid and magnetic separation techniques. Then all suitable crystals were handpicked under the microscope. Separated groundmass fractions were also leached with nitric acid about one hour in an ultrasonic bath to clean the crystals. 10–30 mg of material from each sample was wrapped in Al-foil and loaded in a 15 mm ID quartz vial. Fish Canyon Tuff sanidine standard (28.201 ± 0.023 Ma modified from Renne et al., 1998) was wrapped in Cu-foil and loaded at the top and bottom positions and between each set of 3 or 5 samples. The vial was irradiated in the High Flux Reactor (Petten, the Netherlands) in the cadmium shielded RODEO P3 position for 18 hours. After irradiation, samples and standards were loaded in 2 mm diameter holes of a copper planchet and placed in an ultra-high vacuum extraction line. Samples and standards were stepwise heated or directly fused. The gas was analyzed with a Mass Analyzer Products LTD 215–50 noble gas mass spectrometer.

The crystal fractions have been measured by stepwise heating with a 24W Ar-ion laser. The Fish Canyon standards have been preheated using a defocused laser beam with an output of 2 W (samples did not glow and gas was pumped away) to remove undesirable atmospheric argon. After the preheating step the standards were analyzed by total fusion. Experiments were replicated 7 to 10 times for single crystals of the Fish Canyon standard sample. Beam intensities were measured in a peak-jumping

mode over the mass range 40–36 on a secondary electron multiplier. For data collection, the mass spectrometer is operated with a modified version of standard MAP software. Data reduction was carried out using the *ArArCalc* (v2.2) software of Koppers (2002). Each analysis was corrected for mass discrimination and system blanks. System blanks were measured every 3 steps. Mass discrimination was monitored by frequent analysis of $^{40}Ar/^{38}Ar$ reference gas pipette aliquots. The irradiation parameter J-value for each unknown was determined by interpolation using a second-order polynomial fitting between the individually measured standards.

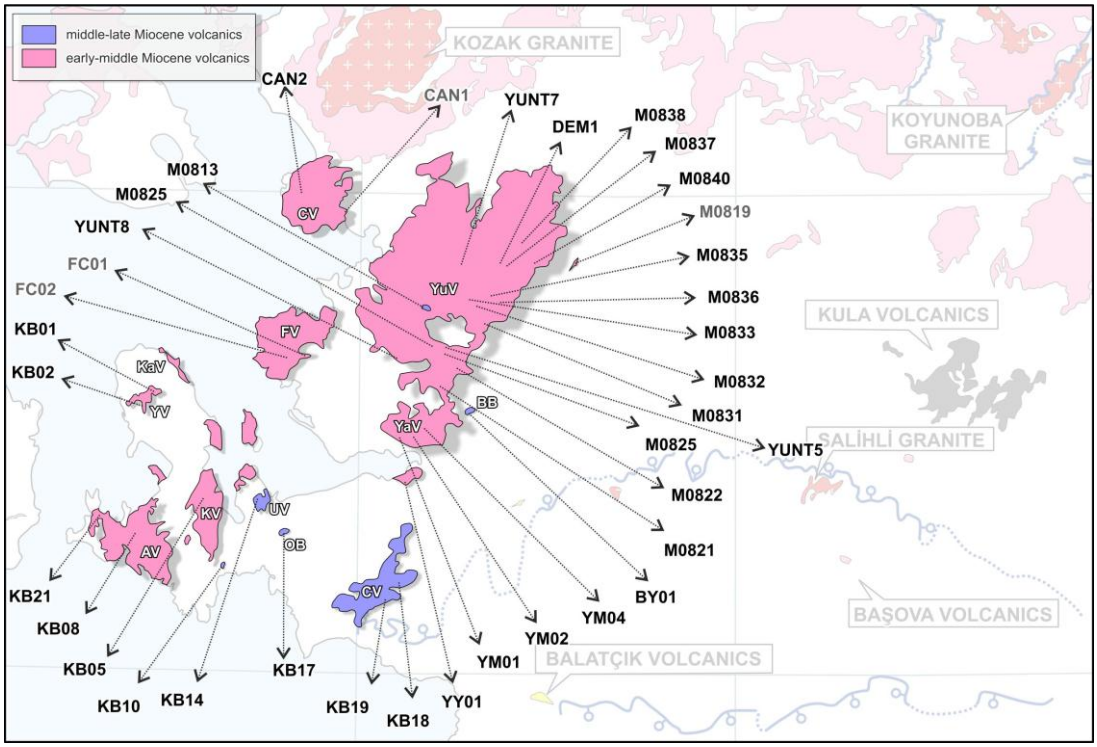


Figure 3.3 Simplified geological map (from Fig. 3.2) of volcanic areas and sample locations for $^{40}Ar/^{39}Ar$ geochronology study. Cv, Çandarlı-Dikili area; Yuv, Yuntdağ volcanics, Fv, Foça volcanics; Yav, Yamanlar volcanics; Bb, Beşyol basalt; Kav, Karaburun volcanics; Yv, Yaylaköy volcanics, Kv, Kocadağ volcanics; Av, Armağandağ volcanics; Uv, Urla volcanics; Ob, Ovacık basalt; Cv, Cumaovası volcanics. Sample codes indicated in gray did not yield any meaningful result.

Table 3.2 Summary of $^{40}Ar/^{39}Ar$ results. MSWD, mean square weighted deviates; N, number of steps included (excluded) in the plateau age; $^{39}Ar_k$ (%), percentage of $^{39}Ar_k$ released by plateau steps. Errors are given at 95% confidence level. Ages were calculated using the *ArArCalc* software developed by Koppers (2002). All $^{40}Ar/^{39}Ar$ ages were calculated using Steiger and Jäger (1977) decay constants at the 2 level and include the analytical error and error in irradiation parameter (J value).

Lab ID	Irradiation	Sample ID	Mineral	Fraction (mm)	J value	MSWD	N	$^{39}Ar_k$ (%) in plateau	K/Ca	Plateau age (Ma)	Total fusion age (Ma)	Inverse isochron age (Ma)
10m0136	VU82-B4	**KB01**	ground mass	250-500	0.0032419	11.63	7(6)	56.74	0.297 ± 0.034	17.96 ± 0.20	18.30 ± 0.25	**16.98 ± 0.36** ✓
10m0139	VU82-B7	**KB03**	ground mass	250-500	0.0031948	1.74	11(4)	92.85	0.177 ± 0.019	**16.50 ± 0.16** ✓	16.57 ± 0.14	15.64 ± 1.16
10m0138	VU82-B6	**KB05**	ground mass	250-500	0.0032095	0.58	8(6)	74.35	0.847 ± 0.053	**17.55 ± 0.18** ✓	18.05 ± 0.17	17.50 ± 0.52
10m0132	VU82-B1	**KB08**	ground mass	250-500	0.0032958	1.38	7 (4)	85.11	0.713 ± 0.049	**16.07 ± 0.11** ✓	15.99 ± 0.10	16.01 ± 0.45
10m0107	VU82-B8	**KB10**	sanidine	400-500	0.0033042	0.35	8(2)	80.46	13.002 ± 0.565	**13.19 ± 0.04** ✓	13.22 ± 0.04	13.20 ± 0.04
10m0133	VU82-B2		ground mass	250-500	0.0032797	1.49	13 (1)	98.96	1.067 ± 0.119	**13.22 ± 0.09** ✓	13.26 ± 0.10	13.3 ± 0.11
10m0137	VU82-B5	**KB14**	ground mass	250-500	0.0032259	0.86	10(3)	78.57	0.409 ± 0.052	**13.02 ± 0.17** ✓	13.29 ± 0.32	12.78 ± 0.49
10m0134	VU82-B3	**KB17**	ground mass	250-500	0.0032627	0.73	9(4)	87.25	0.212 ± 0.033	15.70 ± 0.99	20.45 ± 2.07	**13.69 ± 2.53** ✓
10m0184	VU82-B10	**KB18**	sanidine	400-500	0.0032975	1.83	17(9)	85.65	10.936 ± 5.102	**13.13 ± 0.08** ✓	13.90 ± 0.08	13.10 ± 0.09
10m0183	VU82-B9	**KB19**	sanidine	400-500	0.0033009	1.83	16(6)	83.58	36.463 ± 8.172	**13.12 ± 0.08** ✓	14.02 ± 0.08	13.14 ± 0.09
11m0443	VU88-A3	**KB21**	sanidine	400-500	0.0033890	1.81	7(3)	59.96	0.0267 ± 0.499	**16.27 ± 0.05** ✓	16.26 ± 0.05	16.37 ± 0.13
11m0444	VU88-A4	**YM01**	biotite	250-500	0.0032660	0.46	5(2)	67.65	4.982 ± 0.649	**17.25 ± 0.05** ✓	17.34 ± 0.05	17.19 ± 0.09
11m0484	VU88-A7	**YM02**	biotite	250-500	0.0034058	2.11	7(2)	76.75	3.696 ± 0.572	**17.17 ± 0.05** ✓	17.22 ± 0.04	17.26 ± 0.07
11m0485	VU88-A8	**YM04**	biotite	250-500	0.0034063	1.29	6(3)	62.18	11.938 ± 0.731	**17.44 ± 0.05** ✓	17.50 ± 0.05	17.67 ± 0.23
11m0488	VU88-A15	**YY01**	ground mass	250-500	0.0033927	15.2	5(7)	84.69	0.568 ± 0.313	**17.68 ± 0.16** ✓	17.58 ± 0.11	17.62 ± 0.24
11m0489	VU88-A17	**M0813**	ground mass	250-500	0.0033815	2.05	8(3)	99.74	0.234 ± 0.009	**12.33 ± 0.22** ✓	12.38 ± 0.16	11.43 ± 1.05
	VU88-A18	M0819	plagioclase	200-500	no reliable age	-	-	-	-	-	103.99 ± 0.73	-
11m0508	VU88-A9	**M0821**	biotite	250-500	0.0034063	1.43	13(4)	98.11	4.117 ± 0.462	**17.24 ± 0.05** ✓	16.26 ± 0.05	17.26 ± 0.05
11m0502	VU88-A30	**M0822**	plagioclase	200-500	0.0033010	0.12	2(9)	65.53	0.088 ± 0.003	**17.21 ± 0.18** ✓	17.07 ± 0.15	-
11m0506	VU88-A34	**M0825**	plagioclase	200-500	0.0032772	29.3	3(8)	75.48	0.085 ± 0.006	17.07 ± 0.57	16.97 ± 0.21	**15.99 ± 0.28** ✓
11m0490	VU88-A19	**M0828**	ground mass	250-500	0.0033689	3.76	3(9)	46.78	0.086 ± 0.100	**17.13 ± 0.18** ✓	17.26 ± 0.11	17.60 ± 0.20
11m0492	VU88-A20	**M0831**	ground mass	250-500	0.0033610	2.86	4(8)	53.92	0.082 ± 0.110	19.02 ± 0.13	18.95 ± 0.12	**18.79 ± 0.17** ✓
11m0450	VU88-A10	**M0832**	biotite	200-500	0.0034057	1.42	8(2)	76.94	0.069 ± 0.009	**18.49 ± 0.11** ✓	18.10 ± 0.12	18.45 ± 0.21
11m0452	VU88-A12	**M0833**	biotite	250-500	0.0034282	1.88	8(2)	95.12	0.112 ± 0.015	**18.60 ± 0.12** ✓	18.76 ± 0.11	18.33 ± 0.14
11m0504	VU88-A32	**M0835**	plagioclase	250-500	0.0032895	3.89	2(9)	56.69	0.069 ± 0.010	**18.19 ± 0.31** ✓	18.02 ± 0.15	-
11m0505	VU88-A33	**M0836**	plagioclase	250-500	0.0032841	0.75	7(4)	99.85	0.072 ± 0.010	**18.39 ± 0.15** ✓	18.35 ± 0.16	18.38 ± 0.26
11m0453	VU88-A13	**M0837**	biotite	250-500	0.0034008	0.19	3(7)	41.18	1.764 ± 0.577	**18.31 ± 0.08** ✓	17.54 ± 0.13	18.77 ± 0.73
11m0493	VU88-A22		ground mass	250-500	0.0033498	1.79	8(4)	79.5	5.570 ± 0.270	**18.30 ± 0.11** ✓	18.23 ± 0.11	18.30 ± 0.11
11m0445	VU88-A37	**M0838**	biotite	250-500	0.0032610	1.07	6(1)	85.96	0.133 ± 1.249	**18.68 ± 0.05** ✓	18.31 ± 0.05	18.69 ± 0.08
11m0483	VU88-A5		sanidine	250-500	0.0034001	0.83	10(0)	100.00	0.133 ± 0.014	**18.63 ± 0.35** ✓	18.69 ± 0/.37	18.82 ± 0.62
11m0454	VU88-A14	**M0840**	biotite	250-500	0.0033981	1.05	8(2)	87.32	2.955 ± 0.760	**18.62 ± 0.06** ✓	18.57 ± 0.06	18.76 ± 0.17
11m0494	VU88-A23		ground mass	250-500	0.0033444	0.36	4(8)	59.28	0.660 ± 0.150	**19.66 ± 0.13** ✓	19.70 ± 0.12	19.69 ± 0.16
12m0108	VU92A-11L	**DEM1**	ground mass	250-500	0.0026290	1.55	6(5)	96.06	2.670 ± 0.120	**18.51 ± 0.03** ✓	18.50 ± 0.03	18.48 ± 0.03
12m0105	VU92A-9L	**YUNT5**	ground mass	250-500	0.0026300	1.69	5(6)	91.99	0.524 ± 0.059	**17.27 ± 0.07** ✓	17.09 ± 0.07	17.32 ± 0.15
12m0104	VU92A-8L	**YUNT7**	ground mass	250-500	0.0026340	0.21	4(7)	79.05	1.850 ± 0.240	**18.48 ± 0.05** ✓	18.52 ± 0.05	18.52 ± 0.09
12m0103	VU92A-7L	**YUNT8**	ground mass	250-500	0.0026340	1.58	4(7)	85.42	0.373 ± 0.021	**17.14 ± 0.08** ✓	16.90 ± 0.07	16.03 ± 0.60
		BY01	ground mass	250-500	still on process	-	-	-	-	-	-	-
12m0110	VU92A-13L	CAN1	ground mass	250-500	no reliable age	-	-	-	-	-	51.41 ± 1.09	-
12m0109	VU92A-12L	**CAN2**	ground mass	250-500	0.0026180	1.17	5(6)	96.32	0.362 ± 0.020	**16.15 ± 0.07** ✓	16.07 ± 0.07	16.46 ± 0.39
		FC01	sanidine	250-500	did not radiate	-	-	-	-	-	-	-
12m0106	VU92A-10L	**FC02**	ground mass	250-500	no reliable age	-	-	-	-	-	690.69 ± 18.92	-

All $^{40}Ar/^{39}Ar$-dating samples in this thesis were calculated using the decay constants of Steiger and Jäger (1977). The age for the Fish Canyon Tuff sanidine neutron fluence monitor used in the age calculations is 28.02 Ma (Renne et al., 1998). Errors are quoted at the 1σ level. An age is accepted as an accurate estimate of the crystallization age when the following criteria are fully filled. There should be a well-defined, high temperature plateau for more than 50% of the ^{39}Ar released formed by three or more concordant, contiguous steps. A well-defined isochron should be obtained from the results of the gas fractions on the plateau, while also the $^{40}Ar/^{36}Ar$ intercept for the trapped argon derived from the isochron should not be significantly different from the atmospheric ratio of 295.5 (McDougall and Harrison, 1999). If no plateau age could be calculated or the sample includes atmospheric excess argon, an isochron age was determined. For four samples (M0819, FC01, FC02, and CAN1) plateau age could not be calculated because of high atmospheric excess argon ratio in the specimens (Table 3.2). It should be also noted that the site BY01 is still in process.

3.3.3 Results of $^{40}Ar/^{39}Ar$ Dating

Five samples were collected from the Karaburun area (Fig 3.3). KB01 and KB03 are collected from Yaylaköy volcanics; KB05, KB08 and KB21 represent Kocadağ, Armağandağ, and Foça volcanics, respectively. The $^{40}Ar/^{39}Ar$ dating results indicate that the age of volcanism in Karaburun area ranges between 17.6 and 16.1 My (Fig. 3.4, Table 3.2). Based on these results it can be concluded that these four volcanic events occurred almost in the same time-span (Fig. 3.5).

In the Urla basin three volcanic fields are recognized. They are composed mainly of basalts. From each field representative samples were collected (KB10, KB14, and KB17) (Fig. 3.3). The plateau ages of KB10 (~13.2) and KB14 (~13.0) are relatively similar, however, the plateau age of KB17 is 15.7 Ma which approximately >2.5 My older than those in other two locations. Field evidence indicates that all of these lava flows belong to so called "*upper sequence*", above the mid Miocene unconformity. On the contrary, ~15.7 Ma the plateau age implies that the lava flows in KB17 site

may belong to the *lower sequence*, but this is not the case. Therefore, its decided that 13.7 Ma isochron age suits best for the sample KB17 instead of plateau age because of its stratigraphical position (Fig. 3.4, Table 3.2). In this case, all three ages become consistent (Fig. 3.5).

The samples KB18, KB19, and YY01 are collected from the Cumaovası basin. These samples belong to two different volcanic successions (Fig. 3.3). YY01 characterizes the Yamanlar volcanics in the lower volcano-sedimentary sequence and yielded ~17.7 Ma groundmass age. KB18 and KB19 from the Cumaovası volcanics represents the *upper sequence*, and yielded ~13.1 Ma sanidine age, which is similar to other *upper sequence* ages elsewhere (Figs. 3.4, 3.5; Table 3.2).

Compared to other volcanic fields, more sites (21 sites) were sampled from Yamanlar and Yuntdağ area (Fig. 3.3). This is mainly due to the fact that the internal structures of these areas are very complex and presence of a number of cross-cutting relationships encountered during field studies implies multiple phases of volcanism unlike other areas where the lava flows and related pyroclastics are relatively monotonous. Due to same reasons, the number of paleomagnetic sample locations within this area is also more than the other areas.

The samples labeled as YM01, YM02, YM04, M0821, and M0822 characterize the Yamanlar volcanics. According to $^{40}Ar/^{39}Ar$ results listed on Table 3.2, the analyzed oldest age from these volcanics is 17.4 Ma, and is obtained from the center of the Yamanlar high (biotite age of YM04), while the youngest is 17.3 Ma (biotite age of YM01). These ages are very consistent although the sampling sites are distributed relatively in a very large area (Figs. 3.4, 3.5; Table 3.2).

The Yuntdağ volcanics are the most widespread volcanic rocks in the study area and are aligned approximately NE-SW direction (Fig. 3.3). In order to determine the age of various volcanic pulses within this area geochronological samples were collected from fifteen sites. These include samples M0813, M0825, M0828, M0831, M0832, M0833, M0835, M0836, M0837, M0838, M0840, DEM1, YUNT5,

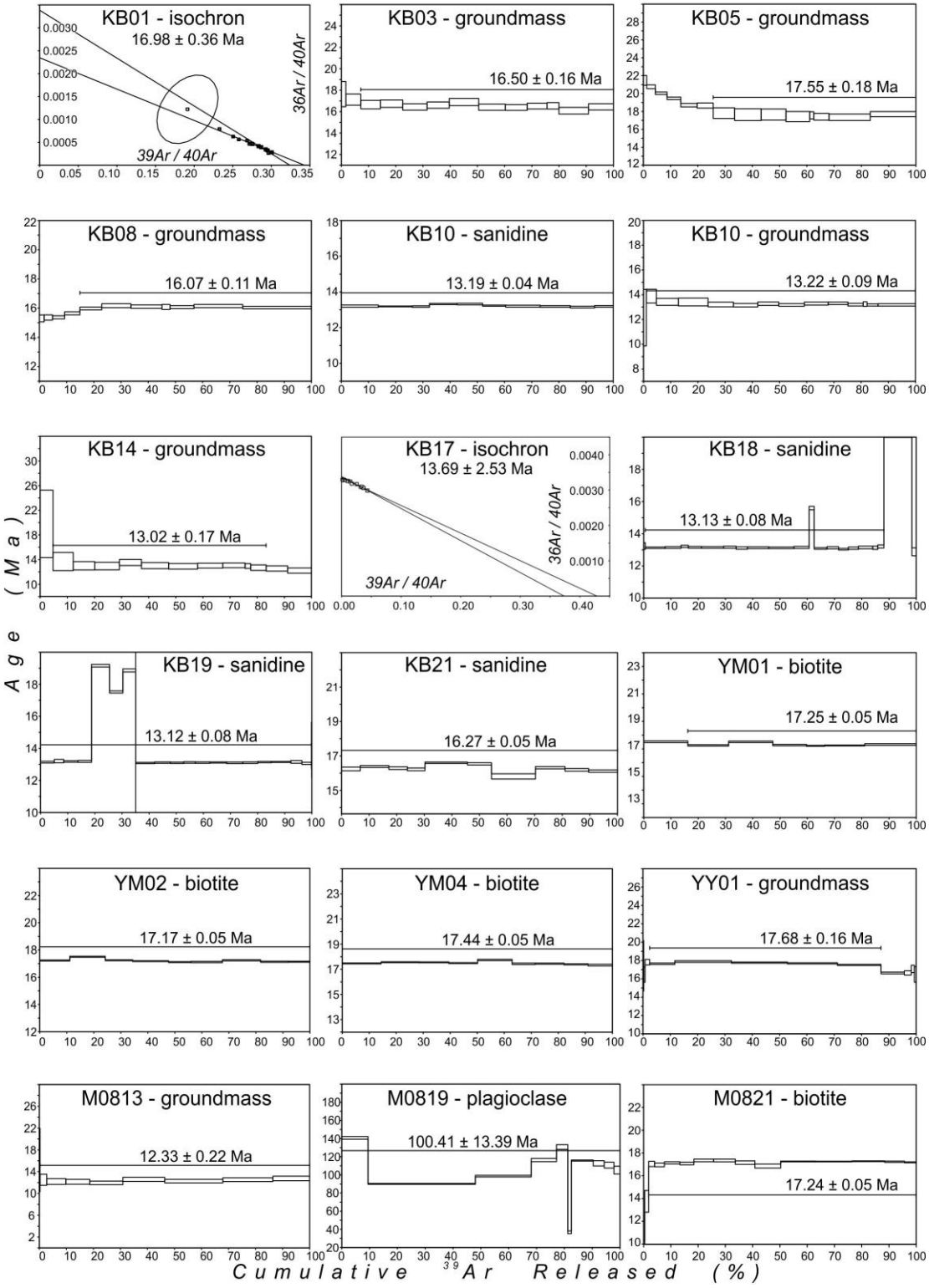


Figure 3.4 Figure showing the incremental heating $^{40}Ar/^{39}Ar$ spectra of 33 samples. The width of the bars/steps represents the 1σ analytical error. Weighed mean plateau ages are displayed. For three samples, the inverse isochron diagrams with their ages are also shown.

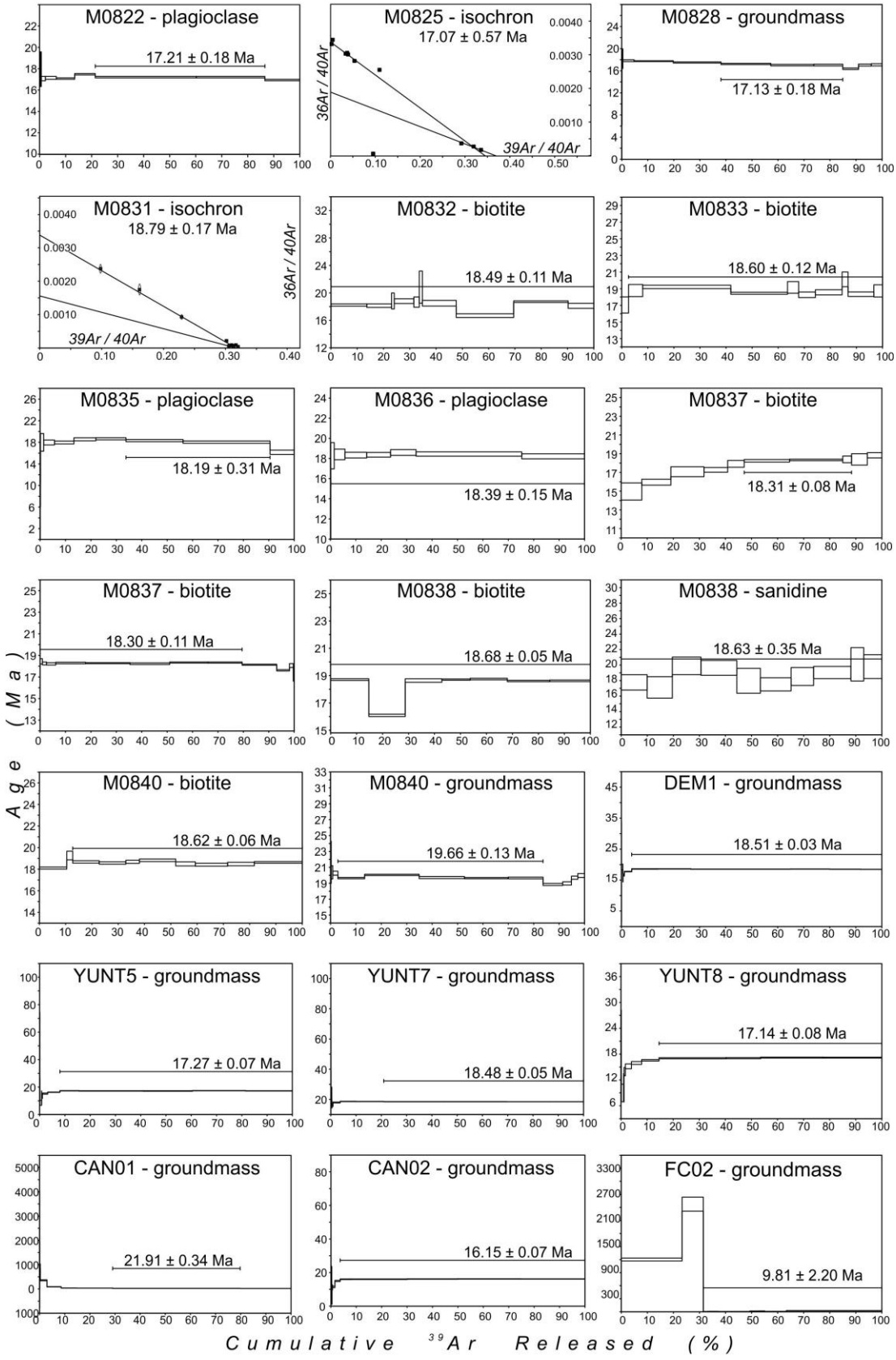


Figure 3.4 continued.

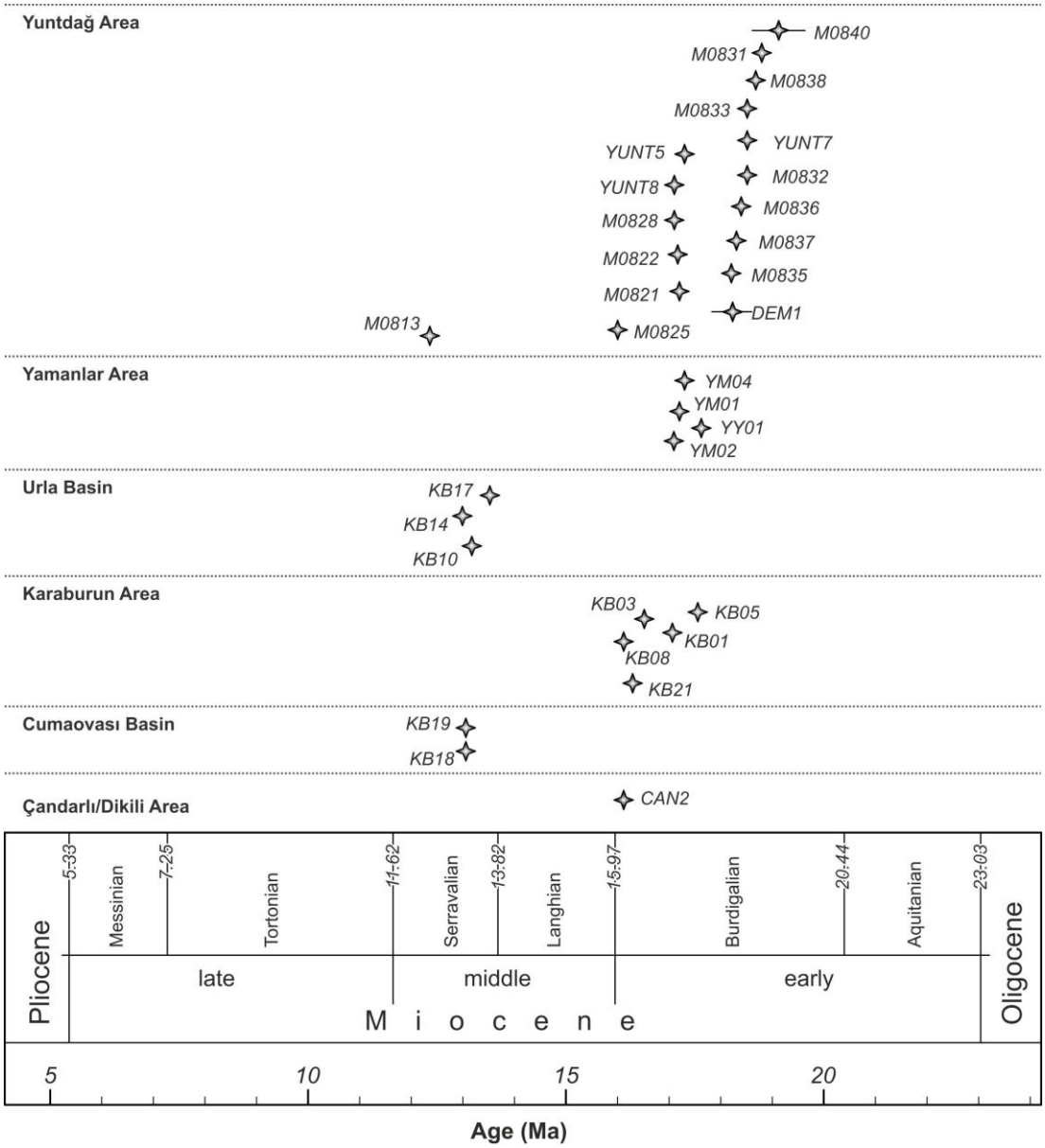


Figure 3.5 Figure showing the chronologic positions of $^{40}Ar/^{39}Ar$ results of this study and spatio-temporal relationship between volcanism and studied areas. It is also surprising that whole volcanic activity along the İBTZ occurred during Burdigalian–Serravalian time interval. Numerical ages for series and stages are taken from 2013-International Chronostratigraphic Cart (http://www.stratigraphy.org/ICSchart/ChronostratChart2013-01.pdf)

YUNT7, and YUNT8; they are processed for the $^{40}Ar/^{39}Ar$ dating. The lithology of the samples includes andesite, dacite, perlite, and basalts. The minerals plagioclase, biotite, and ground mass are used for dating. Except the sample M0813, all other samples yielded ages ranging between 17.1 (ground mass age of M0828) and 19.7

Ma (ground mass age of M0840) (Fig. 3.4, Table 3.2). Surprisingly, the analyzed groundmass material from the sample M0813 collected in the area to southwest of Türkmenköyü yielded 12.3 Ma. The host lithology of the sample has also characteristic features, such as columnar jointing and its olivine-bearing basalt similar to the basaltic lava flows from Urla basin (Fig. 3.5, Table 3.2). Therefore, its concluded that this basalt must be belonging to the upper sequence of middle-late Miocene age and were most probably emplaced along the Güzelhisar fault zone.

In addition to these, in order to check the consistency of the results two different crystals were analyzed from four samples. This is performed first for biotite, and then for groundmass. The obtained ages indicated that the results are consistent. For example, the isotopic age obtained from the biotite minerals and the groundmass for the sample M0837 yielded the same ages as 18.3 Ma (Figure 3.4 and Table 3.2).

CHAPTER FOUR
STRUCTURAL FEATURES AND TECTONICS OF THE İZMİR–BALIKESİR TRANSFER ZONE

4.1 Introduction

The Cenozoic deformation and related basin formation in western Anatolia is one of the hot topics in geoscience research since last decades within the active framework of Africa–Europe convergence zone. This is mainly due to the complex deformation history of the region where intense deformation and associated metamorphism, basin formation and volcanism took place coevally. Şengör et al. (1985), Bozkurt (2001, 2003), and Ersoy et al. (2010) have discussed and summarized the main ideas on Cenozoic tectonics and related basin formation history in this (mainly) extensional system. Despite the large number of studies in the region only few have appreciated the importance of strike-slip faulting in western Anatolia, except the early studies of Kaya (1979, 1981), and Şengör (1987), and the more recent studies of, Ring et al. (1999), Bozkurt (2001), Özkaymak & Sözbilir (2008), Uzel & Sözbilir (2008), Sözbilir et al. (2009, 2011) and Uzel et al. (2012). In particular, Uzel & Sözbilir (2008) provided first convincing field evidence for the existence of a major strike-slip zone in the region, the İzmir–Balıkesir Transfer Zone (İBTZ) that accommodates differential extensional strain between the Cycladic core complex (CCC) in the southwest and the Menderes core complex (MCC) in the northeast (Fig. 4.1). This NE-trending transfer zone also includes a number of secondary strike-slip faults striking generally NE–SW and NW–SE, and normal faults striking E–W, which are seismically active and control the evolution of several Miocene to Recent sedimentary basins (Emre et al., 2005; Uzel and Sözbilir, 2008; Uzel et al., 2012; Sözbilir et al., 2011). The most complete and crucial outcrops of the late Cenozoic sedimentary records and structural evidence are exposed on the coastal part of the Aegean Sea, particularly around İzmir Bay.

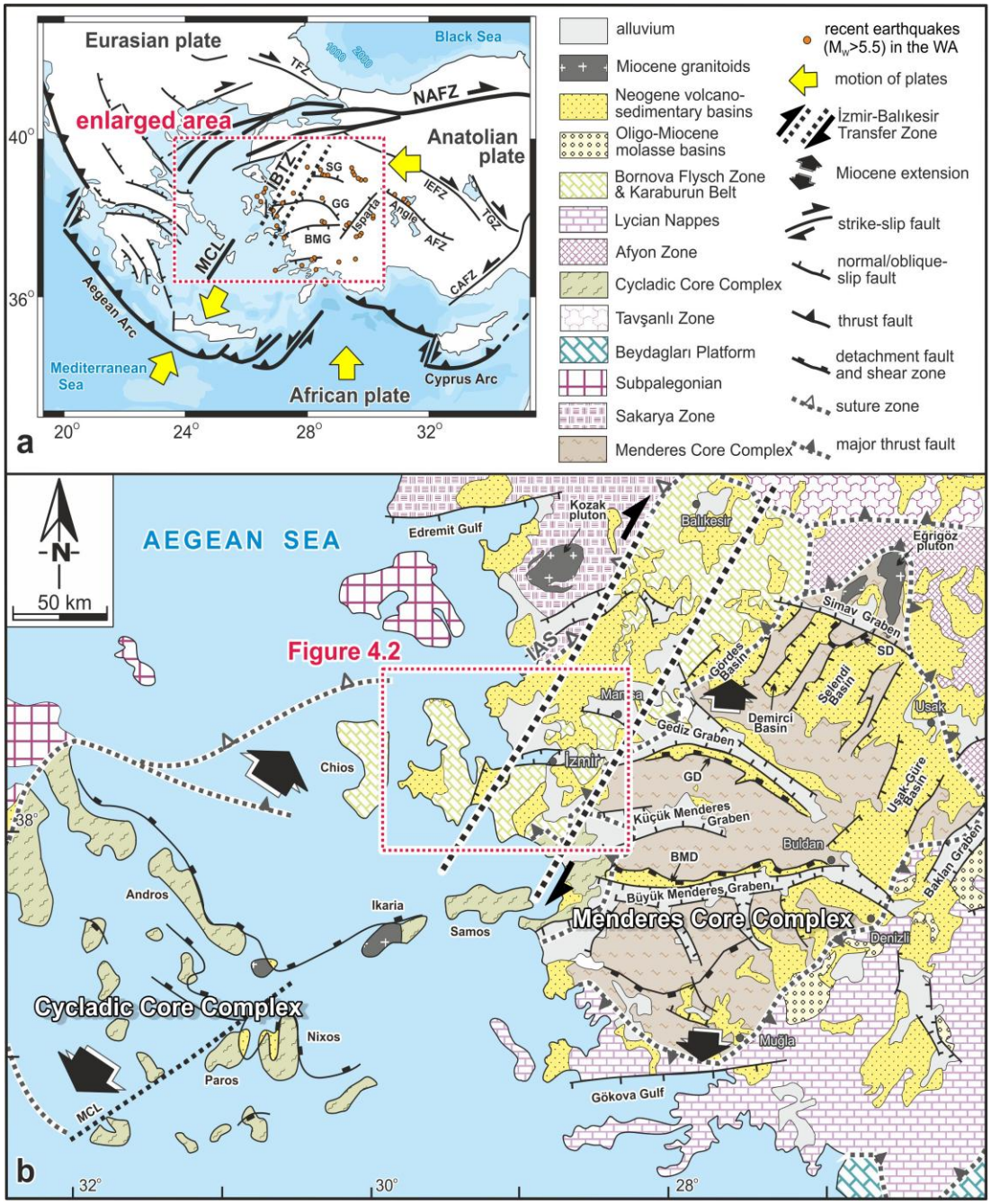


Figure 4.1 a) Simplified map showing the major (plate) tectonic elements and configuration of the Aegean region. NAFZ, North Anatolian fault zone; CAFZ, Central Anatolian fault zone; EPF, Ezinepazarı Fault; TGF, Tuz Gölü Fault; İEFZ, İnönü-Eskişehir fault zone; AFZ, Akşehir fault zone; G, Gökova Bay; BMG, Büyük Menderes Graben; GG, Gediz Graben; SG, Simav Graben; TFZ, Thrace fault zone (redrawn from Taymaz et al., 2007 and compiled from Koçyiğit and Özaçar, 2003; Kaymakçı et al., 2007 and our observations). The seismic data for western Anatolia (WA) are from Tan et al. (2008). b) Simplified tectonic map of western Anatolia (after Sözbilir et al., 2011). GD, Gediz Detachment Fault; BMD, Büyük Menderes Detachment Fault; İAS, İzmir–Ankara Suture Zone.

The İzmir Bay formed in central part of the İBTZ is one of the most distinctive "boot-shaped" bays in the Aegean Sea with Karaburun Peninsula defining its western–northwestern boundary, while the Foça-Yuntdağı and Yamanlar highs delimit it from the north-northeast. The southern boundary is defined by the Seferihisar and Nifdağı highs. It is an approximately 10–20 km wide and 50–60 km long depression. According to topographic and bathymetric data it comprises two depressions, namely the Outer Bay and the Inner Bay (Aksu et al., 1987; Sayın et al., 2006). The Outer Bay is oriented NNW–SSE and forms an approximately 20 km wide and 40 km long depression (Fig. 4.2). The Karaburun Peninsula has a peak altitude of 1200 m (Bozdağ), Foça high is 450 m. Maximum water depth in the Outer Bay is approximately 75 m (Akyarlı et al., 1988; Alpar et al., 1997; Sayın, 2003; Sayın et al., 2006). Based on surface and subsurface morphology, the Outer Bay can be separated into two sub-basins as the Menemen and Gülbahçe sub-basins (Fig. 4.2; Aksu et al., 1987). The inner and the outer bays are separated by a swell where the water depth decreases down to 13 m. The Inner bay trends E–W and approximately 5–7 km wide and 25 km long (Fig. 4.2). It is a relatively small and shallow basin having a maximum depth of 20 m, and it's surrounded by the Yamanlar, Seferihisar and Nifdağı highs. The Yamanlar high has a relatively low peak elevation around 110 m while Seferihisar high rises as high as 1000 m from mean sea level. The eastwards on-shore continuation of the inner bay is the alluvial Bornova plain, delimited in the south by the Nifdağı high.

4.2 Tectonic Framework of the Region

Apart from field-oriented studies, strike-slip activity and recent tectonic activity is also corroborated by earthquake moment tensor solutions of major earthquakes and accumulated GPS data over the last two decades from the region (Kiratzi & Louvari, 2003; Sperner et al., 2003; Zhu et al., 2006; Akyol et al., 2006; Aktuğ & Kılıçoğlu, 2006; Benetatos et al., 2006; Reilinger et al., 2006; Tan et al., 2008; Heidbach et al., 2010). According to Aktuğ and Kılıçoğlu (2006), GPS data obtained around İzmir provides convincing evidence for right-lateral strike-slip faulting and a clockwise

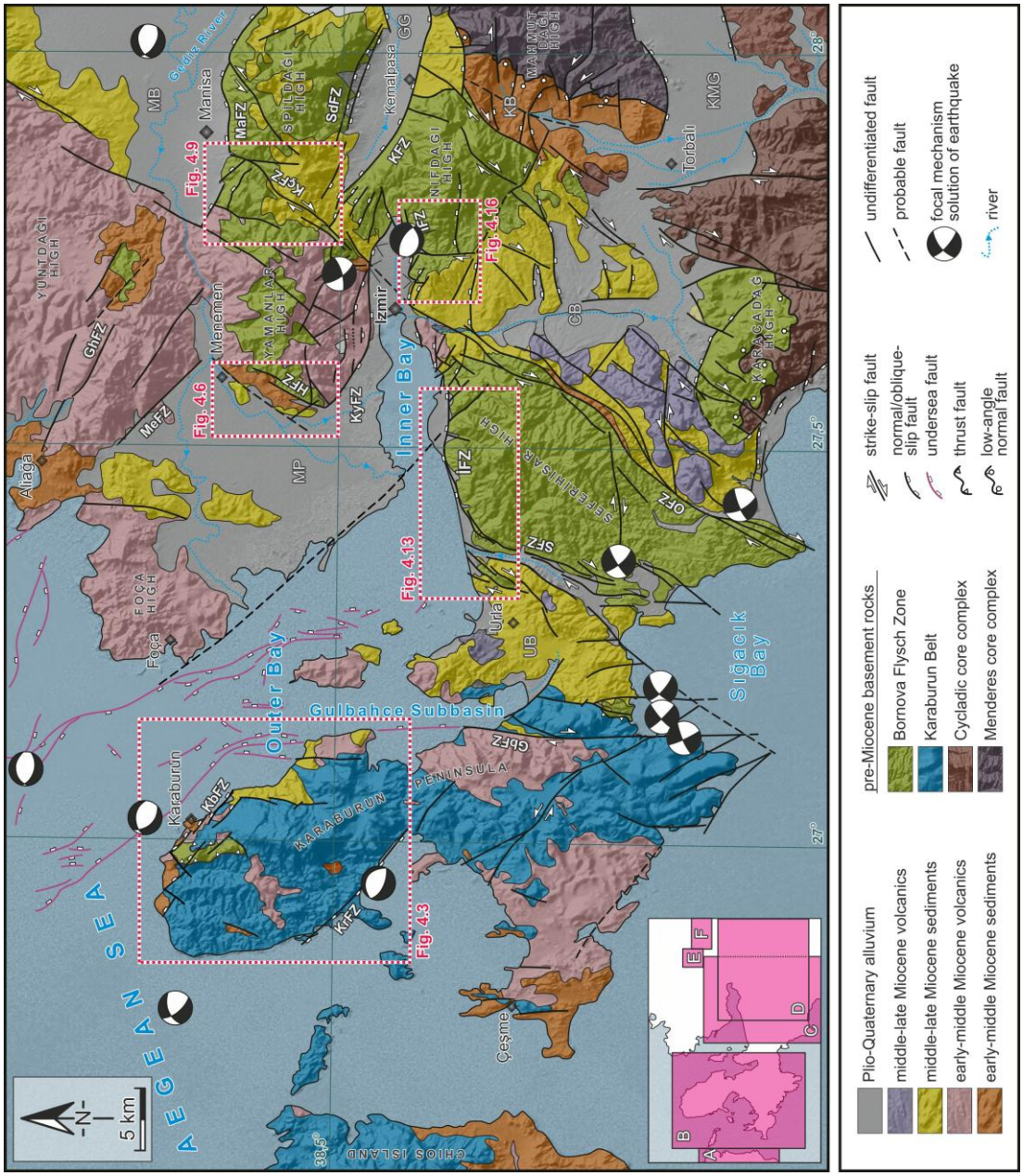


Figure 4.2 Simplified geological map of the İzmir Bay area draped on topographic data. References: (A) Pe-Piper et al. (1995), (B) Çakmakoğlu and Bilgin (2006), (C) Uzel et al. (2012), (D) Sözbilir et al. (2011), (E) Özkaymak et al. (2011), (F) Bozkurt and Sözbilir, 2006); A–F are indicated in the lower-left inset map. Lower hemisphere equal area projection plots of the focal mechanism solutions of main earthquakes are taken from the Earthquake Catalogues for Turkey (Tan et al., 2008); the black (white) parts are compressional (extensional) quadrants. GbFZ, Gülbahçe fault zone; GhFZ, Güzelhisar fault zone; MeFZ, Menemen fault zone; HFZ, Harmandalı fault zone; KyFZ, Karşıyaka fault zone; SFZ, Seferihisar fault zone; OFZ, Orhanlı fault zone; İFZ, İzmir fault zone; KFZ, Kemalpaşa fault zone; SdFZ, Spildağı fault zone; MaFZ, Manisa fault zone; UB, Urla Basin; CB, Cumaovası Basin; KMG, Küçük Menderes Graben; KB, Kocaçay Basin; GG, Gediz Graben; MB, Manisa Basin; MP, Menemen Plain.

rotation, related to E–W shortening and N–S extension. In addition, recent earthquakes around İzmir Bay also provide evidence for distributed strike-slip motion, mainly NE–SW-striking right-lateral and NW–SE-striking left-lateral (Fig. 4.2; Kiratzi and Louvari, 2003; Benetatos et al., 2006; Tan et al., 2008; Tan, 2012). Ocakoğlu et al. (2005) mapped, using seismic reflection data, the off-shore active faults around Karaburun Peninsula and argued that N–S- to NE–SW-trending strike-slip faults are responsible for the deformation and current seismicity in the region. Lykousis et al. (1995) have also reported some Pliocene–Quaternary strike-slip faults around Ikaria and Samos Islands, based on their seismic reflection data. In this contribution, I provide new structural and kinematic data based on recent field studies around İzmir Bay area, which experienced three different phases of deformation since the Miocene. In this context, below I will first describe the general stratigraphy of the late Cenozoic basins in the region. Then, the field data obtained from newly mapped key areas around İzmir Bay will be presented. In the final section, the implications of the presented data will be discussed in the context of the deformation mechanism of the western Anatolian and Aegean region.

In this chapter, I aimed at better constraining the deformation history of the İBTZ by combining field-based structural analysis and a computer-based palaeostress inversion method, using fault slip data. Here, field-based studies mainly focused on: (i) geological mapping of structural elements at a scale of 1/25000, (ii) identifying stratigraphic units for relative dating of the deformation phases, (iii) collection of kinematic data from the mesoscopic structures for construction of palaeostress configurations. The structural data will be presented using stress and strain terminology (Means, 1976; Twiss and Moores, 1992; Marret and Peacock, 1999), and given in text in the order of: first, general description of a structure and supporting field observations; second, presentation and analysis of structural data; third, interpretation of fault kinematics and deformation phases. Depending on the outcrop availability and density of vegetation/urbanization, we collected fault-slip data systematically along the fault zones wherever possible. On some of the faults, overprinting slickensides indicative of two different faulting episodes or deformation phases were observed and they form the basis for the separation of different

deformation phases in the region. Hence, structural observations such as displacement of stratigraphy, style and relative ages of the faults, incompatible shear senses of the cross-cutting faults within the same sampling site, and overprinting/cross-cutting relationships of the features were carefully noted to precisely identify and distinguish the deformation phases. Shear senses along faults were determined by kinematic indicators such as off-set strata, drag of markers, growth fibres in stepped slickensides, crescentic markings, steps and Riedel shear geometry (cf. Means, 1987; Petit, 1987; Hancock and Barka, 1994; Doblas, 1998).

4.3 Late Cenozoic Structures

The first key area is the Karaburun area, located in the northern side of Karaburun Peninsula and covers about 60 km^2. The second key area is the Menemen area, located at the western margin of Yamanlar high and covers approximately 120 km^2. The third one is the Yaka area lying between the Yamanlar and Spildağı highs, and covers some 150 km^2. Finally, with the title of Inner Bay area, I will present two detailed geological map showing the relationships of different fault systems in İBTZ. All key areas are denoted in Figure 4.2.

4.3.1 Karaburun Area

The main late Cenozoic structures mapped around the Karaburun area consist of the Karaburun and Karareis fault zones, NNE-striking conjugate faults and a number of folds (Fig. 4.3).

4.3.1.1 Karaburun Fault Zone (KbFZ)

It is a 2–4 km wide, 25 km long, approximately N50W-striking and NE-dipping fault zone comprising several synthetic faults that display a well-developed step-like morphology with concave/curvilinear range-front. It controls the SW margin of the

İzmir Bay at the NE side of the Bozdağ high (Figs. 4.2 and 4.3). The fault zone starts north of Mordoğan village and runs in a N50°W trend to the Karaburun village, where it bents west to N65°W and bends again to N50°W. Further north, it jumps two times to southwest juxtaposing conjugate faults, and then disappears under the water of the Aegean Sea in a N70°W trend north of Sarpıncık village (Fig. 4.3a). NW of Karaburun village, a couple of relatively small SW dipping antithetic fault is also recognized (Figs. 4.3 and 4.4).

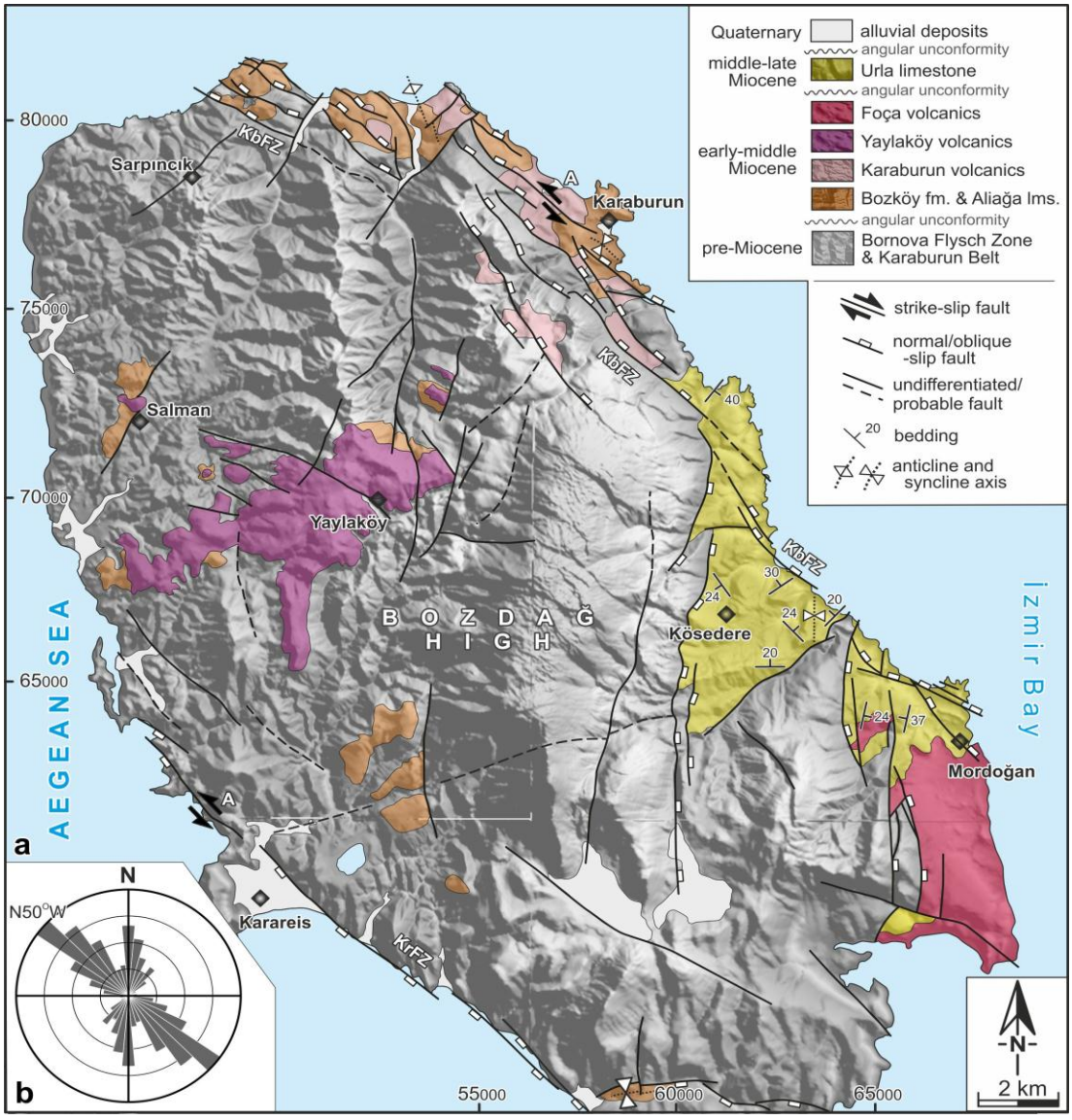


Figure 4.3 (a) Detailed geological map of Karaburun area (compiled from Tatar-Erkül et al., 2008; Helvacı et al., 2009, and this study). "A" refers to older than Miocene strike-slip faulting along the Karaburun and Karareis fault zones. See Fig. 4.2 for location. (b) Length weighted rose diagram of the strikes of all faults in the area. Note that two directions, N50°W and N–S, dominate in the region.

Along the KbFZ, we collected more than 90 fault plane data to establish its kinematic behavior (plots 1A, 2, 3 and 4A in Fig 4.5). The observed slicken-lines along the KbFZ are between 45° and 88°. Depending on the direction of the fault plane and the position of the measurement site along the fault zone, the amount of the obliqueness of the slip vectors and also the orientation of the calculated stress axes (see "4.4. Palaeostress Configuration" section) show some kinematic variation along fault from one tip to the other, in accordance with the nature of faulting (Maniatis and Hampel, 2008). The dip angles of the fault planes are ranging between 50° and 88°, but most of them are more than 75°, surprisingly steep for a normal fault. According to field observations, the general structural style of the KbFZ is identified as an oblique-slip normal fault with an average rake of 60°W, trending in N50°W direction.

Evidence of an older strike-slip faulting with 37 fault slip data, from several locations along the fault zone are also documented along the KbFZ. The computed data is presented (in Fig. 4.5) as projections in 1B and 4B. The observed older slickenside set has a left-lateral strike-slip character represented by slickenlines with an average rake of 20W, and consistently overprinted by younger slickensides having an oblique-slip normal character. Therefore, we suggest that the KbFZ formerly had a strike-slip motion, and has afterwards been reactivated as an oblique-slip normal fault zone. The younger oblique-slip faulting is also documented by seismic events near the KbFZ in outer bay (Fig. 4.2). The KbFZ has cut and displaced the basement rocks of the Karaburun Belt, Bornova Flysch Zone, and the Miocene volcano-sedimentary strata.

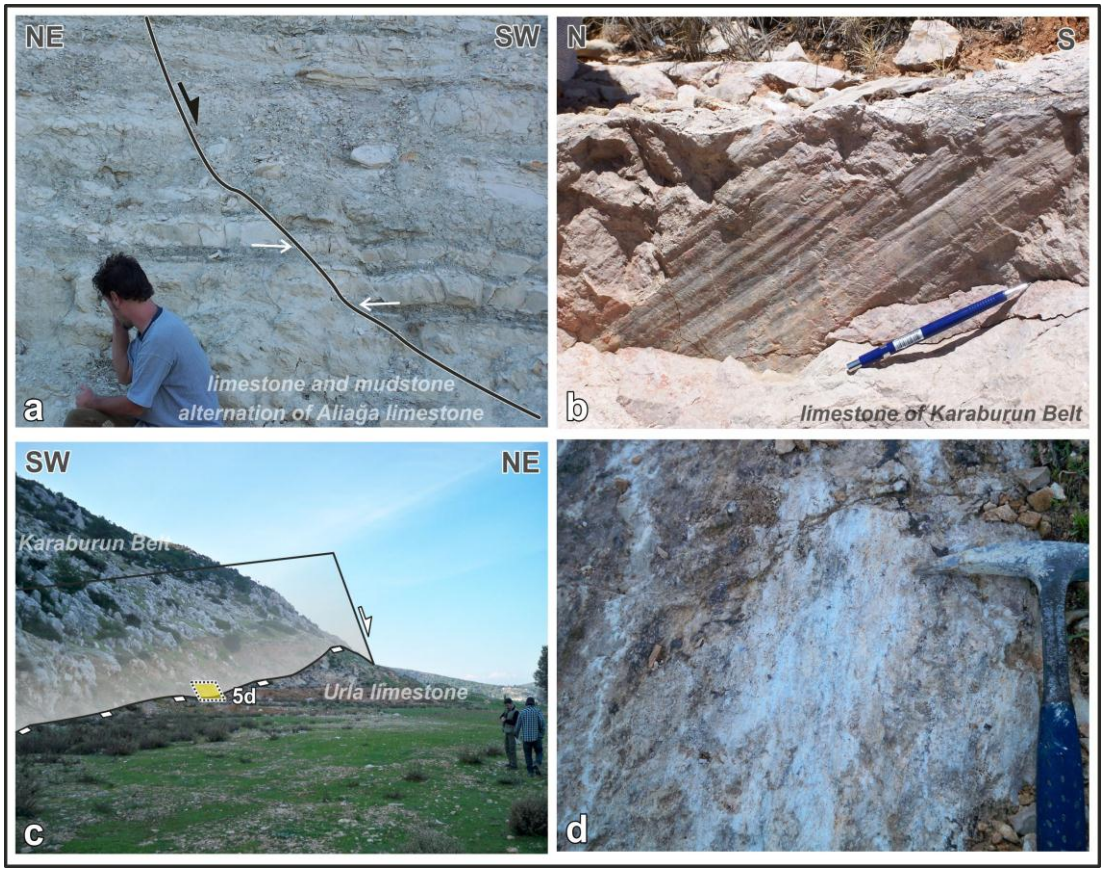


Figure 4.4 Field photos of post-Miocene structures from the Yaka area. (a) A secondary antithetic normal fault parallel to the Karaburun fault zone, W of Karaburun village. (b) Close-up view of older strike-slip faulting along the Karaburun fault zone, SW of Karaburun village. (c) A distinct NNE-striking fault trace west of Kösedere village. (d) Close up view of a normal fault plane with well-preserved slickenlines.

4.3.1.2 Karareis Fault Zone (KrFZ)

The NW-striking KrFZ cuts and displaces the rocks of the Karaburun Belt along the SW margin of Bozdağ High where it delimits the western side of Karaburun Peninsula (Figs. 4.2, 4.3). The zone is 1–3 km wide, 20 km long, and is approximately parallel to the KbFZ on the other side of the Bozdağ high (Fig. 4.3a). The KrFZ also includes several link and antithetic faults with steeply dipping planes. We collected 34 fault plane data along the fault zone. According to computed data, the major strike is around N50°W and the main dip is approximately 75°SW (plots 6, 7A, 7B, and 8 in Fig 4.5). Observed slickenlines range 64 - 80°, characterizing the oblique-slip normal fault character of the KrFZ. Like the KbFZ, the KrFZ also bears

obvious evidence of early left-lateral strike-slip motion: overprinting kinematic indicators show reactivation of the KrFZ as an oblique-slip normal fault zone (plot 7A on Fig. 4.5). On the basis of 8 fault plane data from different locations around Karareis village, the older striation has an average rake of 11°E, whereas the younger ones are around 70°W. Seismicity of the northern Karaburun Peninsula also provides evidence that dip-slip faulting is younger than strike-slip, in good agreement with the field evidence (Fig. 4.2).

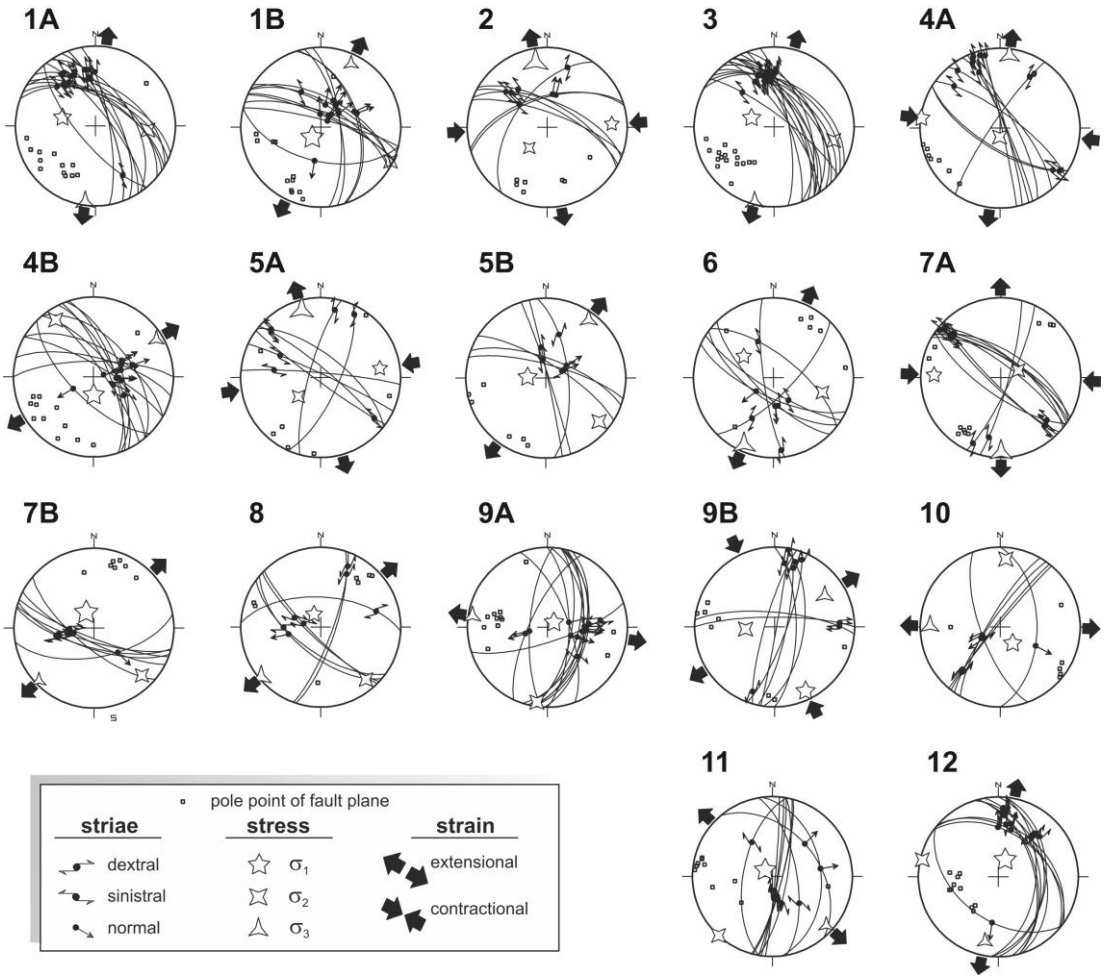


Figure 4.5 Lower-hemisphere equal-area projection of fault planes, slickenlines, and constructed palaeostress configurations for the Karaburun area. Numbers refer to the localities as depicted in Fig. 4.13a.

4.3.1.3 NNE-striking Faults

These faults are predominantly observed around the N and NE sides of the Bozdağ High (Fig. 4.3). More than 50 fault plane measurements along the NNE-striking faults show that they are generally steeply dipping (around 70°) and have mainly a strike-slip character (Fig 4.5). As an example, N of Sarpıncık where the Miocene strata are cut and deformed by a series of left-lateral NE-trending strike-slip faults (Fig. 4.4b), kinematic data show left-lateral strike-slip faulting with a minor normal component as indicated by sub-horizontal rakes (15–25°SW) (plot 9B on Fig. 4.5). The average dip of the fault planes is approximately 80° to NW.

West of Kösedere village, four obvious NNE-striking structural lineaments are mapped, where the limestones of the Karaburun Belt are juxtaposed with Miocene carbonates and clastics of the Urla Formation (Fig. 4.3a, and 4.4c-d). These structures display a typical step-like normal-fault morphology stepping down eastwards. Along these, we collected 14 fault plane data to understand the nature of faulting. Some of the fault planes have locally preserved slickensided surfaces showing normal slip (>60°), on average dipping 60°E (plot 12 on Fig 4.5). West of Mordoğan, another NNE-trending fault set was mapped and archived with 14 fault plane data. It delimits the eastern part of the Bozdağ High, cuts and displaces volcano-clastics of the Foça Formation and lacustrine sediments of the Urla Formation (Fig. 4.3) with several sub-parallel faults having an average dip of 55°E. Well-exposed slickenlines on these planes show normal fault activity with a minor left-lateral strike-slip component as indicated by sub-vertical rakes (50–85°N) (plot 11 on Fig. 4.5). The NNE-striking faults observed around Kösedere and Mordoğan villages have cross-cutting relationships with the fault sets of the KbFZ (Fig. 4.3).

Additionally, along the one NE-striking fault located at 2 km NE of Sarpıncık village, we collected 13 overprinted slickenside data supporting the evidence for two different styles of faulting. Here, the red clastic part of the Miocene strata (Bozköy Formation) is cut and offset by high-angle fault planes dipping NW and shows a well-preserved overprinting expressed as two sets of slickensides. The early set has average rakes of 80°S while the younger set has average rakes of 25°S (projections

9A and 9B, respectively). Likewise, the other NNE-striking faults observed around Sarpıncık and Karaburun villages also have cross-cutting relationships with the faults of the KbFZ.

4.3.1.4 Folds

A series of anticlines and synclines were mapped in the Karaburun distinct. The average lengths of these folds are not more than 2 km. They are developed mainly in the lower sequence of Miocene strata around Karaburun town and at the southernmost part of Karaburun Peninsula (Fig. 4.3). They are relatively small, open to gently plunging folds. Except east of Kösedere village, their axes are mostly parallel to the nearby normal faults, which indicates that they are forced (drag) folds developed on top of rotating fault blocks along horizontal axes (i.e. cover deformation).

4.3.2 Menemen Area

In this area, three different fault and fold sets that are related to deformation of the Miocene units have been recognized during field studies (Fig. 4.6). These structures include NE-striking strike-slip faults (Harmandalı fault zone), approximately E–W striking oblique-slip faults, NW-striking strike slip faults, and NNE-trending folds. Apart from that, part of a regional NE–SW-trending strike-slip fault system, which we named the Harmandalı fault zone and which delimits the Yamanlar high to the west, is documented here for the first time together with its kinematic characteristics.

4.3.2.1 Harmandalı Fault Zone (HFZ)

It runs along the western scarps of the Yamanlar High and can be traced for approximately 15 km between Izmir Bay and Menemen town (Fig. 4.6).

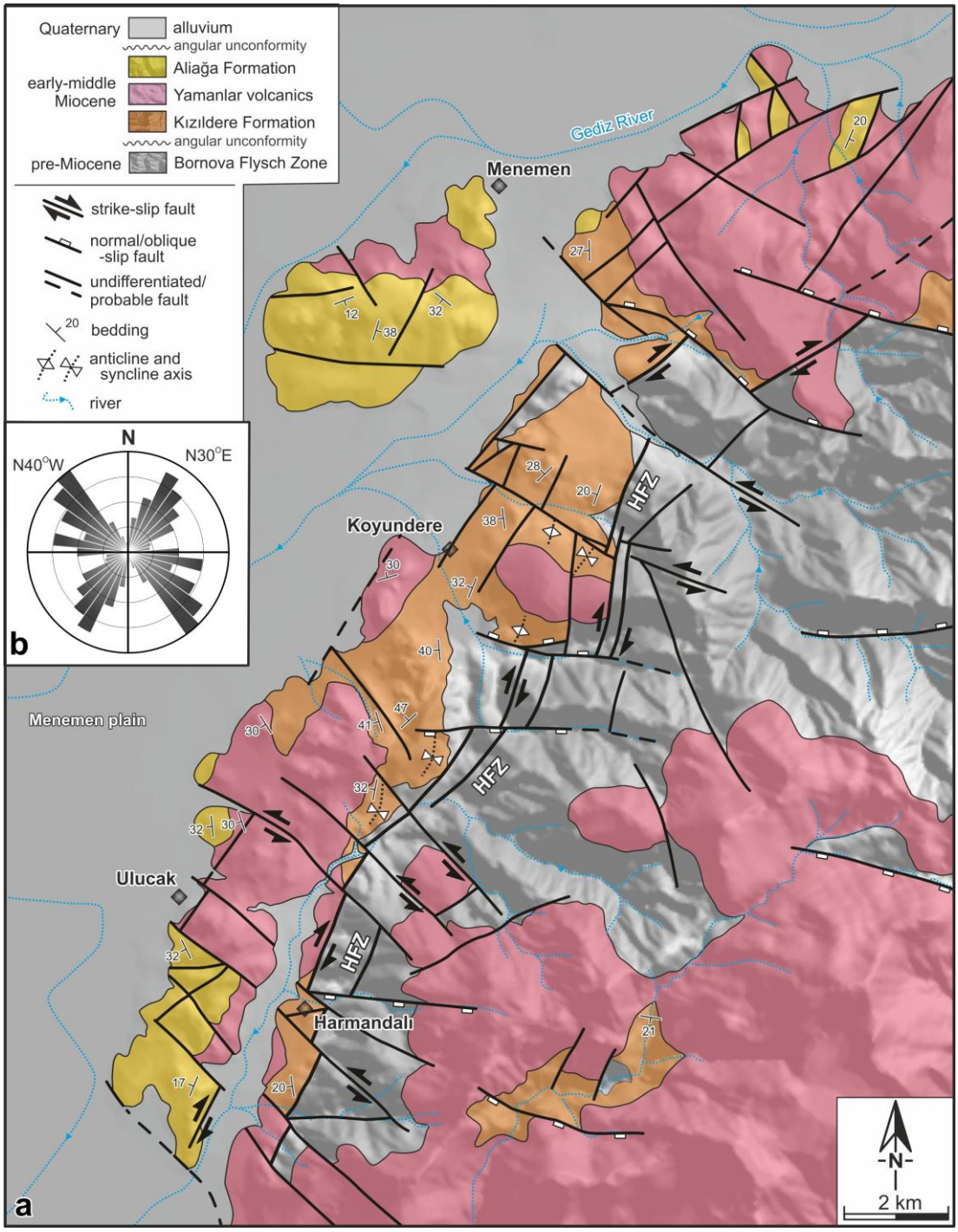


Figure 4.6 (a) Detailed geological map of the Menemen area (see Fig. 4.2 for location), and (b) rose diagram of faults in the area. Note the two dominant directions of N40°W and N30°E. HFZ, Harmandalı fault zone.

The fault zone comprises several relatively small-scale faults striking mainly in a NE–SW-direction. The Yamanlar volcanics, the Kızıldere Formation and the rocks of Bornova Flysch Zone are tectonically juxtaposed along the fault zone (Figs. 4.6a and 4.7a). Sixty nine fault planes were measured along the HFZ, projected as plots of 13, 14, 16, and 18 (Fig. 4.8). According to kinematic data, the main motion on the fault surfaces is right-lateral strike-slip with an average rake of 20° (Fig. 4.7b). Here, the fault planes have an overall strike of between N5°E and N65°E (Figs. 4.6b and 4.8), and dip of approximately 75° to the NW. The HFZ is systematically cut and displaced by E–W-trending faults (Fig. 4.6a). According to the regional picture of the main faults, the distinct NE trending HFZ controls the Menemen plain and it seems that this zone was extending to the south of İzmir Bay into the Seferihisar fault zone. Later, it was dissected by E–W faults that control the northern (Karşıyaka fault zone) and southern margin (İzmir fault zone) of the inner İzmir Bay. The Seferihisar fault zone bends and merges clearly with the İzmir fault zone, but the younger evidence about the joining of Harmandalı fault zone and Karşıyaka fault zone is mostly under the alluvium because of the rapid sedimentation in the Menemen plain (Fig. 4.2).

4.3.2.2 E–W-trending Faults

These faults are developed all along the HFZ, the western margin of Yamanlar high (Fig. 4.6). Several well-exposed fault planes strike approximately E–W (Fig. 4.6b), with an average dip of 65° both N and S (Fig. 8c). Based on 22 fault plane data, well-preserved slickenlines on these planes show oblique-slip motion with right-lateral component as indicated by rakes ranging between 22° and 70° (plots 15 and 17 on Fig 4.8). In map view, the E–W-trending faults cut and displace some faults belonging to the HFZ, and are in turn displaced by NW-trending faults around Harmandalı village (Fig. 4.6).



Figure 4.7 Field photos of post-Miocene structures from Menemen area. (a) The reddish sandstone and conglomerate alternation of the Kızıldere Formation juxtaposed with intensely deformed sandstones of Bornova Flysch Zone along the Harmandalı fault zone. (b) Close up view of slickenside surfaces. (c) Well-exposed fault planes of E–W striking faults. Oblique-slip offset of the Kızıldere Formation is very obvious. (d) A field photo of NW striking strike-slip fault with minor normal-slip component.

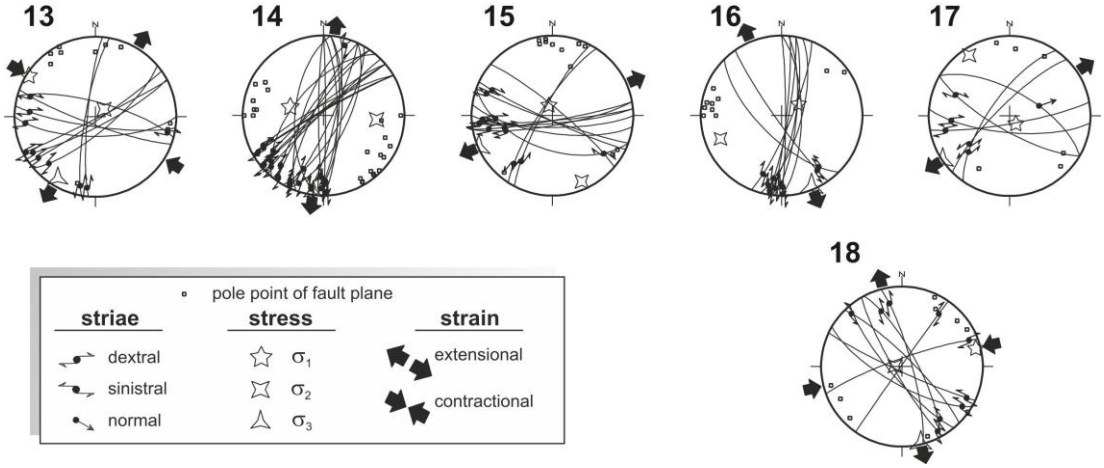


Figure 4.8 Lower-hemisphere equal-area projection of fault planes, slickenlines, and constructed palaeostress configurations for the Menemen area.

4.3.2.3 NW-trending Faults

The mapped NW–SE oriented faults are apparently the youngest structures in the area. These were clearly expressed by the linear NW-trending topographic valleys in the morphology (Fig. 4.6). The observed fault planes show that the main motion along these faults is left-lateral strike-slip with a minor normal component (Fig. 4.7d). The fault planes are well preserved, striking N30–50°W (Fig. 4.6b) with an average dip of 80OSW and NE, and the observed striations having rakes less than 20° (plot 18 on Fig. 4.8). In particular, NE of Koyundere, a series of NW-trending strike-slip faults cut and displaced the Miocene strata, but no Quaternary activity of these faults could be observed because of being mostly concealed by alluvial deposits.

4.3.2.4 Folds

Several mesoscopic anticlines and synclines trending in a NNE-direction are observed in the Menemen area (Fig. 4.6). They have occurred mainly in the Kızıldere Formation and are mostly sub-parallel to the Harmandalı fault zone and are almost always parallel to the nearby oblique faults. They are mostly open and gently plunging southwest to northeast. From the Yamanlar High westwards towards the

basin center, these folds are getting more open and disappear in the younger beds. Based on these relationships we propose that these faults are drag folds developed on the hanging-wall block of normal fault blocks (Fig. 4.6c).

4.3.3 Yaka Area

The area lying between the Yamanlar and Spildağı highs along the northern margin of the inner bay of İzmir is mainly shaped by strike-slip faults, namely of the Karaçay, Gürle, Manisa, Kemalpaşa and Spildağı fault zones (Figs. 4.2 and 4.9). Özkaymak and Sözbilir (2008), and Sözbilir et al. (2011) previously documented some of these structures, especially the normal faults along the margin of the Manisa Basin and along the western rim of the Gediz graben, respectively. In particular, the field observations on the Manisa and Karaçay fault zones by Özkaymak and Sözbilir (2008) support reactivation on NE-trending faults. Here, we provide additional field data and kinematic analyses on their continuation in the Yaka Area, to shed more light on the structural link between NE-SW and E–W striking fault systems - it plays a key role in understanding the kinematic relationship between strike-slip and normal faults in western Anatolian extensional tectonics. Additionally, in the Yaka area two distinct fold patterns, trending N–S and E–W, within the Miocene strata are recognized and mapped during field studies.

4.3.3.1 Karaçay Fault Zone (KçFZ)

This is a 2 km wide and 15 km long NE-striking fault zone tracing between the Yamanlar and Spildağı highs (Figs. 4.2 and 4.9). It cuts and deforms the Bornova Flysch Zone, and the Miocene volcano-sedimentary strata (Fig. 4.10). We collect 59 fault plane data along the KçFZ, and present them as plots 19A, 19B, 20A, and 20B in Fig 4.11. The fault zone includes strike-slip faults, which were formed by a principal displacement zone striking between N5–40°E, and Riedel faults striking between N–S and N45°W (Fig. 4.9b).

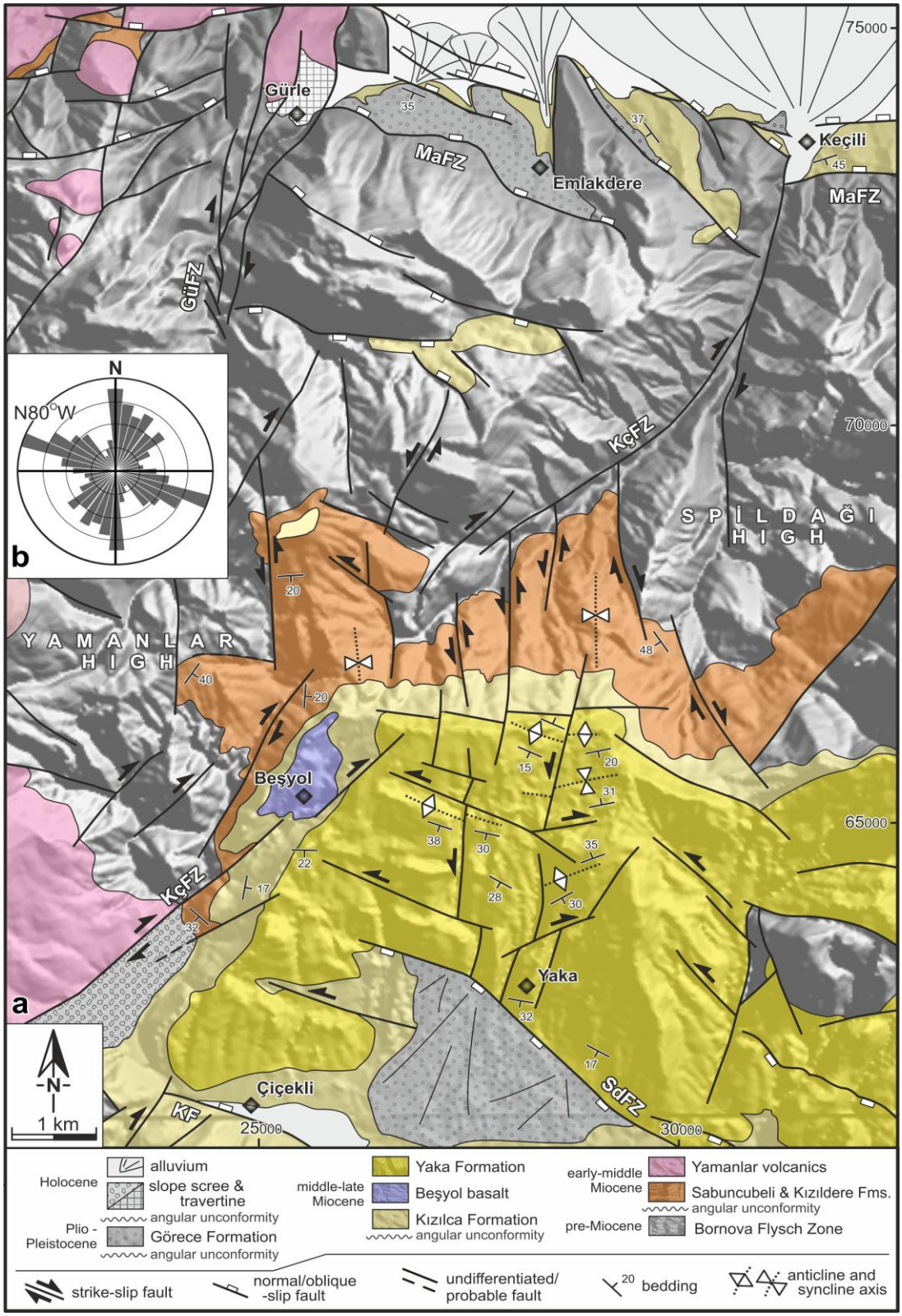


Figure 4.9 Detailed geological map of the Yaka area (northern side of the mapped area is compiled from Özkaymak & Sözbilir, 2008; southern side is from this study). MaFZ, Manisa fault zone; GüFZ, Gürle fault zone; KçFZ, Karaçay fault zone; SdFZ, Spildağı fault zone; KF, Kemalpaşa fault. See Fig. 4.2 for location.

Most of these faults of Karaçay fault zone are generally dipping more than 70° to the S, and are clearly traced by well-developed fracture zones generally having widths of >10 m (Fig. 4.10b). NE of Beşyol and NW of Çiçekli villages, the existence of an early left-lateral strike-slip faulting were documented with 24 fault plane data (plots 19A and 20A). Here, the earlier left-lateral slip lines with rakes ranging 04–20°N have been overprinted by a series of younger right-lateral strike-slip striations with an average rake of 20°S. The measured fault planes have strikes around N35–40°E with an average dip of 85° to the SE. Near Keçili village, reactivation along the KçFZ was also mentioned with kinematic data by Özkaymak and Sözbilir (2008). In map view, the KçFZ shows cross-cutting relationships with the E–W-trending normal faults such as the Manisa, Kemalpaşa and Spildağı fault zones (Figs. 4.2 and 9a).

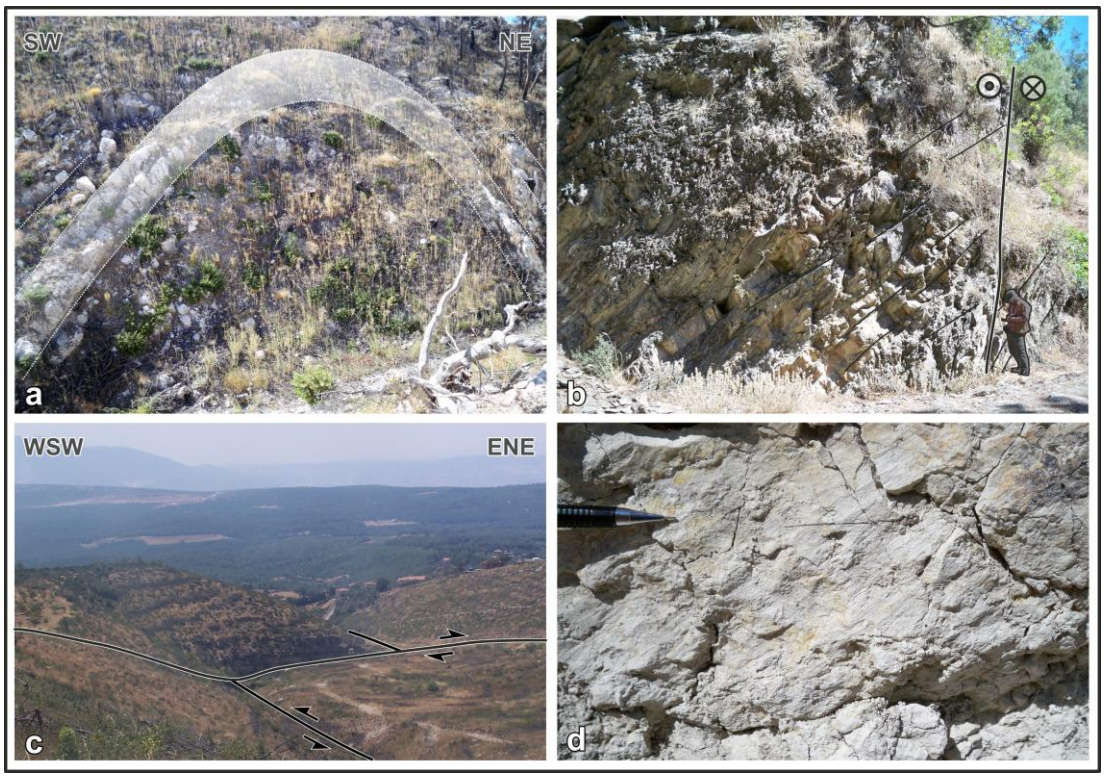


Figure 4.10 Field photos of post-Miocene structures from the Yaka area. (a) Close up view of an approximately E–W trending fold in the Yaka Formation. (b) Nearly vertical fault plane of the NE striking Karaçay fault zone cutting the Bornova Flysch Zone. (c) A field photo showing the left-lateral offset of a N–S striking fault along the NE striking cross fault. (d) Close up view of a NW striking strike-slip fault plane including well-developed slickenlines.

4.3.3.2 Kemalpaşa (KFZ) & Spildağı Fault Zones (SdFZ)

The WNW–ESE to E–W-striking KFZ and SdFZ are developed in the southern part of the Yaka area (Fig. 4.9). They can be traced 3–5 km inside the mapped Yaka area, but the actual lengths are more than a few tens of kilometers. In fact, according to Sözbilir et al. (2011) they are the westernmost rims of the extensional normal faults that bound the modern Gediz graben (Fig. 4.2). In this study, we provide new 11 fault plane data for the KFZ and SdFZ (projection 21 in Fig. 4.11). In the Yaka area, the SdFZ is characterized by a 4 km long, 1 km wide high-angle fault, and includes 3 sub-parallel faults. The observed fault planes dip at an average angle of 65°SW. In the study area, the KFZ is a 500 m wide, 1.5 km long, graben-bounding normal fault cross-cutting the NE–SW striking fault (Fig. 4.9a). The fault displays locally well-preserved slickensided surfaces revealing that the KFZ is a normal fault dipping at an average angle of 70°NE. Along the SdFZ and KFZ, the upper sequence of the Miocene units is displaced and is juxtaposed tectonically with Quaternary sediments exposed on down-thrown blocks.

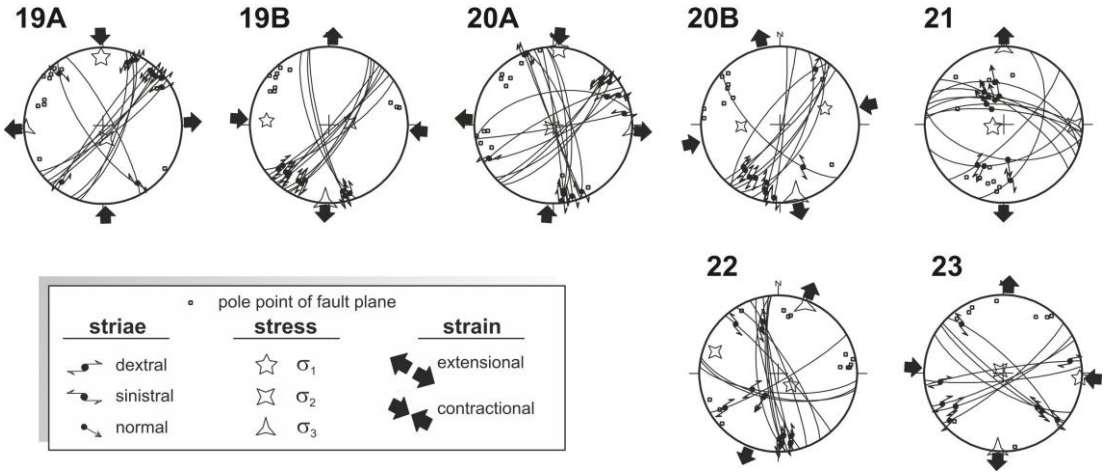


Figure 4.11 Lower-hemisphere equal-area projection of fault planes, slickenlines, and constructed palaeostress configurations for the Yaka area.

4.3.3.3 Cross-faults

These structures are mapped in a triangular area between the Manisa fault zone in the N, the KçFZ in the NW and the SF in the S as three different fault subsets that have NE–SW, NW–SE and N–S strikes (Fig. 4.9). Generally, the lengths of these faults can be traced to a maximum of 3 kilometers. The cross-faults displace the Miocene volcano-sedimentary units and laterally offset the fold axes of Miocene strata. According to the collected 27 fault plane data along these structures (see projections 22 and 23 on Fig. 4.11), NE-striking ones have a left-lateral component, while the NW-trending faults also have a normal fault character but with a right-lateral component (Figs. 4.10c and 4.10d). The third, N–S striking subset has a left-lateral strike-slip character. These second-order faults developed as accommodation structures inside the triangle area formed by the junction of SdFZ, KFZ and KçFZ; it forms the connection of the major normal and strike-slip faults (Fig. 4.12).

4.3.3.4 Folds

Two distinct fold patterns are developed in the Yaka area. These are N–S trending folds that are developed in the lower sequence of Miocene strata, and approximately E–W trending folds observed only in the lacustrine limestones of the Yaka Formation which is the highest unit of the upper sequence (Fig. 4.9). The N–S trending folding is observed within the Sabuncubeli and Kızıldere Formations around the NE of Beşyol village. They are mostly open synclines gently plunging to the N and they are parallel to the nearby faults. The fold axes can be traced over at least 1 km and are overlain by the clastics of the Kızılca Formation. The E–W-trending folds are well exposed between the Yaka and Beşyol villages where they are nearly parallel to NW–SE-trending normal faults (Fig. 4.9a). They are relatively large, open and plunging gently both towards the northwest and to southeast (Fig. 4.10a).

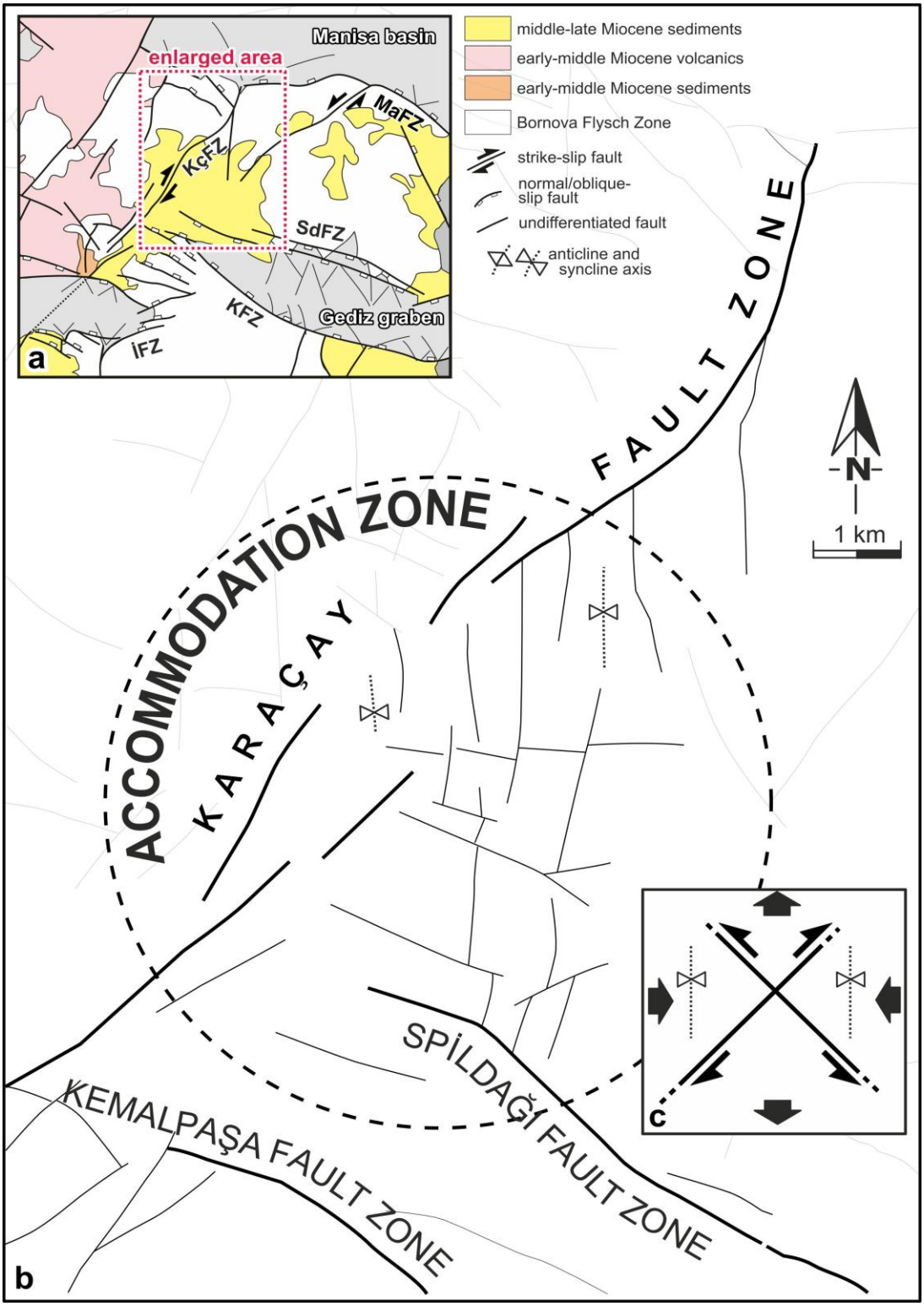


Figure 4.12 Interpretation of fault interactions in the Yaka area (a, inset). (b) Interaction of the Spildağı fault zone with the Karaçay fault zone by a number of N–S striking left-lateral strike-slip faults, (c) simplified model to illustrate the development of N–S folds caused by E–W compression (convergent arrows) and N–S extension (divergent arrows) within the Yaka area.

Towards the north the folds become more open with interlimb angles around 130°. The development of the E–W trending folds are interpreted to be forced folds that developed on the rotating faults blocks, similar to the mechanism proposed for folds in the Menemen area (Fig. 4.6c). A similar extensional folding mechanism is also proposed for the folds in the Gediz graben (Seyitoğlu et al., 2000; Sözbilir, 2001, 2002; Çiftçi & Bozkurt, 2008). On the other hand, the N–S folds that trend parallel to the secondary faults within the accommodation area of the KçFZ and SdFZ make an angle of approximately 45° with both major fault zones (Fig. 4.12).

4.3.4 Inner Bay Area

The Inner Bay of İzmir is an E–W-directed depression clearly outlined on topographic elevation map of the region (Fig. 4.2). A large number of the strike-slip and oblique to dip-slip normal faults are established and mapped around the southern rim of the Inner Bay (Fig. 4.2). Detailed analyses of late Cenozoic faults in the mapped areas enable us to recognize a pre-existing zone of weakness (İBTZ) that intermittently reactivated and is active today. Many of the dip- to strike-slip faults that initiated during the early history of the Miocene basin formation has become inactive, and older basin fill has been uplifted on the footwalls of younger faults. Here, the area provide not only the new field data and kinematic analyses on late Cenozoic structures, but also another perfect structural example letting daylight into the structural relationship between the E–W trending normal faults and the NE-SW trending strike-slip faults.

4.3.4.1 Seferihisar Fault Zone (SFZ)

The fault zone lying between Sığacık Bay and Güzelbahçe district is a 2–5 km wide, 30 km long and NE-trending dextral fault zone (Figs. 4.2 and 4.13). At the northern termination, it consists of a series of parallel and sub-parallel fault segments. It enters into the study area at the Yelki town in N20°E strike and cuts the basement rocks of Bornova Flysch Zone and Holocene alluvial deposits. There are

also a series of actively growing lateral alluvial fans aligned along the fault segments. Towards the north, the strike of the fault changes to N40–50°E and connected to the İzmir fault zone (Fig. 4.13). Holocene activity of the fault is evidenced by observations of the dextral offsets on drainage systems up to 100 m (Emre et al., 2005). Moreover, an intermediate-magnitude (MW= 5.7) earthquake that struck on April 10, 2003 supports the recent dextral strike-slip activity of the SFZ (Fig 4.2; Akyol et al., 2006). Along the northern termination of the SFZ, the fault segments have a strike of N30–50°E and average dips of about 70–87° to the NW. The slickenlines on the fault planes show a rake angle ranging from 03° to 32° (Fig. 4.15). When the SFZ come close to İFZ it bends to the east and their fault planes have a rake angle up to 70° (Fig. 4.14, and plots 24-28 on Fig. 4.15).

4.3.4.2 İzmir Fault Zone (İFZ)

It is the southern incipient margin-bounding structure of the Inner Bay of İzmir. It is an approximately 2–4 km wide, 40 km long, E–W trending and range-front active normal-fault zone (Figs. 4.2, 4.13, and 4.16).

It bounds the Seferihisar and Nifdağı Highs to the north and consists of two main fault sets lying between Güzelbahçe and Altındağ villages. Through Balçova to Güzelbahçe villages, the western fault set of the İFZ is made up of a number of segments trending approximately in an E–W direction (Figs. 4.13, and 4.16). In this section, the İFZ has corrugations with variable size wavelengths, reaching km-scale amplitude. Their map view shows a basin-ward-facing step-like fault pattern, which is convex to north (Fig. 4.13). Towards the east, where the eastern fault set of the İFZ enter into Altındağ village in a WNW–ESE-direction, it includes several en-echelon-arranged synthetic and antithetic fault segments, dipping to the north and south, respectively (Fig. 4.16). Here, the İFZ cuts the basement rocks of the Bornova Flysch Zone (Fig. 4.17) and sedimentary rocks of the older basin fill units, while its northernmost segment separates the Holocene alluvial deposits from the older rocks. Holocene lateral alluvial fan sediments growing on the hanging wall of the İFZ are back-tilted towards the fault.

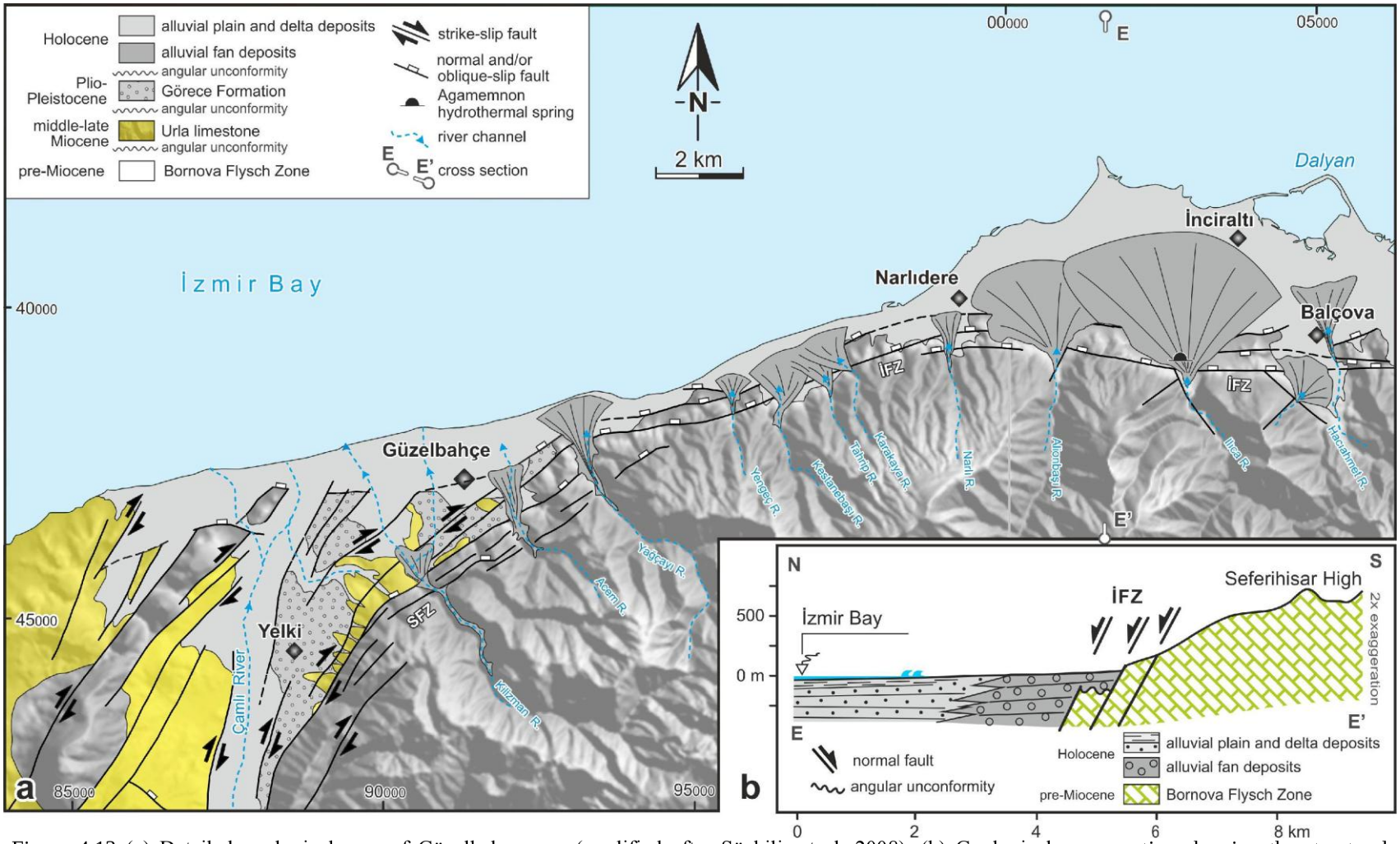


Figure 4.13 (a) Detailed geological map of Güzelbahçe area (modified after Sözbilir et al. 2008). (b) Geological cross-section showing the structural configuration of the southern rim of the Inner Bay of İzmir. SFZ, Seferihisar fault zone; İFZ, İzmir fault zone.



Figure 4.14 a) Field photograph showing the morphologic contrast and linkage of the Seferihisar and İzmir fault zones (view to SE). (b–e) Fresh slip-planes of the Seferihisar fault zone indicating the nearly horizontal slickenlines where it cuts the rocks of Görece Formation and Bornova Flysch Zone.

Along the easternmost segment of the İFZ two differently orientated striation sets on the same slip surface were measured, which strike in approximately E–W and dip 75°N. The younger set is represented by slip lines with rakes of 79–88°W and overprints an older striation set with an average rake of 10°E (Fig. 4.17). There, the observed two slickenside lineation with different plunges and slip senses on the same fault plane suggest that the strike-slip surface was overprinted with dip-slip movements (plots 32A and 32B on Fig. 15).

4.3.4.3 Karşıyaka Fault Zone (KyFZ)

The northern sector of the bay between Bayraklı and Karşıyaka district is bounded by the KyFZ, which is an antithetic fault to the İFZ (Fig. 4.2). It is a 0.5–2.5 km wide, 20 km long, approximately N80°W- to E–W-trending normal fault zone which is characterized by a concave, curvilinear range-front fault trace to the south. The hangingwall of the KyFZ comprises the modern basin fill units, while the footwall includes the Bornova Flysch Zone and volcano-sedimentary rocks of the lower sequence. The fault zone displays a well-developed step-like morphology. There are also a series of actively growing lateral alluvial fans aligned parallel to the fault. The observed fault planes are trending N80°W, dipping an average of 60° to SW (plots 33 and 34 on Fig. 4.15). Through the village of Bornova, it runs between the sedimentary rocks of the lower and upper units, N80°W in strike, and it is characterized by an oblique-slip normal fault dipping to the south.

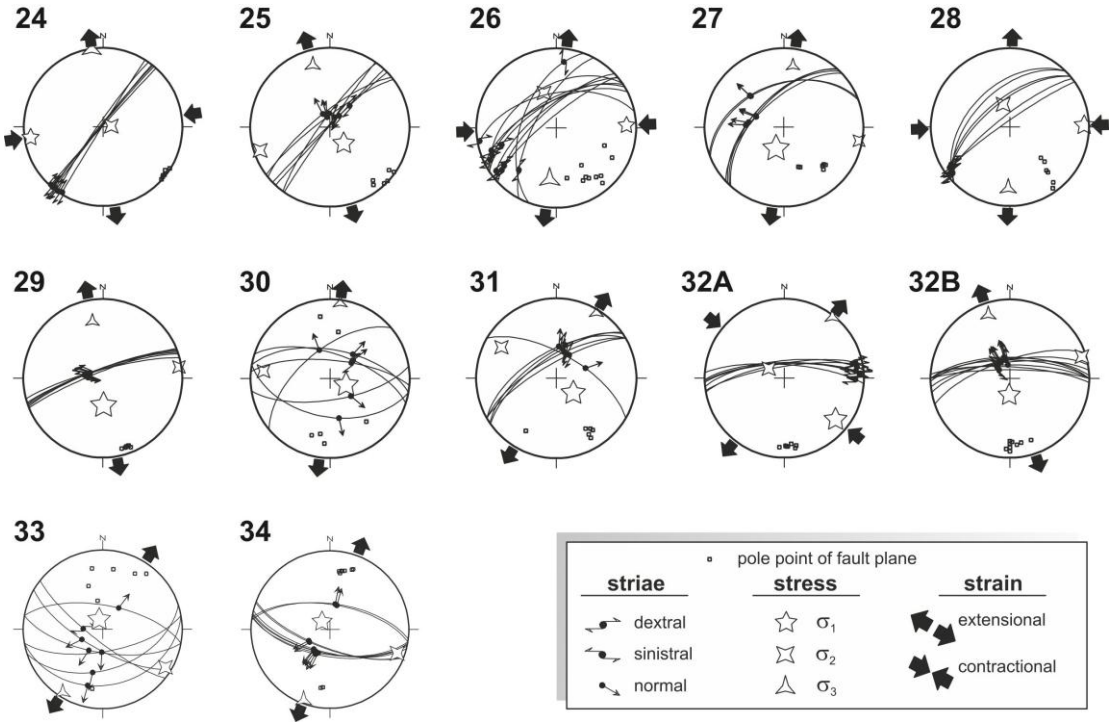


Figure 4.15 Lower-hemisphere equal-area projection of fault planes, slickenlines, and constructed palaeostress configurations for the Inner Bay area.

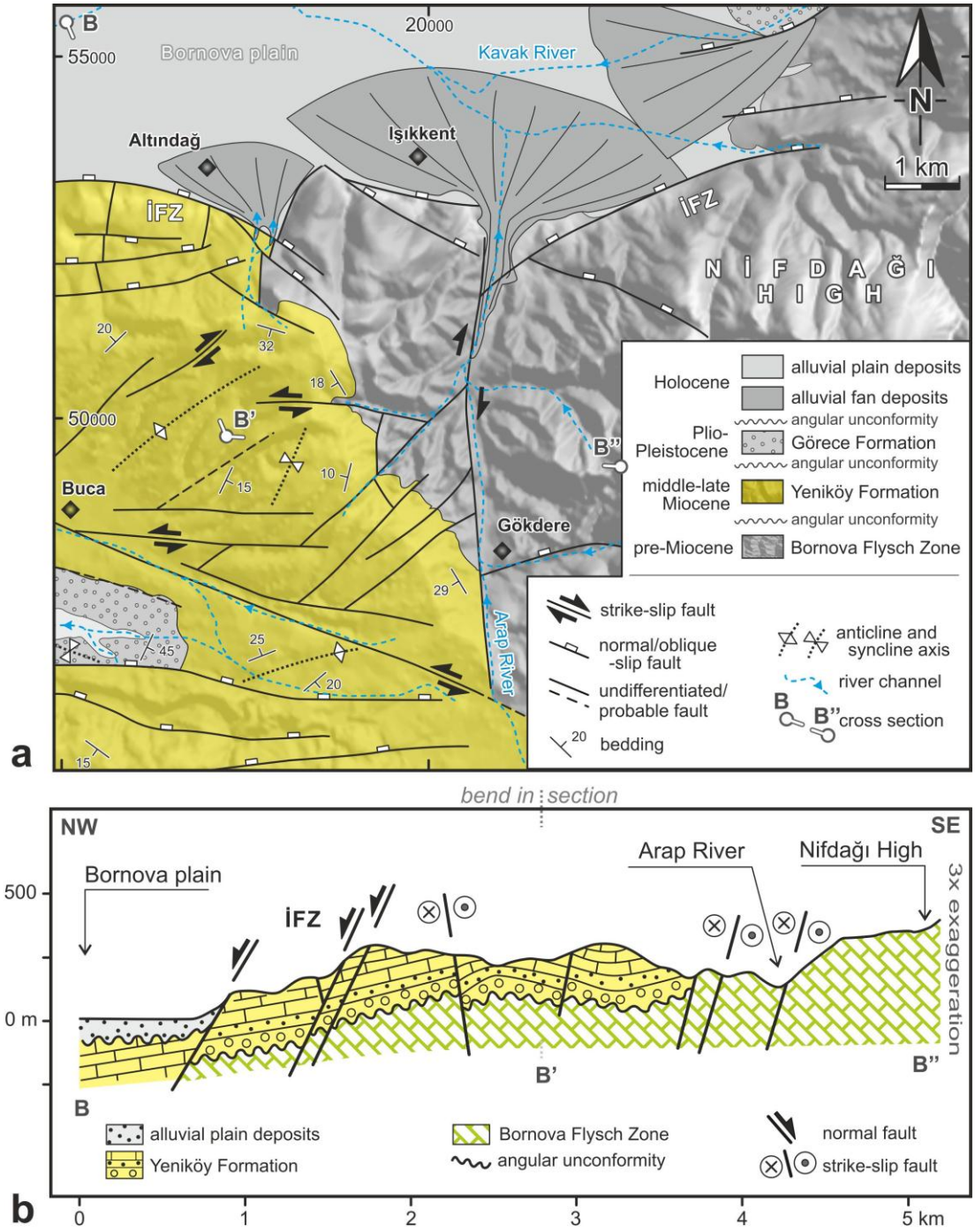


Figure 4.16 Detailed geological map of the southern margin of the Inner Bay area around Altındağ. İFZ, İzmir fault zone. See Fig. 4.2 for location.

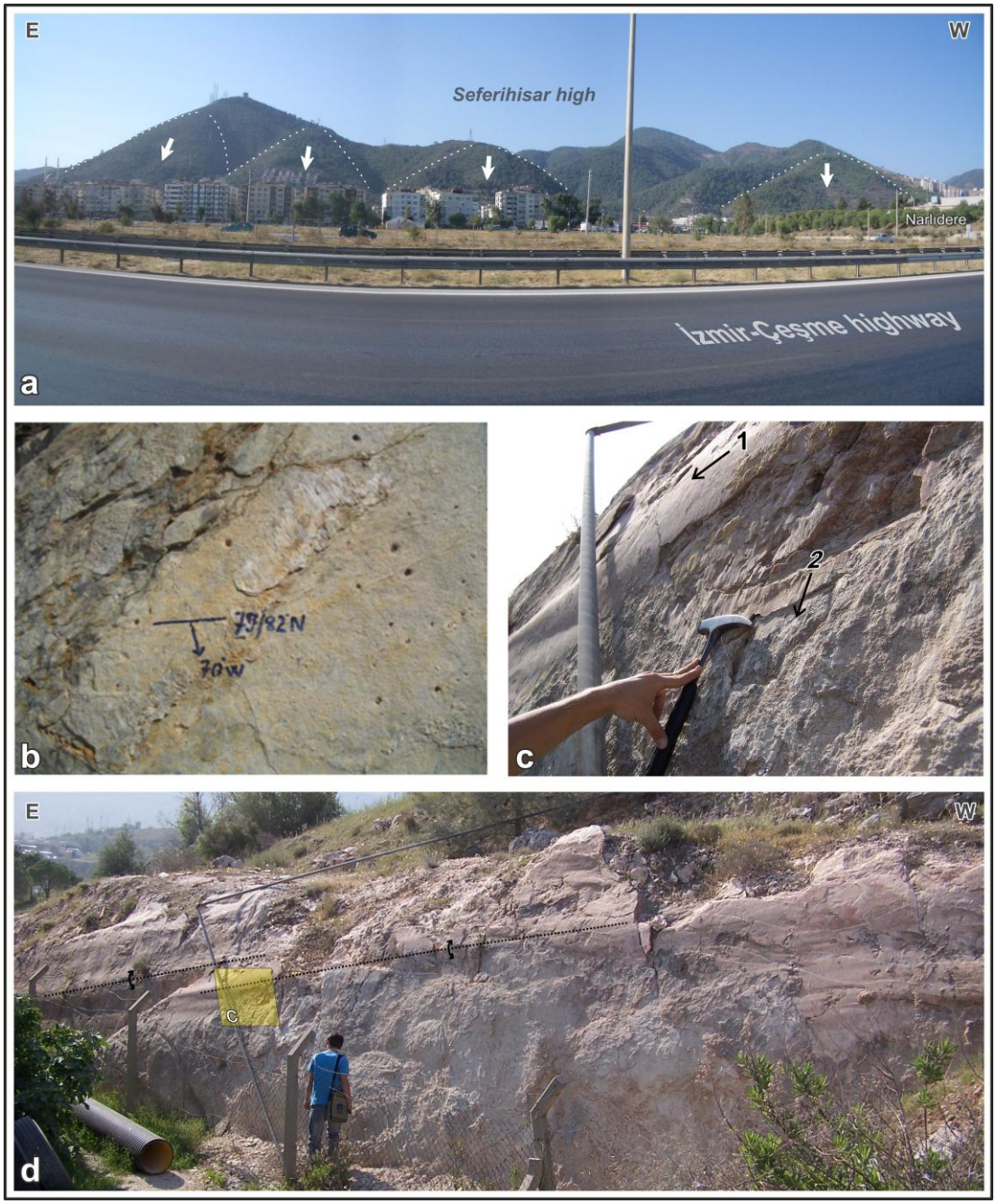


Figure 4.17 Field photographs of the E–W-trending İzmir fault zone. (a) The step-like morphology, and basinward-facing steep fault scarp reflect the active normal-slip character of the fault zone (view to S, between Balçova and Narlıdere villages). (b) Fresh fault-planes of the İzmir fault zone showing nearly vertical slickenlines where it cuts the basement rocks. (c, d) In the easternmost segment of the fault zone we observed and measured two differently orientated striation sets on the same slip surface of the İzmir fault zone. Th ere, the two slickenside lineation with different plunges and slip senses observed on the same fault plane suggest that the strike-slip surface was overprinted with dip-slip movements.

4.3.4.4 Orhanlı Fault Zone (OFZ)

It forms the western margin of the Cumaovası basin, and is also the most prominent structure in the region located to the south of İzmir city (Fig. 4.2). The OFZ bounds the Seferihisar High to the east. It may be traced for about 45 km, between İzmir Bay in the north and Kuşadası Bay in the south. The fault zone includes several dextral fault segments extending mainly in a NE–SW direction. The main motion along the slip surfaces is dextral strike-slip. However, there are some geomorphological and structural evidence for the presence of an earlier sinistral strike-slip motion (Uzel & Sözbilir 2008). Typical tectonic landforms, such as systematically deflected stream channels and ridges, shutter ridges, and fault scarps, are recognized along segments of the OFZ. On the basis of their morphological and structural features, it is interpreted that the early sinistral offsets are later overprinted by dextral offsets. In addition to that, several hot springs occur in the central part of the fault zone, implying that the fault zone provides effective conduits for the geothermal field. This indicates that the hot springs in the area are associated with active faults (Uzel & Sözbilir 2008). Recent dextral strike-slip activity of the OFZ is also evidenced by 6 November 1992 Doğanbey Earthquake (Fig 4.2; Tan et al., 2008).

4.3.4.5 N–S-trending Faults

The N–S faults are steeply dipping, and are mainly of strike-slip nature (Figs. 4.2, and 4.16). Some of these show clear evidence of early left-lateral slip reactivated by later right-lateral motion. In the southern sector of the Inner Bay, NW of Altındağ two sets of slip lines on the fault planes were recognized, and slip lines with rakes 10°N are superimposed by striations with an average rake of 25°S. The length of this fault is approximately 2 km. The fault cuts trough Miocene lacustrine limestone and is in turn cut by approximately E–W trending normal faults of the İFZ. To the southeastern part of the study are, between Işıkkent and Gökdere village, there is a straight fault zone with a N–S trend, for about 6 km. To the east of Buca district, several NE–SW trending dextral strike-slip faults splaying out from the main fault

zone cut, and these displaced the unconformity between the Bornova Flysch Zone and the overlying Miocene units (Fig. 4.16). There are also several oblique-slip normal faults along the west side of the main fault and these are mainly en-echelon or oblique to the trend of the main fault. The en-echelon faults are steeply dipping and have normal separation. Some of the faults have nearly horizontal slickenside striae that are interpreted as consequences of oblique-slip.

The N-S trending strike-slip faults may have acted as extensional tear faults (cross-faults) separating areas that may have experienced different amount of extension. According to Kaya (1979 & 1981) and Kaya et al. (2004 & 2007), the NE–SW and N–S trending faults were inherited from old zones of weakness of Paleocene age. These Paleocene faults a) have significant vertical movements, b) later acted as growth faults during the early Miocene, because they are responsible for variation in thickness of the Miocene volcano-sedimentary units, c) were a zone of weakness that aligned volcanic centers, and d) reactivated intermittently until recent time as indicated by overprinted slickenlines. In case of this thesis, these N–S trending faults are interpreted as the oblique segments of the NE-trending İBTZ.

4.3.4.6 Folds

The folds observed within the Inner Bay area comprise a series of anticlines and synclines. These folds of various sizes characterize the internal deformation of the older basin fill units. Two types of fold-to-fault relationships have been mapped: folding parallel to the normal-fault traces and folds lying oblique to the strike-slip fault traces. Several folds have been mapped that are associated with strike-slip faults and typically are arranged in en echelon patterns oblique to the principal direction of shear in which Miocene rocks are folded into en echelon, NE–SW trending anticlines and synclines that die out within approximately 2 km. Typically, en echelon folds are distributed in a relatively narrow zone adjacent to strike-slip faults (Fig. 4.16). The general trend of the folds indicates a NW–SE-directed compression direction, possibly attributed to the formation of the strike-slip faults.

4.4 Paleostress Analysis of Fault-Slip Data

4.4.1 Methodology

For computer-based inversion of structural data, a number of graphical (e.g. Arthaud, 1969; Alexandrowski, 1986; Krantz, 1988) and numerical palaeostress methods (e.g. Carey and Brunier, 1974; Angelier, 1979, 1984, 1990, 1994; Etchecopar et al., 1981; Armijo et al., 1982; Gephart and Forsyth, 1984; Michael 1984; Reches, 1987; Marrett and Almandinger, 1990; Will and Powell, 1991; Yin and Ranalli, 1993; Hardcastle, 1989; Fry, 1999; Yamaji, 2000; Delvaux and Sperner, 2003; Zalohar and Vrabec, 2007) have been developed and most of the software has been made available. Here, however, we used the Direct Inversion Method (INVD) of Angelier (1990), because of its efficiency and robustness in multi-stage deformed areas (Angelier et al., 1981; Kaymakçı et al., 2000, 2003, 2006; Vandycke and Bergerat, 2001; Brahim et al., 2002; Saintot and Angelier, 2002; Sperner et al., 2003; Bergerat et al., 2007; Hippolyte and Mann, 2011). Here, I refer to Angelier (1994) for a detailed review of the method, and to Sperner and Zweigel (2010), and Hippolyte et al. (2012) for data acquisition/separation techniques.

Principally, the INVD technique is based on the reduced stress tensor concept and the estimation of the stress ellipsoid by the shape factor [$\Phi = (\sigma 2 - \sigma 1) / (\sigma 3 - \sigma 1)$], which varies between 0 and 1. Therefore, in areas where the stress ratio approximates 0 or 1, uni-axial stress conditions prevail and faults are not constrained in any direction. Otherwise stress is tri-axial and all of the principal stress magnitudes are significantly different, and the fault orientations tend to develop parallel to $\sigma 2$ directions and they approximate to an Andersonian mechanism (Anderson, 1951). During the inversion process, we used the ANG and RUP values (Angelier 1994) to separate heterogeneous data. The allowable maximum misfit angle (ANG), i.e. maximum misfit angle between observed slip and computed shear stress direction was taken as 25^{O}. The acceptable maximum quality estimator value (RUP), ranging from 0% (calculated shear stress parallel to actual striae with the same sense and maximum shear stress) to 200% (calculated shear stress maximum,

parallel to actual striae but opposite in sense) was taken as 50%. Fault slip data exceeding these limits were separated from the data set, and then recomputed as separate tensor.

4.4.2 Palaeostress Configurations

In the key areas, more than 320 fault slip data were collected (Table 4.1). The available palaeostress data sets (Table 4.2) were also integrated. Among these, the sites, which are labeled as 1–12 belong to the Karaburun area and they have produced 17 palaeostress configurations. Sites 13–18 belong to the Menemen area have generated 6 palaeostress configurations. Sites 19–23 are located within the Yaka area and they yielded 7 palaeostress configurations. Sites 24–34 characterize the palaeostress constructions of sites in Inner Bay area (Fig. 4.18).

The results of the palaeostress analyses are depicted in Figures 4.5, 4.8, 4.11, 4.16 and Table 4.1. As mentioned in previous sections, during the field studies the overprinted slickensides were encountered in several locations and analyzed separately. These overprinting relationships, together with cross-cutting relationships and stratigraphic information, are used to determine the various deformation phases and their succession in time. However, deformation phases of areas where no cross-cutting or overprinting relationships were encountered were based on the age of host lithology, and the similarity of the stress orientations and stress ratios to other sites for which the deformation phase was already assigned precisely (cf. Sperner and Zweigel 2003).

Within the studied sub-areas along the İBTZ, during the late Cenozoic (Miocene–Quaternary) interval, three different deformation phases have been recognized based on our kinematic analyses and available palaeostress data from literature (Bozkurt & Sözbilir, 2006; Özkaymak & Sözbilir, 2008; Uzel & Sözbilir, 2008; Sözbilir et al., 2011). The first phase (Phase 1) is characterized by N–S directed extension and E–W contraction and likely took place during the early (?) to late Miocene. This transtensional phase formed several volcano-sedimentary basins. It was followed by

a second phase (Phase 2) which caused wrench- to extension-dominated transtension. The structures related to Phase 2 are observed all around İzmir Bay and probably took place during the early Pliocene. The last deformation phase (Phase 3) is characterized by both NW-SE left-lateral and NE– SW right-lateral strike-slip faults and E–W trending normal faults, causing a transtensional deformation phase.

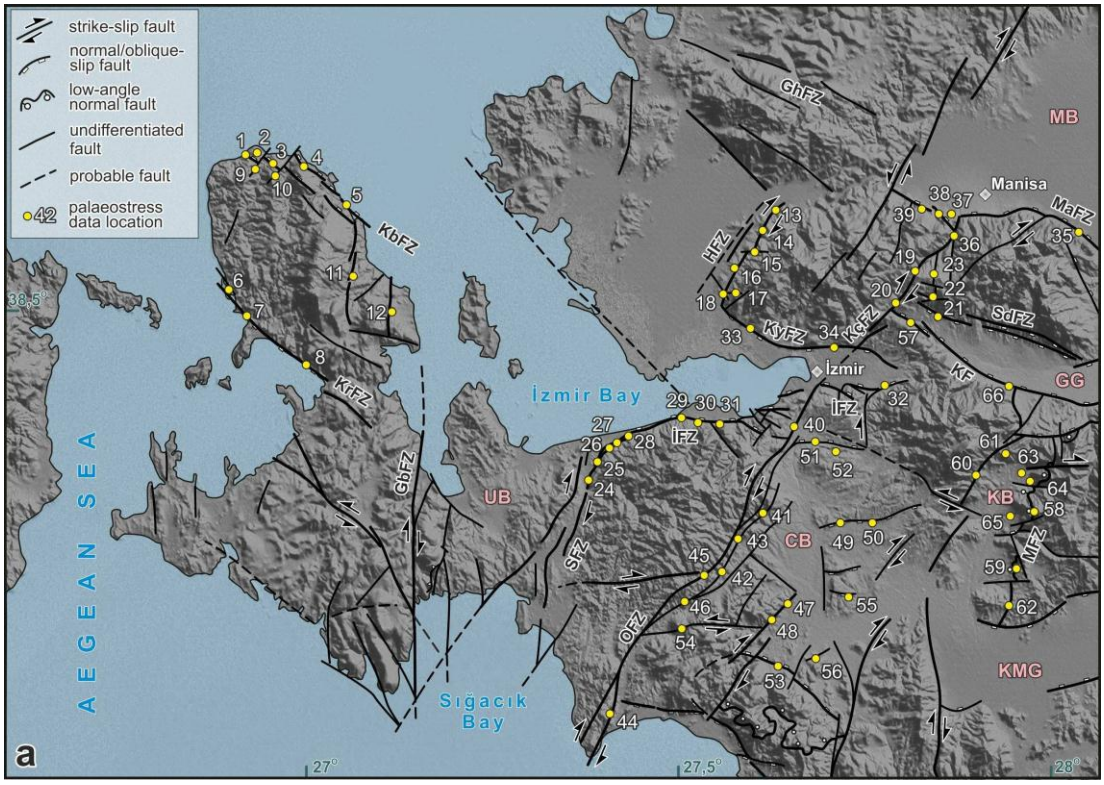


Figure 4.18 Orientation and temporal variation of horizontal components of principal paleostrain axes. (a) Distribution of palaeostress data sites draped on a simplified tectonic map of İzmir Bay area. KbFZ, Karaburun fault zone; KrFZ, Karareis fault zone; HFZ, Harmandalı fault zone; GbFZ, Gülbahçe fault zone; GhFZ, Güzelhisar fault zone; KyFZ, Karşıyaka fault zone; SFZ, Seferihisar fault zone; OFZ, Orhanlı fault zone; İFZ, İzmir fault zone; KF, Kemalpaşa Fault; SdFZ, Spildağı fault zone; MaFZ, Manisa fault zone; MFZ, Mahmutdağı fault zone; UB, Urla Basin; CB, Cumaovası Basin; KMG, Küçük Menderes Graben; KB, Kocaçay Basin; GG, Gediz Graben; MB, Manisa Basin.

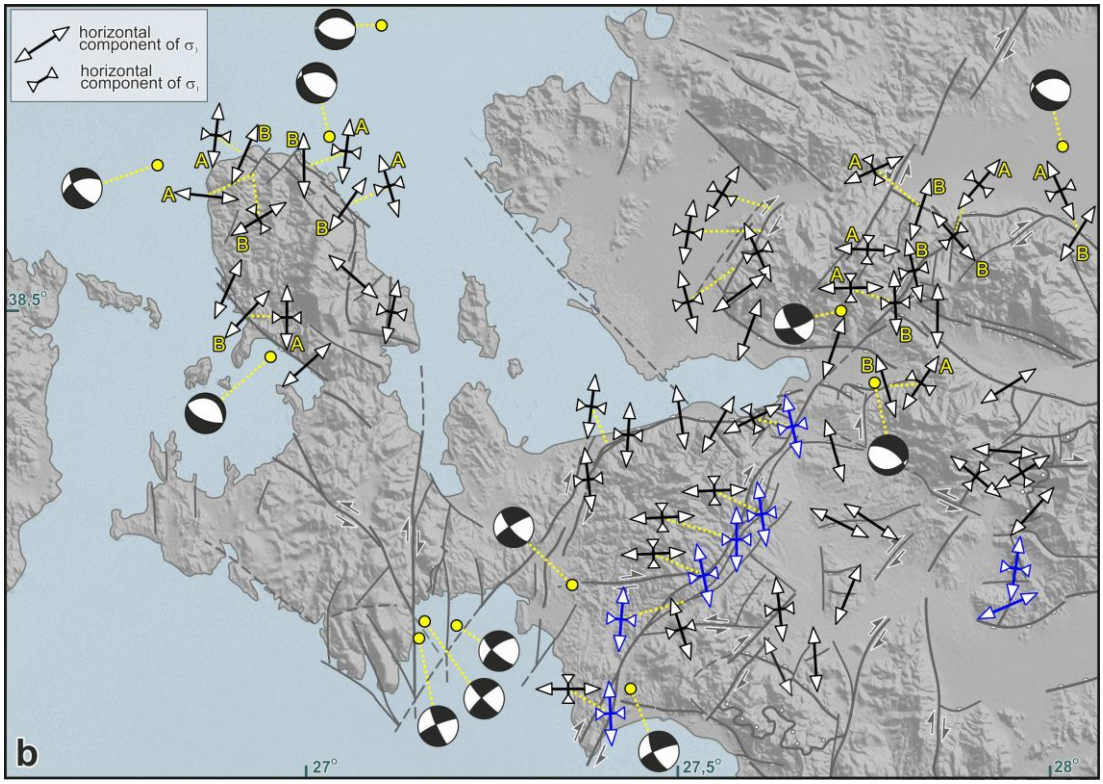


Figure 4.18 continued. (b) Calculated horizontal component of maximum and minimum strain axes directions. Blue arrows related to Miocene faulting along the Mahmutdağı and Orhanlı fault zones (Phase 1). A (B) refers to the older (younger) faulting on reactivated fault planes. The focal mechanism solutions (beach balls) of the main earthquakes are used to identify recent tectonic activity (Tan et al., 2008). Characteristics of local stress states are shown in Tables 1 and 2.

4.4.2.1 Phase 1

It is well documented in two areas, in the Kocaçay basin and along the Orhanlı Fault Zone (OFZ), which forms the western margin of the Cumaovası basin. In the Kocaçay basin, two sites along the Mahmutdağı Fault Zone (58 and 59; Fig. 4.18a) from Sözbilir et al. (2011) at the eastern margin of the İBTZ, provide evidence for two families of faults: NE-trending dextral strike-slip faults and low-angle normal faults. The INVD technique identifies steeply plunging σ_2 axes (71°), but gently plunging σ_1 and σ_3 axes (18° and 08°). The results suggest that strike-slip faulting developed under an approximately N-S-trending extension associated with E–W contraction (Table 4.2).

Table 4.1 Characteristics of stress states used to reconstruct the stress regimes as illustrated in Figs. 4.6, 4.9, 4.12, and 4.17. #, Number of fault slip data; D° and P°, dip and plunge of stress axes in degrees; Φ, ratio of stress magnitude differences [$\Phi = (\sigma_2 - \sigma_3)/(\sigma_1 - \sigma_3)$]. RUP and ANG are quality estimators: average ANG values below 25° and average RUP values below 50% indicate good fits between computed shear stress and actual fault slip data. Rej, number of rejected data because of the low quality.

Site	Name of fault	Principle stress axes (dip°/plunge°)			Φ	#	max ANG	max RUP	Rej
		σ1	σ2	σ3					
Karaburun area									
1A	Karaburun Fault Zone	289/56	091/33	187/09	0,527	14	16	48	2
1B	Karaburun Fault Zone	235/74	118/08	026/14	0,328	12	24	43	1
2	Karaburun Fault Zone	087/20	221/62	350/18	0,882	7	14	30	0
3	Karaburun Fault Zone	276/55	109/34	015/06	0,659	16	10	38	1
4A	Karaburun Fault Zone	105/13	234/69	011/15	0,691	10	18	41	1
4B	Karaburun Fault Zone	179/72	327/15	059/09	0,346	12	22	48	0
5A	Karaburun Fault Zone	081/26	229/60	344/14	0,874	7	23	43	0
5B	Karaburun Fault Zone	265/72	138/11	046/14	0,476	6	19	38	1
6	Karareis Fault Zone	306/52	107/36	204/09	0,723	7	12	44	0
7A	Karareis Fault Zone	266/61	072/29	165/06	0,944	11	11	22	1
7B	Karareis Fault Zone	010/69	154/17	247/12	0,322	7	17	23	1
8	Karareis Fault Zone	354/76	144/12	235/07	0,640	7	11	23	0
9A	Karareis Fault Zone	015/83	191/07	281/01	0,575	12	21	47	1
9B	Karareis Fault Zone	088/87	316/02	226/02	0,749	8	19	36	1
10	West Karaburun	142/69	006/16	271/13	0,520	6	21	39	0
11	West Kösedere	297/75	029/11	119/15	0,523	10	16	44	4
12	West Mordoğan	032/67	286/07	193/22	0,454	11	16	42	3
Menemen area									
13	Harmandalı Fault Zone	306/06	90783	215/04	0,821	10	16	40	3
14	Harmandalı Fault Zone	254/11	029/75	162/11	0,620	22	24	47	7
15	East Koyundere	108/81	328/07	237/06	0,833	12	23	45	4
16	Harmandalı Fault Zone	064/17	287/68	158/14	0,835	10	14	43	5
17	Southeast Ulucak	142/80	326/10	236/01	0,749	6	22	48	0
18	Harmandalı Fault Zone	099/10	255/79	009/04	0,807	22	22	40	3
Yaka area									
19A	Karaçay Fault Zone	353/11	161/79	263/02	0,547	11	15	41	1
19B	Karaçay Fault Zone	285/25	085/63	191/08	0,764	11	18	48	2
20A	Karaçay Fault Zone	017/03	250/84	107/05	0,459	15	19	44	8
20B	Karaçay Fault Zone	064/31	266/57	160/10	0,841	10	21	39	1
21	Kemalpaşa & Spildağı Faults	241/70	091/17	358/10	0,458	11	12	28	3
22	East Beşyol	102/88	295/02	205/01	0,840	13	23	40	4
23	North Beşyol	286/02	036/86	196/04	0,842	9	17	39	3
Inner Bay area									
24	Seferihisar Fault Zone	262/08	084/82	352/00	0,644	6	15	41	1
25	Seferihisar Fault Zone	139/68	252/09	345/20	0,268	6	18	48	2
26	Seferihisar Fault Zone	088/13	341/52	187/65	0,509	10	19	44	8
27	Seferihisar Fault Zone	201/67	100/04	008/23	0,265	6	21	39	1
28	İzmir Fault Zone	089/07	344/65	182/24	0,432	6	12	28	3
29	İzmir Fault Zone	178/62	350/28	082/04	0,150	6	23	40	4
30	İzmir Fault Zone	111/73	276/17	008/04	0,104	6	17	39	3
31	İzmir Fault Zone	131/67	300/22	031/04	0,271	6	12	28	3
32A	İzmir Fault Zone	129/18	301/71	038/02	0,278	7	23	40	4
32B	İzmir Fault Zone	182/73	073/06	341/16	0,328	9	12	28	3
33	Karşıyaka Fault Zone	326/73	108/13	200/10	0,280	7	23	40	4
34	Karşıyaka Fault Zone	315/78	110/10	200/05	0,431	9	17	39	3

Table 4.2 Published palaeostress tensors used for the reconstruction of the deformational history of the area. #, Number of fault slip data; D° and P°, dip and plunge of stress axes in degrees; Φ, ratio of stress magnitude difference [$\Phi = (\sigma_2 - \sigma_3) / (\sigma_1 - \sigma_3)$]. *Reference codes are: (1) Bozkurt and Sözbilir (2006), (2) Özkaymak and Sözbilir (2008), (3) Sözbilir et al. (2008), (4) Uzel and Sözbilir (2008), and (5) Sözbilir et al. (2011).

Site	Name of fault	Principle stress axes (dip°/plunge°)			Φ	#	Ref*
		σ1	σ2	σ3			
Manisa Basin (Gediz Graben)							
35A	Manisa Fault Zone	259/35	058/53	162/10	0,622	9	1
35B	Manisa Fault Zone	208/83	303/01	033/07	0,245	14	1
36A	Karaçay Fault Zone	136/02	261/86	046/03	0,922	11	2
36B	Karaçay Fault Zone	228/08	357/78	136/09	0,798	10	2
37	Manisa Fault Zone	199/72	303/05	036/17	0,195	8	2
38A	Manisa Fault Zone	173/19	024/68	267/10	0,721	8	2
38B	Manisa Fault Zone	343/75	091/04	182/14	0,110	8	2
39A	Manisa Fault Zone	130/65	336/22	242/10	0,630	10	2
39B	Manisa Fault Zone	256/70	113/16	020/12	0,353	11	2
Cumaovası Basin							
40A	Orhanlı Fault Zone	163/17	276/53	062/32	0,613	6	4
40B	Orhanlı Fault Zone	257/06	014/77	166/11	0,315	6	4
41A	Orhanlı Fault Zone	360/23	162/66	267/06	0,716	6	4
41B	Orhanlı Fault Zone	260/40	098/48	001/09	0,651	6	4
42A	Orhanlı Fault Zone	185/05	291/72	094/17	0,565	6	4
42B	Orhanlı Fault Zone	278/39	095/51	187/01	0,626	6	4
43A	Orhanlı Fault Zone	355/15	206/72	088/09	0,336	6	4
43B	Orhanlı Fault Zone	267/22	063/66	173/09	0,579	6	4
44A	Orhanlı Fault Zone	358/04	261/64	090/26	0,434	6	4
44B	Orhanlı Fault Zone	265/17	096/73	356/03	0,212	6	4
45A	Orhanlı Fault Zone	355/15	206/72	088/09	0,336	6	4
45B	Orhanlı Fault Zone	258/11	066/78	167/02	0,821	6	4
46	Orhanlı Fault Zone	275/14	086/76	185/02	0,688	6	4
47	Orhanlı Fault Zone	259/03	154/77	350/12	0,516	6	4
48	Orhanlı Fault Zone	106/07	350/74	198/15	0,715	6	4
49	Kısıkköy Fault	020/69	218/20	126/06	0,320	6	4
50	Kısıkköy Fault	023/65	205/25	114/00	0,182	6	4
51	Buca Fault	208/53	079/25	336/25	0,080	6	4
52	Buca Fault	154/62	250/03	341/27	0,520	6	4
53	Değirmendere Fault	225/73	065/16	333/06	0,220	6	4
54	Deliömer Fault	074/18	239/72	342/04	0,252	6	4
55	Conjugate set	094/66	298/22	204/09	0,336	6	4
56	Conjugate set	010/68	267/15	175/21	0,316	6	4
Kocaçay Basin							
57	Kemalpaşa Fault	334/82	096/04	187/07	0,499	6	5
58	Mahmutdağı Fault Zone	080/72	316/11	223/18	0,418	5	5
59	Mahmutdağı Fault Zone	096/18	300/71	188/08	0,388	6	5
60	Kesmedağı Fault	222/04	116/76	313/13	0,279	5	5
61	Kalkancatepe Fault	291/74	186/04	095/16	0,469	8	5
62	Karabeldere Fault	057/72	156/03	247/18	0,168	7	5
63	Dereköy Fault	152/06	036/77	243/12	0,139	12	5
64	Dereköy Fault	027/78	134/04	225/12	0,363	11	5
65	Karaot Fault	094/22	336/50	199/32	0,652	7	5
66	Spildağı Fault Zone	222/82	332/03	6208	0,702	11	5

The fault slip measurements for the low-angle normal faulting define a near horizontal σ_3, trending approximately 223° with a 15° plunge, whereas σ_1 and σ_2 axes have attitudes of approximately 080°/72° and 316°/11°, respectively. The results suggest a NE–SW directed extension. Phase 1 faults are kinematically congruent with the N–S extensional direction expected to have been associated with the opening of the supra-detachment basins during the early Miocene, an interpretation that is supported by the σ_3 orientation calculated for strike-slip faults.

Structures related to Phase 1 were also documented along the Orhanlı Fault Zone (OFZ), which forms the western margin of the Cumaovası basin and is the most prominent structure in the region south of İzmir city. Along the Orhanlı Fault Zone, crosscutting relationships and superposition of successive striae in fault planes show that sinistral faulting was reactivated as right-lateral strike-slip faulting (Uzel and Sözbilir 2008). The older kinematic structures including sinistral shear sense were determined in Sites 38, 39, 40, 41 and 44 (Figure 4.18b, and Table 4.2). The inverse analysis results of fault-slip measurements for the early phase of sinistral strike-slip faulting define steeply plunging σ_2 axes (53° and 76°), but gently plunging σ3 axes (09° and 32°). The main orientation of the σ1 axis is very variable with an approximately horizontal plunge (10° and 30°). The results suggest that sinistral strike-slip faulting developed under an approximately N–S trending contraction regime associated with E–W extension. The fault-slip measurements for the later phase of dextral strike-slip faulting define a near horizontal σ_1, trending approximately 260° with a 10° plunge, whereas σ_3 axes have attitudes of approximately 160°/10°, respectively. The orientation of σ_2 axes is variable with approximately vertical plunging. The results suggest an approximately N–S directed extension associated with E–W contraction (Table 4.2).

4.4.2.2 Phase 2

Deformation Phase 2 is characterized by an association of strike-slip and oblique-to dip-slip normal faults that deformed the Miocene units. Eight sites (1A, 4A, 5A, 7A, 9, 10, 11, 12, 15, 16 17, 18, 19A, and 20A; Fig. 4.18a and Table 4.1) along the

KbFZ, KrFZ, HFZ and their subsets characterize this phase in the Karaburun and Menemen subareas (Fig. 4.18b). These NE and NW striking fault zones seem to form conjugate sets since they operated at the same time and had right- and left-lateral strike-slip character, respectively. The palaeostress configurations computed from the data of the Karaburun and Menemen areas are reasonably coherent, and define a horizontal component of the σ_3 axes ranging between N20°W and N15°E, with a plunge of < 22°. The plunge of the σ1 axes is nearly vertical (> 56°) in most sites of the Karaburun area, whereas in the Menemen area the plunge of σ_1 is sub-horizontal (< 17°).

The computed data from Yaka area along the KçFZ, however, indicate that here the intermediate (σ_2) stress is steeply plunging. The overall results suggest that in all areas the direction of minimum stress (σ_3) is horizontal and approximately NE–SW to E–W, while in the Karaburun and Menemen areas σ1 is more or less subvertical. In the Yaka area, the direction of σ_3 is horizontal, in a NNW–SSE direction (Table 4.1). The second phase is attributed to the early Pliocene, based on kinematic/stratigraphical information and the geological context of the region by Bozkurt and Sözbilir (2006).According to their palaeostress analyses, and the subsequent analyses of Uzel and Sözbilir (2008), Özkaymak and Sözbilir (2008) and Sözbilir et al. (2011) at several sites of the eastern part of the İzmir Bay (sites 24–27, 38–42, 56, and 60–64 on Fig. 4.18a), the E–W extension and related N–S contractional strain across the region is also related to early Pliocene events as revealed by reactivated structures (Fig. 4.18b).

4.4.2.3 Phase 3

In this deformation phase, palaeostress orientations which indicate both extensional and strike-slip deformation are obtained (Fig. 4.18b, and Table 4.1), similar to what happened during Phase 2, but the other way around. This phase, which is evidenced by the youngest structures of the region, indicates transtensional deformation within the İBTZ. The orientation of extensional strain axes varies between NNW–SSE to NNE–SSW, while contractional strain directions in sites with

a strike-slip solution vary from WNW–ESE to ENE–WSW. Having both extensional and coeval strike-slip deformation implies that Phase 3 is transtensional in nature. This phase postdates Phase 2, and seems to have been active during the late Pliocene–Quaternary time interval (Sperner et al., 2003; Aktuğ and Kılıçoğlu, 2006; Tan et al., 2008; Heidbach et al., 2008). The palaeostress configurations from KbFZ, KrFZ, KçFZ, KFZ, SdFZ and some secondary faults sampled in sites 1B, 2, 3, 4B, 5B, 6, 7B, 8, 9B, 13, 14, 19B, 20B, 21, 22, and 23 (Fig. 4.18a) indicate a combination of an extensional and strike-slip deformation (Fig. 4.18b, and Table 4.1). These fault zones belong to the youngest deformation phase and are the faults fringing İzmir Bay. I therefore conclude that İzmir Bay has developed during the last deformation phase in response to transtensional deformation in the region, based on major Quaternary basin bounding faults in the region (Figs. 4.18a, 4.18b, Tables 4.1, and 4.2).

CHAPTER FIVE
PALEOMAGNETIC STUDIES

5.1 Introduction

Paleomagnetic tools are one of the most successful methods in determining vertical axes rotations of fault blocks. Strike-slip fault zones are generally characterized by vertical axis rotation especially if simple shear conditions are prevailed. In this regard, paleomagnetic studies carried out around İBTZ: (i) aimed at determination of vertical axes rotations of the fault blocks within and adjacent to the İBTZ and (ii) to constrain their timing; here previously established stratigraphical ages from sedimentary units and newly obtained $^{40}Ar/^{39}Ar$ ages are encountered.

A number of paleomagnetic studies have been carried out in western Anatolia after the pioneering work of Kissel et al. (1987). Later Orbay et al. (2000), Şen & Seyitoğlu (2009), van Hinsbergen et al. (2010a, 2010b), and Kondopoulou et al. (2011) contributed to the paleomagnetic database of western Anatolia (Figs. 5.1 and 5.2). In addition to these studies, which directly address fault block rotations and tectonic evolution of western Anatolia, there are also a number of studies concerned with block rotations due to the North Anatolian Fault Zone in the northern Turkey. These include Kissel et al. (1993), Platzman et al. (1994, 1998), Tatar et al. (1996, 2000, 2002, 2004), Piper et al. (1996, 1997, 2006, 2010), Gürsoy et al. (1997, 1999, 2003), Kissel et al. (2002), Kaymakçı et al. (2007), and İşseven & Tüysüz (2006). Apart from these studies, Kissel et al. (1986), Avigad et al. (1998), Duermeijer et al. (1998, 2000), Kondopoulou (2000), van Hinsbergen et al. (2004, 2005, 2007, 2008), Kondopoulou et al. (2010), Bradley et al. (2013) provided large database from Aegean Islands and mainland Greece. Other paleomagnetic studies are mainly related to the paleotectonic events in the central and western Anatolia. These include Gürsoy et al. (1998), Kaymakci et al. (2003), Piper et al. (2002, 2009), Meijers et al. (2010, 2011), and Çinku (2012). Although, there is great number of paleomagnetic

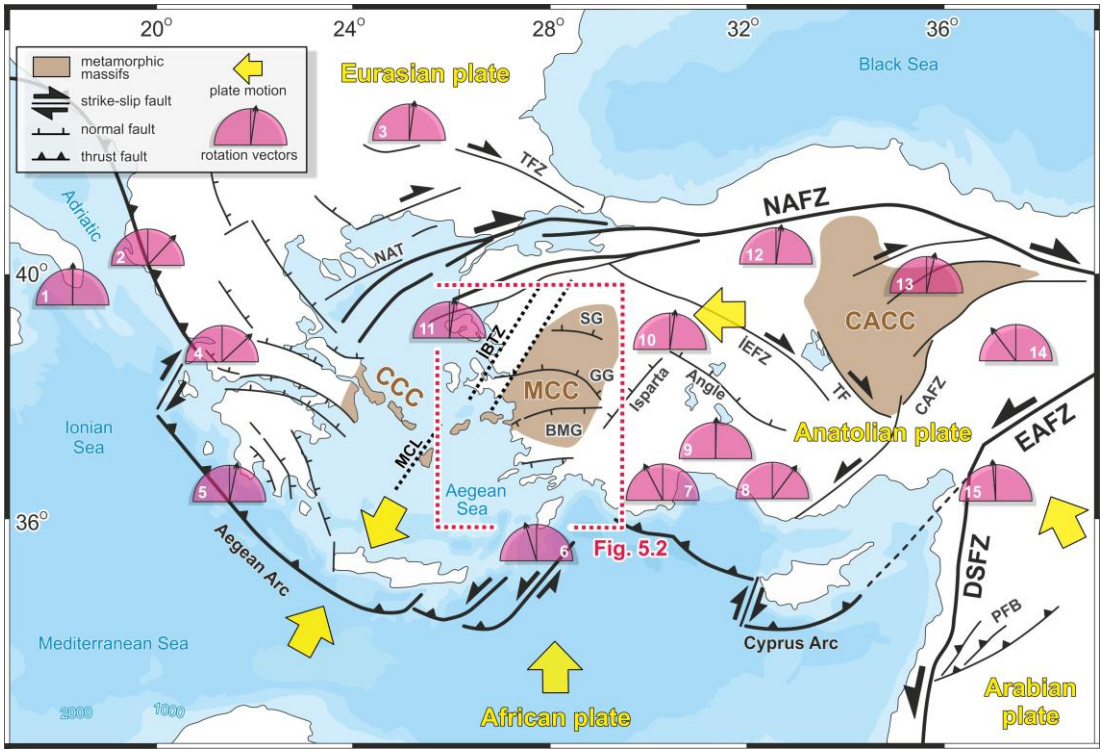


Figure 5.1 Published paleomagnetic results from the eastern Mediterranean region. The map is complied from Şengör et al. (1985), Barka (1992), Bozkurt (2001), Koçyiğit & Özaçar (2003), Uzel et al. (2008), Biryol et al. (2011) and our observations. Pink half circles represent reliable paleomagnetic declinations for post-Eocene: 1) Apulian platform (Tozzi et al., 1988; Scheepers, 1992; Speranza and Kissel, 1993), 2) Albania (Speranza et al., 1992, 1995; Mauritsch et al., 1995, 1996), 3) Moesian platform and Rhodope (van Hinsbergen et al., 2008a), 4) western Greece and Peloponnesus (Horner and Freeman, 1982, 1983; Kissel et al., 1984, 1985; Kissel and Laj, 1988; Márton et al., 1990; Morris, 1995; van Hinsbergen et al., 2005b), 5) Crete (Duermeijer et al., 1998), 6) Rhodos (Laj et al., 1982; van Hinsbergen et al., 2007), 7) Bey Dağları (Kissel and Poisson, 1987; Morris and Robertson, 1993; van Hinsbergen et al., 2010), 8) eastern limb of the Isparta Angle (Kissel et al., 1993), 9) center of the Isparta Angle (Kissel and Poisson, 1986), 10) Afyon (Gürsoy et al., 2003), 11) Lesbos (Kissel et al., 1989; Beck et al., 2001), 12) Galatean province (Krijgsman et al., 1996; Gürsoy et al., 1999), 13) Çiçekdağı basin (Gülyüz et al., 2013), 14) Sivas basin (Krijgsman et al., 1996; Platzman et al., 1998; Gürsoy et al., 1997), 15) NW margin of the Arabian platform (Gaziantep, Kilis) (Gürsoy et al., 2009). NAFZ, North Anatolian Fault Zone; EAFZ, East Anatolian Fault Zone; DSFZ, Dead Sea Fault Zone, PFB, Palmyride Fold Belt; CAFZ, Central Anatolian Fault Zone; TF, Tuzgölü Fault; İEFZ, İnönü–Eskişehir Fault Zone; SG, Simav Graben; GG, Gediz Graben; BMG, Büyük Menderes Graben; NAT, North Anatolian Through, TFZ, Thrace Fault Zone, MCC, Menderes Core Complex; CCC, Cycladic Core Complex; CACC, Central Anatolian Crystalline Complex; İBTZ, İzmir-Balıkesir Transfer Zone; MCL, Mid-Cycladic Lineament.

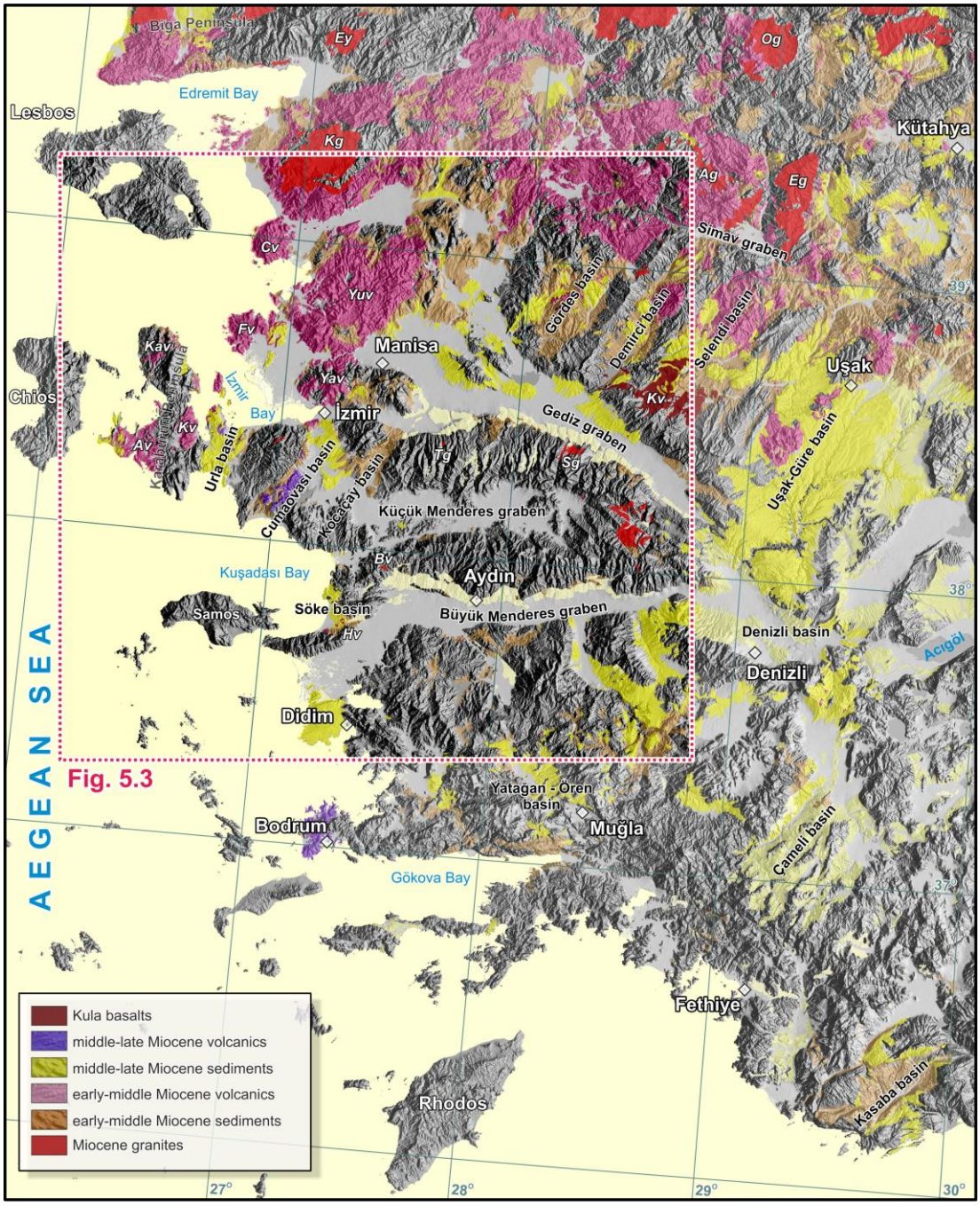


Figure 5.2 Simplified geological map of western Anatolia (MTA, 2002) draped onto a Digital Elevation Model image showing distribution of Neogene sediments, granitoids and volcanic suits. Kg, Kozak granite; Ey, Eybek granite; Og, Orhaneli granite; Eg, Eğrigöz granite; Ag, Alaçamdağ granite; Sg, Salihli granite; Tg, Turgutlu granite; Kav, Karaburun volcanic suite, Kv, Kocadağ volcanic suite; Av, Armağandağ volcanic suite; Yuv, Yuntdağ volcanic suite; Yav, Yamanlar volcanic suite; Fv, Foça volcanic suite; Cv, Çandarlı volcanic suite; Hv, Hisartepe volcanics; Bv, Balatçık volcanics.

data in Anatolian and Aegean region, the number of studies within İBTZ and surrounding region is, however relatively scarce.

It’s important to note that the problem inherited in the contradictory paleomagnetic results, reported in the literature, even from the allegedly same tectonic block is mainly due to lack of reliable age data as well as the nature of paleomagnetic signal in the volcanic rocks. It’s widely known that a volcanic rock cools within few days to few hundred years depending on the thickness and volume of the volcanic material. This implies that the paleomagnetic data that they retain are spot readings and are subjected to secular variations in geomagnetic field (Biggin et al., 2008a, 2008b; Denen et al., 2011). Thus, the deviation of the **Ch**aracteristic **N**atural **R**emanent **M**agnetism (ChNRM) can be as large as few degrees to tens of degrees depending on the position of the area with respect to paleo-pole positions. On the other hand, due to slow sedimentation rates (generally 1 and more orders slower than volcanic rocks) most of the time sedimentary rocks are least affected from secular geomagnetic variations. Since 1.3 m thick sedimentary samples may represent few hundred to thousands of years that smooth out secular variation of geomagnetic field.

One of the strategies to overcome this problem for the volcanic rocks is to sample different lava flows from the same magmatic suit, which many belong to different episodes and increase the number of the sample. The other source of error in vertical axes rotation in western Anatolia could also be size of the rotating blocks and presence of multiple phase deformation (e.g. Uzel et al., 2013). Bearing in mind all of these drawbacks, we have sampled almost all lava flows and associated sedimentary units in the study area. Depending on the availability of magmatic material, each sampled site is dated by Ar–Ar dating methods. Later, the new data set and published paleomagnetic data are integrated in order to develop an up-to-date and working kinematic model since the early Miocene.

5.2 Paleomagnetic Measurements and Analysis

The paleomagnetic sampling includes mainly four stages. These are: (1) Sampling in the field, (2) sample preparation and measurement in the lab, (3) analysis, and (4) interpretation of the results in terms of kinematics and regional tectonics. In this

study the sampling was concentrated mainly on the main magmatic suits in and around the İBTZ and intercalated sedimentary units (Fig. 5.2). Dating of the samples in each site and their stratigraphical position are discussed in the next sections. The measurements and analysis of the samples were carried out in Fort Hoofddijk Paleomagnetic Laboratory, Utrecht University, the Netherlands.

For magnetic cleaning and determination of paleomagnetic vectors, the collected samples were demagnetized using alternating field (AF) and thermal (TH) progressive stepwise demagnetization. The thermal demagnetization was carried out in a magnetically shielded oven, with varying steps from 10–50 °C up to a maximum of 645 °C. The AF demagnetization was carried out with increments of 3-20 mT, up to a maximum of 80 or 100 mT. The natural remanent magnetization (NRM) of all samples was measured on a 2G Enterprises horizontal 2G DC SQUID cryogenic magnetometer (noise level 3 x 10^{-12} Am^2). For AF demagnetization, an in-house developed robot assisted and fully automated 2G DC SQUID cryogenic magnetometer was used.

Thermomagnetic runs to determine magnetic carriers were carried out in air, using a modified horizontal translation type Curie balance, with a sensitivity of ~5 x 10^{-9} Am^2 (Mullender et al., 1993). Approximately 30–65 mg of powdered rock samples was put into a quartz-glass sample holder and was held in place by quartz wool. Heating and cooling rates were 10 °C/min. Temperatures were increased to a maximum of 700 °C. The anisotropy of magnetic susceptibility (AMS) was measured to determine the magnetic fabric of the sediments and to assess whether they have a mainly sedimentary fabric or a tectonic fabric that may be indicative of the amount of strain that the rocks underwent since their deformation (Hrouda, 1982). During deformation, the maximum axis of the AMS tensor (k_{max}) will gradually align with the direction of maximum extension and become perpendicular to the direction of maximum compression. For calculations Jelinek (Jelinek, 1981, 1984) statistics were used. Demagnetization diagrams of the NRM were plotted as orthogonal vector diagrams (Zijderveld, 1967).

To determine characteristic remanent magnetization (ChRM) directions, results from generally five to eight successive temperature or AF steps were analyzed by principal component analysis (Kirschvink, 1980). In several cases, samples with a direction that deviated from the general NRM behavior were analyzed using the great-circle approach (McFadden & McElhinny, 1988). This method was developed to identify the direction on the great circle that lies closest to the average direction obtained from well-determined NRM directions. Fisher statistics (Fisher, 1953) were used to calculate site-means and virtual geomagnetic pole (VGP) means. Because scatter of paleomagnetic directions induced by secular variation of the Earth's magnetic field is circular at the poles, but gradually becomes more ellipsoid towards the equator (Tauxe & Kent, 2004), we calculated the VGPs from all directions. Successively, a variable cut-off (Vandamme, 1994) was applied and the error in declination (Δ_{Dx}) and the error in inclination (Δ_{Ix}) of the site were calculated following Butler (1992). To determine whether two distributions have a common true mean direction (ctmd), we used the reversal test developed by McFadden and McElhinny (1990) and their classifications (A, B, C, indeterminate). The classifications are based on the critical angle γc and the angle γ between the means. Because we use their test with simulation, the test is equivalent to using the V_w statistical parameter of Watson (1983). To correct for a possible shallowing of inclination in sediments caused by compaction during burial, we used the elongation/inclination (E/I) method of Tauxe & Kent (2004).

The common temperature steps using thermal (TH) and alternating field (AF) demagnetization techniques are as follows; the volcanic sites were analyzed using progressive stepwise thermal demagnetization at temperature ranges of 20°, 120°, 180°, 210°, 250°, 300°, 350°, 400°, 450°, 500°, 530°, 560°, 580°, 610°, and 630°, while the sedimentary rocks are analyzed in temperature ranges of 20°, 120°, 150°, 180°, 200°, 225°, 250°, 275°, 300°, 320°, 340°, 380°, 420°, 450°, 500°, 530°, 560°, 580°, and 610°. For the volcanics alternating field demagnetization steps were chosen as 0, 5, 10, 15, 20, 25, 30, 35, 40, 45, 50, 60, 70, 80, 90, 100 mT, while the sedimentary specimens demagnetized alternating field ranges of 0, 6, 9, 12, 15, 18, 21, 24, 24, 27, 30, 35, 40, 50, 60, 70, 80, 100 mT.

5.3 Sampling Procedure

In total, 1398 cores were sampled at 96 localities distributed within the İBTZ and adjacent areas where a minimum of 12 (up to as much as 112) cores per site was collected. A single core often provided multiple specimens (TH and AF) for paleomagnetic analysis. The drilling locations are concentrated on the Miocene volcano-stratigraphic units exposed along the İBTZ, E-W trending graben basins, and NE-trending basins (Fig. 5.3). In addition to these, syn-extensional granites intruded into the Menderes Core Complex during its exhumation are also sampled. In order to avoid soft-sedimentary deformation (especially in early-middle Miocene sediments) both around the volcanic centers and brittle deformation along the fault zones, the undeformed and fresh outcrops are targeted for the sampling where possible.

Samples were collected using a gasoline powered ECHO and Husqvarna brand modified chain-saw engine drills. Sample orientations were measured with a magnetic compass and sun compass, depending on the rock type. The sample core orientations as well as the bedding tilts were corrected for present-day declination (4° W). At least seven standard oriented paleomagnetic cores at each site were taken after removing the weathered surface to reach a fresh outcrop. The fold-test is applied for both hillside of the NE-trending Yuntdağ area that includes YUNT01 –to –13 and DEM1 sites. In the course of this thesis project, 6 locations were re-sampled because of the adverse effects of lightning or low intensity values in the previously collected samples.

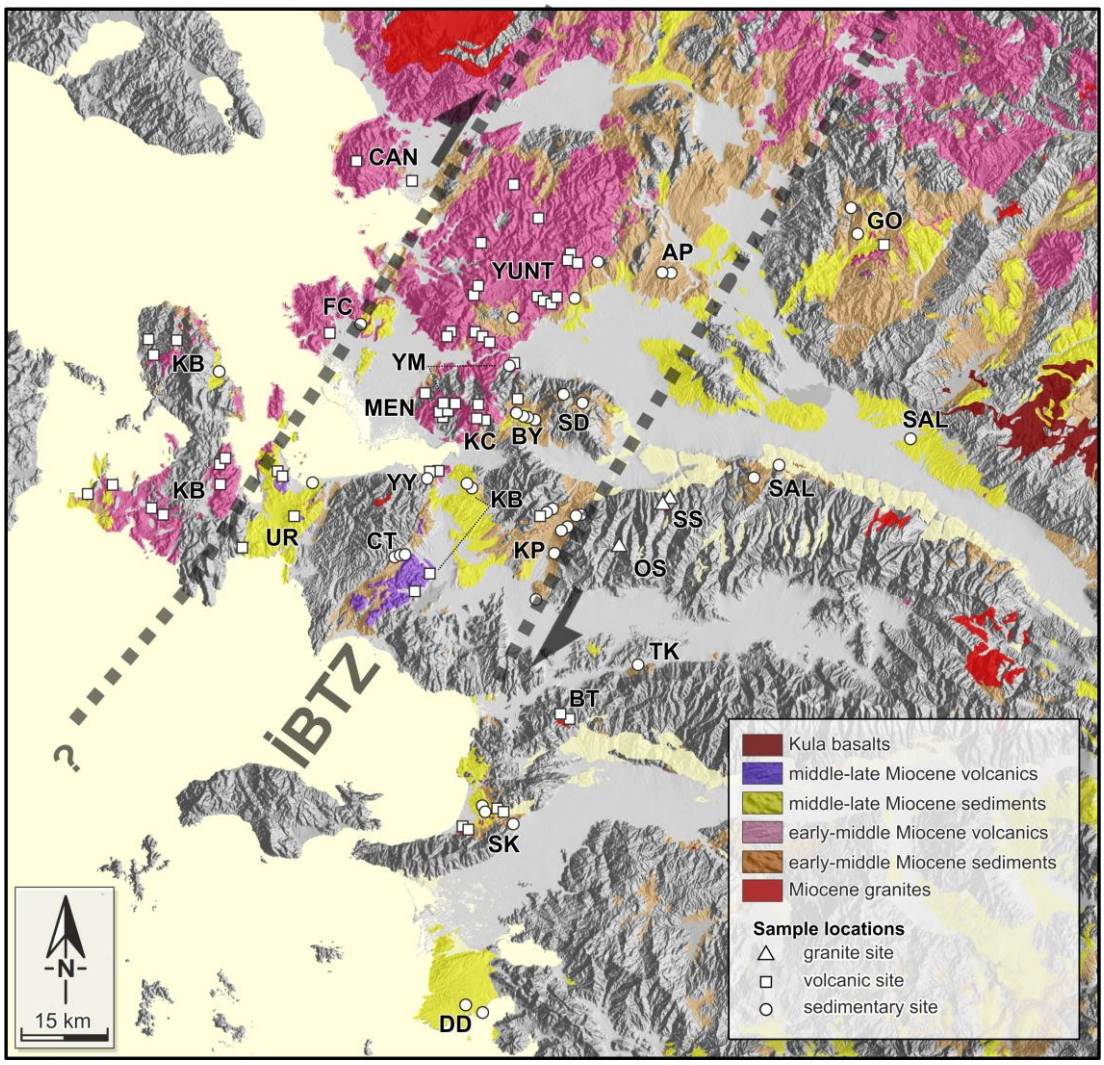


Figure 5.3 Simplified geological map showing the distribution of sampling locations and codes of ninety-six paleomagnetic sampling localities. İBTZ, İzmir-Balıkesir Transfer Zone; other abbreviations shows sample code of localities within and outside the İBTZ (see text for details).

The sampled sites in this study can be divided into two main tectonic domains; (i) the areas within the İBTZ and (ii) sample sites outside the İBTZ. In total, the study area is subdivided into subareas: (1) Yuntdağ, (2) Spildağı-Yamanlar, (3) Urla, (4) Cumaovası, (5) Kocaçay basins (or areas). These are located within the İBTZ while; (6) Dikili-Çandarlı, (7) Foça, (8) Karaburun, (9) Gördes, (10) E–W-trending Gediz, Küçük Menderes, Büyük Menderes grabens, and (11) Söke–Didim areas (or basins) lie outside the İBTZ (Figs. 5.2 and 5.3). The detailed paleomagnetic results and corresponding $^{40}Ar/^{39}Ar$ ages (see Chapter 3 for details) obtained during this PhD

project are summarized in Table 5.1. For each area, in addition to site based result, a common paleomagnetic vector is calculated. In order to obtain common vector mean directions the magnetization vectors merged and averaged using Fisher (1953) statistics. Then, tectonically induced rotations are determined for each tectonic block. 00° is accepted as the reference direction to compare rotations with each other, because it is not yet clear to us stable region the study area formerly belonged to that is why we not able to choose a pole of reference plate.

5.3.1 Paleomagnetic Studies within the İBTZ

5.3.1.1 Yuntdağ Area

About 160 samples From 17 sites are collected and demagnetized in the Yuntdağ area. The samples are from both Miocene sedimentary and volcanic rocks. The sedimentary rocks are collected from the sites AP01, AP02, AV01, YUNT03, and YUNT04, while the volcanic sites are coded as DEM1, YUNT01, YUNT02, and YUNT05–13 (Fig. 5.3).

AP01 includes 14 sedimentary cores taken from northeast hillside of the Yamanlar high where the middle–late Miocene sedimentary rocks are exposed. An approximately 12-m-thick limestone level in the sandstone, mudstone and conglomerate dominated alternation sequence was sampled (Fig. 5.4a). Here, the bedding attitude was noted in the field as N43E/50SE for tilt correction (Table 5.3). AP02 is located at near the Gökbel village (Fig. 5.3). At this location a grayish beige limestone section above greenish beige mudstones is sampled (AP02.1–8; Fig. 5.4b). The orientation of bedding plane is N75E/18SE. In addition to early–middle Miocene volcanic rocks in site DEM1 sub-volcanic dyke is also sampled (Fig. 5.3). General trend of the dyke is N50W. Ten samples were collected from this location (DEM1.1–10; Fig. 5.4c); one sample for $^{40}Ar/^{39}Ar$ dating is also collected.

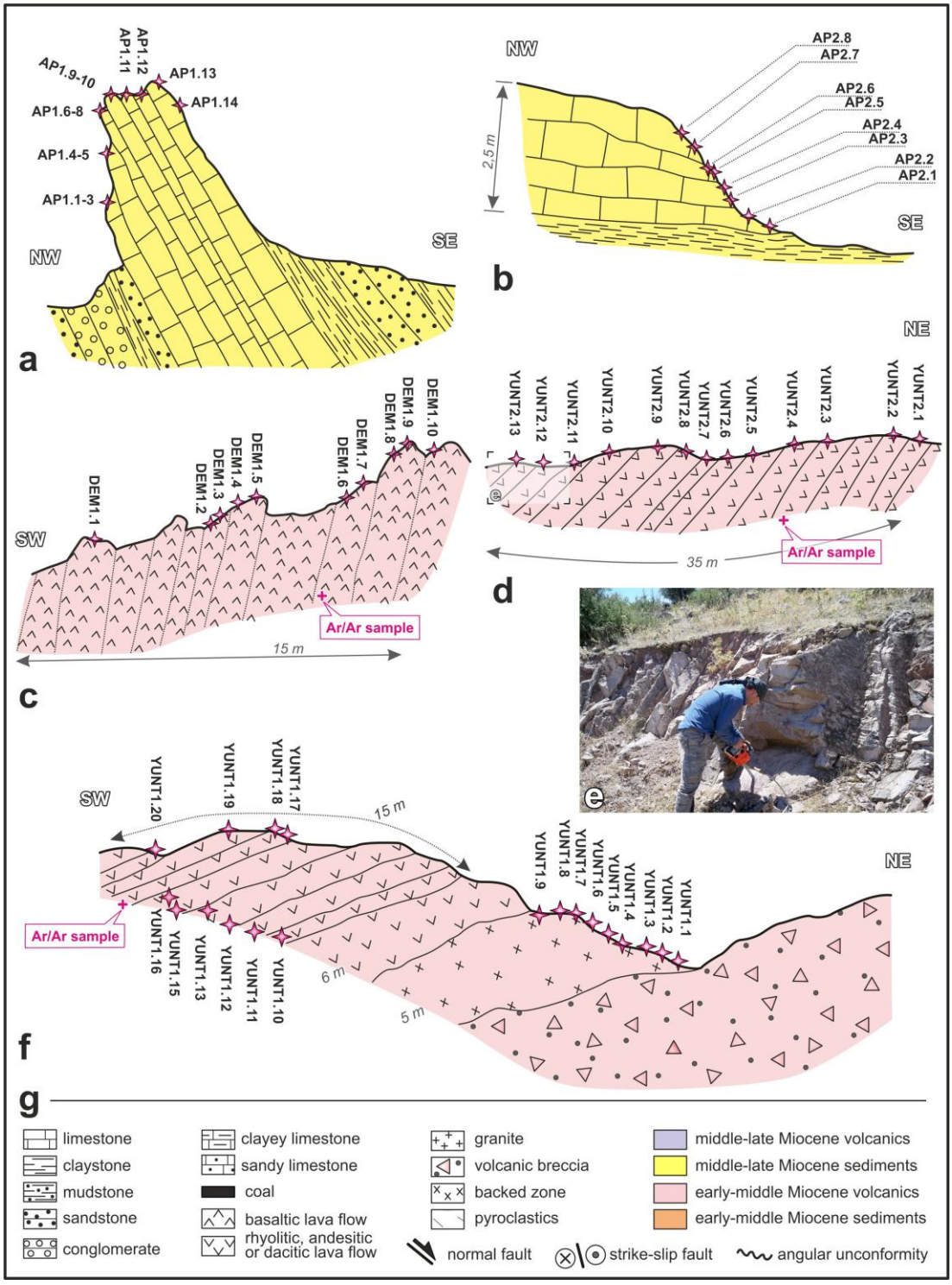


Figure 5.4 Sketch cross-sections and a field picture of the sample sites within the Yuntdağ area. a) AP01, b) AP02, c) DEM1, d–e) YUNT02, and f) YUNT01. Pink and yellow colors refer to Yuntdağ volcanics and Karadağ Formation, respectively. g) Legend for lithologies. See Fig. 5.3 for the locations of sampling sites.

YUNT01 comprise twenty paleomagnetic samples (YUNT01.1–20). The section starts with approximately 20-m-thick volcanic breccia, continues upwards more than 21 m thick dark brown to dark gray massive lava flow with 5-m-thick reddish baked zone at the base (Fig. 5.4f). The orientation of flow surfaces is measured as N15W/25SW. Near the southern hillside of the Yuntdağ high, pinkish grey andesites were sampled at YUNT02 site (Fig. 5.3). Along a road section thirteen paleomagnetic cores were collected in YUNT02, and average attitude of layering in the lava flows is approximately N10W/50SW (Fig. 5.4d–e).

Along the section, which is crossing the stratigraphic contact between the Yuntdağ volcanics and Karadağ formation, the base level of the middle–late Miocene successions were sampled and coded as YUNT03 (Fig. 5.3). Here, a thick and massive volcanic breccia level in pinkish brown color characterizes the Yamanlar volcanics. Karadağ Formation overlies the volcanic rocks of Yuntdağ volcanics with 60 cm thick basal conglomerate made up of volcanic fragments. The formation continuous with sandstone comprising reworked volcanic rocks, and lacustrine limestone alternations; fourteen samples were collected (YUNT03.1–14, Fig. 5.5a–b). The seventeen samples from Çınarlıkuyu characterize the location of YUNT04 (Fig. 5.3), where pyroclastic rocks of the Karadağ Formation are sampled along a river section (YUNT04.1–17, Fig. 5.5c). The lithology of the cores is mostly beige to dirty white tuffite and lacustrine limestone.

The YUNT05 site includes early–middle Miocene volcanic facies of the Yuntdağ volcanics and sampled along a road cut where a series of lava flows, and their baked contacts, with a level of thick volcanic breccia and tuff alternation are exposed (Fig. 5.4d). At the base the section starts with pinkish brown volcanic breccia and 20-m-thick massive grayish beige tuff layer. It continues with several dark gray lava flows, commenced with about 1.1-m-thick reddish brown to dark brown baked base. The first seven samples were taken from the baked zone (YUNT05.1–7), while the other seven samples were collected from the lava flows above (YUNT04.7–14). The bedding planes strike N60W direction and dip approximately 20° to southwest.

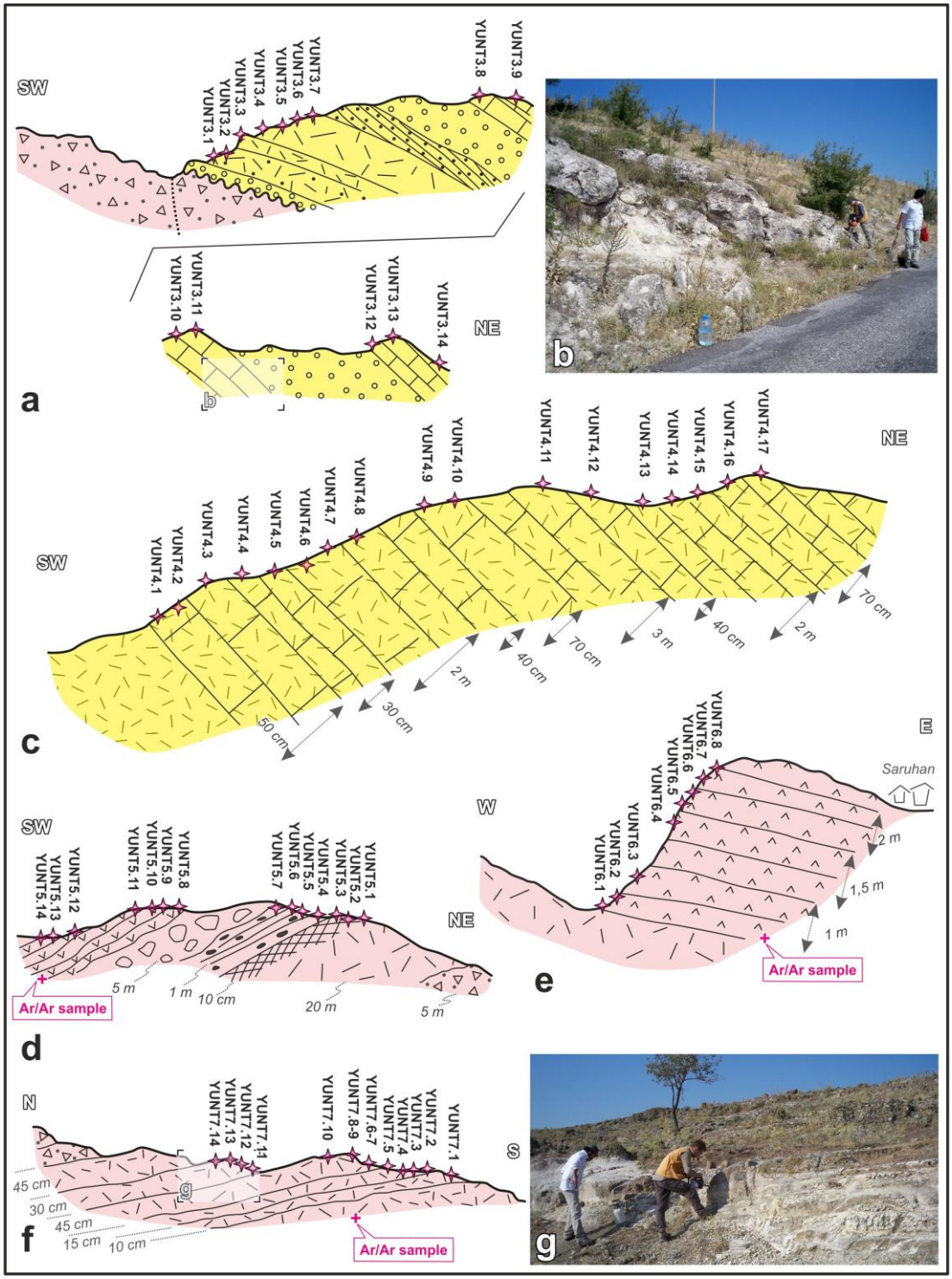


Figure 5.5 Sketch cross-sections and field pictures of the sample sites within the Yuntdağ area. a–b) YUNT03, c) YUNT04, d) YUNT05, e) YUNT06, and f–g) YUNT07. Pink and yellow colors refers to Yuntdağ volcanics and Karadağ Formation, respectively. See Fig. 5.3 for the locations of the sampling sites and see Fig. 5.4g for legend of lithologies.

The dark gray to black basaltic andesites of Yamanlar volcanics are exposed around YUNT06 site (Fig. 5.3). There eight samples were collected. The layering of the lava flows is approximately N-S/15W and is overlying grayish white pyroclastic fall deposits (YUNT06.1–8, Fig. 5.5e). YUNT07 located at the center of the Yuntdağ area and includes pyroclastic fall deposits of the Yuntdağ volcanics (Fig. 5.3). Along an N–S-directed road-cut, fourteen samples were collected at this site, where, at the top of the section, pyroclastic rocks are overlain by a thick and massive volcanic breccia (Fig. 5.5f–g). The sampling sites YUNT08 and YUNT09 are located at the southern hillside of the Yuntdağ high, along highway Çukurköy–Menemen (Fig. 5.3). There dacitic lava flows alternating with volcanic breccias are exposed (Fig. 5.6a–c). YUNT08 includes thirteen; YUNT09 includes nine paleomagnetic cores from gently dipping lava layers. The sampling localities YUNT10, YUNT11, and YUNT13 are located at the central part of the Yuntdağ area (Fig. 5.3). The samples were collected from andesitic-dacitic lava flows and associated pyroclastic deposits of the Yuntdağ volcanics. From the sampling sites YUNT10, YUNT11, and YUNT13; nine, fifteen, and twelve paleomagnetic cores were collected, respectively (Fig. 5.6d–h). At the southeastern part of the Yuntdağ area, dirty white rhyolites are exposed at a significant topographic high. These rhyolites were also sampled along a road cut (Fig. 5.3) where ten cores were collected from the SW-dipping lava layers (Fig. 5.6g).

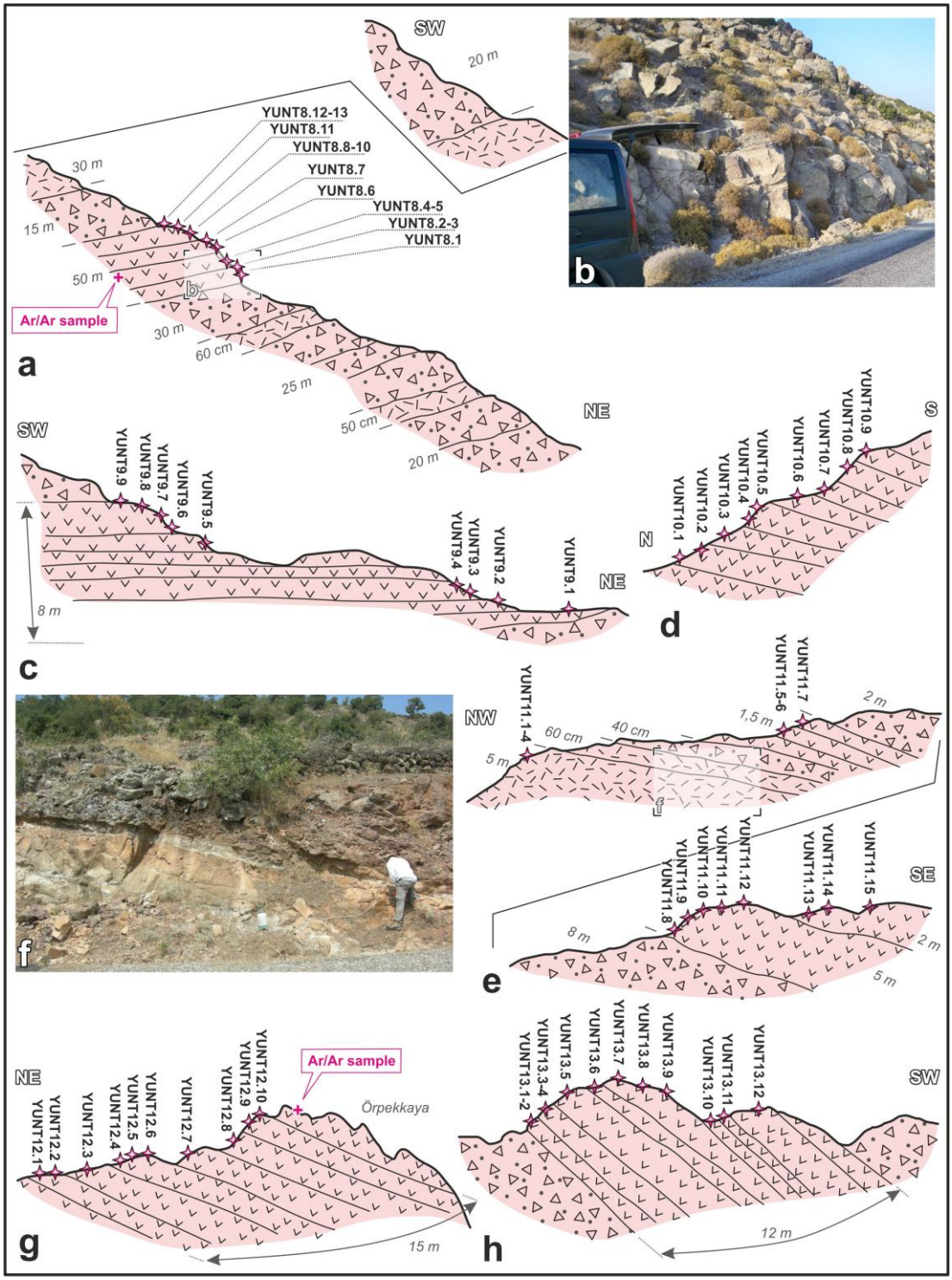


Figure 5.6 Sketch cross-sections and field pictures of the sample sites within the Yuntdağ area. a–b) YUNT08, c) YUNT09, d) YUNT10, e-f) YUNT11, g) YUNT12, and h) YUNT13. Pink color refers to Yuntdağ volcanics (*lower sequence*). See Fig. 5.3 for the locations of the sampling sites and see Fig. 5.4g for legend of lithologies.

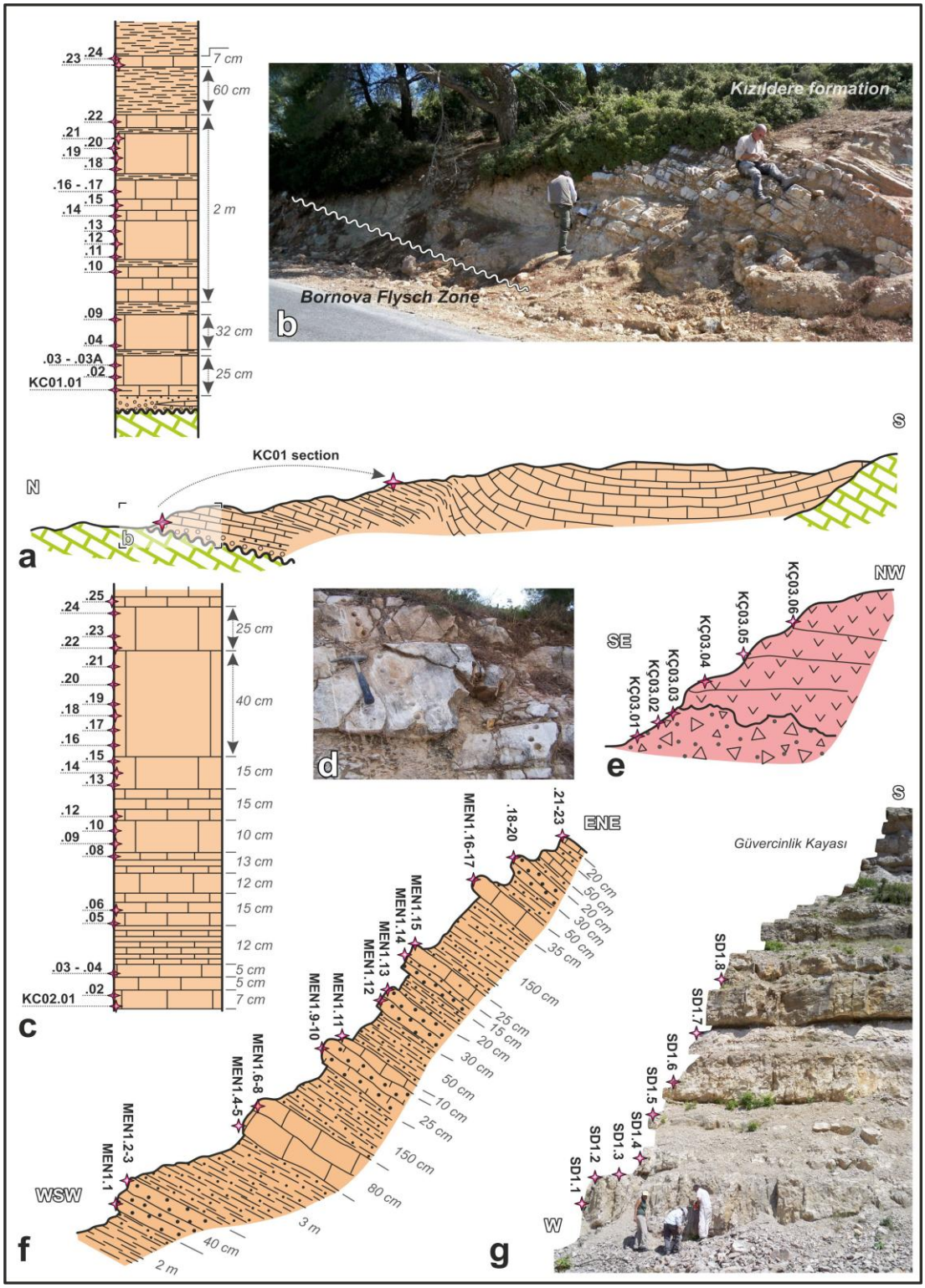


Figure 5.7 Sketch cross-sections and field pictures of the sample sites within the Spil-Yamanlar area: a–b) KC01, c-d) KC02, e) KC03, f) MEN1, and g) SD01. Pink and orange colors refer to Yuntdağ volcanics and Kızıldere Formation, respectively (*lower sequence*). See Fig. 5.3 for the locations of the sampling sites and see Fig. 5.4g for legend of lithologies.

5.3.1.2 Spildağı-Yamanlar Area

Two hundred and fifteen samples from 18 sites were collected and analyzed for the Spildağı-Yamanlar area. The paleomagnetic cores are from both early–middle and middle–late Miocene volcano-sedimentary sequences (Fig. 5.3). KC01–03, MEN1, SD01, SD02, and YM01–07 represent the lower sequence of the Miocene successions, while BY01–04 and SB01 characterize the upper sequence. In total, 112 samples (9 localities) were collected from the sedimentary rocks, 103 samples (9 localities) are from volcanic rocks.

Along the road from Bornova to Eğridere village, early–middle Miocene (*lower sequence*) successions are exposed; there sampling was performed at three sites labeled as KC01 to KC03. The early–middle Miocene Kızıldere Formation overlies the intensely deformed rocks of the Bornova Flysch Zone with an angular unconformity where a basal conglomerate level is observed. KC01 lies at the base and is composed of buff to brown micritic limestone, brownish gray mudstone and grayish green claystone alternation (Fig. 5.7a–b). Stratigraphically upwards, KC02 is sampled from a series of lacustrine limestone beds (KC02.2–25) and include twenty-five samples (Fig. 5.7c–d). Along the Kocaçay River, the stratigraphically uppermost part, KC03 site is characterized by the volcanic rocks of the lower sequence (Fig. 5.7e) where lava flows and related pyroclastic rocks of Yamanlar volcanics are exposed. Site MEN1 is located at the western margin of the Spil-Yamanlar area (Fig. 5.3) and includes twenty-two sedimentary specimens from early–middle Miocene Kızıldere Formation (MEN1.1–22). At the southeast of Menemen town, alternation of reddish brown conglomerate, sandstone and mudstone intercalated with lacustrine limestone are well exposed. Here, along a continuous section, fine-grained sandstone, sandy limestone, and limestone levels are sampled (Fig. 5.7f). In this locality, bedding dips gently to the west and includes some syn-sedimentary deformation structures and several fining upward sequences.

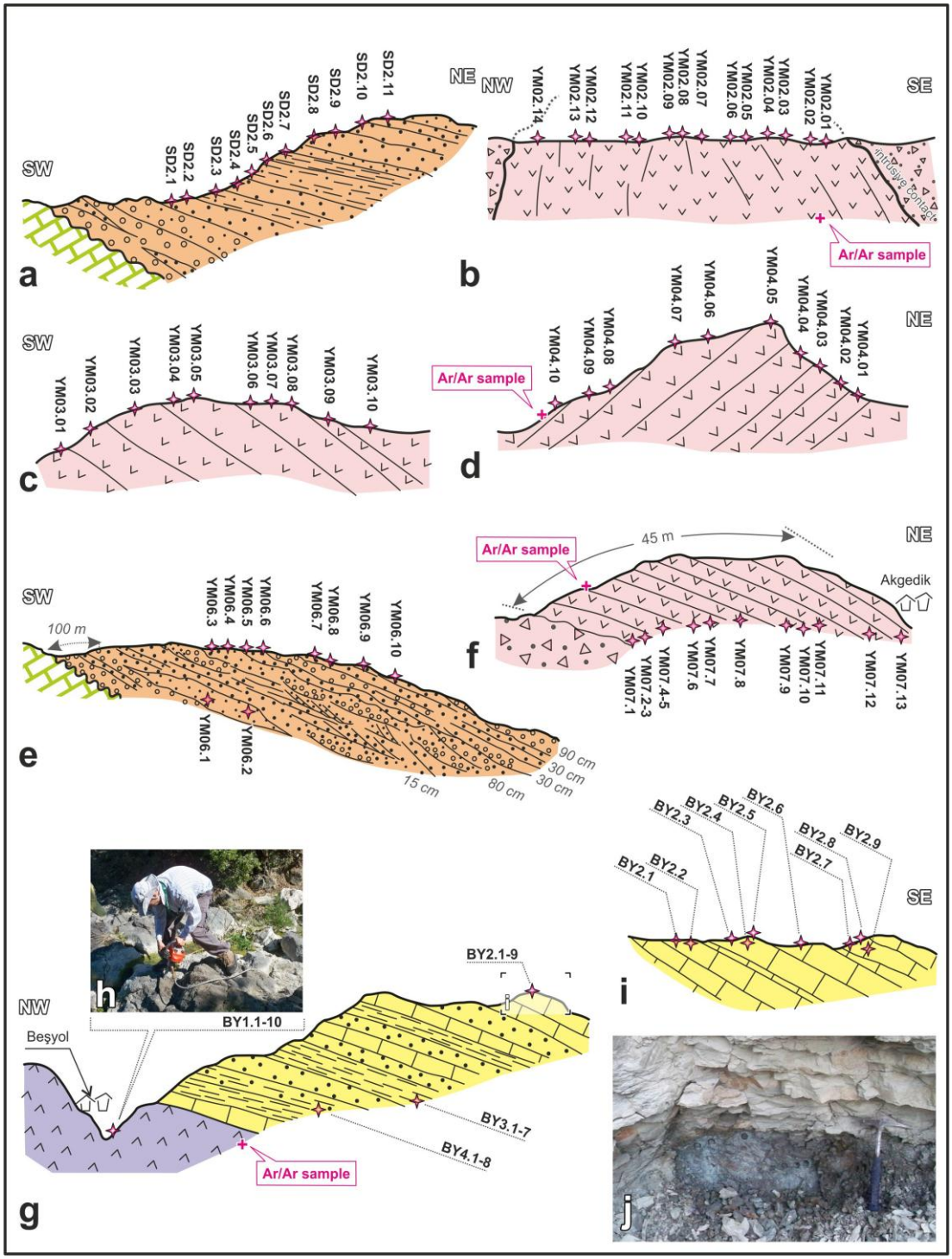


Figure 5.8 Sketch cross-sections and field pictures of the sample sites within the Spil-Yamanlar area. a) SD02, b) YM02, c) YM03, d) YM04, e) YM06, f) YM07, g–h) BY01 to BY04, and i) SB01. Pink color refers to volcanic, orange color sedimentary rocks of the *lower sequence*, similarly yellow and purple colors refer to sedimentary and volcanic rocks of the *upper sequence*. See Fig. 5.3 for the locations of the sampling sites and see Fig. 5.4g for legend of lithologies.

Sites SD01 and SD02 are located at the top of the Spildağı high (Fig. 5.3). SD01 includes eight samples of yellowish brown lacustrine limestone (Fig. 5.7g), while SD02 has eleven cores from a sequence of reddish brown sandstone and reddish gray mudstone alternation (Fig. 5.8a). Across the Yamanlar high, fresh outcrops of the early–middle Miocene rocks are sampled at 7 locations as YM01 to YM07 (Fig. 5.3). Except from YM06, all sites have the andesitic or dacitic lava flows of Yamanlar volcanics (Fig. 5.8b–f). Site YM06 represent the Kızıldere Formation, and is composed mainly of reddish brown fine-grained sandstone (Fig 5.8e).

5.3.1.3 Urla Basin

In total, 85 cores were sampled at six localities distributed throughout the middle–late Miocene lacustrine sedimentary rocks and volcanic bodies (Figs. 2.22 and 5.3). The drilling localities are concentrated mostly on the columnar basalt outcrops..

Along the road-cut between Urla and Güzelbahçe villages, alternation of middle–late Miocene lacustrine limestone and mudstone of the Urla limestone are cropped out. Along this section twenty-three sedimentary specimens are collected, and labeled as UR01 (Fig. 5.9a–b). Here, the bedding planes dip gently dipping to northwest. First, eleven samples were collected from the location (UR01.1–11), and following fieldwork season eleven more (UR01.12–22) samples were collected. The basaltic lavas cropped out in the Urla basin sampled as UR02, UR03 and UR05: from east of İskele, southwest of Yağcılar and south Ovacık, respectively (Fig. 2.22). Each drilling sites comprises basaltic lava flows that is well exposed and traced throughout the basin (Fig. 5.9c–d). Samples consisting mainly of columnar olivine-bearing basaltic lava flows are aligned and possibly emplaced along NE–SW-trending strike-slip faults during the middle–late Miocene. Site UR04 contains eleven specimens from trachyte to porphyritic rhyolite dome of Urla volcanics (Fig. 5.9d). During the paleomagnetic measurements, tectonic corrections of these volcanic sites are performed using the bedding plane attitudes from the sediments above these volcanic rocks.

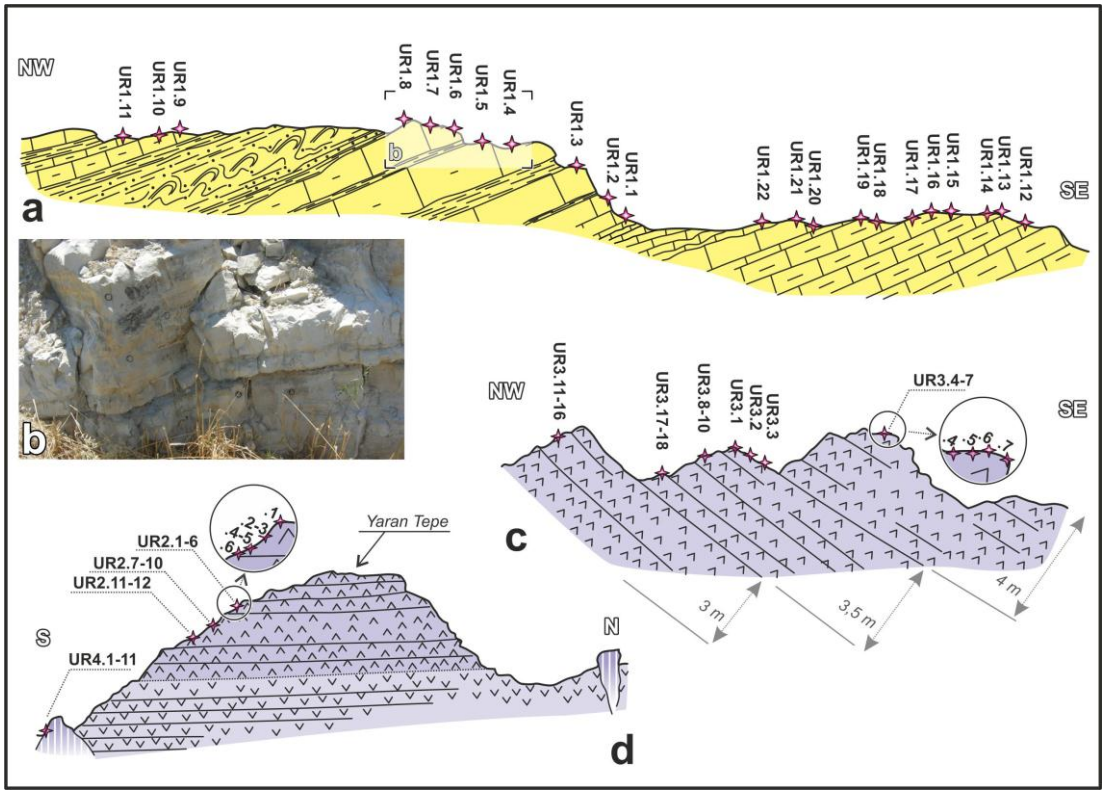


Figure 5.9 Sketch cross-sections and a field photo of the sample sites within the Urla basin: a–b) UR01, c) UR02–04, and d) UR3. Yellow color refers to Urla limestone, while purple refers to the Ovacık basalt of the *upper sequence*. See Fig. 5.3 for the locations of the sampling sites and see Fig. 5.4g for legend of lithologies.

5.3.1.4 Cumaovası Basin

During the field studies, the freshest outcrops of both lower and upper sequences are drilled around Buca, Kunerlik and Çatalca villages (Figs. 2.7 and 5.3). Hundred and twenty seven samples are collected from ten localities (CT01, CT02, CT03, KB11, KB12, KB18, KB19, YY01, YY02, and YY03). Early–middle Miocene volcano-sedimentary strata including the Çatalca Formation and the Yamanlar volcanics crops out at the northern margin of the Cumaovası basin (Fig. 2.7). It starts with brownish gray at the base, and continues upwards with brownish gray mudstone, sandstone, claystone alternation and thin coal-seam intercalations. Along this section, twenty-two samples were collected from the conformably overlying volcanic breccias in the site YY03 (YY03.1–22; Figs. 5.10c–d). Stratigraphically upwards, the strata include first andesitic lava flow and breccia alternation, then thick

and continuous blocky lava layers dipping gently to NE. At this level, thirteen and ten samples are collected, and labeled as YY02 (.1–13), and YY01 (.1–10) respectively (Fig. 5.10a–b).

The sites CT01 and CT02 are located near Çatalca at the northwestern margin of the basin (Fig. 2.7). Along the section the early–middle Miocene sediments lie (Çatalca Formation) on the rocks of the late Cretaceous–Paleocene Bornova Flysch Zone with an angular unconformity (Fig. 5.10e–g). The sequence starts at the base with sub-angular pebbles of greenish brown basal conglomerate, made up of fragments derived from the basement. These conglomerates are covered by light brown, massive sandstones and are overlain by dark gray organic rich mud to coal interlayers. The sequence continues with a few meters thick light brown to gray sandstone and greenish gray mudstone alternations where limestones become dominant at the upper levels. From this part of the section, thirteen samples are collected (CT01.1–13). The top of the section comprises thick yellowish brown lacustrine limestone levels from which eighteen cores are drilled (CT02.1–18).

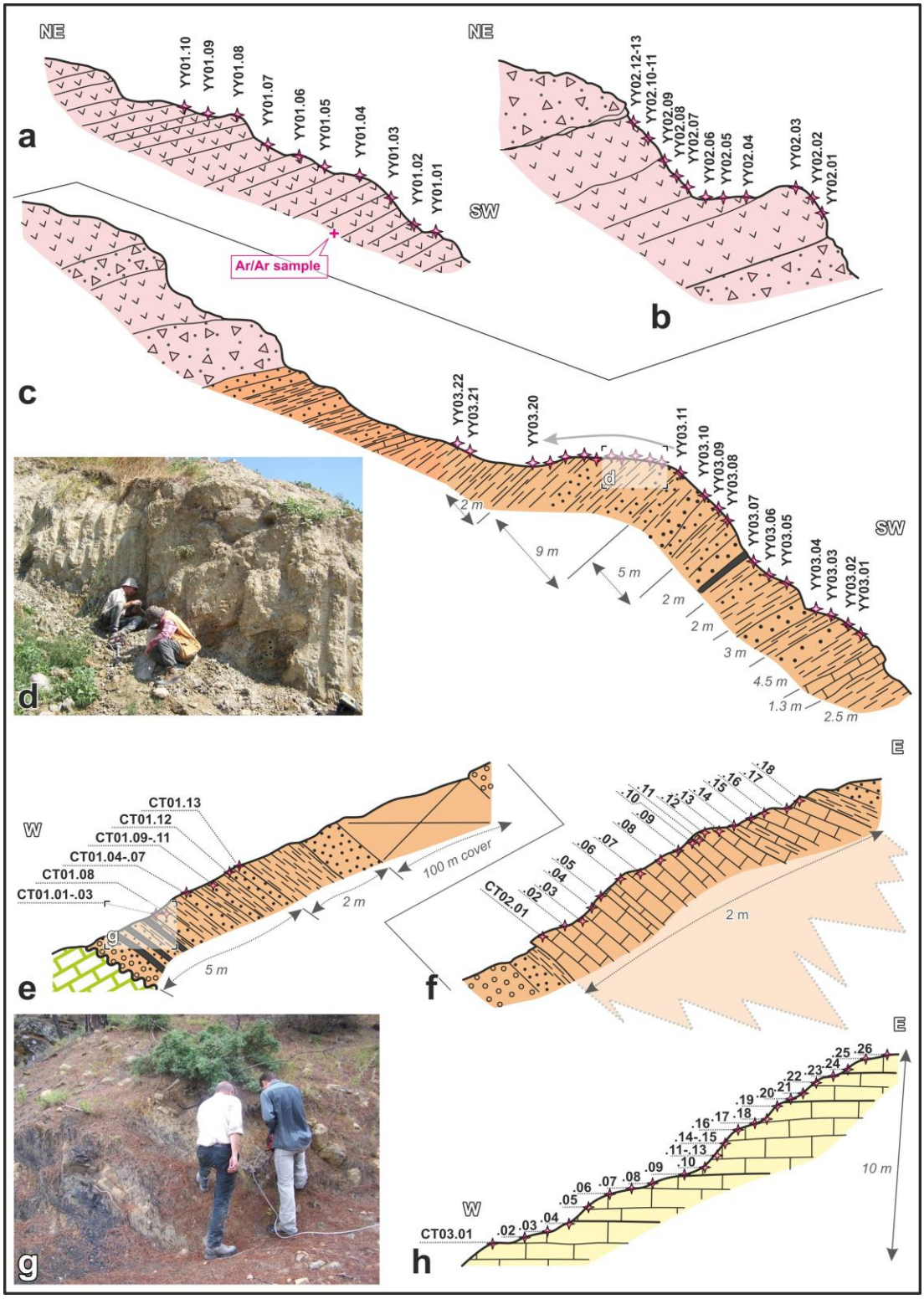


Figure 5.10 Sketch cross-sections and field pictures of the sampling sites illustrating positions of the samples within each section in the Cumaovası basin: a) YY01, b) YY02, c–d) YY03, e–g) CT01, f) CT02, h) CT03. Pink refers to volcanic, orange to clastic and yellow to limestone sequences. See Fig. 5.3 for the locations of the sampling sites and see Fig. 5.4g for legend of lithologies.

The middle–late Miocene Yeniköy Formation unconformably overlies the Çatalca Formation, and the contact relationship is well observed along a river-cut at the northwest of Yeniköy village (Fig. 2.7). The undeformed, yellowish medium to thick bedded, nearly horizontal white lacustrine limestone level of the Yeniköy Formation is drilled, and twenty-six samples as CT03 (.1–26, Fig. 5.10h) were collected. The localities KB18 and KB19 also comprise fresh outcrops of the Yeniköy Formation around Buca (Fig. 2.7). Nine and eleven paleomagnetic cores were drilled from these sites, respectively. Along the road near Kunerlik village, rhyolitic lava flows of the middle–late Miocene Cumaovası volcanics crops out (Fig. 2.7). From these volcanic rocks in two sites (KB18 and KB19) thirty-eight (twenty and eighteen, respectively) paleomagnetic cores were collected. These lava flows represent the volcanic rocks of the upper sequence and at the same time they are the topmost units of the late Miocene volcano-sedimentary successions in the İBTZ.

5.3.1.5 Kocaçay Basin

From the infill of Kocaçay basin nine sites are drilled and 78 samples were collected (Figs. 2.27 and 5.3; Table 5.1). All sites comprise early–middle Miocene Dereköy, and Vişneli Formations. The sample sites marked with KP5 and KP7 belongs to the Vişneli Formation others, Dereköy Formation.

At the eastern side of the basin, the freshest and slightly less deformed outcrops of the Dereköy Formation are exposed between the Karakızlar and Karaot villages (Fig. 2.27). Here the unit comprises a series of grey lacustrine limestone lenses within a brick red to crimson clastic sequence. As sites KP1 and KP2, seven and nine paleomagnetic cores were drilled from the limestones, respectively (KP1.1–7, KP2.1–9). KP3 and KP4 are located along a road-cut to Dereköy village. Along the section, fine-grained reddish sandstones and dark gray mudstones alternating with reddish purple conglomerates are sampled, and fifteen samples (KP3.1–8, KP4.1–7) were collected in stratigraphic order (Fig. 5.11a).

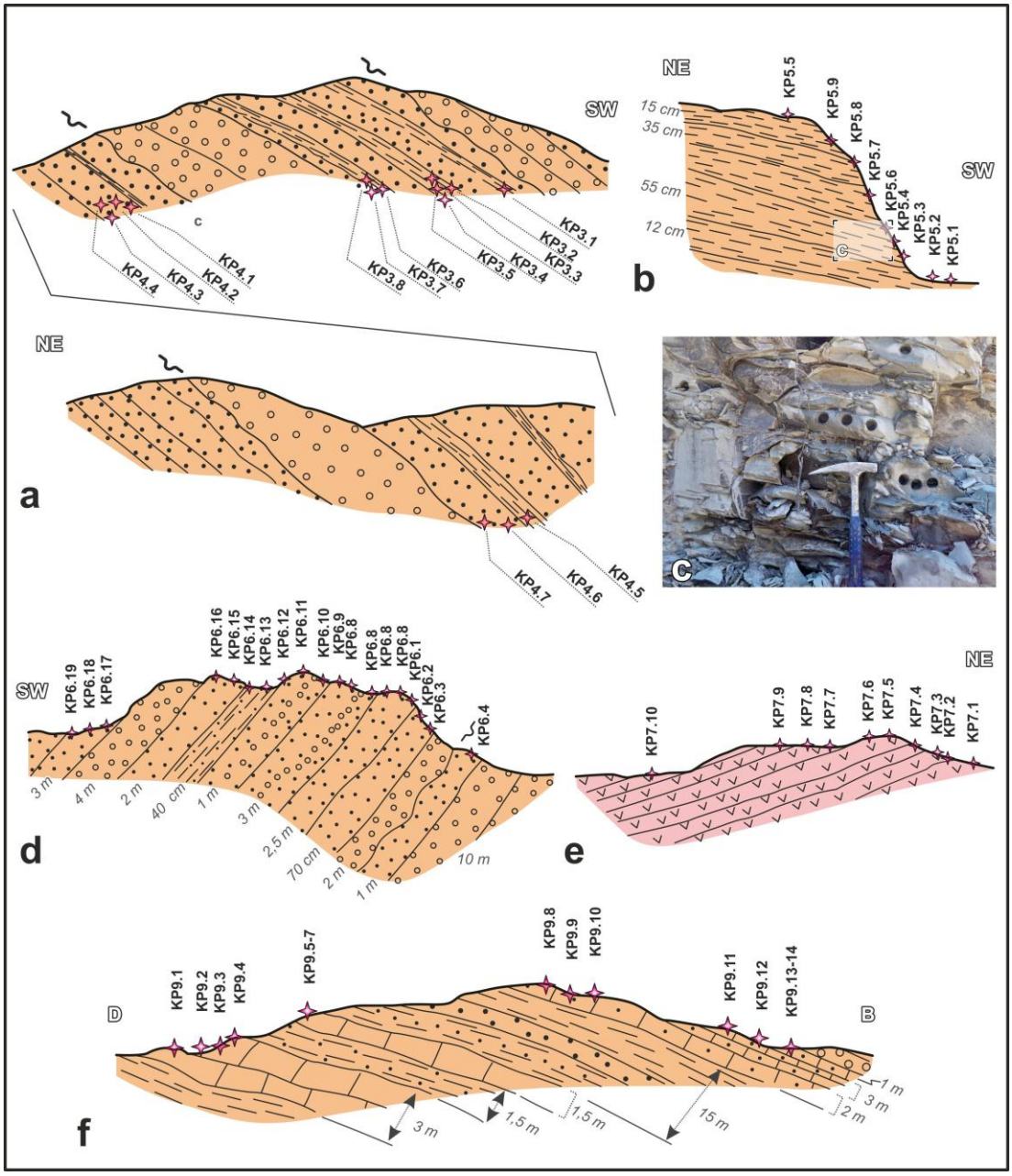


Figure 5.11 Sketch cross-sections and a field photo, indicating stratigraphic positions of the paleomagnetic samples within the Kocaçay basin. a) KP03–KP04, b–c) KP05, d) KP06, e) KP07, and f) KP09. Orange color refers to sedimentary while pink color refers to volcanic rocks of the lower sequence. See Fig. 5.3 for the locations of the sampling sites and see Fig. 5.4g for legend of lithologies.

Along the western side of the Kocaçay basin, fine-grained sediments of the Vişneli Formation, and along the eastern side, relatively coarse-grained sediments of the Dereköy Formation are exposed. Around Vişneli village, the Vişneli Formation starts with conglomerates intercalated with mudstones. After tens of meters,

mudstones became less in amount and the conglomerates appear as the dominant lithology in the unit. Here, nine paleomagnetic samples (KP5.1–9) were drilled in a creamy white to greenish gray, gently dipping, leaf fossils bearing mudstones (Figs. 5.11b–c). The KP6 site is located around Dağkızılca village where Dereköy Formation is exposed. Along a road-section the unit contains reddish, thick and massive conglomerates at the base, which laterally grades into purplish sandstones and buff to pale gray mudstones. From this section nineteen (KP6.1–19) paleomagnetic cores were drilled (Fig. 5.11d). In the western side, a thick tuff lenses radiometrically dated at 13.8 Ma (Sözbilir et al. 2011) were also sampled (KP7.1–10 ten specimens). KP8 and KP9 sites include the limestone lenses of the Dereköy Formation, and are locate at the southeastern part of the basin (Fig. 5.3). From these sites fifteen (KP8.1–15) and ten (KP8.1–10) paleomagnetic samples were collected, respectively (Fig. 5.11f).

5.4.2 Paleomagnetic Studies outside the İBTZ

5.4.2.1 Dikili-Çandarlı Area

From the Dikili-Çandarlı area 26 samples were collected at two sites, these are CAN1 and CAN2 sites (Fig. 5.3). Both sites comprise the early–middle Miocene volcanic rocks (*lower sequence*). The first site is located around Burgaz Hill, along the main road to the Çandarlı village. There, greenish gray mudstone and light brown tuff (and/or volcano-clastic sandstone) alternations are overlain by >35-m-thick dark grey volcanic lava flows with a reddish baked zone at their base are well exposed (Fig. 5.12a–b). Lavas are characterized by 10-cm- to 1-m-thick several flow packages. Twelve samples were collected from these gently south dipping flows (CAN1.1–12). CAN2 is located in the central part of the area, in the vicinity of the Çandarlı village. From this site fourteen cores were drilled (CAN2.1–14). Here, pinkish gray gently south-dipping dacitic lava flows are drilled. Lava flows lie above dark gray to brown volcanic breccias and display baked soles(Fig. 5.12c).

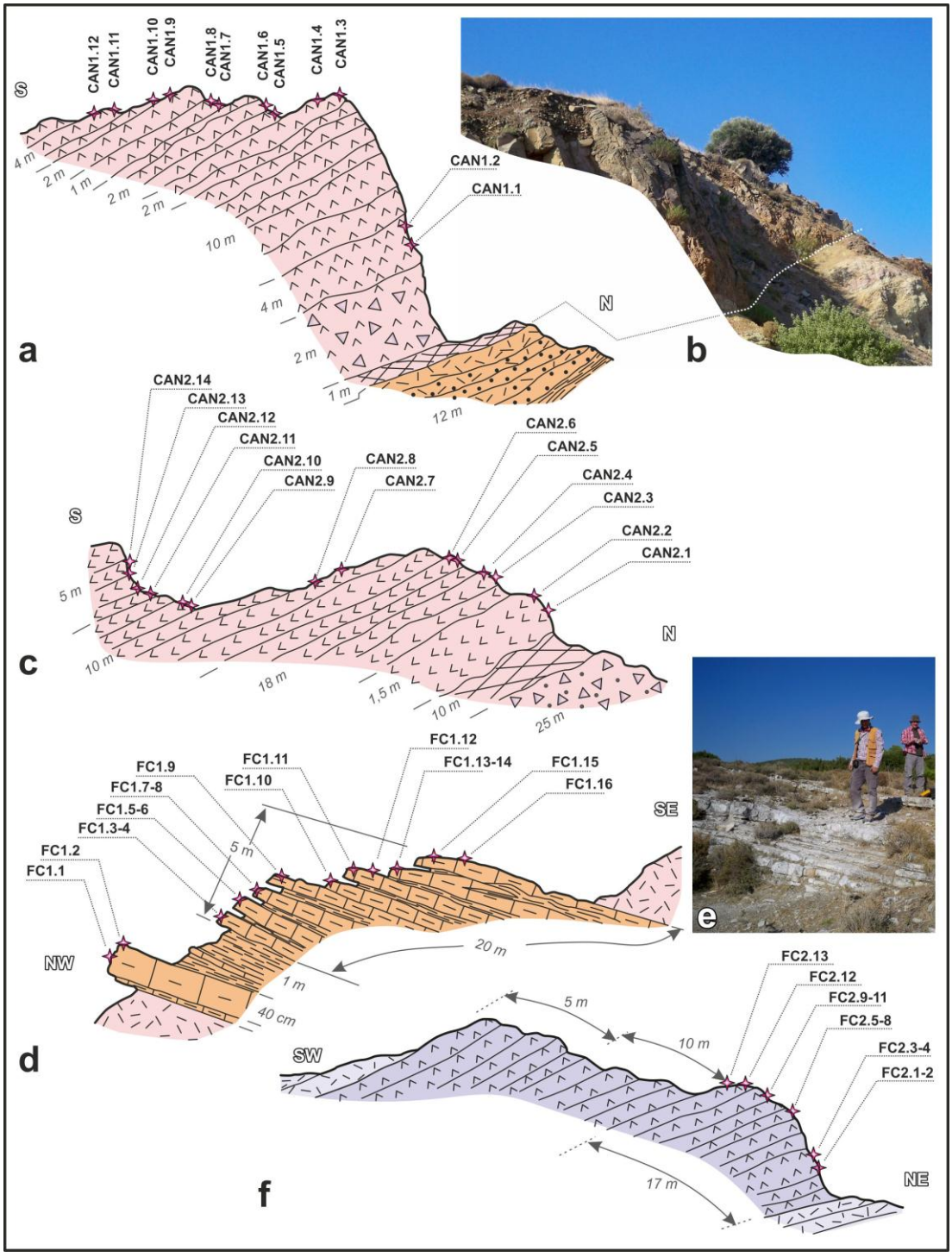


Figure 5.12 Sketch cross-sections and field photos showing stratigraphic positions of the paleomagnetic samples within the Çandarlı-Dikili and Foça areas: a–b) CAN1, c) CAN2, d–e) FC1, f) FC2. Pink and orange colors refer to the *lower*, while purple refers to the *upper sequence*. See Fig. 5.3 for the locations of the sampling sites and see Fig. 5.4g for legend of lithologies.

5.4.2.2 Foça Area

It comprises the early to late Miocene volcano-sedimentary rocks around the Foça village. The sampling was performed mostly along the road cuts of the Menemen–Foça highway. Forty one specimens were drilled at two sites (FC1, and FC2; Fig. 5.3). FC1 is characterized by a lacustrine limestone lens within pyroclastic deposits of the Foça volcanics. Maximum thickness of the lens is about 35 m and is characterized by yellowish to buff color and mostly intercalated with laminated claystone. From the site twenty-six samples were collected (FC1.1–26; Fig. 5.12d–e). Dark gray, gently south dipping columnar basalt layers of Foça alkaline volcanics are exposed at SE of the area where thirteen (FC2.1–13) samples were obtained (Fig. 5.12f). In the locality, the lava flows overlie biotite rich buff to yellowish tuffs which, in turn, are overlain by light brown pyroclastics.

5.4.2.3 Karaburun Area

Early–middle Miocene volcano-sedimentary rocks (*lower sequence*) with several volcanic centers crops out throughout the Karaburun area. In total, 174 paleomagnetic samples from 13 localities (KB01– to– 09, and KB20– to– 23) have been processed to unravel the paleomagnetic history of area (Figs. 5.3, and 5.13).

The sample sites are concentrated mostly on the volcanic outcrops, since they can be dated precisely, which provide means of correlation Yaylaköy volcanics (KB01, KB03, KB22, KB23), Kocadağ volcanics (KB05, KB06, KB07), Armağandağ volcanics (KB08, KB09), and Foça volcanics (KB21) were drilled and from each sites; forty two, forty three, twenty one, and fifty three paleomagnetic cores were collected, respectively. The samples of KB02, and KB20 belongs to the early–middle Miocene (*lower sequence*) sedimentary rocks of the Bozköy Formation, while the site KB04 includes ten specimens from the middle–late Miocene Urla limestone (*upper sequence*) (KB04.1–10).

In the KB20 site, the gently dipping red beds of the Bozköy Formation lying on the Karaburun Belt with an angular unconformity are sampled (Fig. 5.13). Here,

eighty-nine paleomagnetic specimens were drilled along a log section they are useful in unraveling the oldest vertical axis rotation history of the area.

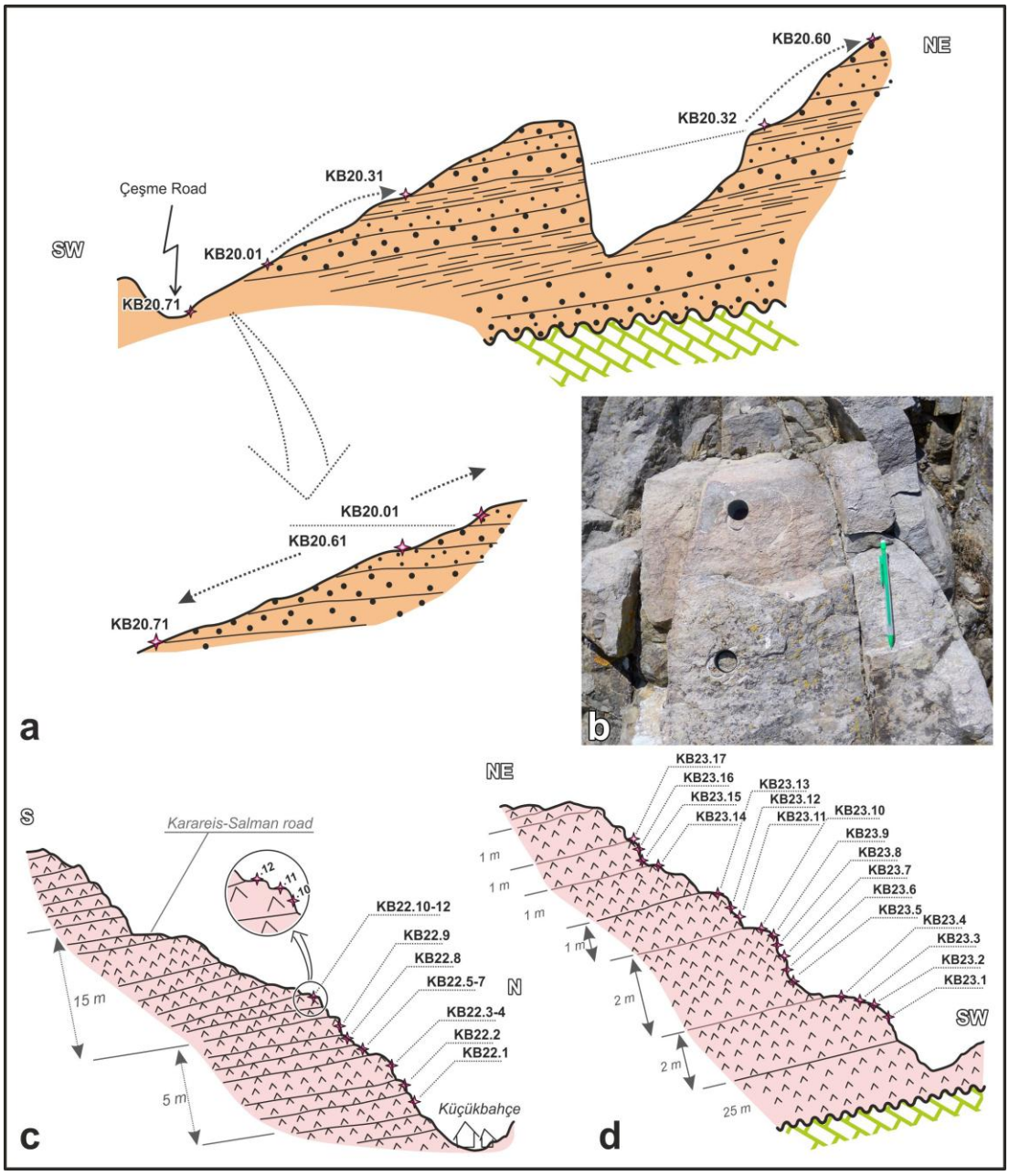


Figure 5.13 Sketch cross-sections and a field photo showing stratigraphic positions of the paleomagnetic samples within the Karaburun area: a) KB20; b–c) KB22, d) KB23. Orange color refers to sedimentary rocks and pink color refers to volcanic rocks of the Lower sequence. See Fig. 5.3 for the locations of the sampling sites and see Fig. 5.4g for legend of lithologies.

5.4.2.4 Gördes Basin

Sampling studies in Gördes basin were performed on the sedimentary rocks of the early–middle Miocene Kuşlukköy Formation, and volcanic rocks of central volcanics dated at 21.7–16.3 Ma by Seyitoğlu and Scott (1994). These rocks were sampled in three sites, GO1, GO2, and GO3 sites (Figs. 5.3, and 5.14). The longest sections of the basin infill is located at the northwest of Kayacık village, where freshest rocks are sampled (GO1). It includes thirty specimens (GO1.1–30) obtained from lacustrine limestone, mudstone and fine-grained sandstone (Fig. 5.14a–c) of the Kuşlukköy Formation. Second locality in the Gördes basin, GO2, represents the central volcanics of the basin. Eleven specimens (GO2.1–11) were analyzed for the rotational history of the basin (Fig. 5.14d). The other locality characterizing the sedimentary infill of the basin is located along Akhisar–Gördes highway. Thirteen paleomagnetic cores (GO3.1–13) were collected from the thick-bedded limy-, sandy- and micritic-lacustrine limestones (Fig. 5.14e).

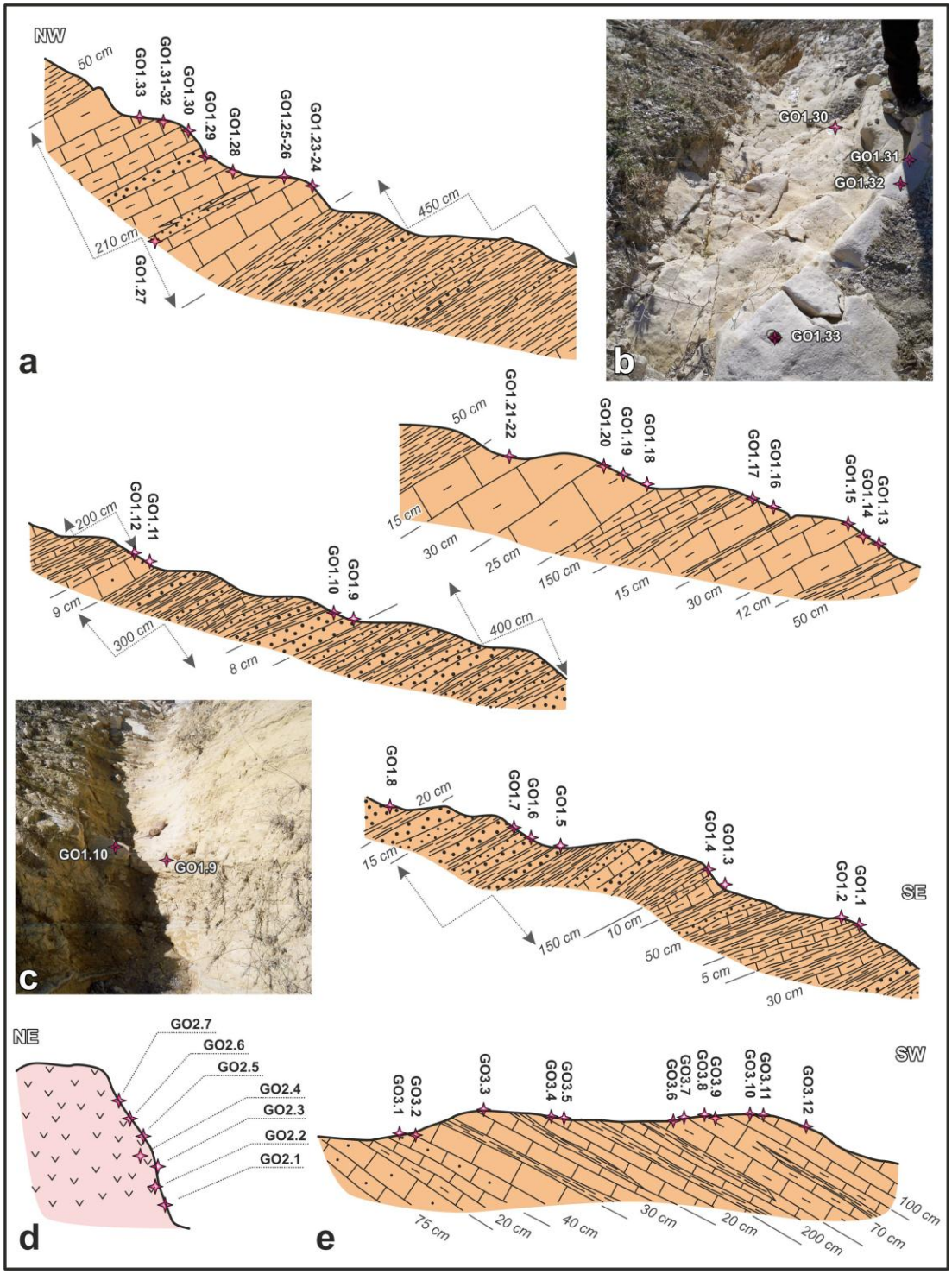


Figure 5.14 Sketch cross-sections and filed photos showing stratigraphic positions of the paleomagnetic samples within the Gördes basin: a–c) GO1; d) GO2, e) GO3. Orange (pink) color refers to sedimentary (volcanic) rocks of the *lower sequence*. See Fig. 5.3 for the locations of the sampling sites and see Fig. 5.4g for legend of lithologies.

5.4.2.5 Gediz, Küçük Menderes, and Büyük Menderes Grabens

A series of actively developing E–W graben and horst form main morphology of the region at the eastern side of the İBTZ. In order to determine relative vertical axis rotations of İBTZ, since the early Miocene, with respect to its intervening blocks paleomagnetic sampling was also performed in nine sites located outside the İBTZ. Sampling within the Gediz graben was performed on the sedimentary rocks, which lie immediately above the Gediz detachment fault (SAL1–3) and southern. In these sites twenty-four samples were collected from sandstone, mudstone, and lacustrine limestones (Fig. 5.15a–e).

Site TK1 is from the early–middle Miocene rocks of the Küçük Menderes graben, which overlie coal seams bearing basal sequence (Fig. 5.15e). In this area gently south dipping, grayish brown limy sandstone and light brown lacustrine limestone alternations are sampled, and eleven specimens were collected (TK1.1–11). Due to scarcity of the sedimentary outcrop, volcanic rocks exposing at the northernmost rim of the Büyük Menderes graben are drilled instead, at sites BT01 and BT02 (Fig. 5.3). Here, twenty-five paleomagnetic cores are collected from the Balatçık volcanics (BT01.1–13, BT02.1–12). Additionally, syn-extensional granitic bodies, which are intruded into the Menderes Core Complex and the Gediz detachment, are also sampled during this study (Fig. 5.3). These sites are very important, in order to test vertical axes rotations of hanging-wall blocks (most of the NE-SW grabens) of the detachment fault with respect to the footwall-blocks, which are represented by these syn-extensional granitoids. For this purpose the freshest outcrops, at the south of Salihli-Turgutlu town, are drilled along a river valley in two sites namely SS1 and SS2 (Figs. 5.15f–h). Third location, OS1 represents a relatively small granitic body exposed near the Osmacalı village, and comprises twenty-seven paleomagnetic cores (OS1.1–27).

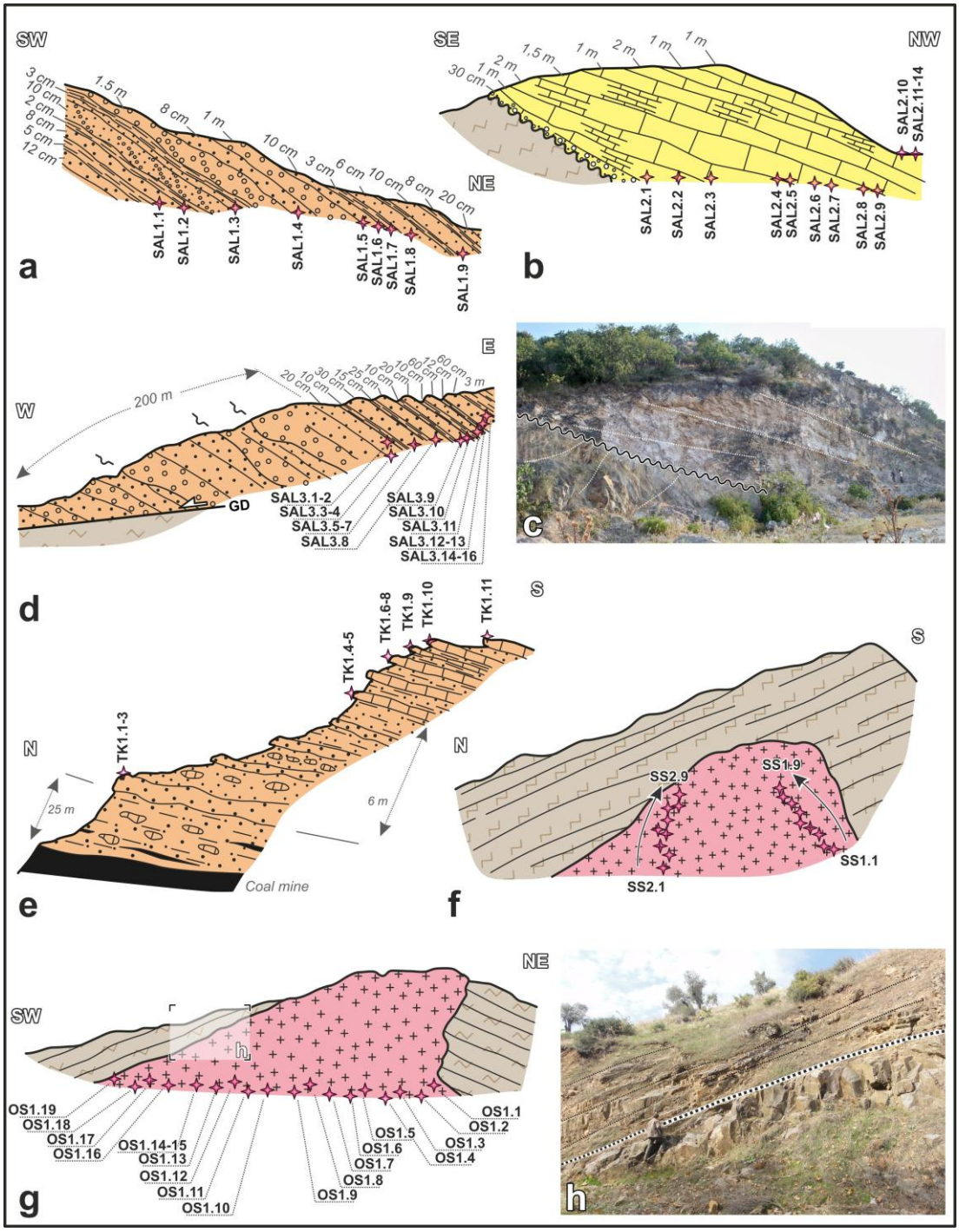


Figure 5.15 Sketch cross-sections and filed photos indicating positions of the paleomagnetic samples within the E–W-trending grabens, a) SAL1; b) SAL2, c–d) SAL3, e) TK1, f) SS1–SS2, g–h) OS1. Orange (yellow), and pink colors refer to lower (upper) volcano-sedimentary sequence, and syn-extensional granite. See Fig. 5.3 for the locations of the sampling sites and see Fig. 5.4g for legend of lithologies.

5.4.2.6 Söke Basin & Didim Area

In total 230 sample cores were collected from the Söke basin (199 cores) and Didim area (31 cores) in 9 localities that include SK1–SK7, DD1–DD2 (Fig. 5.16). Except from the basal part of the SK6 comprising the early–middle Miocene Söke Formation, all of the samples were collected from the middle–late Miocene volcano-sedimentary units.

The sites, SK1 and SK2, located in the center of the basin comprise eighteen and thirteen paleomagnetic samples, respectively (SK1.1–19, and SK2.1–13). The sampled unit is the Kuşadası Formation and it is characterized by pale gray sandy limestone, greenish gray mudstone and gray sandstone (Fig. 5.16a–c). Hisartepe volcanics are exposed within the Söke basin (Gürer et al. 2000) between Söke and Davutlar villages and were sampled at four sites: SK3, SK4, SK5, and SK7. Fifty-three samples were collected from middle–late Miocene basaltic and dacitic rocks (SK3.1–8, SK4.1–16, SK5.1–13, and SK7.1–16) in stratigraphic order (Fig. 5.16d–h). In the SK6 site sampling was performed along a line starting from Söke town and continued upwards in NW direction. It covers lower part of the early–middle Miocene Söke Formation (SK6.1–93; Fig. 5.16k–o) and then middle–late Miocene Kuşadası Formation (SK6.94–107), which were separated by an angular unconformity (Fig. 5.16i–j). Along this section, at the bottom, buff lacustrine limestone, greenish gray fossil-rich (mostly gastropod) laminated mudstone beds of the Söke Formation are drilled. Above the intervening angular unconformity, the Kuşadası Formation is composed mainly of coarse-grained conglomerate and sandstone alternations; samples were collected from the fine-grained levels intercalated within the sandstone beds, and alternating mudstones.

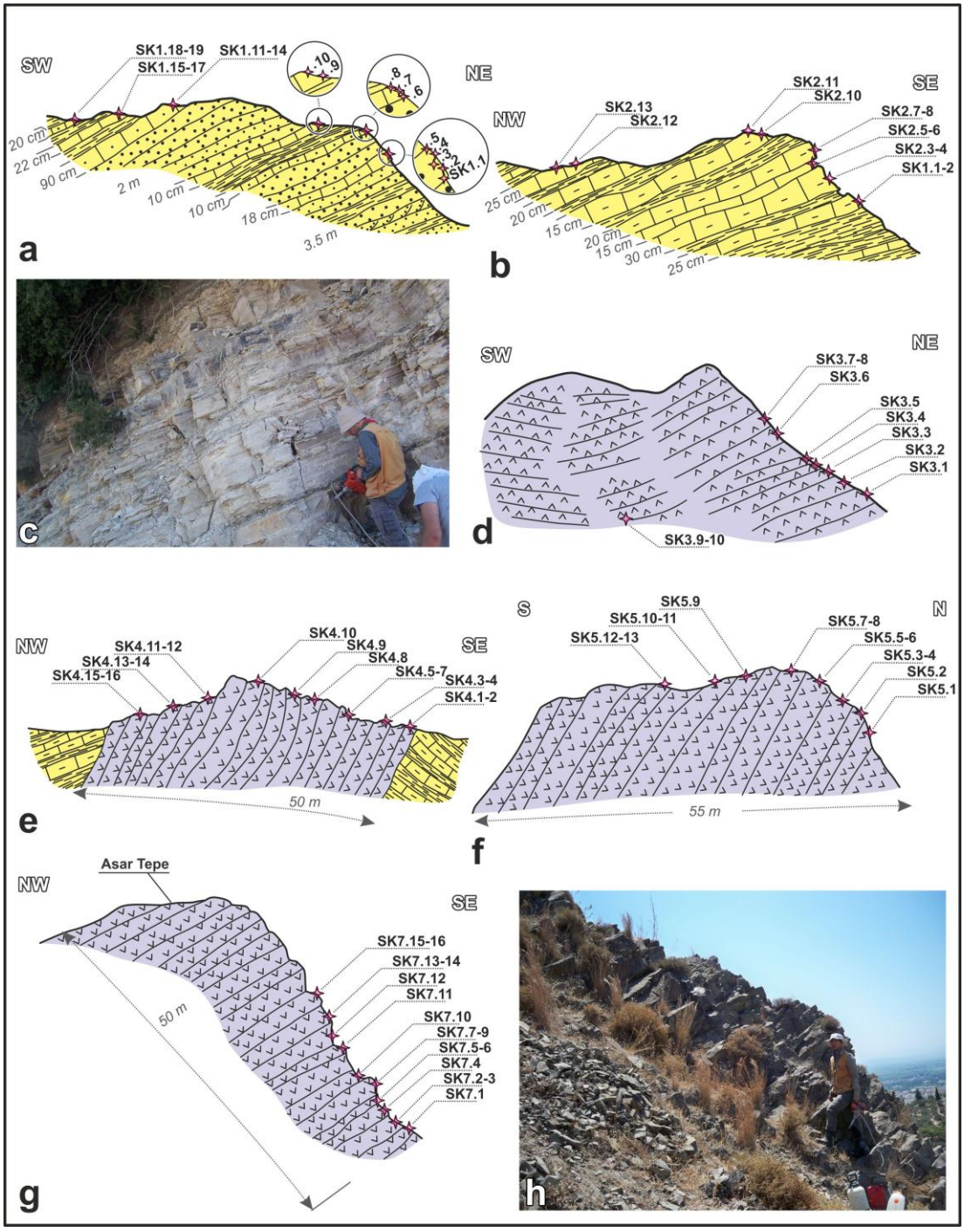


Figure 5.16 Sketch cross-sections and field photos showing stratigraphic positions of the paleomagnetic samples within the Söke basin. a–c) SK1, b) SK2, d) SK3, e) SK4, f) SK5, g–h) SK7. Yellow and purple color refers to sedimentary volcanic rocks of the upper sequence respectively. See Fig. 5.3 for the locations of the sampling sites and see Fig. 5.4g for legend of lithologies.

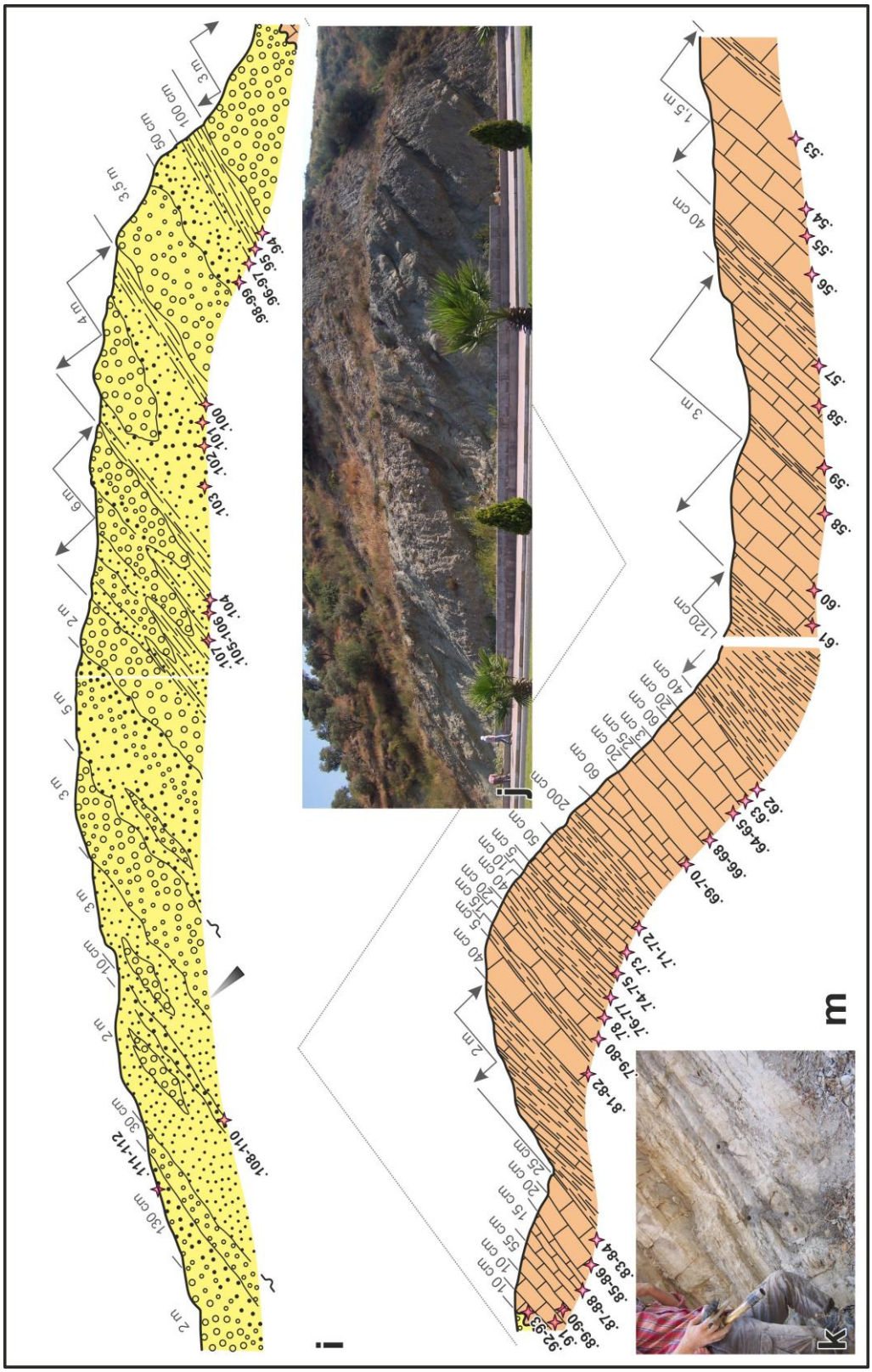


Figure 5.16 continued

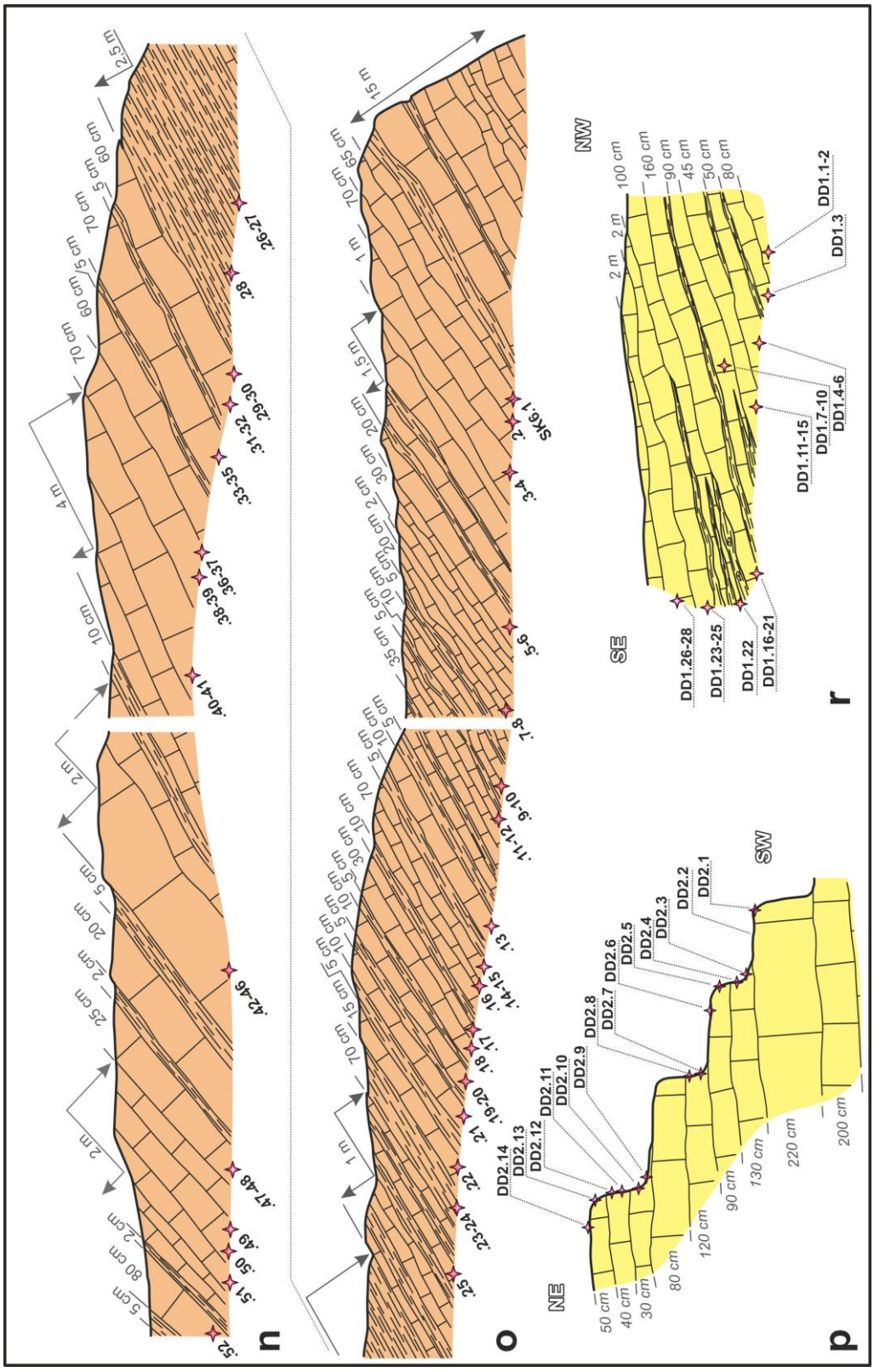


Figure 5.16 continued

In Didim area, 31 paleomagnetic samples were collected from two localities (DD1, and DD2; Fig. 5.3). Both localities include middle–late Miocene lacustrine limestone dominated levels of the Kuşadası Formation. Along the sampling sections, buff to brown, gastropod-rich, thick-bedded micritic limestones are drilled in stratigraphical order (Fig. 5.16p–r). The bedding attitudes are nearly horizontal to gently south dipping.

5.5 Paleomagnetic Results

In all samples the present-day overprint is mostly removed in the low temperature levels around 100–120 °C. In the alternating field present-day overprint is removed around 0–15 mT. In some of the samples, sometimes a secondary component is present, and is generally removed at temperatures around 200–230 °C (Fig. 5.17). In most cases, thermomagnetic curves obtained by Curie Balance measurements are displayed a well-shaped curve, usually between 300 °C and 580 °C. The curve generally hit the bottom around 560–580 °C indicating that the dominant magnetic carrier is magnetite. No major deviation is observed in the Curie Balance diagrams. Demagnetization analysis also supported that the principal magnetic carrier of the ChRM in the samples is magnetite, evidenced by maximum unblocking temperatures around 580 °C and alternating magnetic fields around ~30–90 mT (Figs. 5.17).

5.5.1 Paleomagnetic Results within the İBTZ

In *Yuntdağ area*, twelve of the thirteen early–middle Miocene sites show coherent declination/inclination results. All sites yielded clockwise rotations ranging between 20° and 45° (Table 5.1, Fig. 5.17a). Inclination values are mostly clustered around a range of 50° to 65°. According to paleomagnetic results, the Yuntdağ area underwent a vertical-axis clockwise rotation of about 27° since the deposition of the early–middle Miocene units (Fig. 5.18). On the other hand, the middle–late Miocene sedimentary rocks show no rotation to slightly clockwise rotations somewhat similar to early to middle Miocene rotations (Fig. 5.18; Table 5.1).

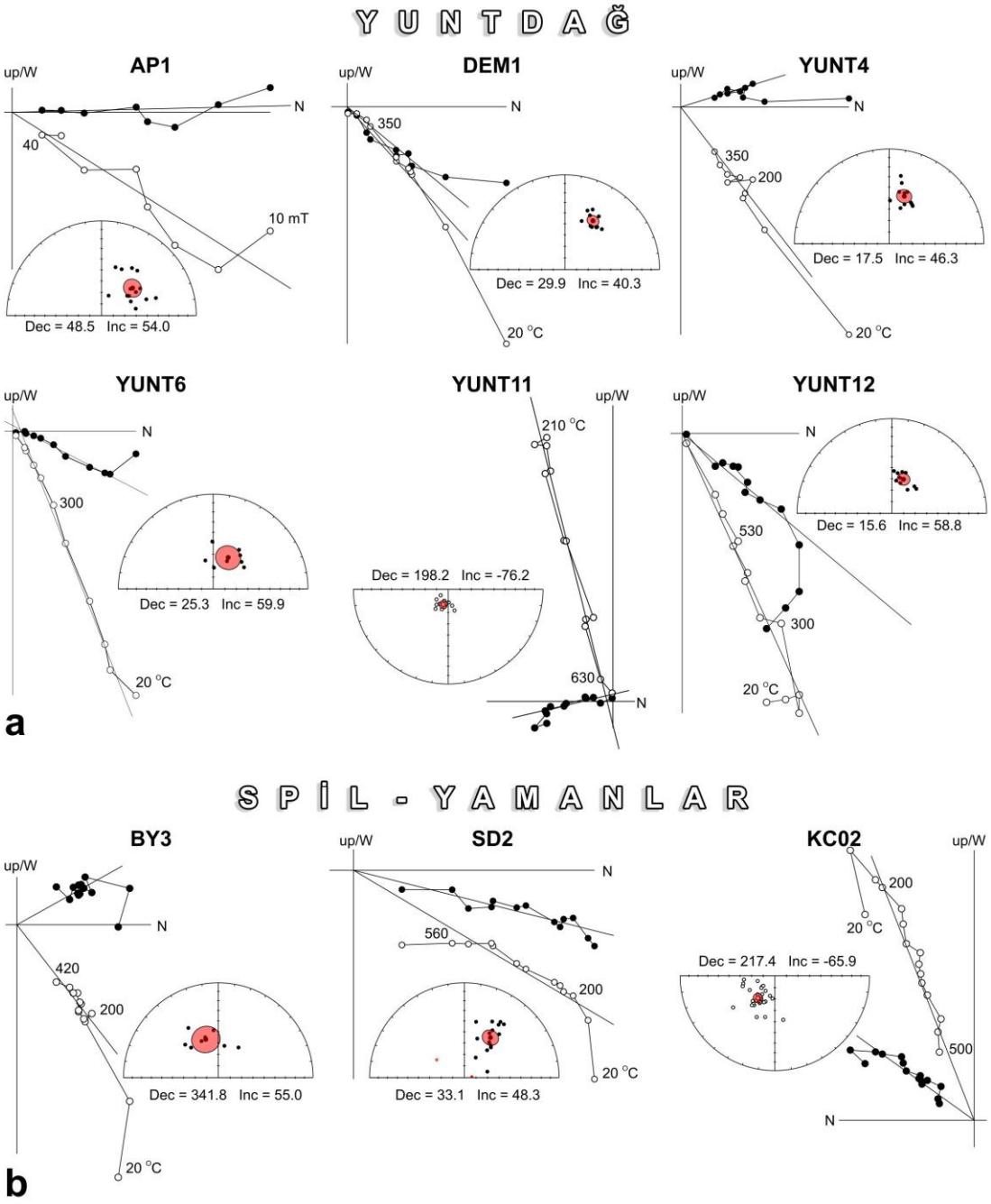


Figure 5.17 Equal area projections of the ChRM directions and orthogonal vector diagrams (Zijderveld, 1967), showing characteristic demagnetization diagrams for representative samples from a) Yuntdağ area, b) Spil-Yamanlar area, c) Urla basin, d) Cumaovası basin, and d) Kocaçay basin. Closed (open) circles indicate the projection on the horizontal (vertical) plane. Alternating field (°C) and thermal (mT) demagnetization steps are indicated. Open (closed) symbols denote projection on upper (lower) hemisphere. Large black symbols with black circle indicate respectively the mean directions and their cone of confidence (α95). Red (small) circles indicate the individual directions rejected after applying a variable cut-off (Vandamme, 1994).

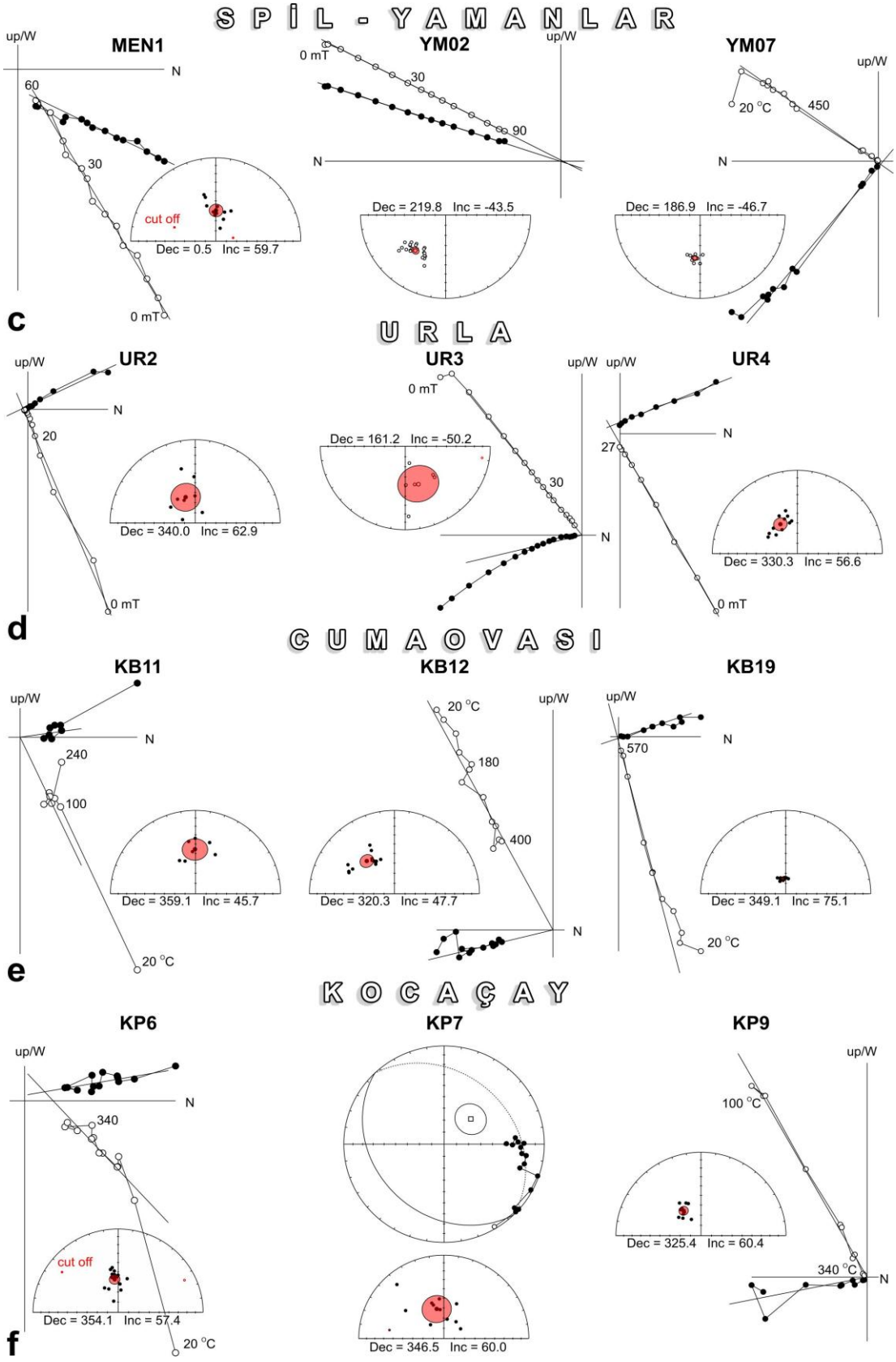


Figure 5.17 continued

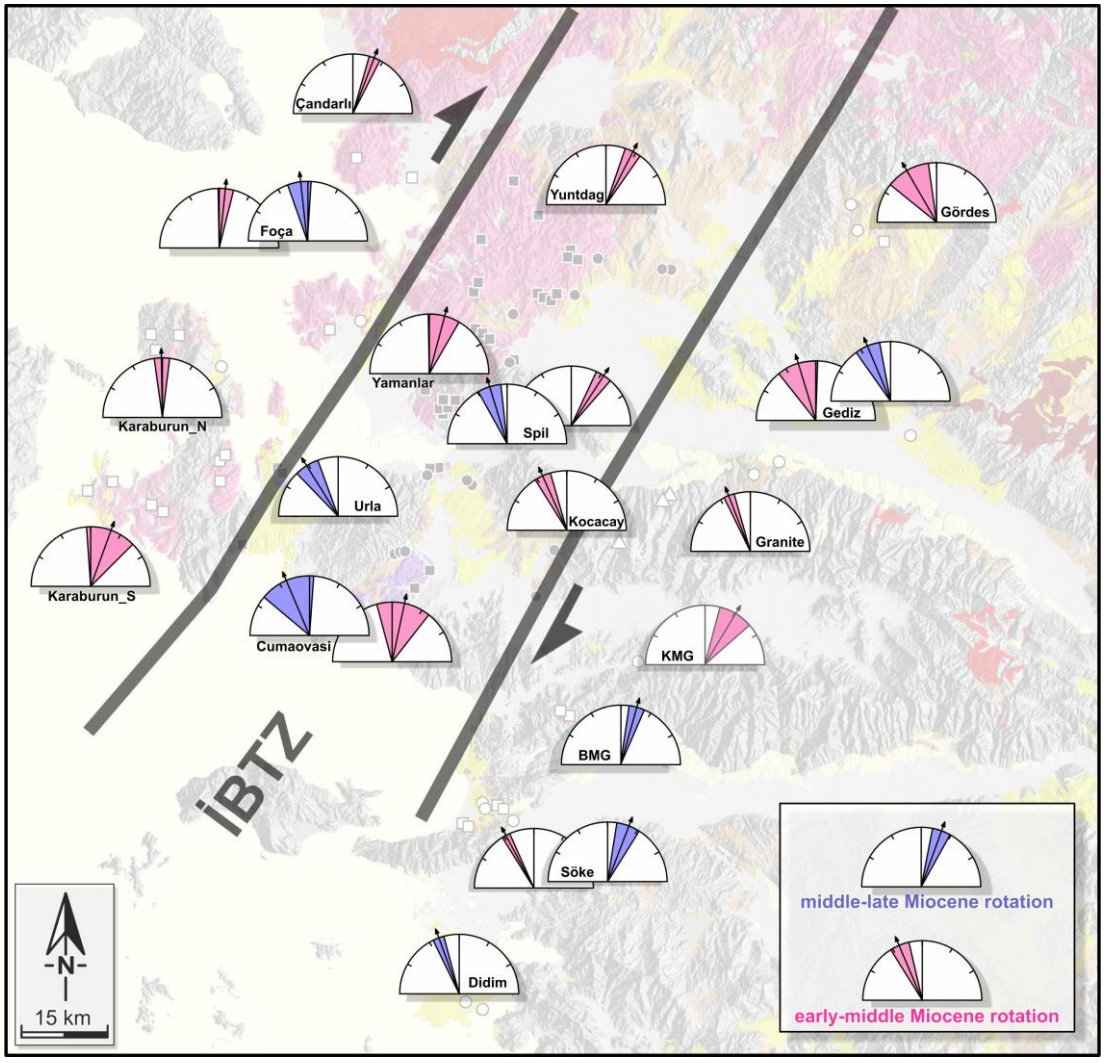


Figure 5.18 Calculated mean directions for each area. All reversed results are normalized.

Only three of the eighteen localities of the Spildağı-Yamanlar area didn't yield any geological meaningful paleomagnetic vector, while other sites showed reliable declination/inclination results (Table 5.1, Fig. 17b). The early–middle Miocene sites on the Spil high (SD01 and SD02) display clearly clockwise rotation with mean direction of 33°, while the middle-late Miocene locations yielded counterclockwise rotation about 17°. The calculated inclinations range between 48° and 50° for the Spildağı high (Table 5.1). The Yamanlar part has eleven early–middle Miocene sites and only one site of middle–late Miocene (SB01) age.

Table 5.1 Table showing all paleomagnetic data from this study. N, number of analyzed samples after interpretation and application of a variable cut-off (Vandamme, 1994); D, declination; I, inclination; k, estimate of the precision parameter determined from the ChRM directions; α95, cone of confidence determined from the ChRM directions;*, Strikethrough sites removed from further analysis because of the lightning-induced direction or statistical reasons.

Locality	Lat	Lon	Na	Nc	D	I	k	a95	Age	*
Candarli			**26**							
CAN1	501422	4311634	12	12	63.3	82.1	72.8	5.1	early-middle Miocene	
CAN2	487770	4316480	14	14	204.2	-42.3	121.2	3.6	early-middle Miocene	
rotation				26	21.3	49.2	49.9	4.1	early-middle Miocene	
Cumaovası			**127**							
CT01-02	503100	4231648	11	11	152.0	-59.1	18.7	10.8	early-middle Miocene	
CT03	504077	4231802	26	26	10.9	53.0	52.6	4.0	middle-late Miocene	
KB11	517998	4249849	7	7	359.1	45.7	29.1	11.4	middle-late Miocene	
KB12	516762	4246433	14	14	320.3	47.7	39.5	6.4	middle-late Miocene	
KB18	511337	4227660	20	20	343.0	44.0	130.3	2.9	middle-late Miocene	
KB19	507300	4222980	18	18	317.3	64.9	908.1	1.1	middle-late Miocene	
YY01	509597	4249097	9	9	206.0	-59.6	53.6	7.1	early-middle Miocene	
YY02	509508	4249336	13	13	215.0	-37.6	87.4	4.5	early-middle Miocene	
YY03	509361	4249068	9	9	169.9	-60.5	131.4	4.5	early-middle Miocene	
YY01-03				31	2.9	62.5	57.9	3.5	early-middle Miocene	
rotation-1					9.7	57.1	16.0	23.7	middle-late Miocene	
rotation-2				127	343.0	52.0	24.8	14.9	early-middle Miocene	
Didim			**42**							
DD1	530687	4147932	28	22	combined				middle-late Miocene	
DD2	531604	4139631	14	9	combined				middle-late Miocene	
rotation				31	339.9	56.1	26.6	5.1	early-middle Miocene	
Foca			**44**							
FC1	594341	4279562	29	26	15.6	59.7	19,5	6.6	early-middle Miocene	
FC2	484656	4279123	17	17	173.5	-58.5	47.9	5.2	middle-late Miocene	
Gördes			**54**							
GO1	591257	4308229	30	30	321.6	42.0	66.6	3.4	early-middle Miocene	
GO2	602714	4307484	11	11	163.9	-52.4	222.5	3.1	early-middle Miocene	
GO3	600061	4315813	13	13	326.4	56.0	107.5	4.2	early-middle Miocene	
rotation				54	326.7	47.8	44.5	2.9	early-middle Miocene	
Karaburun			**228**							
KB01	446662	4268250	11	10	~~212.8~~	~~20.5~~	~~16.5~~	~~13.1~~	early-middle Miocene	L
KB02	445832	4271320	6	6	176.1	-50.8	14.8	18.0	early-middle Miocene	
KB03	453076	4270502	14	9	~~156.2~~	~~-8.9~~	~~44.7~~	~~7.8~~	early-middle Miocene	L
KB04	453076	4270502	14	10	220.4	-17.5	8.8	17.2	middle-late Miocene	
KB22	446854	4267992	10	10	357.1	34.9	12.1	14.5	early-middle Miocene	
KB23	450050	4268133	13	13	~~117.6~~	~~-13.5~~	~~90.3~~	~~4.6~~	early-middle Miocene	L
KB02, KB22			28	28	350.2	32.6	16.6	6.9	early-middle Miocene	
KB05	464901	4246236	12	12	199.4	-43.4	93.2	4.5	early-middle Miocene	
KB06	464887	4245900	18	18	200.8	-51.5	1.8	1.8	early-middle Miocene	
KB07	463520	4240246	13	13	214.3	-55.1	125.7	3.9	early-middle Miocene	
KB08	452500	4236072	7	7	149.0	-54.8	49.5	9.6	early-middle Miocene	
KB09	454715	4232824	14	14	213.5	-26.4	42.6	6.9	early-middle Miocene	
KB20_N			29	29	12.0	70.8	105.4	2.6	early-middle Miocene	
KB20_R			60	60	191.7	-73.4	37.2	1.9	early-middle Miocene	
KB20_N+R	438131	4238022	89	89	11.8	72.6	96.1	1.5	early-middle Miocene	
KB21	439614	4243232	53	9	~~134.1~~	~~-38.7~~	~~12.2~~	~~15.3~~	early-middle Miocene	L
KB05-09, KB20-21				146	200.4	-52.6	12.3	17.9	early-middle Miocene	
Kocaçay			**81**							
KP01-02	538660	4238404	8	8	331.8	55.3	19.4	12.9	early-middle Miocene	
KP03-04	539072	4244436	17	17	162.8	-39.7	97.6	3.6	early-middle Miocene	
KP05	533463	4242849	9	9	157.8	-48.5	40.9	8.1	early-middle Miocene	
KP06	533997	4240574	8	8	141.5	-57.3	27.8	10.7	early-middle Miocene	
KP07	533900	4241945	12	11	346.5	60.0	12.1	13.7	early-middle Miocene	
KP08	532939	4228966	17	15	342.5	49.0	17.4	9.4	early-middle Miocene	
KP09	535697	4235617	10	10	325.4	60.4	123.1	4.4	early-middle Miocene	
Söke			**210**							
SK01	529705	4180421	15	12	25.2	54.4	34.4	7.5	middle-late Miocene	
SK02	528331	4183620	16	15	15.3	43.9	40.1	6.1	middle-late Miocene	
SK03	530625	4180735	9	9	23.3	46.4	63.4	6.5	middle-late Miocene	
SK04	529686	4182338	16	15	33.4	60.3	149.8	3.1	middle-late Miocene	
SK05	527416	4177149	13	low intensity					middle-late Miocene	R
SK06_1	535004	4175126	125	122	331.9	28.8	26.9	2.5	early-middle Miocene	
SK06_2	535004	4175126	22	19	9.7	28.3	17.3	8.3	middle-late Miocene	
SK07	536810	4180652	7	7	207.0	-55.5	248.2	3.8	middle-late Miocene	
rotation-1				77	20.9	48.5	40.3	10.7	middle-late Miocene	
rotation-2				122	352.1	53.2	26.9	2.5	early-middle Miocene	

Table 5.1 continued

Locality	Lat	Lon	Na	Nc	D	I	k	a95	Age	*
Spil			**46**							
BY01	525468	4265078	10	9	245.8	-38.2	37.6	8.5	middle-late Miocene	
BY02-04	527672	4263358	10	7	343.5	44.1	14.6	16.4	middle-late Miocene	
BY03	525484	4264831	8	8	341.8	55.0	23.1	11.8	middle-late Miocene	
SD01-02	526188	4267834	18	16	33.1	48.3	30.6	6.8	early-middle Miocene	
rotation-1				15	342.6	50.0	18.0	9.3	middle-late Miocene	
rotation-2				16	33.1	48.3	30.6	6.8	early-middle Miocene	
Urla			**164**							
KB10	471250	4232453	28	19	~~296.6~~	~~25.6~~	~~15.0~~	~~9.0~~	middle-late Miocene	L
KB14	477445	4266020	28	11	~~22.2~~	~~-11.1~~	~~1.6~~	~~34.2~~	middle-late Miocene	L
KB15	478993	4245492	17	17	~~246.3~~	~~37.2~~	~~69.9~~	~~4.3~~	middle-late Miocene	L
KB17	483284	4238539	11	low intensity					middle-late Miocene	R
UR01	484607	4246495	26	22	319.6	51.5	25.5	5.1	middle-late Miocene	
UR02	477543	4245960	9	8	340.0	62.9	16.8	13.9	middle-late Miocene	
UR03	471250	4232453	18	7	161.2	-50.2	5.7	18.8	middle-late Miocene	
UR04	479003	4245497	11	11	330.3	56.6	52.4	6.4	middle-late Miocene	
UR05	483284	4238539	27	27	124.3	-66.1	51.1	3.9	middle-late Miocene	
rotation				85	328.2	58.1	60.9	9.9	middle-late Miocene	
Grabens			**174**							
BT01	542581	4200989	16	16	21.3	56.3	41.1	5.8	middle-late Miocene	
BT02	542106	4200774	18	18	10.7	57.5	22.5	7.4	middle-late Miocene	
BT01-02			34	34	15.8	57.0	28.4	4.7	middle-late Miocene	
SAL1	584884	4258873	8	4	337.5	28.6	29.3	5.0	early-middle Miocene	
SAL2	511630	4273019	11	10	332.0	39.3	27.5	17.3	early-middle Miocene	
SAL3	577087	4256435	10	10	335.5	47.0	21.5	9.4	middle-late Miocene	
SAL1-2-3			29	23	337.9	54.6	16.6	7.7	early-middle Miocene	
TK01	555095	4212273	7	5	344.4	46.1	84.9	10.7	early-middle Miocene	
OS01	549940	4236714	29	27	339.3	27.4	31.6	5.0	early-middle Miocene	
SS01-02	559058	4248695	12	7	328.3	56.9	13.2	17.2	early-middle Miocene	
rotation-1				39	20.2	59.0	185.1	9.1	middle-late Miocene	
rotation-2				57	337.2	40.3	75.5	10.6	early-middle Miocene	
Yamanlar			**204**							
KC01	520306	4260483	24	12	198.1	-54.8	24.9	8.9	early-middle Miocene	
KC02	520301	4260459	30	29	217.4	-65.9	44.1	4.1	early-middle Miocene	
KC03	519379	4263920	12	12	183.4	-36.4	70.9	5.2	early-middle Miocene	
MEN1	505356	4267839	15	12	0.5	59.7	47.1	6.4	early-middle Miocene	
SB01	526188	4267834	10	9	320.6	67.0	41.7	8.1	middle-late Miocene	
YM01	515209	4265795	23	23	212.4	-61.7	93.6	3.1	early-middle Miocene	
YM02	514790	4265726	23	23	219.8	-43.5	76.8	3.5	early-middle Miocene	
YM03	514024	4266338	16	15	~~110.6~~	~~-32.1~~	~~170.3~~	~~2.9~~	early-middle Miocene	R
YM04	511037	4264465	16	16	~~124.6~~	~~-59.0~~	~~131.5~~	~~3.3~~	early-middle Miocene	L
YM05	510940	4263836	13	13	~~117.2~~	~~-39.8~~	~~281.1~~	~~2.5~~	early-middle Miocene	R
YM06	523399	4275357	9	9	348.2	54.1	39.1	8.3	early-middle Miocene	
YM07	524007	4275842	13	12	186.9	-46.7	263.2	2.7	early-middle Miocene	
rotation-1				9	320.6	67.0	41.7	8.1	middle-late Miocene	
rotation-2				132	14.8	54.2	29.4	10.4	early-middle Miocene	
Yuntdağ			**197**							
AP01	556128	4297321	14	14	48.5	54.0	27.4	7.7	middle-late Miocene	
AP02	539573	4298304	8	low intensity					middle-late Miocene	R
AV01	522375	4287522	22	low intensity					early-middle Miocene	R
DEM1	532826	4299487	10	10	29.9	40.3	101.0	4.8	early-middle Miocene	
YUNT01	515066	4289879	15	15	26.5	37.7	54.6	5.2	early-middle Miocene	
YUNT02	532037	4289232	12	12	17.4	63.6	301.8	2.5	early-middle Miocene	
YUNT03	533799	4288717	8	6	34.4	38.9	34.8	11.5	middle-late Miocene	
YUNT04	535356	4288519	11	11	17.5	46.3	56.9	6.1	middle-late Miocene	
YUNT05	522522	4281140	14	13	29.3	41.4	61.6	5.3	early-middle Miocene	
YUNT06	518626	4281767	8	8	25.3	59.9	28.9	10.5	early-middle Miocene	
YUNT07	523710	4298746	7	6	17.0	49.8	41.1	10.6	early-middle Miocene	
YUNT08	509310	4276771	13	13	35.2	55.6	162.2	3.3	early-middle Miocene	
YUNT09	509322	4280331	9	9	38.0	50.3	301.0	3.0	early-middle Miocene	
YUNT10	525218	4304096	9	9	22.7	54.8	183.7	3.8	early-middle Miocene	
YUNT11	526070	4306530	15	12	18.2	76.2	156.6	3.5	early-middle Miocene	
YUNT12	533684	4297608	10	10	18.9	58.8	84.9	5.3	early-middle Miocene	
YUNT13	520032	4312498	12	12	19.1	43.1	129.1	3.8	early-middle Miocene	
rotation-1				31					middle-late Miocene	
rotation-2				129					early-middle Miocene	

Results from volcano-sedimentary rocks of the *lower sequence* (early–middle Miocene) provide evidence for a 15° clockwise rotation, a small set of sediments from upper sequence display a well-defined counterclockwise rotation about 40°.

Likewise, these opposite rotation senses are very similar to Spildağı high. According to combined results, the first rotation of the area took place after the deposition of the early–middle Miocene units and underwent 20° to clockwise around vertical-axis. Then the area rotated approximately 20° counterclockwise since the middle–late Miocene (Fig. 5.18).

In *Urla basin*, calculated site means from the paleodeclination directions using Fisher statistics (Fisher, 1953) showed that some specimens affected by lightning (Fig. 5.17c) as well as the specimens with low intensity are omitted from further analysis (Table 5.1). After that, the accepted volcanic sites include UR02–05, in addition UR01 comprises sedimentary rocks, which also produced reliable results. According to demagnetization diagrams, the main components are usually lies between 20 and 60 mT in the alternating field and temperature ranges between 300–580 °C for the volcanic specimens, while the sedimanter rocks retain ChRM in magnetic fields ranging between 15–45 mT and temperature ranges of 120–380 °C. Five of six middle–late Miocene sites produced coherent declination/inclination attitude. Despite a large uncertainty on the result of the sedimentary site (UR01) all locations yielded counterclockwise rotations ranging between 20° and 40° (Fig. 17d, Table 5.1). Except for the site UR04 where very steep paleoinclination (75°) is obtained (Fig 5.17d), the paleoinclinations in all other sites are relatively consistent and range between 47° and 56°. After the statistical analysis of the results the calculated mean ChRM direction for the basin is 33° (Table 5.1).

The sedimanter specimens from the *Cumaovası basin* show that the main paleomagnetic directions are obtained at temperature levels between 180 °C and 400 °C (or 20 and 60 mT, in alternating field), whereas these ranges are between 200 °C and 530 °C (or 20–90 mT) for the volcanic rocks. For some sites such as CT3 reversal tests were performed and very good results are obtained (Fig. 5.17e). The rotation results are quite dispersed in both early–middle and middle–late Miocene localities. Despite big error margins, however, the calculated average results indicate two different rotation senses. These mean rotations are more or less similar to other areas within the İBTZ. In the basin, the early–middle Miocene sites yielded 17°

counterclockwise rotation, while for the middle–late Miocene sites 10° clockwise rotation is obtained (Fig. 5.18).

The *Kocaçay basin*, which is located adjacent to and at eastern rim of the İBTZ, has nine localities of early–middle Miocene age. The calculated mean paleomagnetic directions produced very reliable results. After tilt correction, all sites yielded counterclockwise rotations between 15° and 40° (Table 5.1, Fig. 17f). The mean values of all sites show that the basin rotated counterclockwise 24° since the early Miocene (Fig. 5.18).

5.5.2 Paleomagnetic Results outside the İBTZ

West of the İBTZ, two early–middle Miocene sites of *Çandarlı-Dikili area* showed coherent paleo-declination/inclination directions with a small uncertainty. The individual results are clustered in the NE quadrant (clockwise) of the lower hemisphere (Fig. 5.19a, and Table 5.1). These results show that the area underwent a clockwise vertical-axis rotation of about 21° since the emplacement of early–middle Miocene volcanics.

From the *Foça area* lying outside and west of the İBTZ, 41 specimens of both sedimentary and volcanic rocks were analyzed. The sediments, which derived from early–middle Miocene units yielded clockwise rotations of about 16° (Table 5.1). However, volcanic rock samples resulted in very large rotation values. The combined analyses of sedimentary and volcanic samples indicate that the area rotated counterclockwise about 7° since the middle–late Miocene (Fig. 5.19b, Table 5.1).

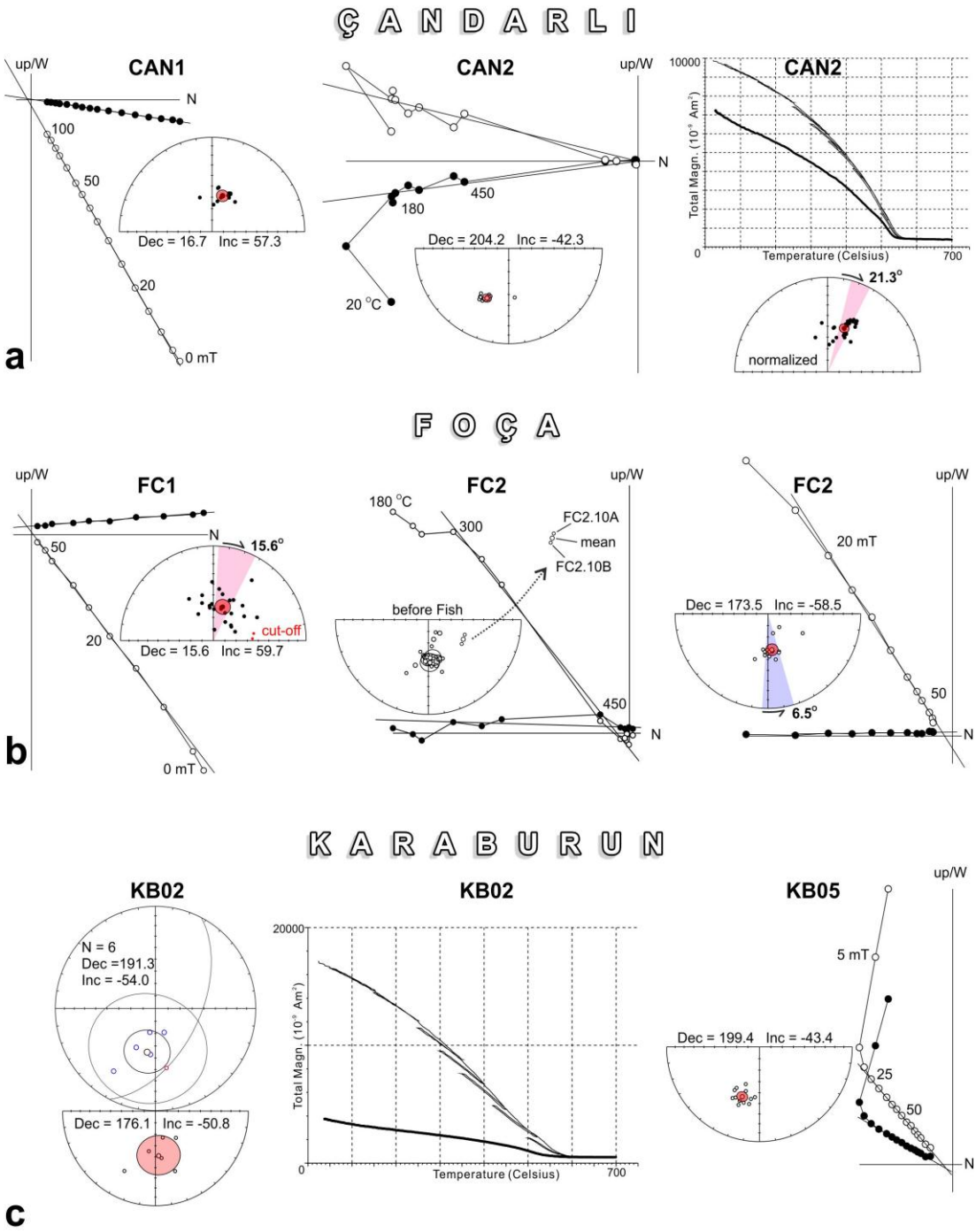


Figure 5.19 Equal area projections of the ChRM directions and orthogonal vector diagrams (Zijderveld, 1967), showing characteristic demagnetization diagrams for representative sampled sites from a) Foça, b) Çandarlı, c–d) Karaburun, e) Gördes, f–g) E–W-trending Gediz, Küçük Menderes, and Büyük Menderes grabens, h) Söke-Didim area. See Fig. 18 for detailed descriptions of symbols and abbreviations in figure.

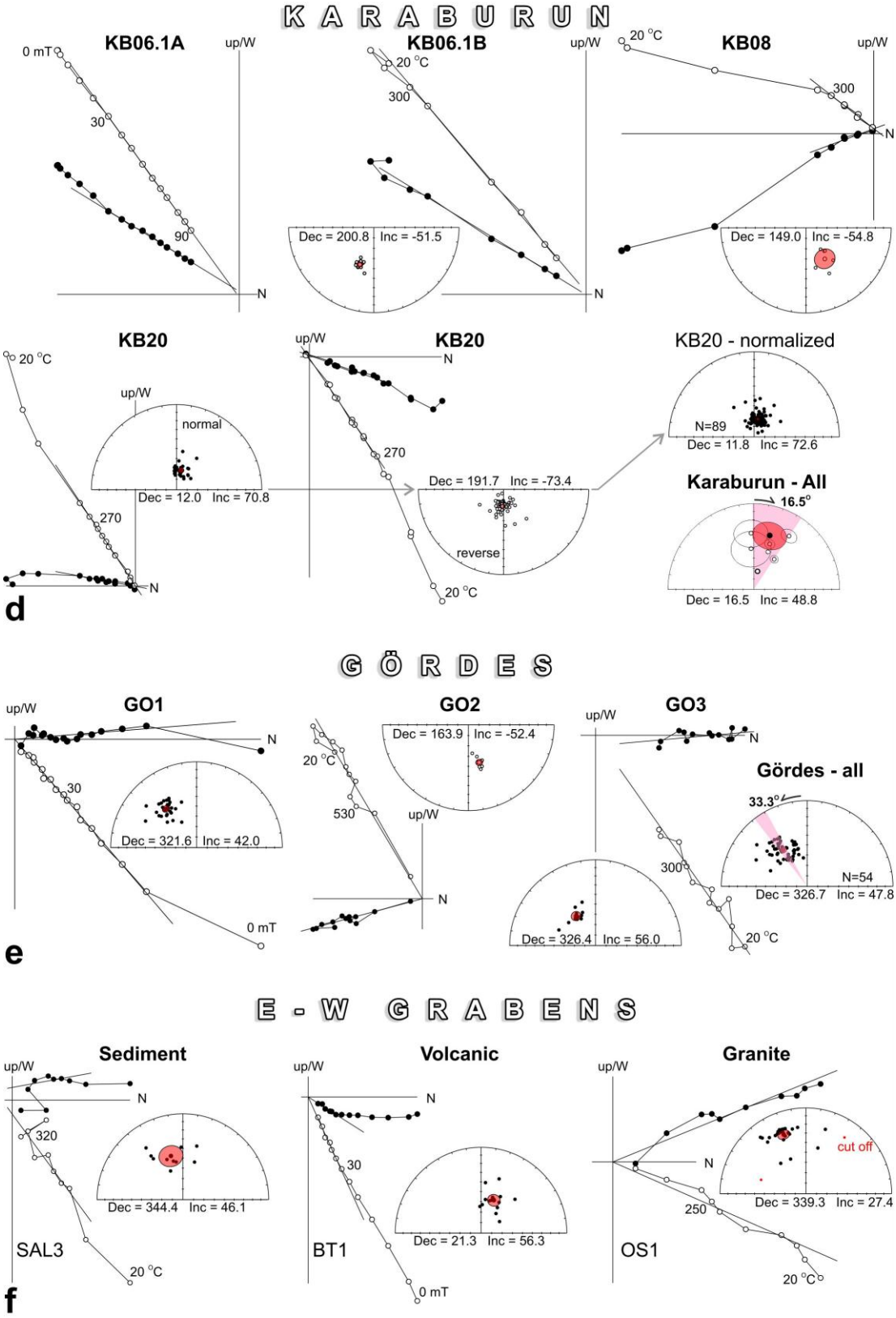


Figure 5.19 continued

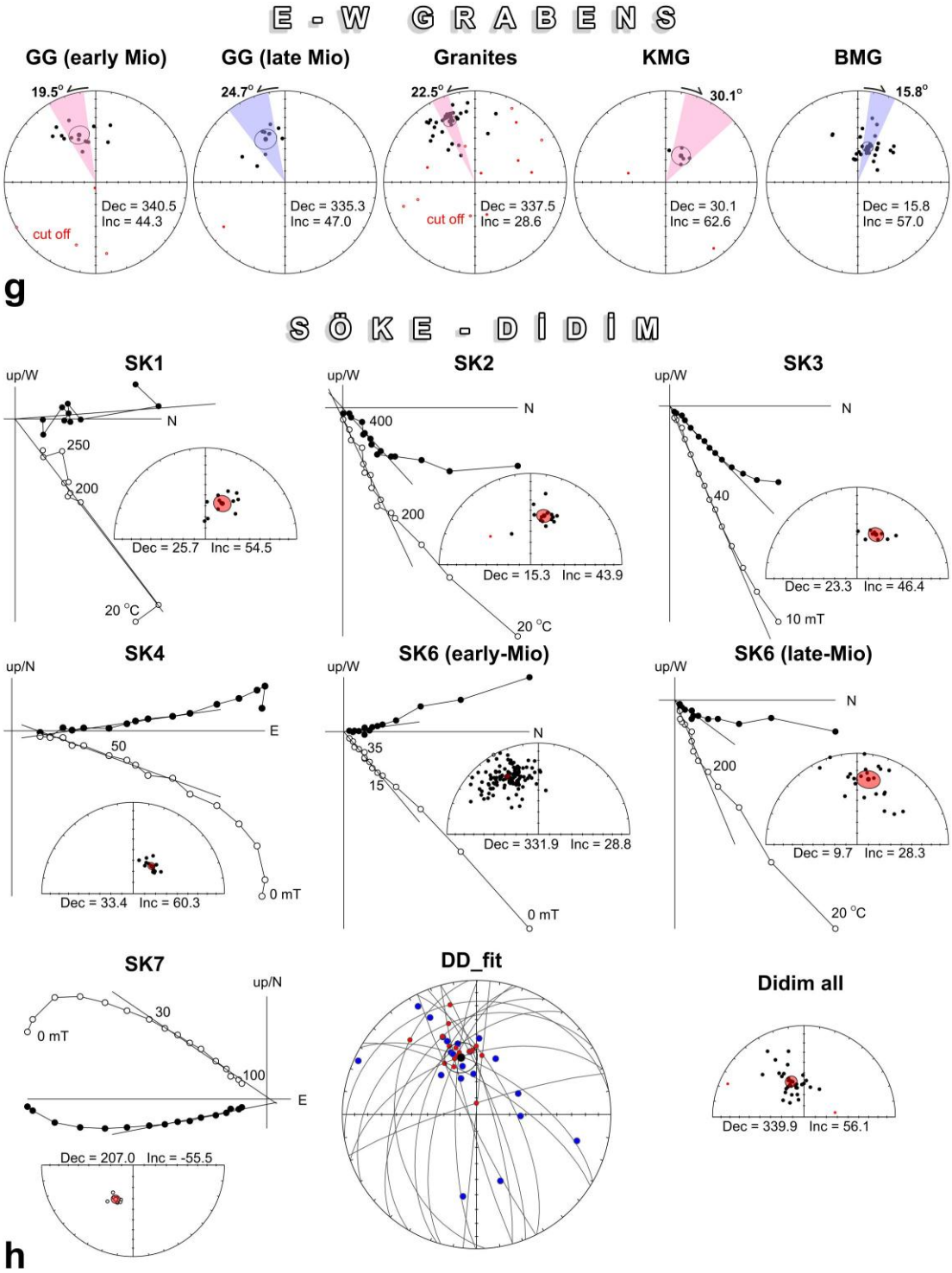


Figure 5.19 continued

Demagnetization diagrams of the *Karaburun area* showed that some localities (KB01, KB03, KB21, and KB23) affected by lightning, thus did not yield any appreciable results. In addition, KB04 yielded very low paleoinclination of 18° which is highly unlikely for this area for early-middle Miocene. Northern side of the area did show no significant rotation, while southern part of the area rotated about 20° clockwise (Fig. 19c–d, Table 5.1). In average, 17° clockwise rotation is calculated for the whole area (Figs. 5.18 and 19c–d; Table 5.1).

The samples sites included in *Gediz, Küçük Menderes, and Büyük Menderes grabens*, *Gördes* and *Söke basins* together with *Didim area* are located within the blocks lying at the east of the İBTZ. Except for the Küçük Menderes Graben, all early–middle Miocene sites yielded counterclockwise rotations ranging from 8° and 33° for these basins (Fig. 5. 19e–h). The rotation values, from north to south are; 33°, 23°, 16°, and 8° for Gördes basin, Gediz, Büyük Menderes, grabens and Söke basin, respectively (Fig. 5.18, Table 5.1). Unlike other areas east of the İBTZ Küçük Menderes graben yielded 21° clockwise rotation for the early-middle Miocene. In addition to this, three sites representing syn-extensional granites yielded reliable results clockwise rotations between 21° (OS01) and 32° (SS01-02) (Fig. 5.18, Table 5.1). The data indicate that all the middle–late Miocene sites located in the areas to the east of İBTZ and north of the Küçük Menderes graben underwent almost a uniform vertical-axis counterclockwise rotation of about 20° (Fig. 5.18, Table 5.1).

CHAPTER SIX
DISCUSSION AND CONCLUSION

6.1 Spatio-Temporal Characteristics of Volcanism and Sedimentation

Present day distribution of Cenozoic volcanic and depositional centers are controlled by the tectonic processes that gave way to the structures related to the development of the tectonic scheme of the western Anatolia and inherited weakness zones developed during the evolution and closure of the Tethys ocean. Among these structures the İBTZ has the primary role since seems to localize the eruption centers and directly or indirectly controlled the evolution of the Neogene basins in the region.

In order to understand the timing of the events and their interaction in time and space, radiometric dating was very crucial since they have the potential to provide very precise age data. In this context, the radiometric ages obtained during the course of this study and published reliable ages are compiled from the literature. The results have shown that there are two episodes of volcanism in the region, separated by a regional unconformity. The first volcanic activity along the İBTZ took place during the Burdigalian (Fig. 6.1); the $^{40}Ar/^{39}Ar$ results indicate that the oldest recorded age for the volcanism within the İBTZ is 19.7 Ma and it is obtained from the samples of the Yuntdağ volcanics (Figs. 3.4 and 6.2). These volcanics and age data belong to the base of *lower sequence*. The youngest age for the youngest part of the *lower sequence* is obtained from Dikili Group (samples collected from CAN2 sites) and the $^{40}Ar/^{39}Ar$ data yielded 16.1 Ma (Table 3.2). Aldanmaz et al. (2000), however, reported 15.2 and 15.5 Ma (K–Ar ages) from these volcanics. It's commonly accepted that $^{40}K/^{40}Ar$ techniques generally produce relatively younger results. Therefore, it can be concluded that the youngest age for the volcanic activity of the *lower sequence* corresponds approximately to boundary between Burdigalian and Langhian (Fig. 6.1). The volcanic rocks of the *lower sequence* are mainly dominated by rhyolite, andesite, and related pyroclastic rocks with minor basaltic andesites with calc-alkaline to alkaline nature (Kaya, 1981; Ercan et al., 1996; Erkül et al., 2005;

Aldanmaz et al., 2010; Altunkaynak et al., 2010). This implies that, the volcanism was bimodal and subduction related magmatism was still dominant during the Burdigalian, although, extensional deformation was effective in the region as indicated by kinematic analysis of the fault slip data discussed in Chapter 4.

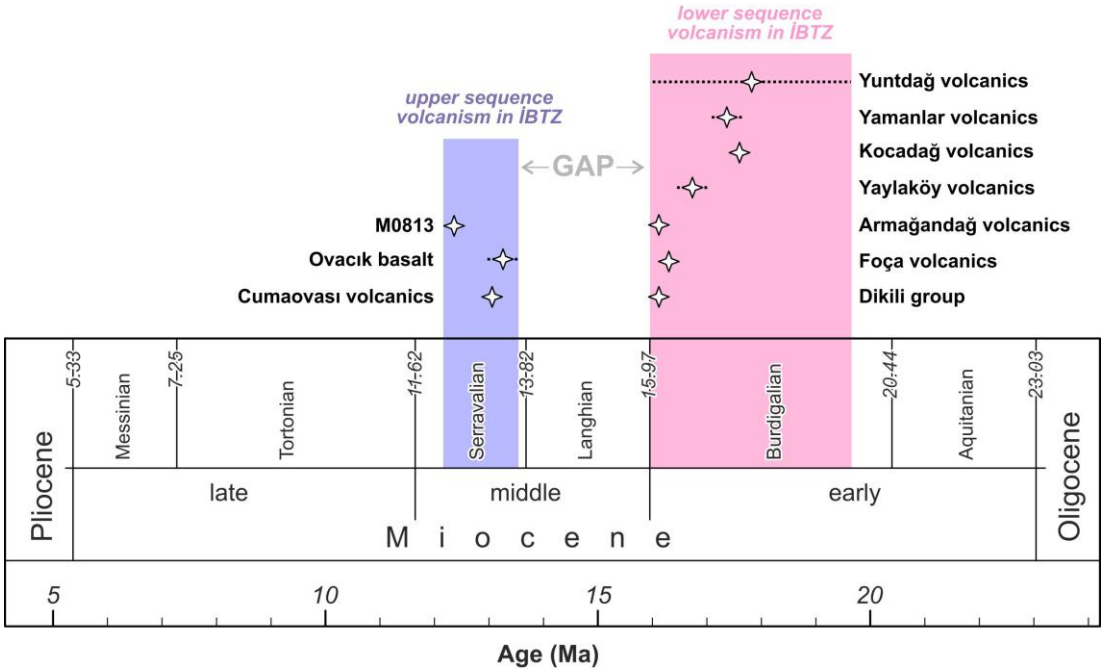


Figure 6.1 Figure showing temporal relationship between the different volcanic edifices in İBTZ. There are clearly two age groups that are also stratigraphically appeared in lower (pink) and upper (purple) sequences of the Miocene sedimentary units. Note that M0813 fallen down in upper sequence volcanism is representing the olivine-bearing basaltic volcanism in the Yuntdağ area.

Based on radiometric age results of this study, the second stage of volcanic activity, *upper sequence* units, took place during the Serravalian (Fig. 6.1). Genç et al. (2001), however, proposed younger ages (~9 Ma) for Cumaovası volcanics, our data did not confirm this argument. The volcanic rocks of the *upper sequence* are composed mainly of rhyolite, trachyte (Urla and Cumaovası volcanics) and olivine (Ovacık) basalt; this means that the volcanism is also bimodal in character. According to $^{40}Ar/^{39}Ar$ ages, the rhyolitic volcanic rocks were emplaced around 13.1 Ma, while the basaltic columnar lavas extruded between 13.0 and 13.7 Ma time interval (Figs. 3.4 and 6.1; Table 3.2).

The spatial distribution of the age data implies that the youngest ages lie mostly in lower altitudes, while the oldest ages are exposed at the highest peaks (Fig. 6.2). This relationship is statistically tested by using correlation analysis. According to correlation coefficient, this is about 0.32; the relationship between altitude and age of the volcanic rock is very poor. In fact the youngest age data is obtained from the rocks lie around 400 m while the oldest age is obtained around 200 m (Figure 6.2b), the relationship between the age and altitude of the volcanism is not clear (Fig. 6.2b). Nevertheless, the bulk of the highest isochrones are concentrated around the peaks and the bulk of the lowest isochrones are around lowest peaks. In addition, the youngest volcanic rocks (~13–14 Ma) are located close to the western boundary of the İBTZ and are obtained from the samples collected around Urla-Yağcılar and Menemen regions (Figure 6.2a). This implies that the emplacement of some the youngest volcanic rocks are controlled by the faults located at the western margin of the İBTZ.

The İBTZ is composed of NE–SW-trending Miocene volcano-sedimentary basins that are dissected by mainly E–W-trending Plio–Quaternary depressions. Miocene stratigraphy is typified by a folded (normal and strike-slip faulted) volcano-sedimentary sequence characterized by coal-bearing clastic to carbonate sediments, andesitic to rhyolitic pyroclastic deposits and lava flows, and lacustrine carbonates. The younger and recent basin-fill is represented by continental alluvial to fluvial deposits and coastal clastics of the Aegean Sea. The Neogene–Quaternary evolution of the zone is characterized by variable wrench to extension dominated transtension, and has resulted in a complex fault pattern. Three different deformation phases have been encountered around İzmir Bay area for the late Cenozoic time interval.

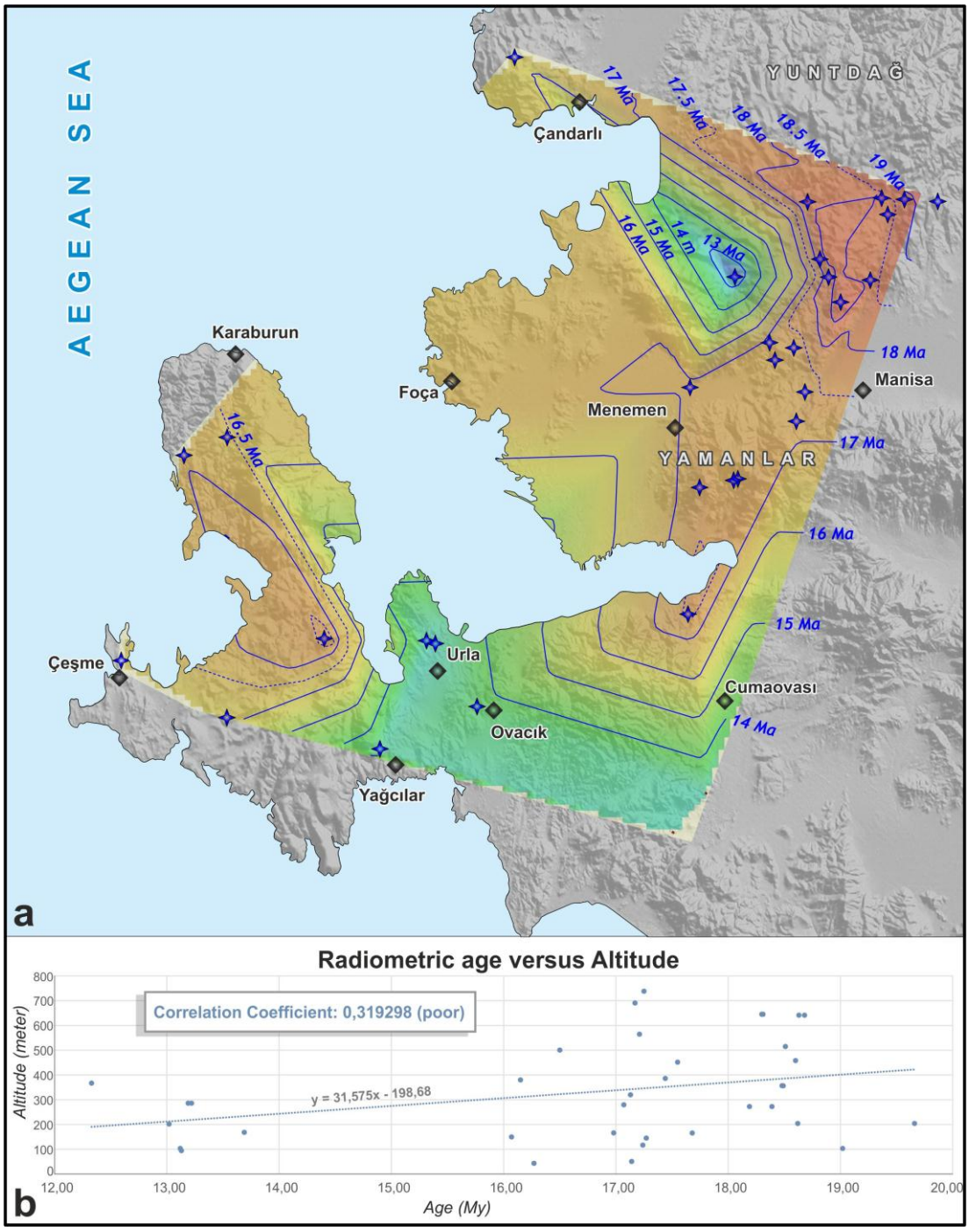


Figure 6.2 a) Iso-age contour map of the Miocene volcanics. The ages are complied from 32 $^{40}Ar/^{39}Ar$ results of this thesis. b) Age versus altitude diagram showing the possibly effect of the volcano-chronology on morphology. Blue stars indicate dated sample locations (See Chapter 3 for details).

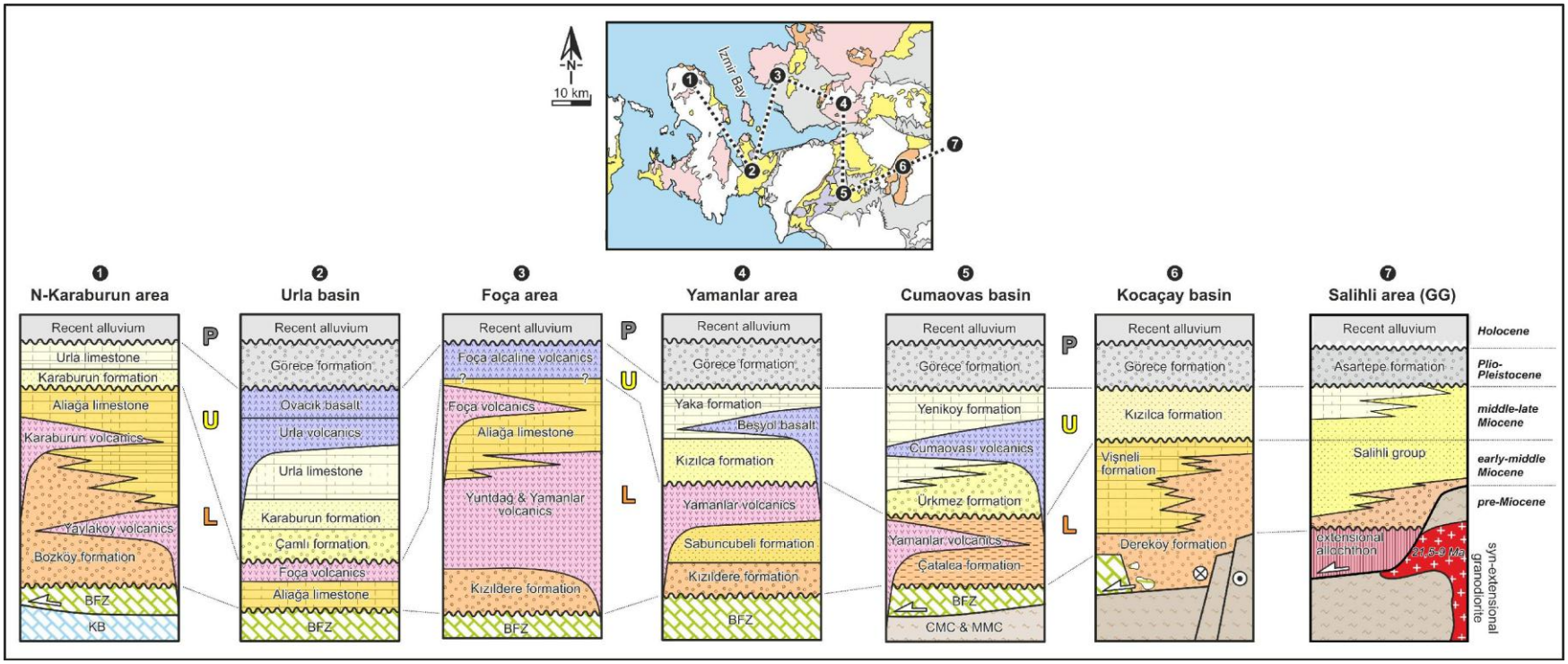


Figure 6.3 Stratigraphical correlation of the Cenozoic basins in the İzmir Balıkesir Transfer Zone. U (L), Upper (Lower) sequence of Miocene deposits; BFZ, Bornova Flysch Zone; KB, Karaburun Belt; CMC, Cycladic Metamorphic Core Complex; MMC, Menderes Metamorphic Core Complex. See text for references on radiometric ages, indicated by purple stars.

As discussed previously, there are also two different Miocene sequences within the İBTZ. These mainly lacustrine sequences (*lower* and *upper sequences*) within which two different volcanic rocks are interlayered (Fig. 6.3). The compiled age data together with the results of this study and published micro-mammal ages indicate that the earliest deposition in the region commenced by the beginning of Burdigalian (MN3 locality of Kaya et al., 2007 within the *lower sequence* around Bornova). This phase was ended by ~16 Ma (CAN2 from Dikili) after the emplacement of younger volcanics of the lower sequence. There is a regional unconformity between lower and upper sequences. The oldest radiometric ages obtained from the upper sequence indicates that deposition during the second phase commenced by ~13.7 Ma. This implies that the hiatus, in other words, time gap between *lower* and *upper sequences* is around 2.3 Ma (16.0–13.7 Ma). Unfortunately, there is no reliable age data for the younger part of the upper sequence. However, According to Kaya (2005), based on rodent ages, the deposition of the *upper sequence* lasted until Tortonian. The youngest mammal locality within the *upper sequence* documented from the outcrops around eastern end of the Büyük Menderes graben (Denizli basin) support this age with MN 11–12 mammal zones indicating late Miocene time interval (Kaymakci, 2006). It is important to note that the major unconformity between the *lower* and the *upper sequences* is also noticeable from both the geochronological data and the field observations; however, no evidence has been published about this mid-Miocene unconformity from the grabens and the other basins in western Anatolia. It is speculated that, while the middle Miocene sedimentation was uninterrupted within the basins such as Büyük Menderes and Gediz grabens, however, it was interrupted within the İBTZ, which indicates activity of the İBTZ during the middle Miocene.

6.2 Deformation Phases

The first field-based studies of Kaya (1979, 1981) reported that the region between İzmir and Balıkesir was divided into NNE-trending depressions of Neogene age by steep, oblique-slip faults with a considerable left-lateral strike-slip component. He indicated that these faults appear to be older than the E–W- to WNW-trending normal faults and hence might follow older structural trends. These

major strike-slip cross-faults offset the main Gediz detachment fault near its western end, and Şengör (1987) delineated them as a transfer fault zone. This zone might be classified as a transverse or replacement structure, defined by Şengör et al. (1985) as a configuration coincident in space with paleotectonic structures but that does not have the same function during a later tectonic episode. Its origin may be attributed to the influence of the basement structure inherited from the transform nature of the zone during the late Cretaceous. This is supported by faults within the İBTZ which may have their earliest record in the Late Cretaceous convergence, related to an existing transform zone perpendicular to the Neotethys. It later acted as a wrench- to extensional-dominated transfer fault zone during the late Cenozoic (Okay & Siyako, 1993; Okay et al., 1996; Ring et al., 1999; Uzel & Sözbilir, 2008; Özkaymak & Sözbilir, 2008; Uzel et al., 2012; Özkaymak et al., 2012; Okay et al., 2012).

The deformation phases within the study area are based on regional field studies and paleostress inversion studies. For the late Cenozoic, two different deformation styles and three different deformation phases have been recognized in the mapped areas within and adjacent to the İBTZ (Fig. 6.4). During Phase 1, all studied subareas were dominated by strike-slip faulting and related structures. For Phases 2 and 3, however, there is structural consistency between the Menemen and Yaka subareas within the İBTZ, in the sense that these areas were dominated by strike-slip tectonics, whereas the Karaburun area outside of the İBTZ was dominated by extensional deformation during Phase 3. The geometry and kinematics of brittle structures in the Karaburun Peninsula are consistent with wrench-dominated deformation. Simple shear within the zone is accommodated by right-lateral R shears (NE–SW-trending faults) and left-lateral R’ shears (NW–SE-trending faults).

The documented reactivation on some of the NW–SE trending faults in the Karaburun Peninsula predicts that R’ shears initiated as left-lateral shear fractures are later reactivated as normal oblique-slip faults, possibly caused by vertical axis rotation. This can be explained by the progressive deformation produced by the switch from simple strike-slip to extension-dominated transtension. This new local strain field favors the development of new dip- to oblique-slip normal faults or

reactivation of the earlier strike-slip faults. This relationship implies that the Karaburun area was kinematically decoupled from the eastern areas at the end of deformation Phase 2, by the Pliocene. After the initiation of Phase 2, differential stretching between the Menderes Core Complex and the area west of it, including İzmir Bay, caused the İBTZ to develop as a transfer zone (Fig. 6.4). Most probably, dominance of strike-slip deformation during Phases 1 and 2, within and outside the İBTZ, implies that the İBTZ evolved from a wider shear zone into a relatively narrow discrete fault zone by the late Pliocene, during which the strike-slip and extensional deformation completely decoupled from each other.

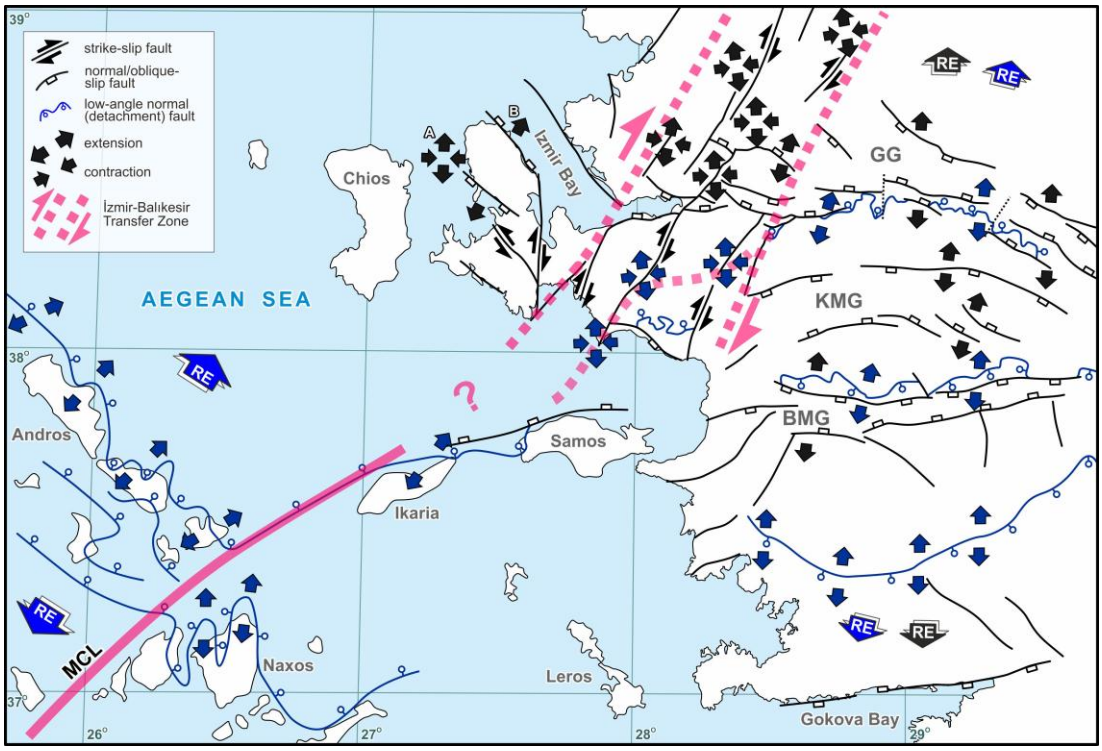


Figure 6.4 Miocene (blue arrow) and post-Miocene (black arrow) kinematic data from the İBTZ combined with published data from the Aegean and West Anatolian Extensional Systems (Walcott and White, 1998; Bozkurt and Satır, 2000; Lips et al., 2001; Sözbilir, 2002; Ring et al., 2003; Bozkurt and Sözbilir, 2004, 2006; Emre and Sözbilir, 2007; Uzel and Sözbilir, 2008; Gürer et al., 2009; Jolivet et al., 2010; Sözbilir et al., 2011; Uzel et al., 2013). Miocene extensional detachment faults show NE-SW oriented regional extension (RE) that almost parallel to the İBTZ and Mid-Cycladic Lineament while a post-Miocene NNE-SSW oriented regional extension (RE) has been documented in the West Anatolian Extensional System, east of the İBTZ. A (B) refers to the older (younger) faulting around Karaburun Peninsula.

In addition, the faults that control the margins of the inner and outer parts of the İzmir Bay have been active during the latest deformation phase since the late Pliocene. These faults generally have a normal component but are connected to NE–SW right-lateral strike-slip faults. This implies that İzmir Bay is a transtensional basin developed in response to synchronous strike-slip and normal faulting along the İBTZ.

6.3 Paleomagnetism

6.3.1 Previous Paleomagnetic Studies in the Region

A number of paleomagnetic studies have already been carried out in western Anatolia. The first work has carried out by Kissel et al. (1987). They sampled volcanic rocks at 42 locations from the coastal area between the Biga and Karaburun Peninsulas (Fig. 6.5 and Table 6.1). The results of this study provided quite complex rotation pattern. It was proposed that the Lesbos and Çanakkale regions have not undergone any significant rotation, the İzmir, Foça, and Dikili regions have rotated approximately 40° counterclockwise, and Karaburun has undergone a 45° clockwise rotation. Northern side of the Yuntdağ high has been affected also by an approximately 20° clockwise rotation similar to the Karaburun Peninsula. Despite the lack of age data for the sampling sites, Kissel et al. (1987) interpreted each different rotation result as a different but coherent tectonic block, and explained the large amount of rotation with the existence of strike-slip faults in the region.

Orbay et al. (2000) provided results from 37 volcanic sites in the Karaburun, İzmir, and Foça regions for three different time intervals as (i) early Miocene, (ii) late Miocene, and (iii) Pliocene. According to their results, the region has rotated 40-45° clockwise since the early Miocene and approximately 45° counterclockwise after late Miocene. They explained this different rotation amounts within the context of westward escape and N-S extension of the Anatolian block proposed previously by Şengör et al. (1985). Using the data from Yamanlar volcanics exposed at the southern margin of İzmir Bay, they argued that there is no significant rotation since the Pliocene.

Table 6.1 Published paleomagnetic results in western Anatolia. Lat, latitude; Lon, longitude; Na, number of demagnetized samples; Nc, number of samples used to calculate average; D, declination; I, inclination; k, Fisher (1953) precision parameter; a95, 95% cone of confidence; Strikethrough sites removed from further analysis by the authors because of the lightning-induced direction or statistical reasons. References for ages are: 1, Fytikas et al. (1984); 2, Pe-Piper and Piper (1993); 3, Bingöl (1977); 4, Seyitoğlu et al. (1997); 5, Purvis et al. (2005); 6, Ercan et al. (1996); 7, Ersoy et al. (2008); 8, Yılmaz et al. (2000); 9, Aldanmaz et al. (2000); 10, Borsi et al. (1972); 11, Benda et al. (1974); 12, Altunkaynak et al. (2010); 13, Helvacı et al. (2010).

Locality	Lat	Lon	Na	Nc	D	I	k	a95	Age
Lesbos (Kissel et al., 1987)									**16.0–20.0 (1, 2)**
LE249	unknown	unknown		10	8.0	37.0	280.0	2.6	
LE252	unknown	unknown		8	0.2	49.0	153.0	4.0	
LE253	unknown	unknown		9	13.6	59.5	196.0	4.0	
LE255	unknown	unknown		11	11.3	53.3	704.0	1.6	
LE256	unknown	unknown		11	340.5	55.0	229.0	2.8	
LE257	unknown	unknown		10	350.0	69.0	262.0	3.0	
LE263	unknown	unknown		9	177.8	−49.0	1333.0	1.3	
LE269	unknown	unknown		8	146.0	−63.6	177.0	3.7	
LE271	unknown	unknown		11	214.0	−20.0	15.0	10.0	
LE272	unknown	unknown		10	191.7	−44.7	181.0	3.3	
LE273	unknown	unknown		10	31.4	58.5	257.0	2.7	
LE274	unknown	unknown		10	358.6	44.3	134.0	3.8	
LE275	unknown	unknown		9	17.3	64.0	233.0	3.0	
LE277	unknown	unknown		9	349.5	45.5	170.0	3.5	
LE278	unknown	unknown		9	10.0	44.5	72.0	5.0	
LE279	unknown	unknown		7	199.5	−20.0	144.0	4.4	
LE280	unknown	unknown		7	191.0	−41.0	46.0	7.8	
İzmir-Bergama (Kissel et al., 1987)									**15.2–21.0 (9–12)**
IZ06	unknown	unknown		12	128.0	-47.0	158.0	4.2	
IZ07	unknown	unknown		8	141.0	-39.5	249.0	3.3	
IZ09	unknown	unknown		12	127.2	-41.0	93.0	4.2	
IZ10	unknown	unknown		8	144.0	-47.5	500.0	2.2	
IZ24	unknown	unknown		7	348.0	64.0	56.0	7.0	
IZ28	unknown	unknown		8	349.6	57.0	57.0	4.0	
IZ44	unknown	unknown		9	342.0	71.0	828.0	1.6	
IZ46	unknown	unknown		8	314.0	53.8	540.0	2.3	
IZ57	unknown	unknown		9	325.0	14.7	35.0	8.0	
IZ59	unknown	unknown		18	336.0	58.5	27.0	6.3	
IZ60	unknown	unknown		10	331.0	67.5	76.0	5.0	
IZ61	unknown	unknown		9	333.0	31.7	47.0	6.7	
IZ64	unknown	unknown		10	165.2	-67.2	115.0	4.1	
South of Bergama (Kissel et al., 1987)									**15.2–21.0 (9–12)**
IZ22	unknown	unknown		11	190.0	-48.0	387.0	2.4	
IZ47	unknown	unknown		9	7.2	34.5	45.0	7.0	
IZ48	unknown	unknown		8	226.5	-28.8	12.0	14.0	
Karaburun (Kissel et al., 1987)									**16.0–21.3 (13)**
IZ08	unknown	unknown		11	267.0	-34.5	23.0	8.5	
IZ14	unknown	unknown		8	181.0	-51.0	264.0	3.2	
IZ15	unknown	unknown		5	226.0	-84.5	35.0	10.5	
IZ16	unknown	unknown		6	43.5	16.3	97.0	5.8	
IZ43	unknown	unknown		8	234.0	-53.5	450.0	2.6	
CESME1	unknown	unknown		7	254.0	-51.9	189.0	4.4	
CESME2	unknown	unknown		7	237.0	-51.5	52.0	8.4	
CESME3	unknown	unknown		5	207.0	-59.5	132.0	6.7	
Lesbos (Beck et al., 2001)									**16.0–20.0 (1, 2)**
Lesbos01	39.3790	26.2130		8	261.1	−63.5	304.3	3.1	
Lesbos02	39.3750	26.3000		8	27.3	67.8	184.2	4.1	
Lesbos03	39.3610	26.2490		8	197.5	−19.3	318.2	3.1	
Lesbos04	39.3620	26.2630		7	208.2	−15.9	400.0	3.0	
Lesbos05	39.3510	26.3060		9	192.1	−41.7	320.0	2.9	
Lesbos06	39.3510	26.3060		7	169.8	−31.1	166.7	4.7	
Lesbos07	39.3640	26.3430		11	203.1	−54.1	500.0	2.2	
Lesbos08	39.3650	26.3210		8	342.1	64.8	148.9	4.5	
Lesbos09	39.3740	26.3170		8	99.0	−60.6	333.3	3.0	
Lesbos10a	39.2500	26.1810		6	180.1	−69.0	1250.0	1.9	
Lesbos10b	39.2500	26.1810		6	195.9	−55.5	74.6	7.8	
Lesbos11	39.2510	26.1720		9	215.1	−55.4	38.8	8.4	
Lesbos12	39.3630	26.2720		5	194.3	−40.3	500.0	3.4	
Lesbos13	39.3650	26.3000		9	247.8	−49.4	101.3	4.3	
Lesbos14	39.2570	26.1090		10	11.4	17.3	33.1	8.5	
Lesbos15	39.2620	26.0650		10	19.0	49.2	333.3	2.6	
Lesbos16	39.2460	26.0510		10	355.5	8.2	160.7	3.8	
Lesbos17	39.2370	26.0310		6	326.9	48.8	625.0	2.7	
Lesbos18	39.2370	26.0310		11	305.9	76.8	500.0	2.3	
Lesbos19	39.2350	26.0340		5	325.9	41.8	148.1	6.3	
Lesbos20	39.2390	26.2620		8	181.7	−18.0	142.9	4.6	
Lesbos21	39.2670	26.2850		10	12.4	53.5	428.6	2.3	

Table 6.1 continued

Locality	Lat	Lon	Na	Nc	D	I	k	a95	Age
Lesbos21	39.2670	26.2850		10	12.4	53.5	428.6	2.3	
Lesbos22	39.2990	26.3130		9	356.1	67.8	347.8	2.7	
Lesbos23	39.3230	26.3020		8	321.9	54.4	269.2	3.4	
Lesbos24	39.3490	26.3220		8	154.9	−46.0	875.0	1.9	
Lesbos26	39.1560	25.9570		10	25.8	45.1	187.5	3.5	
Lesbos27	39.1050	26.0150		7	320.7	41.6	272.7	3.6	
Lesbos28	39.3630	26.1990		7	150.9	−62.3	18.6	14.4	
Lesbos29	39.3480	26.2240		5	204.1	−15.9	46.5	11.3	
Lesbos30	39.2360	26.0170		8	334.6	78.4	106.1	5.4	
Lesbos31	39.2340	26.0200		7	39.5	73.2	333.3	3.3	
Lesbos32	39.2430	26.0110		6	31.2	68.2	294.1	3.9	
Lesbos33	39.2830	26.0040		9	10.0	26.5	210.5	3.5	
Lesbos34	39.2460	25.9870		7	10.0	51.3	111.1	5.8	
Lesbos35	39.2080	26.0330		8	9.0	44.7	189.2	4.0	
Lesbos36	39.2150	26.0300		7	353.3	48.9	400.0	3.0	
Lesbos37	39.2880	26.1200		10	13.0	63.1	204.5	3.4	
Lesbos38	39.1910	26.1670		8	196.4	−42.4	538.5	2.4	
Lesbos39	39.1520	26.1360		8	194.1	−56.5	194.4	4.0	
Lesbos40	39.1360	26.1180		8	193.4	−49.4	777.8	2.0	
Lesbos41	39.1180	26.0910		7	155.3	−35.0	9.0	21.2	
Lesbos42	39.1350	26.0830		8	179.7	−49.8	411.8	2.7	
Lesbos43	39.1500	26.0580		8	178.2	−64.5	636.4	2.2	
Lesbos44	39.1480	25.9830		7	359.3	54.1	1000.0	1.9	
Lesbos45	39.1720	25.9380		8	8.5	26.7	241.4	3.6	
Lesbos46	39.2270	25.9730		10	1.5	17.3	88.2	5.2	
Lesbos47	39.2500	26.0470		10	344.4	16.4	187.5	3.6	
Lesbos48	39.3170	26.2350		6	34.8	70.5	185.2	4.9	
Lesbos49	39.3170	26.2530		4	51.6	47.6	300.0	5.2	
Lesbos50	39.3170	26.2530		8	230.9	−40.6	72.9	6.5	
Gediz (Şen and Seyitoğlu, 2009)				**173**					**early–middle Miocene**
Zetyinçayır River (normal)	unknown	unknown		24	342.2	49.4	31.8	5.3	
Zetyinçayır River (reverse)	unknown	unknown		75	149.7	-53.6	21.8	3.6	
Zetyinçayır Road (normal)	unknown	unknown		6	323.3	43	5.5	31.4	
Zetyinçayır Road (reverse)	unknown	unknown		16	155.2	-55.3	25.4	7.5	
Eycelli (normal)	unknown	unknown		6	43.4	39.4	20.4	15.2	
Eycelli (reverse)	unknown	unknown		46	210.2	-48.6	10.6	6.8	
Uşak (van Hinsbergen et al., 2010)			**69**						**16.9–20.8 (3)**
US1	38.7915	29.5543	7	7	73.2	44.6	99.2	6.8	
US2	38.7904	29.5534	7	7	2.3	40.9	135.2	5.2	
US3	38.7857	29.5487	7	7	193.3	-41.9	72.1	7.2	
US4	38.7847	29.5493	7	7	~~19.8~~	~~11.4~~	~~14.3~~	~~16.5~~	
US5	38.7831	29.5496	7	7	~~347.4~~	~~32.7~~	~~16.2~~	~~15.5~~	
US6	38.7818	29.5580	7	7	~~326.3~~	~~-15.4~~	~~11.4~~	~~18.7~~	
US7	38.7800	29.5527	6	6	~~271.8~~	~~44.7~~	~~11.5~~	~~20.7~~	
US8	38.7780	29.5543	7	5	314.0	61.0	173.8	5.8	
US9	38.7620	29.5555	7	6	342.8	57.8	134.7	5.8	
US10	38.7744	29.5432	7	6	159.6	72.1	67.6	7.4	
Güre (van Hinsbergen et al., 2010)			**42**						**15.9 (4)**
GU1	38.7796	29.2699	7	6	195.4	-46.8	53.6	9.2	
GU2	38.7798	29.2691	7	7	~~98.1~~	~~-70.6~~	~~4.7~~	~~31.3~~	
GU3	38.7798	29.2691	7	4	~~213.1~~	~~-65.1~~	~~39.3~~	~~14.8~~	
GU4	38.7798	29.2691	7	3	195.5	-46.6	519.9	5.4	
GU5	38.7801	29.2683	7	6	273.7	75.7	137.9	5.2	
GU6	38.7801	29.2683	7	7	192.6	-47.8	161.9	4.8	
Ahmetler (van Hinsbergen et al., 2010)			**48**						
AH1	38.4437	29.1547	7	7	166.9	18.1	177.1	4.5	
AH2	38.4468	29.1535	6	6	168.0	14.7	82.4	7.4	
AH3	38.4483	29.1523	7	6	167.5	17.3	74.2	7.8	
AH1,2,3			21	19	167.0	15.8	105.0	3.3	
AH4	38.4548	29.1544	7	7	~~193.2~~	~~-61.0~~	~~10.3~~	~~19.8~~	
AH5	38.4545	29.1545	7	7	~~184.0~~	~~-68.2~~	~~9.3~~	~~20.9~~	
AH6	38.4544	29.1550	7	7	151.9	8.9	77.2	6.9	
AH7	38.4550	29.1541	7	7	~~284.3~~	~~0.6~~	~~1.4~~	~~95.6~~	
Selendi (van Hinsbergen et al., 2010)									**14.9–20.2 (4–7)**
SL1	38.8246	28.8697	7	7	198.5	-59.5	375.0	3.1	
SL2	38.8617	28.9249	7	7	213.6	-42.1	267.7	3.7	
SL3	38.8750	28.9289	7	5	203.6	-58.5	1121.9	2.3	
SL4	38.8751	28.9290	7	7	202.6	-62.5	846.4	2.1	
SL5	38.8731	28.9287	7	7	198.1	-59.7	252.9	3.8	
SL6	38.8658	28.9281	7	4	176.8	-56.2	108.2	8.9	
SL7	38.9110	28.9369	7	7	356.5	50.8	204.8	4.2	
SL8	38.9107	28.9416	7	3	184.9	-53.0	106.8	12.0	
SL9	38.9093	28.9598	7	7	6.1	58.4	283.5	3.6	
SL10	38.9093	28.9598	7	7	166.9	-60.0	86.0	6.5	
SL11	38.9093	28.9598	7	7	353.9	54.6	91.3	6.4	
SL12	38.9131	28.9674	7	7	7.8	56.7	27.0	11.8	
SL13	38.9130	28.9676	7	7	7.3	56.7	92.2	6.3	
SL14	38.9130	28.9678	7	6	358.2	56.7	144.1	5.6	
SL15	38.9130	28.9681	7	7	~~2.9~~	~~56.2~~	~~41.5~~	~~9.5~~	
SL16	38.9129	28.9686	7	7	354.2	51.8	110.2	5.8	
SL17	38.9127	28.9690	7	7	352.2	54.5	251.5	4.2	
SL18	38.9129	28.9683	7	7	~~311.6~~	~~44.2~~	~~21.2~~	~~13.4~~	
SL19	38.8458	28.8845	7	7	210.0	-18.9	172.4	4.6	
SL20	38.8412	28.8795	7	7	174.0	-37.2	125.3	6.0	

Table 6.1 continued

Locality	Lat	Lon	Na	Nc	D	I	k	a95	Age
Demirci (van Hinsbergen et al., 2010)			**117**						**early Miocene (6–8)**
DC1	38.8812	28.5778	7	7	32.0	39.0	627.5	2.4	
DC2	38.8807	28.5770	7	7	26.8	39.2	176.5	4.6	
DC3	38.8802	28.5763	7	6	31.1	38.7	186.2	4.9	
DC4	38.8799	28.5759	7	7	33.1	41.9	363.2	3.2	
DC5	38.8800	28.5755	7	7	34.0	43.4	328.7	3.3	
DC1-5			35	33	31.9	40.5	272.3	1.5	
DC6	38.88546	28.57002	7	7	14.0	29.6	676.9	2.3	
DC7	38.88546	28.57000	7	6	2.2	301.0	362.1	3.5	
DC8	38.88546	28.57000	7	7	5.4	30.8	284.7	3.6	
DC9	38.88546	28.57000	7	7	1.8	31.8	440.5	2.9	
DC10	38.88546	28.57000	6	6	357.5	29.2	337.8	3.7	
DC7-10	38.88546	28.57002	27	26	1.9	30.6	277.3	1.7	
DC11	38.9405	28.5463	7	6	48.7	49.9	417.0	3.3	
DC12	38.9405	28.5460	7	7	53.5	46.4	70.2	7.3	
DC13	38.9403	28.5453	6	6	71.9	61.4	385.3	3.4	
DC14	38.9399	28.5439	7	7	60.6	64.2	281.0	3.6	
DC15	38.9400	28.5437	7	7	353.8	26.5	179.6	4.5	
DC16	38.94009	28.54253	7	7	~~75.7~~	~~44.8~~	~~8.9~~	~~21.4~~	
DC17	38.93959	28.54189	7	7	42.8	42.8	1309.5	1.7	
Gördes (van Hinsbergen et al., 2010)			**69**						**17.6–20.9 (4–6)**
GR1	38.8875	28.1719	7	7	167.4	-64.9	818.2	2.1	
GR2	38.8879	28.1719	7	7	161.2	-62.6	232.6	4.0	
GR3	38.8888	28.1718	7	7	153.2	-66.3	2547.1	1.2	
GR4	38.8892	28.1715	7	7	167.9	-66.3	380.7	3.1	
GR1-4	38.8875	28.1719	28	28	162.5	-65.1	139.1	2.4	
GR5	38.8901	28.1705	7	7	164.0	-81.2	421.5	2.9	
GR6	38.8907	28.1705	7	0	~~0~~	~~0~~	~~0~~	~~0~~	
GR7	38.9027	28.1427	6	6	251.2	-57.7	261.7	4.1	
GR8	38.9032	28.1424	7	7	248.3	-61.8	145.1	5.0	
GR9	38.9032	28.1427	7	7	261.0	-60.9	325.4	3.4	
GR10	38.9040	28.1430	7	7	247.3	-58.6	187.4	4.4	
GR7-10	38.9027	28.1427	27	27	248.7	-60.1	173.3	2.1	
Ayvalık (van Hinsbergen et al., 2010)			**97**						**19.7–20.9 (9)**
AY1	38.2929	26.6678	7	5	181.0	-58.7	182.7	5.7	
AY2	39.2876	26.6720	7	5	206.8	-48.8	425.9	3.7	
AY3	39.2882	26.6730	6	5	205.3	-42.3	3068.4	1.4	
AY4	39.2895	26.6729	7	7	34.3	48.6	21198.7	0.5	
AY5	39.2904	26.6726	7	6	6.5	58.6	1785.8	1.6	
AY6	39.2741	26.6694	7	3	~~200.7~~	~~-34.1~~	~~196.1~~	~~8.8~~	
AY7	39.3017	26.6259	7	7	194.8	-45.0	212.4	4.2	
AY8	39.3162	26.6566	7	6	340.3	41.3	75.4	7.8	
AY9	39.3027	26.6339	7	7	175.7	-39.7	58.3	8.0	
AY10	39.2924	26.6330	7	7	227.4	-47.6	231.1	4.0	
AY11	39.2913	26.6375	7	6	184.9	-40.4	441.7	3.2	
AY12	39.2843	26.6430	7	7	158.1	-51.1	640.7	2.6	
AY13	39.2844	26.6432	7	7	159.0	-41.1	96.1	6.2	
AY14	39.2874	26.6425	7	7	~~184.2~~	~~-44.0~~	~~15.9~~	~~11.6~~	
Dikili (van Hinsbergen et al., 2010)			**175**						**15.2–18.5 (9–12)**
DI1	38.9306	26.8941	7	7	207.5	−24.1	423.3	2.9	
DI2	38.9297	26.8924	7	6	203.9	−32.5	339.5	3.6	
DI3	38.9283	26.8894	7	6	191.6	−63.4	92.5	6.3	
DI4	38.9263	26.8903	7	6	181.8	−56.4	1323.0	1.8	
DI5	38.9284	26.8788	7	7	~~32.9~~	~~-33.2~~	~~167.8~~	~~4.7~~	
DI6	38.9301	26.8751	7	7	325.2	20.8	765.1	2.2	
DI7	38.9315	26.8678	7	7	352.9	73.8	498.2	2.7	
DI8	38.9350	26.8606	7	7	~~211.1~~	~~18.1~~	~~46.3~~	~~9.0~~	
DI9	38.9374	26.8566	7	7	~~298.3~~	~~-21.0~~	~~185.8~~	~~4.4~~	
DI10	38.9463	26.8336	7	7	7.1	36.9	254.4	2.5	
DI11	38.9564	26.8152	7	7	208.9	5.6	620.3	2.4	
DI12	38.9573	26.8088	7	7	211.9	−25.7	1194.9	1.7	
DI13	38.9686	26.8024	7	7	226.7	−35.0	52.1	8.4	
DI14	38.9698	26.8017	7	7	240.0	−27.1	1142.1	1.8	
DI15	38.9783	26.8026	7	7	~~299.0~~	~~-24.3~~	~~72.0~~	~~7.2~~	
DI16	38.9801	26.8021	7	7	237.1	−25.6	720.0	2.3	
DI17	38.9823	26.8010	7	7	209.3	−28.3	93.0	6.3	
DI18	38.9842	26.7994	7	7	~~143.8~~	~~-47.9~~	~~55.7~~	~~8.2~~	
DI19	38.9855	26.7986	7	7	209.0	−35.0	276.4	3.6	
DI20	38.9848	26.7995	7	7	211.7	−38.6	137.2	5.2	
DI21	39.0328	26.8572	7	7	~~278.5~~	~~-11.9~~	~~178.6~~	~~4.5~~	
DI22	39.0346	26.8362	7	7	9.4	15.7	625.9	2.4	
DI23	39.0447	26.8427	7	7	326.9	21.4	72.9	7.1	
DI24	39.0481	26.8451	7	6	8.2	15.2	1677.6	1.6	
DI25	39.0545	26.8506	7	7	241.7	−4.9	549.7	2.6	
Bergama (van Hinsbergen et al., 2010)									**15.2–18.5 (9–12)**
BG1	39.0528	27.0623	7	7	346.6	54.3	161.9	4.8	
BG2	39.0537	27.0619	7	7	329.2	51.6	112.5	5.7	
BG3	39.0571	27.0694	7	7	16.6	15.4	1687.6	1.5	
BG4	39.0603	27.0703	7	7	327.6	63.9	268.5	3.7	
BG5	39.0757	27.0923	7	7	353.8	60.4	425.1	2.9	
BG6	38.0830	27.1121	7	7	~~133.2~~	~~73.2~~	~~47.1~~	~~8.9~~	
BG7	39.0783	27.1021	7	7	332.6	67.4	359.3	3.2	
BG8	39.0759	27.0878	7	7	28.6	52.7	217.8	4.1	

Table 6.1 continued

Locality	Lat	Lon	Na	Nc	D	I	k	a95	Age
BG9	39.0791	27.0794	7	7	3.7	35.8	1684.8	1.5	
BG10	39.0648	27.0232	7	7	~~133.1~~	~~−67.0~~	~~172.8~~	~~4.6~~	
BG11	39.0642	27.0157	6	6	297.3	−79.9	37925.5	0.3	
BG12	39.0647	27.0128	7	7	81.7	67.8	993.4	1.9	
BG13	39.0480	27.0205	7	7	18.0	63.4	435.5	2.9	
BG14	39.0529	27.0265	7	7	17.0	32.6	1238.0	1.7	
Yuntdağ (van Hinsbergen et al., 2010)			**119**						**16.8–21.0 (10)**
YD1	38.9700	27.1776	7	7	~~289.9~~	~~−13.4~~	~~86.8~~	~~6.5~~	
YD2	38.9686	27.1780	7	6	198.1	−8.7	96.7	6.2	
YD3	38.9643	27.1768	7	6	~~118.6~~	~~−16.8~~	~~64.8~~	~~8.4~~	
YD4	38.9577	27.1824	7	7	~~191.0~~	~~−17.3~~	~~36.1~~	~~10.2~~	
YD5	38.9573	27.1828	7	7	179.7	11.8	809.1	2.1	
YD6	38.9538	27.1822	7	7	~~91.5~~	~~−23.0~~	~~65.1~~	~~7.5~~	
YD7	38.9502	27.1845	7	6	~~112.7~~	~~−82.1~~	~~44.9~~	~~10.1~~	
YD8	38.9417	27.1930	7	7	234.5	−65.8	1499.3	1.6	
YD9	38.9368	27.2040	7	7	~~294.5~~	~~−14.2~~	~~79.9~~	~~6.8~~	
YD10	38.9353	27.2075	7	7	34.8	−38.7	1425.0	1.6	
YD11	38.9391	27.2082	7	7	~~264.3~~	~~−55.4~~	~~323.1~~	~~3.4~~	
YD12	38.9420	27.2081	7	6	203.4	−29.5	367.5	3.5	
YD13	38.9499	27.2042	7	6	247.0	−38.5	8657.8	0.7	
YD14	38.9542	27.2031	7	7	~~104.6~~	~~−44.1~~	~~79.1~~	~~6.8~~	
YD15	38.9575	27.2041	7	7	238.5	−37.1	1643.0	1.5	
YD16	38.9600	27.2042	7	7	~~358.8~~	~~−28.3~~	~~212.3~~	~~4.3~~	
YD17	38.9663	27.2067	7	7	~~151.9~~	~~−1.0~~	~~494.7~~	~~2.7~~	

Şen and Seyitoğlu (2009) provided detailed magnetostratigraphic data from the E–W-trending Gediz (the Zeytinçayı river and road sections) and Büyük Menderes grabens (The Eycelli section) that are supposed to be Miocene supradetachment basin deposits (Fig. 6.5, and Table 6.1). The Zeytinçayı sections belong to Alaşehir and Kurşunlu Formations and measure in an area are lying at the transition zone between Gediz and Büyük Menderes grabens. Fifty two samples were collected from The Eycelli section within the Büyük Menderes graben and includes 52 samples of Hasköy and Gökkırantepe Formations. Both Zeytinçayı river and road sections from 121 samples show that this area underwent anticlockwise rotation of about 25° about vertical axis, since their deposition (Fig. 6.5). On the other hand, the samples from the Eycelli section have reversed and normal polarities indicating clockwise rotation of about 30–40°. They suggested that the cause of these opposite rotations might be due to local tectonics and are the result of extensional deformation characterized by detachment faults that gave way to the Gediz and Büyük Menderes grabens (Fig. 6.5).

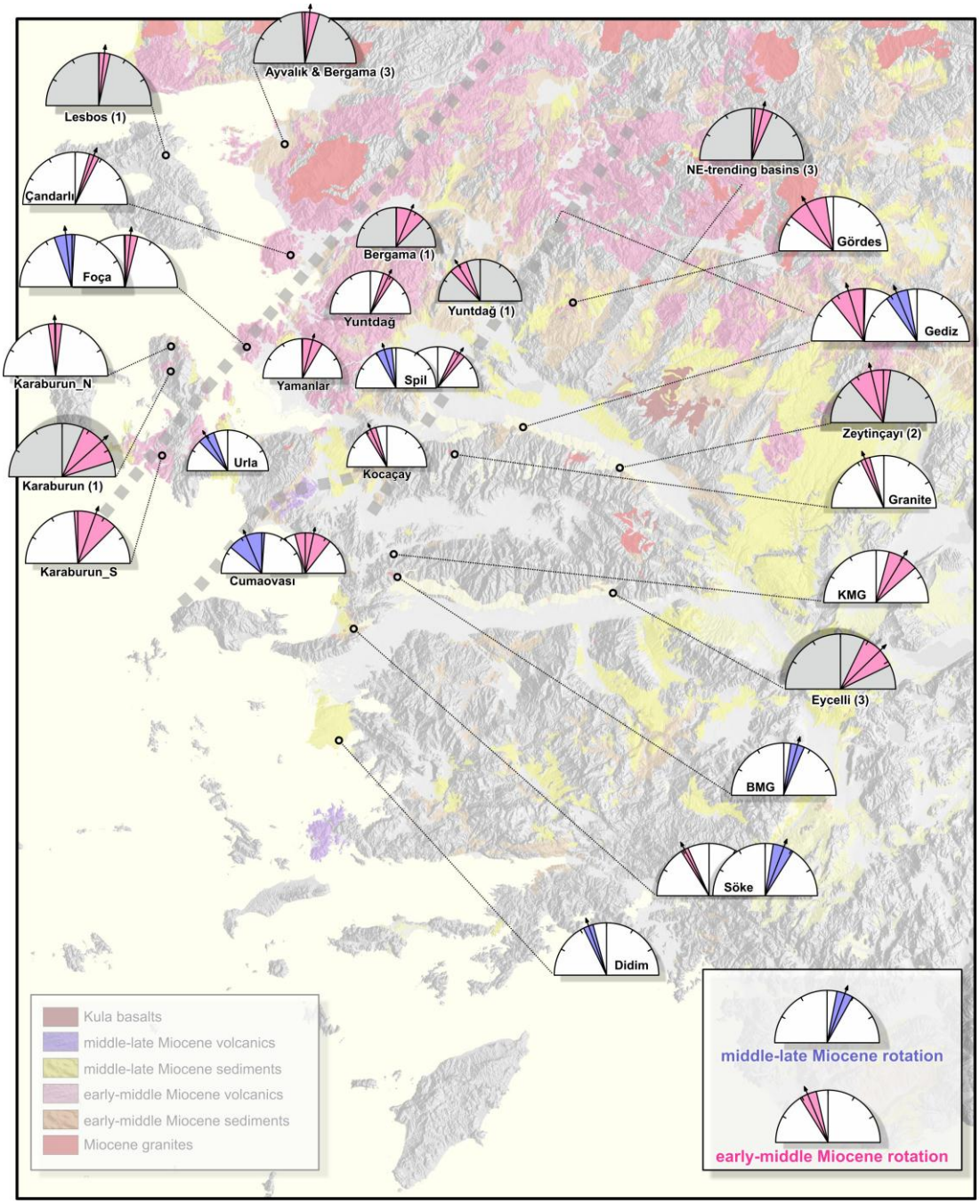


Figure 6.5 Paleomagnetic data from this study and previous paleomagnetic studies. Reference codes are: (1) Kissel et al. (1987); (2) Şen & Seyitoğlu (2006); (3) van Hinsbergen et al. (2010).

Van Hinsbergen et al. (2010a, 2010b) provided an extensive paleomagnetic database for the paleomagnetism of western and southwestern Anatolia. This study includes approximately 1850 samples from 240 sites disturbed in several Neogene basins top the Lycian Nappes and Menderes Core Complex (Table 6.1). They also provided a broad review of published data and applied very rigorous statistical

criteria to check the validity of published paleomagnetic data, and then they integrated the ones that passed the statistical test into their own database. They conclude that the region to the north of the Gediz detachment exhibits two paleomagnetically coherent rotation domains: (i) the domain defined by the region around Afyon, having approximately 20° clockwise rotation since the middle Miocene, and (ii) domain covering from the NE-trending basins to the Lesbos Island, having no significantly rotation (Fig. 6.5). The southern side of the Büyük Menderes detachment is rotating 20° counterclockwise since the Oligocene. The study also defined a pivot point, at the intersection point of the Gediz and Büyük Menderes detachments, to accommodate the vertical axis rotations. They attributed these rotations to the exhumation of MCC, ascent of which gave way to the Gediz and Büyük Menderes detachments and related basins and rotation of the intervening blocks away from the locus of ascent with respect to pivot.

Most recently, Kondopoulou et al. (2011) attempted to solve complex pattern of clockwise and counterclockwise rotational history of the Chios Island. They analyzed 295 samples from the middle Miocene sediments and lava flows. However, results from sedimentary rocks provide evidence for a 15° counterclockwise rotation with a very large error margin. A small set of lavas provided poorly defined but significant (70°) counterclockwise rotation. They did not explain these conflicting rotations, but attributed to a somewhat complex deformation in the region in reference to complex interaction of extensional and strike-slip deformation and they justified this by referring to Uzel et al. (2008). In other words, they suggested that these conflicting rotations might have been resulted from the activity of İBTZ, which implies that the İBTZ extends in to the west to Chios Island including the Karaburun, Dikili, Foça, and Yuntdağ regions.

6.3.2 Discussion on the Paleomagnetic Results of This Study

It has been discussed in previous sections that study area comprises two well-defined stratigraphical sequences separated by a major unconformity. The older sequence is informally names as *lower sequence* and the younger sequence as the

upper sequence. Stratigraphical relationships and kinematic results indicate that these sequences belong, at least, to two different deformation phases during which vertical axis rotations must have been taken place. Due to such kinematic necessity and newly obtained very precise $^{40}Ar/^{39}Ar$ ages paleomagnetic results are analyzed categorized and analyzed for two time intervals; (i) early–middle Miocene phase (Fig. 6.6a), and (ii) middle–late Miocene phase (Fig. 6.6b).

6.3.2.1 Early-Middle Miocene Rotations

The spatial distribution of the rotation senses and amounts for the early-middle Miocene rocks can be classified into three areas. The areas to the east of Söke-Gördes line, the areas east and west of Karaburun and Çandarlı line. Its proposed that the area between west of Söke-Gördes line and to the east of Karaburun-Çandarlı line is the İBTZ. As seen in Figure 6.6a the rotation amounts and senses within the İBTZ and the areas to the east and the west of it are obviously different.

The rotation amounts from the eastern part of the İBTZ ranges between ~10°–40° (Fig. 6.6a) with ~25° counterclockwise average values (Fig. 6.6). The rotation sense and amounts are relatively consistent for this area. The sampled site in the east İBTZ belongs to structurally different tectonic domains. Although, clockwise rotations dominate within the İBTZ there are some counterclockwise rotations (Fig. 6.6). The counterclockwise rotations are generally associated with the local faults and are thought to be related to local fault-block rotations related to local complications and space problem. It's further speculated that the clockwise rotations reflects the main rotations within the İBTZ. Disregarding the counterclockwise rotations, the average clockwise rotation within the İBTZ is around 31°.

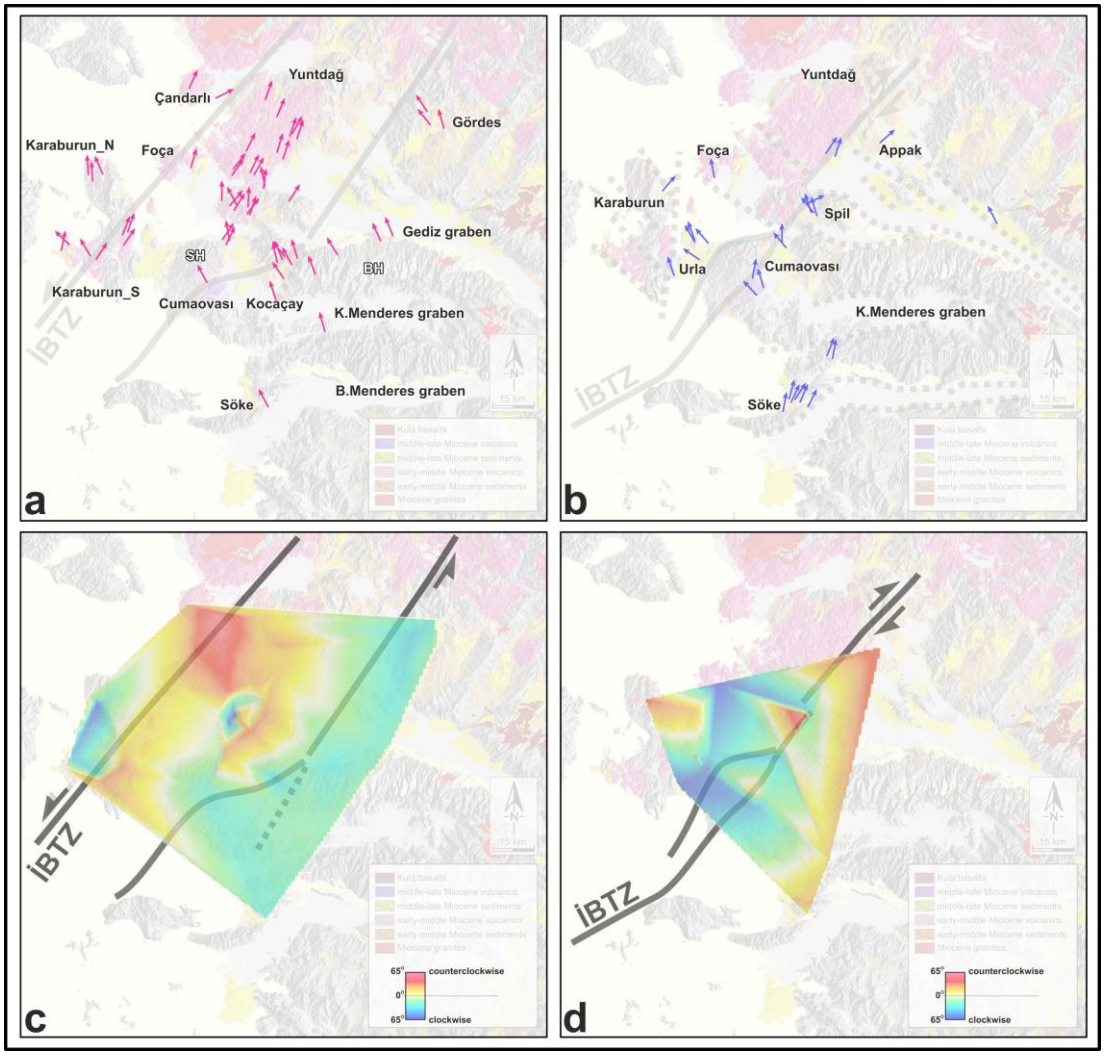


Figure 6.6 Paleomagnetic results from this study. The rotation vectors for; a) early–middle Miocene rocks and b) middle–late Miocene rocks, c. Interpolated early-middle Miocene Rotations, d) interpolated middle-late Miocene rotations. BH, Bozdağ Horst; SH, Seferihisar High.

The rotations west of the İBTZ are also relatively consistent except for some sites at the NW part of the study area around Çandarlı and a site at the western end of the Karaburun Peninsula. Disregarding these inconsistent clockwise rotations which could be considered as spurious, the average of the vertical axis rotation west of İBTZ is 24° counterclockwise. This is very much similar to the areas east of İBTZ and the rotations around Çandarlı area are somewhat similar to the rotations within İBTZ. This may imply that the Çandarlı area is also part of İBTZ and the boundary of the İBTZ is not very linear, or the Çandarlı area is coupled with the western boundary of the İBTZ and rotated similarly.

6.3.2.2 Implications Early Miocene Rotations

As mentioned earlier some of the early-middle Miocene sites include granites located within the footwall block of the Menderes Core Complex while the sites in Söke and Kocaçay basins are located at the supradetachment basin fill; there are also other sites located on the hanging-wall block of the MCC. Van Hinsbergen et al (2010) proposed that the early–middle Miocene rotations in the region are related to ascent and exhumation of the Menderes Core Complex. Some of the site such a Söke and Küçük Menderes are located south of the line where no rotations could be developed according to model proposed by van Hinsbergen et al. (2010).

Having similar rotation senses all the way from the northern parts of the MCC and central and southern part of it, implies that this is a regional rotation rather than local block rotations. Absence of amount and polarity change with respect to any pivot implies that the model proposed by van Hinsbergen et al. (2010) cannot be applied for the early-middle Miocene rotations in the region. Similarly, relatively consistent results from the western part of the İBTZ rules out the connotation of "region of chaotic rotations" proposed by Kondopoulou et al. (2011). In addition to this, relatively consistent rotations within the İBTZ and very sharp changes at its margins implies that the İBTZ was delimiting the western margin of Menderes Core Complex and İBTZ was a very well defined through-going shear zone.

Considering similar and consistent rotations outside of the İBTZ its speculated that the overall study area experienced 25° counterclockwise rotation while İBTZ experienced 31° homogeneous internal clockwise rotation (Figure 6.6). This model does not exclude 56° clockwise rotation of the İBTZ during the early-middle Miocene, 25° of which is taken up by regional counterclockwise rotation that resulted in 31° net clockwise rotation (Figure 6.7c).

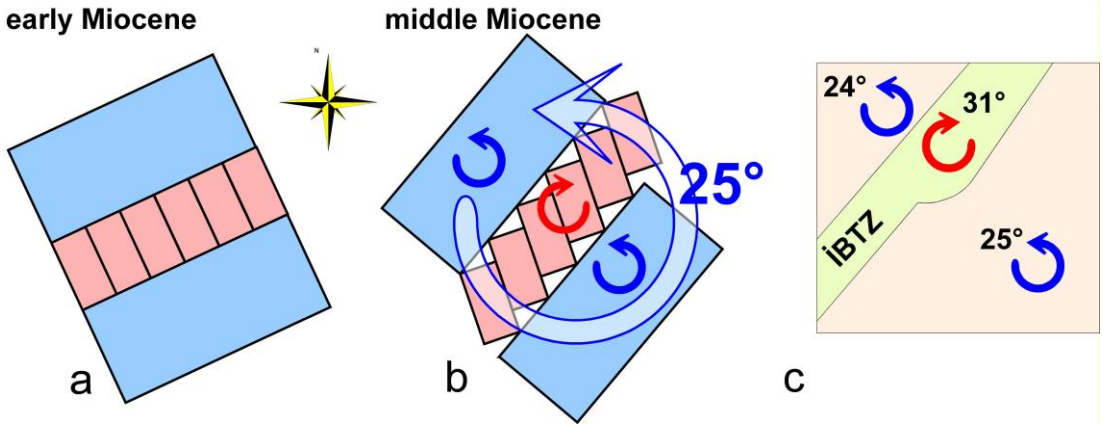


Figure 6.7 Rigid body rotation model for the study area. a) early Miocene, b,c) middle Miocene, c) present configurations. Please note that rotations of the blocks to the west and east of İBTZ are ascribed to regional rotations. Therefore, there is a possibility that the total rotation of the İBTZ was 56° clockwise and counterclockwise regional rotation took away 25° of it.

6.3.2.3 Middle-Late Miocene Rotations

Compared to early-middle Miocene rotations, the middle-late Miocene rotations are relatively chaotic. Nevertheless, there are very obvious patterns especially for determining the boundary of the İBTZ during the middle-late Miocene. As seen in Fig. 6.6. there is very marked change in the rotation amounts and senses on either side of a zone from Cumaovası to eastern margin of Yuntdağ. All the sites east of the zone from Söke to Appak indicate clockwise rotations coherently. However, contrasting, i.e. clockwise and counterclockwise rotations occur within the zone. Except for one site around Karaburun all other sites indicate relatively large counterclockwise rotations for the areas to the west of the line.

6.3.2.4 Implications Early Miocene Rotations

Having coherent rotations on either side and conflicting rotations within the zone from Urla-Yuntdağı, we propose that this line represents the İBTZ in middle-late Miocene. This implies that the İBTZ which was a large shear zone during the early-middle Miocene, evolved into a narrow, well-defined and discrete shear zone during the middle-late Miocene. Evolution from a large shear zone into a narrow zone is

general behavior of most of the strike-slip fault zones (Naylor et al., 1986), provided that strain softening prevailed during its deformation. This may be facilitated by heat generated by the ascending magmatic material.

6.4 Regional Implications

The İBTZ is a NE–SW trending strike-slip dominated shear zone that delimits the western margins of the E-W striking horst-graben complex of west Anatolia that define the loci of maximum extension. These E-W grabens include from north to south; Gediz, Küçük Menderes and Gediz grabens. The İBTZ is recognized previously and it is interpreted as the NE continuation of the Mid-Cycladic Lineament (MCL) (Pe-Piper et al. 2002) to mark the boundary between the eastern and western Aegean domains (Morris and Anderson, 1996). The MCL ceased its activity in the latest Miocene–Early Pliocene coevally with the development of the North Anatolian Fault (Walcott and White, 1998). Regional kinematic studies have also suggested that a major change in the kinematics of the Aegean occurred in the latest Miocene–early Pliocene (Le Pichon et al., 1995).

The oldest deformation phase of the region (Phase 1) is characterized by strike-slip deformation controlled by vertical intermediate stress, E–W contraction and N–S extensional strain axes. In addition, the faults active during this phase controlled the locus of the eruption centers and are generally aligned in NE–SW direction within the İBTZ. Paleostress data for this phase in the eastern margin of the İBTZ indicate that transtensional deformation was dominant and the IBTZ and was kinematically linked with the E–W-trending low-angle normal faults and NE–SW-trending strike-slip faults such as the one that controlled the evolution of the Kocaçay basin (Sözbilir et al., 2011). Major movements along the nearby Gediz detachment also took place at this phase. This was associated with the exhumation of the metamorphic core complexes in the footwalls of the Gediz and Büyük-Menderes detachment faults (Hetzel et al., 1995; Emre & Sözbilir, 1997; Koçyiğit et al., 1999; Lips et al., 2001; Sözbilir, 2001, 2002; Seyitoğlu et al., 2002; Işık et al., 2003, 2004; Bozkurt & Sözbilir, 2004). The footwall metamorphic rocks were progressively mylonitised,

exhumed, and intruded by syn-deformational granitoids, the Turgutlu and Salihli granodiorites indicate clockwise vertical axis rotations. The Salihli granodiorite yielded a wide range of ages, all obtained from the same granitoids: $^{40}Ar/^{39}Ar$ amphibole isochron and biotite plateau cooling ages of 19.5 ± 1.4 and 12.2 ± 0.4 Ma (Hetzel et al., 1995), U-Pb crystallization ages of 15.0 ± 0.3 Ma from allanite (Glodny and Hetzel, 2007), and Th-Pb ion microprobe monazite ages ranging from 21.7 ± 4.5 Ma to 9.6 ± 1.6 Ma (Catlos et al., 2010). In addition, the timing of the syn-extensional plutonism in the footwall of the Gediz detachment coincides with a period of widespread volcanism between 21.5 and 12 Ma in the NE trending transtensional basins located within the İBTZ. The available radiometric age data placed Phase 3 into 21.5 to 9 Ma, and suggest that when the E-W trending grabens developed under the control of the NNE–SSW pure extension while the İBTZ underwent N–S strike-slip dominated transtension (Özkaymak et al., 2013). This implies that the extension and strike-slip motion is partitioned along the İBTZ.

According to paleomagnetic data, the region to the east of the İBTZ, which is mainly the MCC region, underwent a counterclockwise rotation during the Phase 1, while the areas within the İBTZ rotated opposite sense (Figs. 6.6 & 6.7). Here, the rotation sense and amount of the MCC region was mostly uniform suggesting that the exhumation of the MCC must be related to an orthogonal extension. In other words, the rotation amounts and the senses on the MCC show that this rotation was not directly related to detachment faulting, which means the post-orogenic rotation related to exhumation of the core of the MCC occurred as “rigid-body” rotation, i.e. without major internal inhomogeneous deformation. In addition, the stretching lineations of Jolivet et al. (2010 and references therein) from both MCC and CCC are also support this orthogonal extension geometry, rather than round a pivot point (van Hinsbergen et al., 2010).

Clockwise rotations within the İBTZ and counterclockwise rotations of the intervening blocks suggest that the İBTZ was a dextral shear zone during the oldest deformation phase. By linking/accommodating the Miocene extension the İBTZ and MCL have played an important role in tectonics of the region and the exhumation of

MCC, together. Both the end of the activity of the MCL and a concurrent major change in the kinematics of the Aegean occurred in the latest Miocene–early Pliocene. In contrast to the MCL, however, the activity of the İBTZ has continued until recently.

Integrating with surface (topography analysis of Gessner et al., 2013) and mantle tomography images of van Hinsbergen et al. (2010b) and Biryol et al. (2011), there are big differences in the upper mantle and lithospheric characteristics of the region between the MCC and the western side of it. Additionally, the geochemical analyses of Miocene volcanism suggest that the thickness of the lithosphere beneath the western Anatolia is significantly different between under the MCC and İBTZ and it is thinning east to west (Ersoy et al., 2012). The nature of the volcanism along this pattern also changes shoshonitic and ultrapotassic to high potassic (Ersoy et al., 2012) affinies, where the strike-slip tectonics became dominant. Hence, the map view of the Miocene volcanic rocks and their eruption centers indicate that volcanic activity was mostly followed the NE-trending İBTZ as a zone of weakness to reach to the surface (Fig. 3.2). All of these information suggest that, although it is not conclusive, there is a great possibility that İBTZ was not only separating two core complexes (MCC and CCC), but also a deep seated structure that might be related to tear along the subducting northern edge of the African Plate, as a STEP fault suggested by van Hinsbergen et al. (2010) (Fig. 6.8).

The second stage of deformation (Phase 2) closely follows a major change in Aegean kinematics in time and space. It is characterized by two different stress configurations: a strike-slip regime within the İBTZ and an extensional regime outside. It prevailed during the early Pliocene because the strike-slip faults cut and displaced the late Miocene lacustrine carbonates. Even though the regional stress field has essentially been characterized by a sub-vertical maximum principal stress axis, the stress field within the İBTZ was different than the rest of the region during the Phase 2. Within the fault zone, palaeostress analysis points to a local stress field with NW–SE subhorizontal major compression and NE–SW sub-horizontal minor compression (indirect tension).

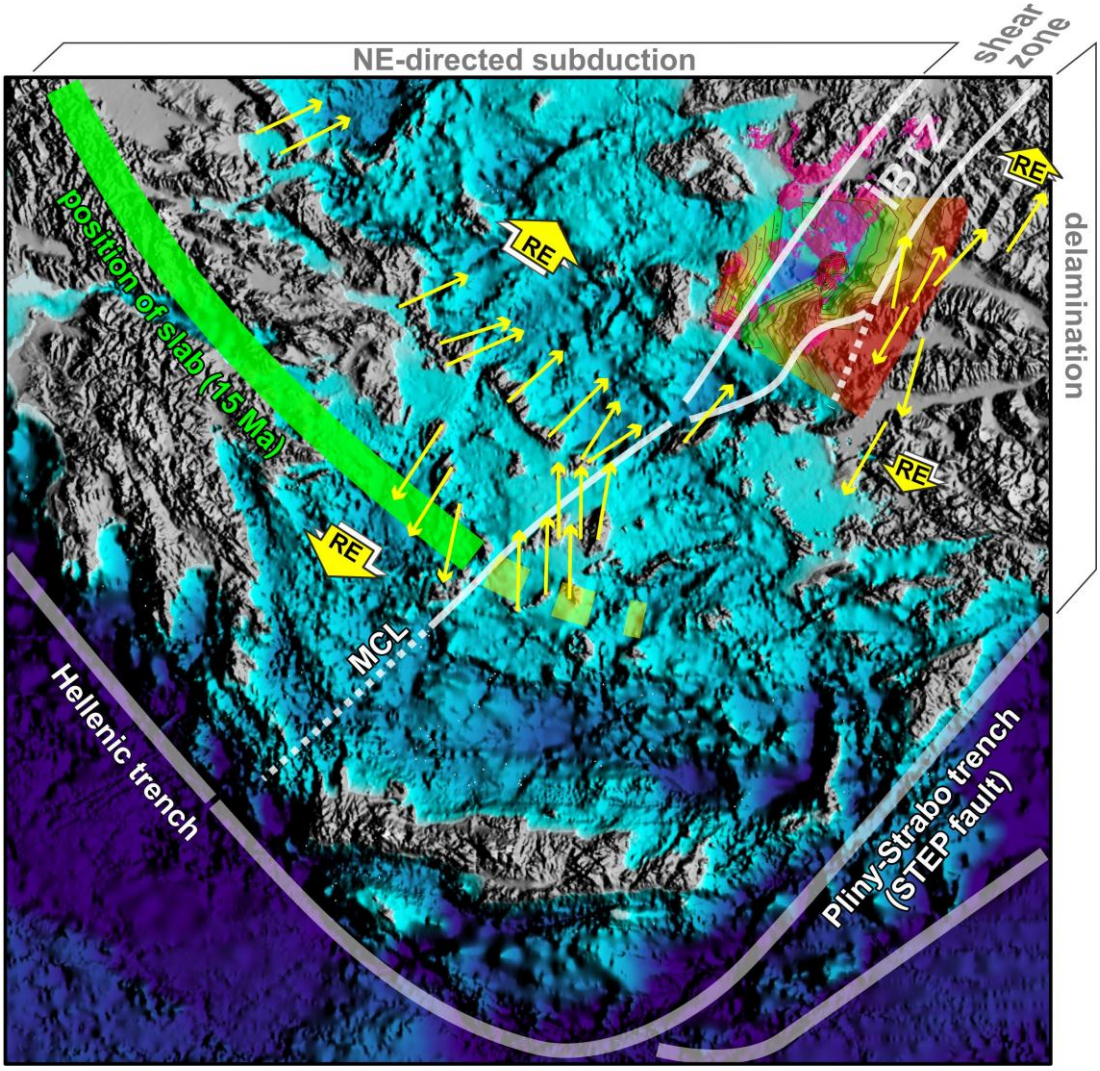


Figure 6.7 Present dynamics in western Anatolian and Aegean region drapped on the surface/subsurface topography (compied from Walcott and White, 1998; Bozkurt and Satır, 2000; Lips et al., 2001; Ring et al., 2003; Jolivet et al., 2010, 2012). Yellow arrows indicate stretching lineations from both MCC and CCC of Miocene extensional detachment faults showing NE-SW oriented regional extension (RE) that almost parallel the İzmir-Balıkesir Transfer Zone (İBTZ) and Mid-Cycladic Lineament (MCL).

With increasing deformation intensity, the former wrench-dominated transtension changed into extension-dominated transtension where maximum extension direction is always horizontal, but the maximum shortening direction changed with time. Available palaeostress analyses of the post-Miocene faults along the E–W trending grabens suggest that they were formed under the control of N−S to NNE−SSW extension, which is compatible with the regional N−S extension. However, in the western end of the grabens, within the İBTZ, wrench- to extension-dominated

transtension was prevailing (Özkaymak et al., 2013). This was associated with a shift from wrench- to extension-dominated deformation within the İBTZ. Field evidence also suggests that some older strike-slip faults might be reactivated as oblique-slip normal faults caused by a switch from strike-slip to extension-dominated deformation. The timing of Phase 2 can be correlated both with the termination of MCL activity and with the onset of N-S rifting in the West Anatolian Extensional System that occurred between 5 and 7 Ma (Lips et al., 2001; Armijo et al., 1999). The $^{40}Ar/^{39}Ar$ ages of syn-extensional muscovites in the footwall rocks of the Gediz detachment fault, of 6.7 ± 1.1 Ma and 6.6 ± 2.4 Ma constrain the timing of late-stage extension and the reactivation of the Gediz detachment fault (Lips et al., 2001). In addition, Gessner et al. (2001) presented two zircon and apatite fission-track ages of 5.2 ± 0.3 Ma from the Salihli granitoid that show accelerated cooling rates in the central Menderes Massif in the earliest Pliocene. These results strongly indicate that the last exhumation of the central Menderes Massif under the footwall of the Gediz detachment fault was coeval with the Plio-Quaternary transtension within the İBTZ. During post-Miocene period (Phase 2), the rotation of eastern part of the MCC was gently clockwise, while the İBTZ has slightly chaotic rotational pattern (Fig. 6.6b).

The youngest stage of deformation (Phase 3) occurs from the late Pliocene onwards. The earlier strike-slip dominated regime (Phase 2) is then replaced by this younger extension-dominated transtensional deformation phase, producing grabens in the early Pleistocene (Özkaymak et al., 2013). Inside the İBTZ, the extension caused segmentation into two branches: the western end of the Gediz Graben (e.g. Kocaçay and Manisa basins) and the inner part of İzmir Bay. Outside the İBTZ, Phase 3 is characterized by dominantly extensional deformation, resulting in the development and growth of the outer part of İzmir Bay and the Gediz graben.

In conclusion, the İBTZ was almost always dominated by strike-slip faulting during the late Cenozoic. The motion was changed through the time depending on the change in the differential motion caused by change in the extension directions and amounts between the MCC and CCC. In addition to this, based on existing published and new stratigraphical and kinematical data, it was concluded that İzmir

Bay originated in the Pliocene as a transtensional basin, within the middle of the İBTZ. The moment tensor solutions for recent earthquakes corroborate that strike-slip motions along the NE–SW- and NW-SW-trending strike-slip faults of the İBTZ coexist with dip-slip E–W-trending faults. This regime agrees well with the regional extensional framework related to NNE–SSW crustal stretching.

REFERENCES

Akartuna, M. (1962). İzmir-Torbalı-Seferihisar-Urla bölgesi jeolojisi hakkında (Geology of İzmir-Torbalı-Seferihisar-Urla region). *Bulletin of the Mineral Research and Exploration of Turkey, 59,* 1–18.

Akay, E. & Erdoğan, B. (2004). Evolution of Neogene calc-alkaline to alkaline volcanism in the Aliağa-Foça region (Western Anatolia, Turkey). *Journal of Asian Earth Science, 21,* 367–387.

Akdeniz, N., Konak, N. & Öztürk, Z. (1986). *İzmir-Manisa dolaylarının jeolojisi* (Geology of İzmir-Manisa surroundings). Mineral Research and Exploration of Turkey (unpublished) Report no: 7929.

Akgün, F. & Akyol, E. (1999). Palynostratigraphy of the coal-bearing Neogene deposits in Büyük Menderes Graben, western Anatolia. *Geobios, 32,* 367–383.

Aksu, A.E., Piper, D.J.W. & Konuk, T. (1987). Late Quaternary tectonic and sedimentary history of outer İzmir and Çandarlı bays, western Turkey. *Marine Geology, 76,* 89–104.

Aktuğ, B. & Kılıçoğlu, A. (2006). Recent crustal deformation of İzmir, western Anatolia and surrounding regions as deduced from repeated GPS measurements and strain field. *Journal of Geodynamics, 41,* 471–484.

Akyarlı, A., Arısoy, A. & Er, T. (1988). Current and sea level measurements performed in the Izmir Bay. Proceedings of the Environmental Science and Technology Conference, İzmir, Turkey. *Environment, 1,* 1–12.

Akyol, N., Zhu, L., Mitchel, B.J., Sözbilir, H. & Kekovalı, K. (2006). Crustal Structure and Local Seismicity in Western Anatolia. *Geophysical Journal International, 166 (3),* 1259–1269, doi: 10.1111/j.1365-246X.2006.03053.x.

Aldanmaz, E., Pearce, J.A., Thirlwall, M.F. & Mitchell, J.G., (2000). Petrogenetic evolution of late Cenozoic, post-collision volcanism in western Anatolia Turkey. *Journal of Volcanology and Geothermal Research, 102*, 67–95.

Alexandrowski, P. (1986). Graphical determination of principal directions for slickenside lineation populations: an attempt modify Arthaud's method. *Journal of Structural Geology, 7,* 73–82.

Allen, P.A., Homewood, P.W. & Williams, G.D. (1986). Foreland basins: an Introduction. In: Allen, P.A. & Homewood, P. (Eds.), Foreland basins. *International Association of Sedimentologists Special Publication, 8*, 3-12.

Alpar, B., Burak, S. & Gazioğlu, C. (1997). Effect of weather system on the regime of sea level variations in İzmir Bay. *Turkish Journal of Marine Sciences, 3,* 83–92.

Altunkaynak, Ş. & Yılmaz, Y. (1998). The Kozak magmatic complex; western Anatolia. *Journal of Volcanology and Geothermal Research ,85 (1–4),* 211–231.

Altunkaynak, Ş. & Yılmaz, Y. (1999). The Kozak Pluton and its emplacement. *Geological Journal, 34*, 257–274.

Altunkaynak, Ş. & Yılmaz, Y. (2000). Geology and active tectonics of Foça region, Western Anatolioa [Foça yöresinin jeolojisi ve aktif tektoniği, Batı Anadolu]. *Batı Anadolu'nun Depremselliği Sempozyumu (BADSEM 2000), Abstracts Book*, 160–165.

Altunkaynak, İ. & Genç, İ.C., (2008). Petrogenesis and time-progressive evolution of the Cenozoic continental volcanism in the Biga peninsula, NW Anatolia (Turkey). *Lithos, 102*, 316–340.

Altunkaynak, İ. & Yılmaz, Y., (1998). The Mount Kozak magmatic complex, Western Anatolia. *Journal of Volcanology and Geothermal Research, 85*, 211–231.

Altunkaynak, İ., Rogers, N.W. & Kelley, S.P., (2010). Causes and effects of geochemical var- iations in late Cenozoic volcanism of the Foça volcanic centre, NW Anatolia, Turkey. *International Geology Review, 52*, 579–607.

Anderson, E.M. (1951). *The Dynamics of Faulting*. Oliver & Boyd, Edinburgh, 206 pp.

Angelier, J. (1979). Determination of the mean principal directions of stress for a given fault population. *Tectonophysics, 56*, 17–26.

Angelier, J. (1984). Tectonic analysis of fault slip data sets. *Journal of Geophysical Research, 80*, 5835–5848.

Angelier, J. (1990). Inversion of field data in fault tectonics to obtain the regional stress: III. A new rapid direct inversion method by analytical means. *Geophysical Journal International, 103*, 363– 376.

Angelier, J. (1994). Fault slip analysis and paleostress reconstruction. In *Continental Deformation* (101–120), Pergamon, Oxford.

Angelier, J., Dumont, J.F., Karamanderesi, İ.H., Poisson, A., Şimşek, Ş. & Uysal, Ş. (1981). Analyses of fault mechanisms and expansion of southwestern Anatolia since the Late Miocene. *Tectonophysics, 79*, 11–19.

Armijo, R., Carey, E. & Cisternas, A. (1982). The inverse problem inmicrotectonics and the separation of tectonic phases. *Tectonophysics, 82*, 145–169.

Armijo, R., Meyer, B., Hubert, A. & Barka, A. (1999). Westwards propagation of the North Anatolian Fault into the Northern Aegean: Timing and kinematics. *Geology, 27*, 267–270.

Arthaud, F. (1969). Me´thode de determination graphique des directions de reccourcissement, d'allongement et interme´diaire d'une population de failles. *Bulletin de la Societe´ Ge´ologique de France, 7*, 729–737.

Avigad, D., G. Baer, & Heimann, A., (1998). Block rotations and continental extension in the central Aegean Sea: Palaeomagnetic and structural evi- dence from Tinos and Mykonos (Cyclades, Greece), *Earth Planet. Sci. Lett., 157*, 23–40, doi:10.1016/ S0012-821X(98)00024-7.

Barka, A.A. (1992). The North Anatolian fault zone. *Annales Tectonicae, 6,* 164-195.

Becker-Platen, J.D. (1970). Lithostratigraphische Untersuchungen im KaÈnozoikum SuÈdwest-Anatoliens (TuÈrkei) (KaÈnozoikum und Braunkohlen der Turkei, 2). *Beihefte zum geolgischen Jahrbuch*, 97, 1-243.

Benetatos, C., Kiratzi, A., Ganas, A., Ziazia, A., Plessa, A. & Drakatos, G. (2006). Strike-slip motions in the Gulf of Sığacık (western Anatolia): properties of the 17 October 2005 earthquake seismic sequence. *Tectonophysics, 426,* 263–279.

Bergerat, F., Angelier, J. & Andreason, P. (2007). Evolution of paleostress fields and brittle deformation of the Tornquist Zone in Scania (Sweden) during Permo-Mesozoic and Cenozoic times. *Tectonophysics, 444*, 93–110.

Biggin, A., van Hinsbergen, D.J.J., Langereis, C.G., Straathof, G.B., & Deenen, M.H., (2008a). Geomagnetic secular variation in the Cretaceous Normal Superchron and in the Jurassic. *Phys. Earth Planet. Inter., 169*, 3–19, doi:10.1016/j.pepi.2008.07.004.

Biggin, A.J., Strik, G.H.M.A. & Langereis, C.G., (2008b). Evidence for a very- long- term trend in geomagnetic secular variation, *Nat. Geosci., 1*, 395–398, doi:10.1038/ngeo181.

Borsi, S., Ferrara, G., Innocenti, F. & Mazzuoli, R. (1972). Geochronology and petrology of recent volcanics in the eastern Aegean Sea (west Anatolia and Leovos Island). *Bulletin of Volcanology*, *36*, 473–496.

Bozkurt, E. (2000). Timing of extension on the Büyük Menderes Graben, western Turkey, and its tectonic implications, in Tectonics and Magmatism in Turkey and the Surrounding Area, E. Bozkurt et al. (Eds.). *Geol. Soc. Spec. Publ., 173*, 385–403, doi:10.1144/GSL.SP.2000.173.01.18.

Bozkurt, E., (2001a). Late Alpine evolution of the central Menderes Massif, western Turkey. *International Journal of Earth Sciences, 89*, 728–744.

Bozkurt, E. (2001b). Neotectonics of Turkey—a synthesis. *Geodinamica Acta, 14*, 3–30.

Bozkurt, E. (2003). Origin of NE-trending basins in western Turkey. *Geodinamica Acta, 16*, 61–81.

Bozkurt, E., (2007). Extensional vs. contractional origin for the southern Menderes shear zone, SW Turkey: tectonic and metamorphic implications. *Geological Magazine, 144*, 191–210.

Bozkurt, E., & Park, R.G. (1994). Southern Menderes Massif: an incipient metamorphic core complex in western Anatolia, Turkey. *Journal of Geological Society*, 151, 213-216.

Bozkurt, E. & Park, R.G. (1997). Microstructures of deformed grains in the augen gneisses of southern Menderes massif and their tectonic significance, western Turkey. *Geologische Rundschau, 86*, 101–119.

Bozkurt, E. & Satır, M. (2000). The southern Menderes Massif (western Turkey): Geochronology and exhumation history. *Geological Journal, 35*, 285–296, doi:10.1002/gj.849.

Bozkurt, E. & Oberhänsli, R., (2001). Menderes Massif (western Turkey): structural, metamor- phic and magmatic evolution. *International Journal of Earth Sciences, 89*, 679–882.

Bozkurt, E. & Sözbilir, H. (2004). Tectonic evolution of the Gediz Graben: field evidence for an episodic, two extension in western Turkey. *Geological Magazine, 141*, 63–79.

Bozkurt, E. & Rojay, B., (2005). Episodic, two-stage Neogene extension and short-term intervening compression in western Anatolia: field evidence from the Kiraz basin and Bozdağ horst. *Geodinamica Acta, 18*, 299–316.

Bozkurt, E. & Mittwede, S.K., (2005). Introduction: evolution of Neogene extensional tectonics of western Turkey. *Geodinamica Acta, 18*, 153–165.

Bozkurt, E. & Sözbilir, H. (2006). Evolution of the large-scale active Manisa Fault, Southwest Turkey: implications on fault development and regional tectonics. *Geodinamica Acta, 19*, 427–453.

Brahim, L.A., Chotin, P., Abdelouafi, A., El Adraoui, A., Nackha, C., Dhont, D., Charroud, M., Alaoui, F.S., Amrhar, M., Bouaza, A., Tabyaoui, H. & Chaouni, A. (2002). Paleostress evolution in the Moroccan African margin from Triassic to Present. *Tectonophysics, 357*, 187– 205.

Butler, R. F. (1992), *Paleomagnetism: Magnetic Domains to Geologic Terranes*, 195 pp., Blackwell Sci., Boston, Mass.

Candan, O., Dora, O.Ö., Oberhänsli, R., Oelsner, F. & Dürr S., (1997). Blueschist relics in the Mesozoic cover series of the Menderes Massif and correlations with Samos Island, Cyclades. *Schweiz. Mineral. Petrogr. Mitt., 77,* 95–99. doi:10.1016/j.

Candan, O., Dora, O.Ö., Oberhanslı, R., Çetinkaplan, M., Partzsch, J.H.,Warkus, F.C. & Dürr, S. (2001). Pan-African high-pressure metamorphism in the Precambrian basement of the Menderes Massif, Western Anatolia, Turkey. *International Journal of Earth Science, 89*, 793–811.

Candan, O., Cetinkaplan, M., Oberhänsli, R., Rimmelé, G. & Akal C., (2005). Alpine high- P/low- T metamor- phism of the Afyon Zone and implications for the metamorphic evolution of western Anatolia, Turkey, *Lithos, 84*, 102–124.

Carey, E. & Brunier, B. (1974). Analyse the´orique et nume´rique d'une mode`le me´chanique e´le´mentaire applique´ a l'e´tude d'une population de failles. *Comptes Rendus de l'Acade´mie des Sciences Series, D279*, 891–894.

Catlos, E.J. & Çemen, İ., (2005). Monazite ages and rapid exhumation of the Menderes Massif, western Turkey. *International Journal of Earth Sciences, 94,* 204–217.

Catlos, E.J., Baker, C., Sorensen, S.S., Çemen, İ. & Hançer, M. (2010). Geochemistry, geochronology, and cathodoluminescence imagery of the Salihli and Turgutlu granites (central Menderes Massif, western Turkey): implications for Aegean tectonics. *Tectonophysics, 48*, 110–130.

Cavazza, W., Okay, A.İ. & Zattin, M., (2009). Rapid early–middle Miocene exhumation of the Kazdağ Massif (Western Anatolia). *International Journal of Earth Sciences, 98,* 1935–1947.

Çakmakoğlu, A. & Bilgin, Z.R. (2006). Pre-Neogene stratigraphy of the Karaburun Peninsula (W of İzmir Turkey). *Bulletin of the Mineral Research and Exploration of Turkey, 132,* 33–61.

Çiftçi, N.B. & Bozkurt, E. (2008). Folding of the Gediz Graben fill, SW Turkey: extensional and/or contractional origin? *Geodinamica Acta, 21*, 145–167.

Çiftçi, N. B., & E. Bozkurt (2009). Evolution of the Miocene sedimentary fill of the Gediz Graben, SW Turkey, *Sedimentary Geology*, *216*, 49–79, doi:10.1016/j. sedgeo.2009.01.004.

Çiftçi, N.B. & Bozkurt, E., (2010). Structural evolution of the Gediz Graben, SW Turkey: temporal and spatial variation of the graben fill. *Basin Research, 22,* 846–873.

Delvaux, D. & Sperner, B. (2003). Stress tensor inversion from fault kinematic indicators and focal mechanism data: the TENSOR program. In: New Insights into Structural Interpretation and Modelling (D. Nieuwland Ed.). *Geological Society, London, Special Publications, 212,* 75–100.

Dewey, J.F., & Şengör, A.M.C. (1979). Aegean and surrounding regions: complex multiple and continuum tectonics in a convergent zone. *Geological Society of America Bulletin, 90,* 84–92.

Doblas, M. (1998). Slickenside kinematic indicators. *Tectonophysics, 295,* 187–197.

Dora, O., Kun, N., & Candan, O. (1990). Metamorphic history and geotectonic evolution of the Menderes massif. *International Earth Sciences Congress on Aegean Regions,* İzmir, Turkey, Proceedings, p. 102–115.

Duermeijer, C.E., Krijgsman, W., Langereis, C.G., & ten Veen, J.H. (1998). Post early Messinian count- er- clockwise rotations on Crete: Implications for the late Miocene to Recent kinematics of the southern Hellenic Arc. *Tectonophysics, 298 (1–3),* 77–89.

Emre, T. & Sözbilir, H. (1997). Field evidence for metamorphic core complex, detachment faulting and accomodation faults in the Gediz and Büyük Menderes grabens (Western Turkey). *International Earth Sciences Colloquium on the Aegean Region IESCA-95 Vol I,* pp. 73–94.

Emre, T. (1996). Geology and tectonics of Gediz Graben. *Turkish Journal of Earth Sciences, 5,* 171–185 (in Turkish with English abstract).

Emre, T. & Sözbilir, H. (2007). Tectonic evolution of the Kiraz Basin, Küçük Menderes Graben: evidence for compression/uplift-related basin formation overprinted by extensional tectonics in West Anatolia. *Turkish Journal of Earth Science, 16,* 441–470.

Emre, Ö., Özalp, S., Doğan, A., Özaksoy, V., Yıldırım, C. & Göktaş, F. (2005). *İzmir Yakın Çevresinin Diri Fayları ve Deprem Potansiyelleri* (The Active Faults of the İzmir Region and their Earthquake potentials). Mineral Research and Exploration of Turkey, Report no: 10754.

Ercan, T., Satır, M., Kreuzer, H., Türkecan, A., Günay, E., Çevikbaş, A., Ateş, M. & Can, B. (1985). Batı Anadolu Senozoyik volkanitlerine ait yeni kimyasal, izotopik ve radyometrik verilerin yorumu (Interpretation of the new geochemical, isotopic and radiometric age data from the western Anatolia Cenozoic volcanics). *Bulletin of the Geological Society of Turkey, 28,* 121–136.

Ercan, T., Akat, U., Günay, E. & Savaşçın, Y. (1986). Söke-Selçuk-Kuşadası dolaylarının jeolojisi ve volkanik kayaçların petrokimyasal özellikleri (Geology of the Söke-Selçuk-Kuşadası region and petrochemical features of the volcanic rocks). *Mineral Research and Exploration (MTA) Bulletin, Turkey, 105/106,* 15–38.

Ercan, E., Satır, M., Sevin, D. & Türkecan, A. (1996). Batı Anadolu' daki Tersiyer ve Kuvaterner yaşlı volkanik kayaçlarda yeni yapılan radyometrik yaş ölçümlerinin yorumu (Some new radiometric ages from Tertiary and Quaternary volcanic rocks from West Anatolia). *Bulletin of Mineral Research and Exploration Institute of Turkey, 119,* 103–112.

Erdoğan, B. (1990). Tectonic relations between İzmir–Ankara Zone and Karaburun Belt. *Bulletin of Mineral Research and Exploration Institute of Turkey, 110,* 1–15.

Erkül, F. (2010). Tectonic significance of synextensional ductile shear zones within the Early Miocene Alaçamdağ granites, northwestern Turkey. *Geological Magazine, 147,* 611–637.

Erkül, F., Helvacı, H. & Sözbilir, H. (2005). Stratigraphy and geochronology of the Early Miocene volcanic units in the Bigadic¸ borate basin, Western Turkey. *Turkish Journal of Earth Sciences, 14,* 227–253.

Ersoy, Y., Helvacı, C., Sözbilir, H., Erkül, F. & Bozkurt, E. (2008). A geochemical approach to Neogene–Quaternary volcanic activity of western Anatolia: an example of episodic bimodal volcanism within the Selendi Basin, Turkey. *Chemical Geology, 255,* 265–282.

Ersoy, Y. & Helvacı, C. (2007). Stratigraphy and geochemical features of the Early Miocene bimodal (ultrapotassic and calc-alkaline) volcanic activity within the NE-trending Selendi Basin, Western Anatolia, Turkey. *Turkish Journal of Earth Sciences, 16,* 117–139.

Ersoy, E.Y., Helvacı, C. & Sözbilir, H. (2010). Tectono-stratigraphic evolution of the NE-SW-trending superimposed Selendi basin: implications for late Cenozoic crustal extension in Western Anatolia, Turkey. *Tectonophysics, 488,* 210–232.

Ersoy, E.Y., Helvacı, C. & Palmer, M.R. (2011). Stratigraphic, structural and geochemical features of the NE–SW-trending Neogene volcano-sedimentary basins in western Anatolia: implications for associations of supradetachment and transtensional strike–slip basin formation in extensional tectonic setting. *Journal of Asian Earth Science, 41,* 159–183.

Ersoy, Y.E., Helvacı, C., Uysal, İ., Karaoğlu, Ö., Palmer, M.R. & Dindi, F. (2013). Petrogenesis of the Miocene volcanism along the İzmir-Balıkesir Transfer Zone in western Anatolia, Turkey: Implications for origin and evolution of potassic volcanism in post-collisional areas. *Journal of Volcanology and Geothermal Research, 241–242,* 21–38.

Eşder, T. & Şimsek, Ş. (1975). Geology of İzmir (Seferihisar) geothermal area western Anatolia of Turkey determination of reservoirs by means of gradient driling. *Proceedings of 2nd UN. Symposium, San Francisco,* 349–361.

Etchecopar, A., Visseur, A. & Daignieres, M. (1981). An inverse problem in microtectonics for the determination of stress tensors from fault striation analysis. *Journal of Structural Geology, 3,* 51–65.

Fytikas, M., Innocenti, F., Manetti, P., Mazzuoli, R., Peccerillo, A. & Villari, L. (1984). Tertiary to Quaternary evolution of volcanism in the Aegean region. In: Dixon, J.E. & Robertson, A. H. F. (Eds). The Geological evolution of the Eastern Mediterranean. *Geological Society Special Publication, 17,* 687-699.

Fry, N. (1999). Striated faults: visual appreciation of their constraint on possible paleostress tensors. *Journal of Structural Geology, 21,* 7–21.

Genç, S.C., Altunkaynak, Ş., Karacık, Z. & Yılmaz, Y. (2001). The Çubukludağ Graben, Karaburun peninsula: it's tectonic significance in the Neogene geological evolution of the western Anatolia. *Geodinamica Acta, 14*, 45–55.

Gephart, J.W. & Forsyth, D.W. (1984). An improved method for determining the regional stress tensor using earthquake focal mechanism data. *Journal of Geophysical Research, B89*, 9305–9320.

Gessner, K., Piazolo, S., Güngör, T., Ring, U., Kroner, A. & Passchier, C.W. (2001). Tectonic significance of deformation patterns in granitoid rocks of the Menderes nappes, Anatolide belt, southwest Turkey. *International Journal of Earth Sciences, 89*, 766–780.

Gessner, K., Gallardo, L.A., Markwitz, V., Ring, U & Thomson, S.N. (2013). What caused the denudation of the Menderes Massif: Review of crustal evolution, lithosphere structure, and dynamic topography in southwest Turkey. *Gondwana Research 24/1*, 243–274.

Glodny, J. & Hetzel, R. (2007). Precise U–Pb ages of syn-extensional Miocene intrusions in the central Menderes Massif, Western Turkey. *Geological Magazine, 144*, 235–246.

Görür, N., Şengör, A.M.C., Sakınç, M., Tüysüz, O., Akkök, R., Yiğitbas,, E., Oktay, F.Y., Barka, A.A., Sarıca, N., Ecevitoğlu, B., Demirbağ, E., Ersoy, Ş., Algan, O., Güneysu, C., & Akyol, A. (1995). Rift formation in the Gökova region, southwest Anatolia: implications for the opening of the Aegean Sea. *Geological Magazine*, 132, 637–650.

Gürer, O., Sarica-Filoreau, N., Özburan, M., Sangu, E. & Doğan, B. (2009). Progressive development of the Büyük Menderes Graben based on new data, western Turkey. *Geological Magazine, 146*, 652–673.

Gürsoy, H., Piper, J.D.A., Tatar, O. & Mesci, L. (1998). Palaeomagnetic study of the Karaman and Karapinar volcanic complexes, central Turkey: Neotectonic rotation in the south- central sector of the Anatolian Block, *Tectonophysics, 299*, 191–211, doi:10.1016/S0040-1951(98)00205-4.

Gürsoy, H., Piper, J.D.A. & Tatar O. (2003). Neotec- tonic deformation in the western sector of tectonic escape in Anatolia: Palaeomagnetic study of the Afyon region, central Turkey, *Tectonophysics, 374*, 57–79, doi:10.1016/S0040-1951(03)00346-9.

Hancock, P.L. & Barka, A.A. (1987). Kinematic indicators on active normal faults in western Turkey. *Journal of Structural Geology, 9* (5/6), 573–584.

Hardcastle, K.C. & Hills, L.S. (1991). BRUTE3 and SELECT: Quick Basic 4 programmes for determination of stress tensor configurations and separation of heterogeneous populations of fault slip data. *Computer Geoscience, 17*, 23–43.

Hasözbek, A., Akay, E., Erdoğan, B., Satır, M. & Siebel, W. (2010). Early Miocene gran- ite formation by detachment tectonics or not? A case study from the northern Menderes Massif (Western Turkey). *Journal of Geodynamics, 50*, 67–80.

Hasözbek, A., Erdoğan, B., Satır, M., Siebel, W., Akay, E., Doğan, G.D. & Taubald, H. (2011). Al-in-hornblende thermobarometry and Sr–Nd–O–Pb isotopic compo- sitions of the early Miocene Alacam Granite in NW Anatolia (Turkey). *Tukish Journal of Earth Science*, doi:10.3906/yer-1007-33.

Heidbach, O., Tingay, M., Barth, A., Reinecker, J., Kurfess, D. & Müller, B. (2010). Global crustal stress pattern based on the World Stress Map database release 2008. *Tectonophysics, 482*, 3–15.

Helvacı, C., Ersoy, Y., Sözbilir, H., Erkül, F., Sümer, Ö. & Uzel, B. (2009). Geochemistry and $^{40}Ar/^{39}Ar$ geochronology of Miocene volcanic rocks from the

Karaburun Peninsula: implications for amphibole-bearing lithospheric mantle source, Western Anatolia. *Journal of Volcanology and Geothermal Research, 185*, 181–202.

Hetzel, R., Ring, U., Akal, C. & Troesch, M. (1995). Miocene NNE-directed extensional unroofing in the Menderes Massif, southwestern Turkey. *Journal of the Geological Society of London, 152*, 639–654.

Hetzel, R., Passchier, C.W., Ring, U. & Dora, Ö.O. (1995b). Bivergent extension in orogenic belts: the Menderes massif (southwestern Turkey). *Geology, 23*, 455–458.

Hippolyte, J.C. & Mann, P. (2011). Neogene–Quaternary tectonic evolution of the Leeward Antilles islands (Aruba, Bonaire, Curaçao) from fault kinematic analysis. *Marine and Petroleum Geology, 28*, 259–277.

Hippolyte, J.-C., Bergerat, F., Gordon, M.B., Bellier, O. & Esput, N. (2012). Keys and pitfalls in mesoscale fault analysis and paleostress reconstructions, the use of Angelier's methods. *Tectonophysics (inpress)*, doi:10.1016/j.tecto.2012.01.012.

İnci, U. (1998). Miocene synvolcanic alluvial sedimentation in lignite-bearing Soma Basin, Western Turkey. *Turkish Journal of Earth Science, 7*, 63–78.

Innocenti, F., Kolios, N., Manetti, P., Rita, F. & Villari, L. (1982). Acid and basic late Neogene volcanism in central Aegean Sea: its nature and geotectonic significance. *Bulletin of Volcanology, 45*, 87– 97.

Işık, V. & Tekeli, O. (2001). Late orogenic crustal extension in the northern Menderes Massif (western Turkey): evidence for metamorphic core complex. *International Journal of Earth Sciences, 89*, 757–765.

Işık, V., Seyitoğlu, G. & Çemen, İ. (2003). Ductile–brittle transition along the Alaşehir detachment fault and its structural relationship with the Simav detachment fault, Menderes Massif, Western Turkey. *Tectonophysics, 374*, 1–18.

Işık, V., Tekeli, O. & Seyitoğlu, G. (2004). The Ar-40/Ar-39 age of extensional ductile deformation and granitoid intrusion in the northern Menderes core complex: implications for the initiation of extensional tectonics in Western Turkey. *Journal of Asian Earth Sciences, 23*, 555–566.

Jackson, J., & D. McKenzie (1988). The relationship between plate motions and seismic moment tensors, and the rates of active deformation in the Mediterranean and Middle East. *Geophysical Journal of the Royal Astronomical Society*, 93(1): 45-73.

Jolivet, J., Rimmelé, G., Oberhänsli, R., Goffé, B. & Candan, O. (2004). Correlation of syn- orogenic tectonic and metamorphic events in the Cyclades, the Lycian Nappes and the Menderes Massif. Geodynamic implications. *Bulletin de la Société Géologique de France, 17*5, 217–238.

Jolivet, L., Lecomte, E., Huet, B., Denèle, Y., Lacombe, O., Labrousse, L., Le Pourhiet, L. & Mehl, C. (2010). The North Cycladic Detachment System. *Earth and Planetary Science Letters, 289*, 87–104.

Karacık, Z., Yılmaz, Y. & Pearce, J.A. (2007). The Dikili-Çandarlı Volcanics, Western Turkey: magmatic ınteractions as recorded by petrographic and geochemical features. *Turkish Journal of Earth Science, 16*, 493–522.

Kaya, O. (1979). Ortadoğu Ege çöküntüsünün (Neojen) stratigrafisi ve tektoniği (Neogene Stratigraphy and tectonics of the middle-east Aegean depression). *Bulletin of the Geological Society of Turkey, 22*, 35–58.

Kaya, O. (1981). Miocene reference section for the coastal parts of West Anatolia. *Newsletters on Stratigraphy, 10*, 164–191.

Kaya, O., Ünay, E., Göktaş, F. & Saraç G. (2007). Early Miocene stratigraphy of central west Anatolia, Turkey: Implications for the tectonic evolution of the eastern Aegean area, *Geological Journal, 42*, 85–109, doi:10.1002/gj.1071.

Kaymakçı, N., White, S. H. & van Dijk, P. M. (2000). Paleostress inversion in a multiphase deformed area: kinematic and structural evolution of the Çankırı Basin (central Turkey), Part 1. In: Bozkurt, E., Winchester, J. A., Piper, J. A. D. (Eds.), Tectonics and Magmatism in Turkey and the Surrounding Area. *Geological Society London, Special Publications, 173*, 445–473.

Kaymakçı, N., White, S. H. & van Dijk, P. M. (2003). Kinematic and structural development of the Çankırı Basin (Central Anatolia, Turkey): a palaeostress inversion study. *Tectonophysics, 364*, 85–113.

Kaymakçı, N., İnceöz, M. & Ertepınar, P. (2006). 3D-architecture and Neogene evolution of the Malatya Basin: inferences for the kinematics of the Malatya and Ovacık fault zones. *Turkish Journal of Earth Sciences, 15*, 123–154.

Kiratzi, A. & Louvari, E. (2003). Focal mechanisms of shallow earthquakes in the Aegean Sea and the surrounding lands determined by waveform modelling: a new database. *Journal of Geodynamics, 36*, 251–274.

Kissel, C., & Laj, C. (1988). The tertiary geodynamical evolution of the Aegean arc: A paleomagnetic reconstruction. *Tectonophysics, 146*, 183–201, doi:10.1016/0040-1951(88)90090-X.

Kissel, C., & Poisson, A. (1986). Étude paléomagne- tique des formations néogènes du bassin d'Antalya Taurides occidentales- Turquie). *C. R. Acad. Sci., Ser. II, 302 (10)*, 711–716.

Kissel, C., & Poisson A. (1987), Étude paléomagnetique préliminaire des formations cénozoïques des Bey Daglari (Taurides occidentales, Turquie). *C. R. Acad. Sci., Ser. II, 304(8),* 343–348.

Kissel, C., Jamet, M. & Laj, C. (1984). Paleomagnetic evidence of Miocene and Pliocene rotational defor- mations of the Aegean area, (in) *The Geological Evolution of the Eastern Mediterranean*, (Eds.) Dixon J.E. & Robertson, A.H.F. Geological Society, Special Publication, 17, 669–679, doi:10.1144/GSL.SP.1984.017.01.53.

Kissel, C., Laj, C. & Müller C. (1985). Tertiary geodynamical evolution of northwestern Greece: Paleomagnetic results. *Earth Planet. Sci. Lett., 72*, 190–204, doi:10.1016/0012-821X(85)90005-6.

Kissel, C., Laj, C., Poisson, A. & Simeakis K. (1989). A pattern of block rotations in central Aegean, (in) *Paleomagnetic Rotations and Continental Deformation*, (Eds.) Kissel C. & Laj C., NATO ASI Ser., Ser. C, 254, pp. 115–129, Kluwer Acad., Dordrecht, Netherlands.

Kissel, C., Averbuch, O., Frizon de Lamotte, D., Monod, O. & Allerton S. (1993). First paleomag- netic evidence for a post-Eocene clockwise rotation of the western Taurides thrust belt east of the Isparta reentrant (southwestern Turkey). *Earth Planet. Sci. Lett., 117(1–2),* 1–14, doi:10.1016/0012-821X(93) 90113-N.

Kissel, C., Laj, C., Poisson, A. & Görür N. (2003). Paleomagnetic reconstruction of the Cenozoic evo- lution of the eastern Mediterranean. *Tectonophysics, 362*, 199–217, doi:10.1016/S0040-1951(02)00638-8.

Koçyiğit, A. (2005). The Denizli graben-horst system and the eastern limit of western Anatolian continental extension: basin fill, structure, deformational mode, throw amount and episodic evolutionary history, SW Turkey. *Geodinamica Acta*, 18/3, 167–208.

Koçyiğit, A. & Özaçar, A.A. (2003). Extensional neotectonic regime through the NE edge of the Outer Isparta Angle, SW Turkey: New field and seismic data. *Turkish Journal of Earth Sciences, 12*, 67–90.

Koçyiğit, A., Yusufoğlu, H. & Bozkurt, E. (1999). Evidence from the Gediz Graben for episodic two-stage extension in western Turkey. *Journal of the Geological Society London, 156*, 605–616.

Kozur, H. (1997). Pelagic Permian and Triassic of the western Tethys and its paleogeographic and stratigraphic significance. *XLVIII. Bergund Hüttenmannisher Tag, Technische Universitat Bergakademie Freiberg, Abstract book*, pp. 21–25.

Krantz, R.W. (1988). Multiple fault sets and three-dimensional strain: theory and application. *Journal of Structural Geology, 10*, 225–237.

Laj, C., Jamet, M., Sorel, D. & Valente J.P. (1982). First paleomagnetic results from Mio- Pliocene series of the Hellenic Sedimentary arc. *Tectonophysics, 86*, 45–67, doi:10.1016/0040-1951(82) 90061-0.

Le Pichon, X., & Angelier J. (1979). The Hellenic arc and trench system: A key to the neotectonic evolu- tion of the eastern Mediterranean area. *Tectonophysics, 60*, 1–42, doi:10.1016/0040-1951(79)90131-8.

Lips, A.L.W., Cassard, D., Sözbilir, H., Yılmaz, H. & Wijbrans, J.R. (2001). Multistage exhumation of the Menderes Massif, western Anatolia (Turkey). *International Journal of Earth Science, 89*, 781–792.

Lykousis V., Anagnostou, C., Pavlakis, P., Rousakis, G. & Alexandri, M. (1995). Quaternary sedimentary history and neotectonic evolution of the eastern part of Central Aegean Sea, Greece. *Marine Geology, 125*, 59–71.

Maniatis, G. & Hampel, A. (2008). Along-strike variations of the slip direction on normal faults: Insights from three-dimensional finite-element models. *Journal of Structural Geology, 30,* 21–28.

Marret, R. & Allmendinger, R.W. (1990). Kinematic analysis of fault- slip data. *Journal of Structural Geology, 12,* 973–986.

Marret, R. & Peacock, D.C.P. (1999). Strain and stress. *Journal of Structural Geology, 21,* 1057–1063.

Márton, E., Papanikolaou, D.J. & Lekkas E. (1990). Paleomagnetic results from the Pindos, Paxos and Ionian zones of Greece. *Phys. Earth Planet. Inter., 62*, 60–69, doi:10.1016/0031-9201(90)90192-Z.

Mauritsch, H.J., Scholger, R., Bushati, S.L. & Ramiz H. (1995). Palaeomagnetic results from south- ern Albania and their significance for the geo- dynamic evolution of the Dinarides, Albanides and Hellenides. *Tectonophysics, 242*, 5–18, doi:10.1016/0040-1951(94)00150-8.

Mauritsch, H.J., Scholger, R., Bushati, S.L. & Xhomo A. (1996). Palaeomagnetic investigations in northern Albania and their significance for the geodynamic evolution of the Adriatic- Aegean realm. In: Morris, A. & Tarling, D.H. (Eds.), Palaeomagnetism and Tectonics of the Mediterranean Region. *Geological Society Special Publications, 105*, 265– 275, doi:10.1144/GSL.SP.1996.105.01.23.

McKenzie, D.P. (1978). Active tectonics of the Alpine–Himalayan belt: the Aegean Sea and surrounding regions. *Geophys. J. Royal Astron. Soc.*, 55, 217–254.

McDougall, I. & Harrison, T.M. (1999). *Geochronology and Thermochronology by the $^{40}Ar/^{39}Ar$ Method,* Second ed. Oxford University Press, New York, 212p.

McFadden, P.L. & McElhinny M.W. (1988). The combined analysis of remagnetisation circles and direct observations in paleomagnetism. *Earth Planet. Sci. Lett., 87*, 161–172, doi:10.1016/0012- 821X(88)90072-6.

McFadden, P C. & McElhinny M.W. (1990). Clas- sification of the reversal test in palaeomagnetism. *Geophys. J. Int., 103*, 725–729, doi:10.1111/ j.1365-246X.1990.tb05683.x.

Means, W.D. (1976). *Stress and Strain*. Springer-Verlag, New York.

Means, W.D. (1987). A newly recognized type of slickenside striation. *Journal of Structural Geology*, *9*, 585–90.

Meulenkamp, J. E., Wortel, M.J.R., Van Wamel, W.A., Spakman, W. & Hoogerduyn Strating, E. (1988). On the Hellenic subduction zone and the geodynamical evolution of Crete since the late middle Miocene. *Tectonophysics, 146*, 203–215, doi:10.1016/ 0040-1951(88)90091-1.

Michael, A.J. (1984). Determination of stress from slip data: faults and folds. *Journal of Geophysical Research, B89*, 11517–11526.

Morris, A. (1995). Rotational deformation during Palaeogene thrusting and basin closure in eastern central Greece: Palaeomagnetic evidence from Mesozoic carbonates. *Geophys. J. Int., 121*, 827– 847, doi:10.1111/j.1365-246X.1995.tb06442.x.

Morris, A. & Robertson A.H.F. (1993). Miocene remagnetisation of carbonate platform and Antalya Complex units within the Isparta Angle, SW Turkey. *Tectonophysics, 220*, 243–266, doi:10.1016/0040- 1951(93)90234-B.

MTA. (2002). Mineral Research and Exploration Institute of Turkey, *Geological map of Turkey, scale 1:500,000*, Ankara.

Mullender, T.A.T., Van Velzen, A.J. & Dekkers M.J. (1993). Continuous drift correction and separate identification of ferrimagnetic and paramagnetic contribution in thermomagnetic runs. *Geophysical Journal International, 114*, 663–672, doi:10.1111/j.1365-246X.1993.tb06995.x.

Ocakoğlu, N., Demirbağ E., & Kuşcu İ. (2004). Neotectonic structures in the area offshore of Alaçatı, Doğanbey and Kuşadası (western Turkey): evidence of strike-slip faulting in the Aegean extensional province. *Tectonophysics*, 391, 67-83.

Ocakoğlu, N., Demirbağ, E. & Kuşcu, İ. (2005). Neotectonic structures in İzmir Gulf and surrounding regions (western Turkey): evidences of strike-slip faulting with compression in the Aegean extensional regime. *Marine Geology, 219*, 155–171.

Okay, A.İ. (1984). Distribution and characteristics of the northwest Turkish blueschists. In: Dixon J.E. & Robertson, A.H.F. (Eds.), The Geological Evolution of the Eastern Mediterranean. *Geol. Soc. Spec. Publ., 17*, 455–466, doi:10.1144/GSL. SP.1984.017.01.33.

Okay, A.İ. (1986). High pressure/low temperature metamorphic rocks of Turkey. In: *Blueschists and Eclogites*, (Eds.) Evans B. & Brown, E.H., Mem. Geol. Soc. Am., 164, 333–348.

Okay, A.İ. (1989). Geology of the Menderes Massif and the Lycian Nappes south of Denizli, western Taurides. *Miner. Resour. Explor. Bull., 109*, 37–51.

Okay, A.İ. (2001). Stratigraphic and metamorphic inversions in the central Menderes Massif: A new structural model. *Int. J. Earth Science, 89*, 709–727, doi:10.1007/s005310000098.

Okay, A.İ. (2001). Stratigraphic and metamorphic inversions in the central Menderes Massif: a new structural model. *International Journal of Earth Science, 89*, 709–727.

Okay, A.İ. & Siyako, M. (1991). The new position of the İzmir-Ankara Neo-Tethyan Suture between İzmir and Balıkesir. *Proceedings of the Ozan Sungurlu Symposium*, pp. 333–355.

Okay, A.İ. & Tüysüz, O. (1999). Tethyan sutures of northern Turkey. In: Durand, B., Jolivet, L., Horvath, E. & Seranne, M. (Eds.), The Mediterranean Basins: tertiary extension within the Alpine Orogen. *Geological Society, London, Special Publications, 156*, pp. 475–515.

Okay, A.I. & Satır, M. (2000). Coeval plutonism and metamorphism in a latest Oligocene metamorphic core complex in northwest Turkey. *Geological Magazine, 137*, 495–516.

Okay, A.I. & Altıner, D. (2007). A condensed Mesozoic section in the Bornova Flysch Zone: A fragment of the Anatolide-Tauride carbonate platform. *Turkish Journal of Earth Sciences, 16*, 257–279.

Okay, A.İ., İşinteki İ., Altıner, D., Özkan-Altıner, S. & Okay, N. (2012). An olistostrome-melange belt formed along a suture: Bornova Flysch zone, western Turkey, *Tectonophysics (in press)*, doi:10.1016/j.tecto.2012.01.007.

Özer, S. & Sözbilir, H. (2003). Presence and tectonic significance of Cretaceous rudist species in the so-called Permo- Carboniferous Göktepe formation, central Menderes Massif, western TurkeyInternational *Journal of Earth Science, 92*, 397–404.

Özer, S., Sözbilir, H., Özkar, İ., Toker, V. & Sarı, B. (2001). Stratigraphy of Upper Cretaceous-Paleocene sequences in the southern and eastern Menderes Massif. *International Journal of Earth Science, 89*, 852–866.

Özgenç, İ. (1978). Cumaovası (İzmir) asitvolkanitlerde saptanan iki ekstrüzyon aşaması arasındaki göreceli yaş ilişkisi (Relative age relationships between two

extrusion phases of Cumaovası acidic volcanics (İzmir)). *Bulletin of the Geological Society of Turkey, 21,* 31–34.

Özkaymak, Ç. & Sözbilir, H. (2008). Stratigraphic and structural evidence for fault reactivation: the active Manisa fault zone, western Anatolia. *Turkish Journal of Earth Sciences 17* (3), 615–635.

Özkaymak, Ç., Sözbilir, H. & Uzel, B. (2011). Geological and palaeoseismological evidence for late Pleistocene−Holocene activity on the Manisa Fault Zone, western Anatolia. *Turkish Journal of Earth Sciences, 20,* 1–26, doi:10.3906/yer-0906-18.

Özkaymak, Ç., Sözbilir, H. & Uzel, B. (2013). Neogene-Quaternary Evolution of the Manisa Basin: Evidence for Variation in the Stress Pattern of the İzmir-Balıkesir Transfer Zone, Western Anatolia. *Journal of Geodynamics, 65,* 117–135.

Pe-Piper, G., Piper, D.J.W., Kotopouli, C.N. & Panagos, A.G. (1995). Neogene volcanoes of Chios, Greece. The relative importance of subduction and back-arc extension: *Geological Society London, Special Publications, 81,* 213–232.

Pe-Piper, G., Piper, D.J.W. & Matarangas, D. (2002). Regional implications of geochemistry and style of emplacement of Miocene I-type diorite and granite, Delos, Cyclades, Greece. *Lithos, 60,* 47–66.

Petit, J.P. (1987). Criteria for the sense of movement on fault surfaces in brittle rocks. *Journal of Structural Geology, 9,* 597–608.

Piper, J.D.A., Moore, J.M., Tatar, O., Gürsoy, H. & Park R.G. (1996). Palaeomagnetic study of crustal deformation across an intracontinental transform: The North Anatolian Fault Zone in northern Turkey. In: Morris A. & Tarling, D.H. (Eds.), Palaeomagnetism and Tectonics of the Mediterranean Region.

Geological Society Special Publications, 105, 299–310, doi:10.1144/GSL.SP.1996.105.01.26.

Piper, J.D.A., Tatar, O. & Gursoy H. (1997). Deformational behaviour of continental lithosphere deduced from block rotations across the North Anatolian Fault Zone in Turkey. *Earth Planet. Sci. Lett., 150*, 191–203, doi:10.1016/S0012-821X (97)00103-9.

Piper, J.D.A., Gürsoy, H. & Tatar O. (2002). Palaeomagnetism and magnetic properties of the Cappadocian ignimbrite succession, central Turkey and Neogene tectonics of the Anatolian collage. *J. Volcanol. Geotherm. Res., 117*, 237–262, doi:10.1016/S0377-0273(02)00221-4.

Platzman, E.S., Platt, J.P., Tapirdamaz, C., Sanver, M. & Rundle C.C. (1994). Why are there no clock- wise rotations along the North Anatolian Fault Zone? *J. Geophys. Res., 99*, 21,705–21,715, doi:10.1029/94JB01665.

Platzman, E. S., Tapirdamaz, C. & Sanver M. (1998). Neogene anticlockwise rotation of Anatolia (Turkey): Preliminary palaeomagnetic and geochro- nological results. *Tectonophysics, 299*, 175–189, doi:10.1016/S0040-1951(98)00204-2.

Purvis, M. & Robertson, A.H.F. (2004). A pulsed extension model for the Neogene–Recent E–W-trending Alaşehir Graben and the NE–SW-trending Selendi and Gördes Basins, western Turkey. *Tectonophysics, 391*, 171–201.

Piper, D. J. W., H. Gürsoy, M. Tatar, M. E. Beck, A. Rao, F. Kocbulut, and B. L. Mesci (2010), Distributed neotectonic deformation in the Anatolides of Turkey: A palaeomagnetic study. *Tectonophysics*, doi:10.1016/j.tecto.2010.03.008.

Purvis, M., Robertson, A. & Pringle, M. (2005). Ar-40-Ar-39 dating of biotite and sanidine in tuffaceous sediments and related intrusive rocks: Implications for the

Early Miocene evolution of the Gördes and Selendi basins, W Turkey. *Geodinamica Acta, 18*, 239–253.

Reches, Z. (1987). Determination of the tectonic stress tensor from slip along faults that obey the Coulomb yield criterion. *Tectonics, 6*, 849–861.

Reilinger, R.E., Mcclusky, S.C., Vernant, P., Lawrence, S., Ergintav, S., Çakmak, R., Nadariya, M., Hahubia, G., Mahmoud, S., Sakr, K., Arrajehi, A., Paradissis, D., Al- Aydrus, A., Prilepin, M., Guseva, T., Evren, E., Dmitritsa, A., Filikov, S.V., Gomes, F., Al-Ghazzi, R. & Karam, G. (2006). GPS constraints on continental deformation in the Africa-Arabia-Eurasia continental collision zone and implications for the dynamics of plate interactions: *Journal of Geophysical Research, 111*, B05411, doi: 10.1029/ 2005JB004051.

Richardson-Bunbury, J.M. (1996). The Kula volcanic field, western Turkey: the devel- opment of a Holocene alkali basalt province and the adjacent normal faulting graben. *Geological Magazine, 133*, 275–283.

Rimmelé, G., Oberhänsli, R., Candan, O., Goffé, B. & Jolivet L. (2006). The wide distribution of HP- LT rocks in the Lycian Belt (western Turkey): Implica- tions for accretionary wedge geometry. In: Robertson A.H.F. & Mountrakis, D. (Eds.), Tectonic Development of the Eastern Mediterranean Region. *Geol. Soc. Spec. Publ., 260*, 447–466, doi:10.1144/GSL.SP.2006.260.01.18.

Ring, U. & Collins, A.S. (2005). U–Pb SIMS dating of syn-kinematic granites: timing of core-complex formation in the northern Anatolide belt of western Turkey. *Journal of the Geological Society, London, 162*, 289–298.

Ring, U., Glodny, J., Will, T. & Thomson, S.N. (2007). An Oligocene extrusion wedge of blueschist- facies nappes on Evia, Aegean Sea, Greece: Implications for the early exhumation of high- pressure rocks. *J. Geol. Soc., 164*, 637–652, doi:10.1144/0016- 76492006-041.

Ring, U., Susanne, L. & Matthias, B. (1999). Structural analysis of a complex nappe sequence and late orogenic basins from the Aegean Island of Samos, Greece. *Journal of Structural Geology, 21*, 1575–1601.

Ring, U., Johnson, C., Hetzel, R. & Gessner, K. (2003). Tectonic denudation of a Late Cretaceous-Tertiary collisional belt: Regionally symmetric cooling patterns and their relation to extensional faults in the Anatolide belt of western Turkey. *Geological Magazine, 140* (4), 421–441, doi:10.1017/S0016756803007878.

Robertson, A.H.F. & Pickett, E.A. (2000). Paleozoic–Early Tertiary Tethyan evolution of mélanges, rift and passive margin units in the Karaburun Peninsula (western Turkey) and Chios Island (Greece). In: Bozkurt, E., Winchester, J.A., Piper, J.D.A. (Eds.), Tectonics and Magmatism in Turkey and Surrounding Area. *Geological Society London, Special Publications, 173*, 43–82.

Rojay, B., Toprak, V., Demirci, C. & Süzen, L. (2005). Plio–Quaternary evolution of the Küçük Menderes Graben, southwestern Anatolia, Turkey. *Geodinamica Acta, 18*, 317–331.

Saintot, A. & Angelier, J. (2002). Tectonic paleostress fields and structural evolution of the NW-Caucasus fold-and-thrust belt from Late Cretaceous to Quaternary. *Tectonophysics, 357*, 1 –31.

Sarı, B. (2012). Late Maastrichtian–Late Palaeocene planktic foraminiferal biostratigraphy of the matrix of the Bornova Flysch Zone around Bornova. *Turkish Journal of Earth Sciences (in press)*, doi:10.3906/yer-1107-2.

Sarıca, N. (2000). The Plio−Pleistocene age of Büyük Menderes and Gediz Grabens and their tectonic significance on N−S extensional tectonics in West Anatolia: mammalian evidence from the continental deposits. *Geological Journal, 35*, 1–24.

Savaşçın, Y. (1978). *Foça- Urla Neojen Volkanitlerinin Mineralojik ve Jeokimyasal İncelenmesi ve Kökensel Yorumu* (Mineralogical and Geochemical Investigations and Source Interpretations of Foça-Urla Neogene Volcanites). PhD Thesis, pp. 1–15.

Sayın, E. (2003). Physical features of the İzmir Bay. *Continental Shelf Research, 23,* 957–970.

Sayın, E., Pazı, İ. & Eronat, C. (2006). Investigation of water masses in İzmir Bay, western Turkey. *Turkish Journal of Earth Sciences, 15*, 343–372.

Scheepers, P. (1992), No tectonic rotation for the Apulia- Gargano foreland in the Pleistocene, *Geophys. Res. Lett., 19 (22),* 2275–2278, doi:10.1029/ 92GL02440.

Şen, S., & Seyitoğlu G. (2009). Magnetostratigraphy of early–middle Miocene deposits from east- west trending Alaşehir and Büyük Menderes grabens in western Turkey, and its tectonic implications. In: D. J. J. van Hinsbergen et al (Eds.), Collision and Collapse at the Africa- Arabia- Eurasia Subduction Zone. *Geol. Soc. Spec. Publ., 311,* 321–342, doi:10.1144/SP311.13.

Şengör, A.M.C. (1987). Cross-faults and differential stretching of hanging walls in regions of low-angle normal faulting: examples from Western Turkey. In: Continental Extensional Tectonics. *Journal of the Geological Society. Special Publications, London,* 575–589.

Şengör, A.M.C. & Yılmaz, Y. (1981). Tethyan Evolution of Turkey: A Plate Tectonic Approach. *Tectonophysics, 75,* 181–241.

Şengör, A.M.C. (1979). The North Anatolian Transform Fault: its age, offset and tectonic significance. *Journal of the Geological Society of London*, 136, 269–282.

Şengör, A.M.C. (1980). Türkiye'nin Neotektoniğinin esasları. *Türk. Jeol. Kur. Konf. Ser*. 2, 40.

Şengör, A.M.C. (1982). Ege'nin neotektonik evrimini yöneten etkenler, Batı Anadolu'nun Genç Tektoniği ve Volkanizması Paneli. *Congress of the Geological Society of Turkey,* 59–72.

Şengör, A.M.C., Görür, N. & Şaroğlu, F. (1985). Strike-slip faulting and related basin formation in zones of tectonic escape: Turkey as a case study. In: Biddle, K., Christie-Blick, N. (Eds.), Strike-Slip Deformation, Basin Formation and Sedimentation. *Society of Economic Paleontologists and Mineralogists, Special Publications, 37*, pp. 227–264.

Seyitoğlu, G., Scott, B.C. & Rundle, C.C. (1992). Timing of Cenozoic extensional te ctonics in west Turkey. *Journal of the Geological Society, London, 149,* 533–538.

Seyitoğlu, G. (1997a). Late Cenozoic tectono-sedimentary development of the Selendi and Uşak-Güre basins: a contribution to the discussion on the development of east-west and north trending basins in western Anatolia. *Geological Magazine, 134*, 163–175.

Seyitoğlu, G. (1997b). The Simav graben: An example of young E-W trending structures in the late Cenozoic extensional system of Western Turkey. *Turkish Journal of Earth Science, 6,* 135–141.

Seyitoğlu, G. & Scott, B.C. (1991). Late Cenozoic crustal extension and basin formation in west Turkey. *Geological Magazine, 128,* 155–166.

Seyitoğlu, G. & Scott, B.C. (1994). Late Cenozoic basin development in west Turkey. Gördes basin: tectonics and sedimentation. *Geological Magazine, 131*, 631–637.

Seyitoğlu, G., Çemen, İ. & Tekeli, O. (2000). Extensional folding in the Alaşehir (Gediz) Graben, western Turkey. *Journal of the Geological Society London, 157*, 1097–1100.

Seyitoğlu, G., Tekeli, O., Çemen, İ., Şen, Ş. & Işık, V. (2002). The role of the flexural rotation/rolling hinge modeling the tectonic evolution of the Alaşehir graben, Western Turkey. *Geological Magazine, 139*, 15–26.

Sözbilir, H. (2001). Extensional tectonics and the geometry of related macroscopic structures: field evidence from the Gediz detachment, western Turkey. *Turkish Journal of Earth Sciences, 10*, 51–67.

Sözbilir, H. (2002). Geometry and origin of folding in the Neogene sediments of the Gediz Graben, Western Anatolia, Turkey. *Geodinamica Acta, 15*, 277–288.

Sözbilir, H. (2005). Oligo–Miocene extension in the Lycian orogen: evidence from the Lycian molasse basin, SW Turkey. *Geodinamica Acta, 18*, 257–284.

Sözbilir, H., & Emre, T., 1996, Supra-detachment basin and rift basin developed during the neotectonic evolution of the Menderes Massif, *The Geological Congress of Turkey*, Abstracts, 30–31.

Sözbilir, H., Sarı, B. Akgün, F., Gökçen, N., Akkiraz, S., Sümer, Ö. & Erkül, F. (2004). First example of a transtensional supradetachment basin in western Anatolia: The Kemalpaşa-Torbalı Basin, Turkey. *32nd Internatinonal Geological Congress, Italy, Abstracts* 2, p. 894.

Sözbilir, H., Uzel, B., Sümer, Ö., İnci, U., Ersoy, Y.E., Koçer, T., Demirtaş, R. & Özkaymak, Ç. (2008). Evidence for a kinematically linked E-W trending İzmir Fault and NE-trending Seferihisar Fault: Kinematic and paleoseismogical studies carried out on active faults forming the İzmir Bay, Western Anatolia (D-B uzanımlı İzmir Fayı ile KD-uzanımlı Seferihisar Fayı'nın birlikte çalıştığına dair

veriler: İzmir Körfezi'ni oluşturan aktif faylarda kinematik ve paleosismolojik çalışmalar, Batı Anadolu). *Bulletin of the Geological Society of Turkey, 51* (2), 91–114.

Sözbilir, H., Kaymakçı, N., Langereis, C., Uzel, B., Özkaymak, Ç., Özkaptan, M. & Gülyüz, M. (2009). Transfer zonlarının jeolojik evrimi ve bu zonların Batı Anadolu'daki K-G genişleme tektoniğine katkısı: İzmir-Balıkesir Transfer Zonu (Geological evolution of transfer zones and their contribution to N-S Extensional tectonics in western Anatolia: İzmir-Balıkesir Transfer Zone). *13th Meeting of Active Tectonics Research Group, Abstracts*, p. 51.

Sözbilir, H., Sarı, B., Uzel, B., Sümer, Ö. & Akkiraz, S. (2011). Tectonic implications of transtensional supradetachment basin development in an extension-parallel transfer zone: the Kocaçay Basin, western Anatolia, Turkey. *Basin Research, 23*, 423–448, doi: 10.1111/j.1365-2117.2010.00496.x.

Speranza, F., Kissel, C., Islami, I., Hyseni, A. & Laj C. (1992). First paleomagnetic evidence for rotation of the Ionian zone of Albania, *Geophys. Res. Lett., 19(7)*, 697–700, doi:10.1029/92GL00575.

Speranza, F., & Kissel C. (1993). First paleomagnetism of Eocene rocks from Gargano: Widespread overprint or non‐rotation? *Geophys. Res. Lett., 20(23)*, 2627–2630, doi:10.1029/93GL02816.

Speranza, F., Islami, I., Kissel, C. & Hyseni A. (1995). Palaeomagnetic evidence for Cenozoic clockwise rotation of the external Albanides. *Earth Planet. Sci. Lett., 129*, 121–134, doi:10.1016/0012-821X (94)00231-M.

Sperner, B. & Zweigel, P. (2010). A plea for more caution in fault–slip analysis. *Tectonophysics, 482*, 29–41.

Sperner, B., Müller, B., Heidbach, O., Delvaux, D., Reinecker, J. & Fuchs, K. (2003). Tectonic stress in the Earth's crust: advances in the World Stress Map project. *Geological Society London, Special Publications, 212*, 101–116.

Steiger, R.H. & Jäger, E. (1977). Subcommission on geochronology: convention on the use of decay constants in geo- and cosmochronology. *Earth and Planetary Science Letters, 36*, 359–362.

Sümer, Ö. (2007). *Güzelbahçe (İzmir) çevresinin alüvyonal sedimantolojisi ve aktif tektoniği* (Alluvial sedimentology and active tectonics of Güzelbahçe (İzmir) surroundings). M.Sc. Thesis, p. 114.

Tan, O. (2012). The dense micro-earthquake activity at the boundary between the Anatolian and South Aegean microplates. *Journal of Geodynamics (inpress)*, doi:10.1016/j.jog.2012.05.005.

Tan, O., Tapırdamaz, C. & Yörük, A. (2008). The Earthquake Catalogues for Turkey. *Turkish Journal of Earth Sciences, 17*, 405–418.

Tatar, O., Piper, J.D.A., Gürsoy, H. & Temiz H. (1996). Regional significance of neotectonic counter- clockwise rotation in central Turkey. *Int. Geol. Rev., 38*, 692–700, doi:10.1080/00206819709465353.

Tatar, O., Gürsoy, H. & Piper J.D.A. (2002). Differ- ential neotectonic rotations in Anatolia and the Tauride Arc: Palaeomagnetic investigation of the Erenlerdag Volcanic Complex and Isparta volcanic district, south- central Turkey. *J. Geol. Soc., 159*, 281–294, doi:10.1144/0016-764901-035.

Tatar-Ekrül, S., Sözbilir, H., Erkül, F., Helvacı, C., Ersoy, E.Y. & Sümer, Ö. (2008). Geochemistry of I-type granitoids in the Karaburun Peninsula, West Turkey: Evidence for Triassic continental arc magmatism following closure of the Palaeotethys. *Island Arc, 17*, 394–418.

Taymaz, T., Yılmaz, Y. & Dilek, Y. (2007). The Geodynamics of the Aegean and Anatolia: Introduction. In *The Geodynamics of the Aegean and Anatolia* (1–16). Geological Society of London, Special Publications, 291.

Tauxe, L., & D.V. Kent (2004). A simplified statisti- cal model for the geomagnetic field and the detec- tion of shallow bias in paleomagnetic inclinations: Was the ancient magnetic field dipolar? In: Channell et al. (Eds.), Time-scales of the Paleomagnetic Field. *Geophys. Monogr. Ser., 145*, 101–115.

Thomson, S.N. & Ring, U. (2006). Thermochronologic evaluation of postcollision extension in the Anatolide orogen, western Turkey, *Tectonics, 25*, TC3005.

Tokçaer, M., Agostini, S. & Savaşçın, M.Y. (2005). Geotectonic setting and origin of the youngest Kula volcanics (Western Anatolia), with a new emplacement model. *Turkish Journal of Earth Sciences, 14*, 143–166.

Tozzi, M., Kissel, C., Funiciello, R., Laj, C. & Parotto M. (1988). A clockwise rotation of southern Apulia? *Geophys. Res. Lett., 15(7),* 681–684, doi:10.1029/ GL015i007p00681.

Twiss, R.J. & Moores, E.M. (1992). *Structural Geology*. W.H. Freeman, New York.

Uzel, B. & Sözbilir, H. (2008). A First record of strike-slip basin in western Anatolia and its tectonic implication: The Cumaovası basin as an example. *Turkish Journal of Earth Sciences, 17*, 559–591.

Uzel, B., Sözbilir, H. & Özkaymak, Ç. (2012). Neotectonic evolution of an actively growing superimposed basin in western Anatolia: The inner bay of İzmir, Turkey. *Turkish Journal of Earth Sciences, 22* (4), 439–471, doi: 10.3906/yer-0910-11.

Uzel, B., Sözbilir, H., Özkaymak, Ç., Kaymakci, N. & Langereis, CGL. (2013). Structural evidence for strike-slip deformation in the İzmir–Balıkesir transfer zone

and consequences for late Cenozoic evolution of western Anatolia (Turkey*). Journal of Geodynamics, 65,* 94–116.

van Hinsbergen, D.J.J. (2010). A key extensional metamorphic core complex reviewed and restored: the Menderes Massif of western Turkey. *Earth-Science Reviews, 102,* 60–76.

van Hinsbergen, D.J.J., Hafkenscheid, E., Spakman, W., Meulenkamp, J.E. & Wortel, R. (2005) Nappe stacking resulting from subduction of oceanic and continental lithosphere below Greece. *Geology, 33,* 325–28.

van Hinsbergen, D.J.J., Langereis, C.G. & Meulenkamp J.E. (2005b). Revision of the timing, magnitude and distribution of Neogene rotations in the western Aegean region. *Tectonophysics, 396,* 1–34, doi:10.1016/j.tecto.2004.10.001.

van Hinsbergen, D.J.J., Krijgsman, W,.Langereis, C.G., Cornée, J.J., Duermeijer, C.E. & van Vugt N. (2007). Discrete Plio- Pleistocene phases of tilting and counterclockwise rotation in the southeastern Aegean arc (Rhodos, Greece): Early Pliocene forma- tion of the south Aegean left- lateral strike- slip system. *J. Geol. Soc., 164,* 1133–1144, doi:10.1144/0016-76492006-061.

van Hinsbergen, D.J.J., Dupont- Nivet, G., Nakov, R., Oud, K. & Panaiotu C. (2008a). No significant post- Eocene rotation of the Moesian Platform and Rhodope (Bulgaria): Implications for the kinematic evolution of the Carpathian and Aegean arcs. *Earth Planet. Sci. Lett., 273,* 345–358, doi:10.1016/j. epsl.2008.06.051.

van Hinsbergen, D.J.J., Straathof, G.B., Kuiper, K.F., Cunningham, W.D. & Wijbrans J.R., (2008b), No rotations during transpressional orogeny in the Gobi Altai: Coinciding Mongolian and Eurasian apparent polar wander paths. *Geophys. J. Int., 173,* 105–126, doi:10.1111/j.1365-246X.2007.03712.x.

van Hinsbergen, D.J.J., Dekkers, M.J., Bozkurt, E. & Koopman, M. (2010). Exhumation with a twist: Paleomagnetic constraints on the evolution of the Menderes metamorphic core complex, western Turkey. Tectonics, 29, TC3009.

Vandycke, S. & Bergerat, F. (2001). Brittle tectonic structures and palaeostress analysis in the Isle of Wight, Wessex basin, southern U.K. *Journal of Structural Geology, 23,* 393–406.

Walcott, C.R. & White, S.H. (1998). Constraints on the kinematics of post-orogenic extension imposed by stretching lineations in the Aegean region. *Tectonophysics, 298,* 155– 175.

Will, T.M. & Powell, R. (1991). A robust approach to the calculation of paleostress fields from fault plane data. *Journal of Structural Geology, 13,* 813–821.

Yamaji, A. (2000). The multiple inverse method: a new technique to separate stresses from heterogeneous fault-slip data. *Journal of Structural Geology, 22,* 441–452.

Yılmaz, Y. (1989). An approach to the origin of young volcanic rocks of Western Turkey. In: Şengör, A.M.C. (Ed), Tectonic evolution of the Tethyan Region. *Kluwer Academic Publishers,* 159–189.

Yılmaz, Y., Genç, S.C., Gürer, O.F., Bozcu, M., Yılmaz, K., Karacık, Z., Altunkaynak, Ş. & Elmas, A. (2000). When did the western Anatolian grabens begin to develop? In: Bozkurt, E., Winchester, J. A. & Piper, J. D. A. (Eds.), Tectonics and Magmatism in Turkey and the Surrounding Area. *Geological Society, London, Special Publications, 173,* 353–384.

Yin, Z.M. & Ranalli, G. (1993). Determination of tectonic stress field from fault slip data, toward a probabilistic model. *Journal of Geophysical Research, 98,* 12165–12176.

Zalohar, J. & Vrabec, M. (2007). Paleostress analysis of heterogeneous fault-slip data: the Gauss method. *Journal of Structural Geology, 29*, 1798–1810.

Zhu, L., Akyol, N., Mitchell, B.J. & Sözbilir, H. (2006). Seismotectonics of western Turkey from high resolution earthquake relocations and moment tensor determinations. *Geophysical Research Letters, 33*, L07316, doi: 10.1029/2006GL025842.

Zijderveld, J. D. A. (1967). A.C. demagnetisation of rocks: Analysis of results. In: Collinson D.W., et al. (Eds.), *Methods in Palaeomagnetism*, Elsevier, Amsterdam, 254–286.